Development and Application of an Oxygen Electrochemical Sensor

by

Nga Chi Yip

A thesis submitted to
The University of Birmingham
for the degree of
DOCTOR OF PHILOSOPHY

School of Chemical
Engineering
College of Physical Sciences and Engineering
The University of Birmingham

Feb 2016

UNIVERSITY OF BIRMINGHAM

University of Birmingham Research Archive

e-theses repository

Acknowledgments

There are many people I would like to thank who have helped and supported me throughout my years of research, and the write up of my thesis. To all who have helped I would like to say a big personal thank you, whether your support has been on a personal or professional level, it has all been a great help in reaching this point.

Thanks first and foremost has to go to Prof. Paula Mendes for giving me this opportunity to study in her research group, and under her guidance. Her guidance and support has been invaluable, particularly her patience and help throughout the years bringing me to a point where I have the skills I needed to write this thesis. Her ability to assess and provide the extra support where I needed it and to give freedom to explore my work where I wanted to has allowed me to grow throughout the years of my PhD. In particular her belief in my laboratory work where I have been able to drive my research the way I felt I needed to but also the way she has helped me to develop my writing and presentation skills through constant support. She has given me opportunities to go to international conferences and many opportunities to learn as I have progressed.

Dr Frankie Rawson has been a massive help with all aspects of my electrochemistry work and knowledge. He has taken me from a background in biology to this stage where I can confidently merge both my biological and electrochemical knowledge and skills to develop new experiments

and project ideas. He has also been a great friend throughout the years being very supportive and kept me motivated.

I would also like to give thanks to the Head of School Prof. Mark Simmons. In the moment of crisis over my PhD he has been very supportive and understanding, quickly responding to the situation.

The staffs in the school of chemical engineering administration office have always been very helpful and friendly throughout the years. Lynn Draper has been a constant source of advice and help with everything course related and personal and funding documentation. All those things that are a pain if you don't have the right person to help with. Janet Lee has always been a friendly face to see, welcoming and supportive and caring. Anna Ott being so friendly and supportive in a major crisis. You showed amazing selflessness, empathy, and supportiveness while things seemed to be all going wrong. Everyone in the office are a great credit to the school and a wonderful asset for the students.

Dr Aaron Acton, you were a massive help with technical advice, helping to make sense of the chemistry work related in my project. Thanks also for your hard work synthesizing coupling compounds for me and the advice throughout the coupling work. Also a big thank you to Dr James Watton, who taught me about screen printing and how to use the department's printer.

Finally to my parents, thank you for all the hard work throughout your life, sending me to the UK and supporting me throughout my academic life, letting me grow into who I am today. Also thanks for physically taking care of my daily life in the last stages of my write up when I really struggled with my health.

Abstract

In this project, we developed a real-time electrochemical mediator assay to enable the assessment of cell numbers and cell viability. It allows us to monitor metabolism calculable down to a single cell in a low cost easy to use rapid assay, as yet not possible with current technology. The developed assay is based on the determination of oxygen. This was made possible via the use of electrochemical mediator ferrocene carboxylic acid (FcA). The FcA showed distinctive catalytic properties in interacting with reactive oxygen species generated from oxygen when compared to ferrocene methanol (FcMeOH). A deeper insight into the chemistry controlling this behaviour is provided. The behaviour is then taken advantage of to develop a cellular aerobic respiration assay. We describe the properties of the FcA system to detect, in real-time, the oxygen consumption of *Escherichia coli* DH5α (*E. coli*). We demonstrated that the FcA-based oxygen assay is highly sensitive, and using a population of cells, oxygen consumption rates could be calculated down to a single cell level. More importantly, the results can be accomplished in minutes, considerably outperforming current commercially available biooxygen demand assays. The developed assay is expected to have a significant impact in diverse fields and industries, ranging from environmental toxicology through to pharmaceutical and agrochemical industries. A significant start has been made into optimisation of the system into a commercially marketable product, including much work on mediator immobilisation and electrode synthesis.

Chapter 1

Introduction to "The Development of an Oxygen Electrochemical Sensor" reviewing the importance of metabolic rate, cell viability, and biochemical oxygen demand (BOD) assays and the systems currently in use and under development. This chapter critically assesses current system applications and reviews newly developing systems. The advantages and disadvantages of these systems are explored and an explanation is given for how this project aims to exploit and improve on these points for the design and development of a brand new assay.

Chapter 2

The electrochemical and biological theory and techniques used within this project, for the development of a new electrochemical biosensor, are covered in this chapter.

Chapter 3

This chapter describes in detail the investigation and assessment in the use of ferricyanide and ferrocene carboxylic acid (FcA) as electrochemical mediators for the direct measurement of metabolic rate. This is measured via direct electron production, as a result of cellular metabolism using *E. coli* as a model of study.

Chapter 4

The detailed experimental characterisation and investigation of the electro-catalytic properties of ferrocene derivatives, FcA, ferrocene dicarboxylic acid (FcDA), and ferrocene methanol

(FcMeOH) towards oxygen are presented in this chapter. This includes critical analysis of their use as mediator in an electrochemical oxygen sensor, and the discovery of the application of the second oxygen peak, and the vital role it plays in the BOD assay using FcA as mediator are covered. In addition, the application and investigation of an FcA-based BOD sensor for cell number detection, cell viability and cytotoxicity, and oxygen production are detailed providing proof of concept in the application of this FcA-based BOD sensor. This work to the application of a patent (patent application number WO2015036612 A1) and publication of a paper ('Real-time electrocatalytic sensing of cellular respiration').

Chapter 5

This chapter details a series of studies and application of mediator immobilisation techniques for the optimisation of the FcA-based BOD sensor. The attempted immobolisation techniques, as described in this chapter, includes screen printing, drop coating, and chemical immobilisation by self assembled monolayer (SAM) and diazonium electrode surface modification.

Chapter 6

This chapter concludes the current project and critically reviews the future direction of the current project in the research and development of a commercially viable product.

Contents

Chapter 3 : The study of electrochemical biosystems for cellular sensing

Chapter 1

Introduction

1.0 Introduction

The applications of electrochemical sensors are diverse and are found in many analytical instruments used in environmental [1] and food industries [2], pharmaceutical and clinical laboratories [3, 4], as well as, point-of-care (bedside testing) devices [5-7]. In recent years, there has been marked interest in the use of electrochemical sensors in the field of biological (electrochemical biosensors) analysis because of their high sensitivity, selectivity and efficacy [8-10]. Currently Biochemical Oxygen Demand (BOD) assay techniques are limited and it is envisaged that an electrochemical approach in the development of BOD assays could address these limitations. The current methods used to determine BOD are time consuming, taking up to 5 days, and the results can vary by up to 20% depending on the laboratory [11]. BOD assays are predominantly used in monitoring water quality [11], however with the development of an electrochemical biosensor with the qualities of high sensitivity, selectivity and efficacy it could have much broader scope for use within a BOD assay. Besides the obvious benefits to the water treatment industry there could be opportunities in areas such as the food industry, environmental industry and in medical research.

1.1 Metabolism: Aerobic respiration

Biochemical Oxygen Demand assays could facilitate biological studies in many ways, for example, in cell cycle and cell viability studies. Life forms metabolise energy sources, e.g.

sugars, protein and fat, into useable energy, stored as adenosine triphosphate (ATP) by respiration [12]. In the majority of cases, organisms convert the different kinds of food sources from their complex forms in to glucose and consume oxygen in the metabolism process to producing ATP. Therefore, further discussion herein will be focus on using respiration of glucose and the consequent consumption of oxygen as an example. Aerobic respiration is a metabolic pathway that relies on oxygen as a terminal electron acceptor. Aerobic respiration generates a maximum theoretical yield of 38 ATP from every single glucose molecule, although figures range between 30 and 38 ATP due to complexities and variations in the electron transport chain and ATP synthase [13] compared to 2 ATP in anaerobic pathway [14]. Though many organisms can use anaerobic respiration for a short period of time, aerobic respiration tends to be the favoured pathway. Some bacteria such as *Escherichia coli* (*E.coli*), are classified facultative anaerobes, and will switch between aerobic, anaerobic or fermentative metabolism dependent on environmental conditions even in the presence of oxygen.

The aerobic respiration pathway is essentially the same between different types of organisms and can be broken down and simplified into the following steps (**figure 1.1.1**) [14]. 1) Glycolysis, which is the conversion of glucose into pyruvate. 2) The conversion of pyruvate into acetyl CoA. 3) The citric acid cycle, also known as tricarboxylic acid cycle (TCA) or Krebs cycle in which the electron donors NADH and $FADH_2$ are generated. 4) Electron are transferred from the aforementioned electron donors through the electron transport chain and results in the reduction of molecular oxygen and in the process forms metabolic water (**equation 1.1**) [15]. In eukaryotic cells, step 1 to 3 is take place inside the mitochondria and the electron transport chain is located on the inner mitochondria membrane. Whereas

2

prokaryotic cells, step 1 to 3 is taken place inside the cytoplasm and the electron transport chain is located on the cell membrane.
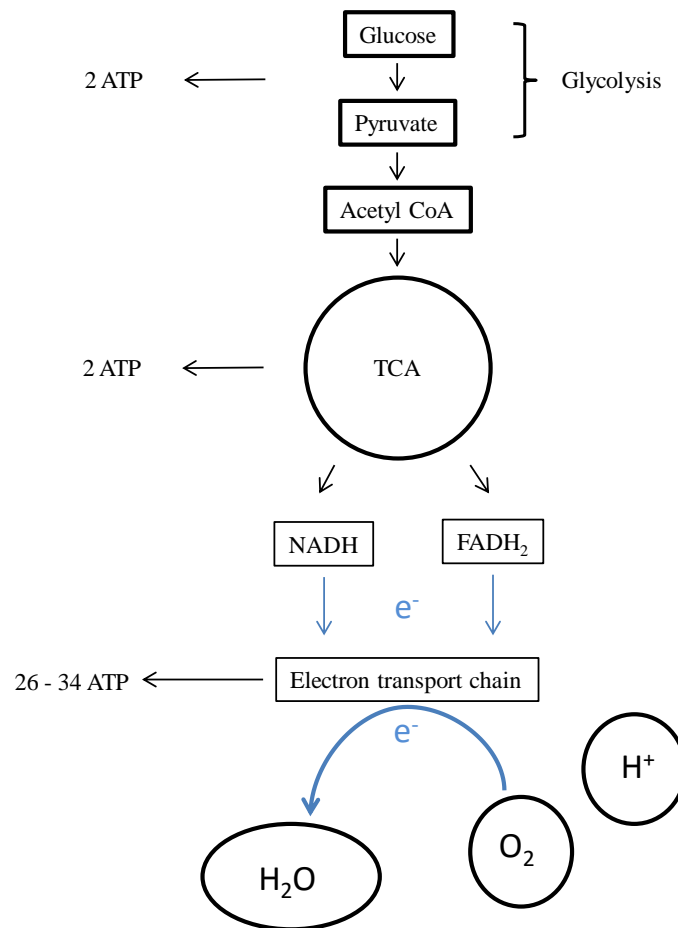
Figure 1.1.1 A simplified diagram of the aerobic respiration pathway[14].

$$2H^+ + 2e^- + \tfrac{1}{2}O_2 \rightarrow H_2O \qquad\qquad \textbf{(Equation 1.1)}$$
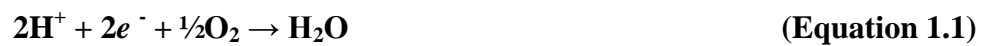
In summary, electron production and oxygen consumptions always occur in the aerobic metabolism pathway. The measurement of either/both electron production or oxygen consumption could therefore be utilised for indirectly measuring the aerobic metabolic rate.

1.2 Direct and indirect measurement metabolism

1.2.1 Direct measurement of metabolism

Assays that are based upon direct measurement of metabolism are widely used in cell biology research mainly as viability assays. They are often used as a tool in pharmaceutical and medical industries, especially for drug testing and research, for example to measure cell cytotoxicity for cancer drug testing [16], and cytotoxicity of plastic additives, 2,2-bis(4-hydroxyphenyl)propane [17]. Drugs/chemicals that are toxic to the cell will kill the cell, thus disrupting cellular metabolism and causing the cell to die. Tetrazolium salt (MTT) assay is the most commonly used viability assay in biomedical research [18]. It directly measures metabolism by incubation of the cell samples, with a specific metabolite which can be selectively measured by colourimetric techniques. The MTT assay is carried out by incubating the yellow tetrazolium dye, 3-(4,5- dimethylthiazol-2-yl)-2,5-diphenyltetrazolium bromide, with cell samples for 1 to 4 hours allowing time for the cells to take up the dye. As the dye enters the living cells, through metabolism the yellow tetrazolium dye is reduced to form an insoluble formazan salt (purple) by NADH-dependent oxidoreducatase enzymes [19, 20] (**figure 1.2.1.1**). This formazan salt acts as a marker for viable cells and is measured by absorbance of light at 560 nm wavelength. A higher measurement of absorbance at this wavelength is a sign of a high percentage of cell viability calculated comparatively to zero cell, and untreated cell controls (negative and positive controls). As dead cells do not metabolise the yellow tetrazolium dye to form the formazan salt, a low percentage viability will show low absorbance.
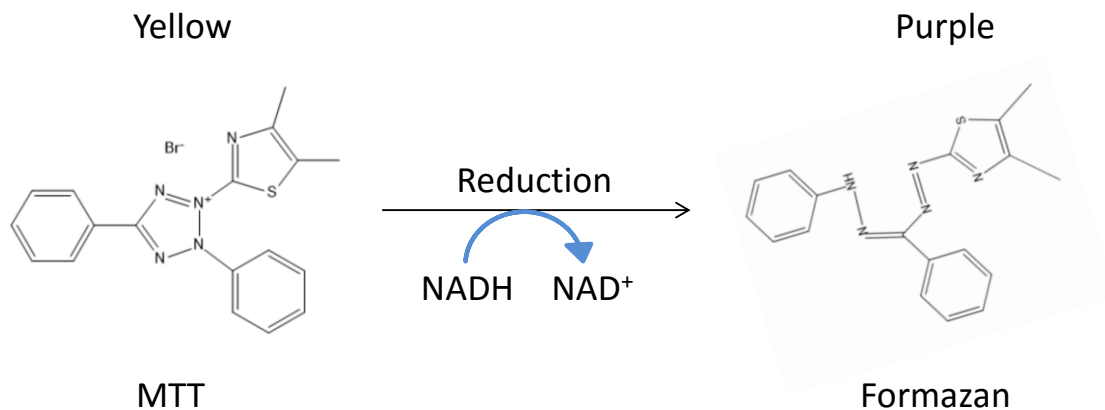
Figure 1.2.1.1 MTT being reduced by NADH to form formazan.

The biggest disadvantage of the MTT assay is it is an end point assay and it only measures the viability as a percentage relative to the positive and negative controls. Therefore in order to perform a cytotoxicity concentration or time point cytotoxicity experiment, a large amount of cell culture is required. This is a time consuming, labour intensive and costly process relative to a non-end point assay. In addition, the multi-step protocol of washing and cell fixation introduces higher risk of error due to sample loss. A real time, non-end point metabolic rate related viability assay would greatly shorten the time, and labour intensiveness, of viability determination. Continual recording of a single sample under different experimental conditions would also reduce greatly the error due to sample inconsistencies. This would greatly benefit the pharmaceutical and medical research industries in advancing drug research, by providing more accurate data with respect to drug toxicity.

1.2.2 Indirect measurement of metabolism – biochemical oxygen demand

The alternative means of measuring metabolic rate is by measuring the rate of oxygen consumption, as oxygen is the terminal electron acceptor as seen in the electron transport

chain **section 1.1**. Oxygen consumption is proportionally linked to cell numbers, viability, growth rate and the phase of cell cycle that an individual cell is in [21, 22]. Biochemical Oxygen Demand (BOD) could potentially be used in many industries. Currently, BOD is mainly used in wastewater treatment and food industry [23]. Domestic waste water and waste water from the food industry or the paper industry contain different levels of waste contaminants. These need to be monitored and cleaned to avoid environmental damage. In waste water treatment, microorganisms are used as part of the treatment to remove organic contaminants. Microorganisms metabolises organic contaminants as an energy source and in the process, oxygen is consumed. The level of oxygen consumption, gives a measurement of the metabolism of the organic contaminants in waste water by microorganisms, and as such is an indirect measurement of the level of organic contaminants in the waste water. This is normally conducted using a 5 days BOD (BOD_5) assay, however longer assay time has been reported, such as the 7 days BOD (BOD_7) used in Finland [23]. This is carefully monitored to ensure effective waste water treatment. In addition, after organic contaminants are removed, the microorganisms in the treated waste water must also be removed before the treated waste water could be released back into the environment. If not removed the microorganisms may also have detrimental affects to the ecosystems at release sites. Therefore careful monitoring of both the treatment process and the microorganism removal process is vital to prevent release of contaminants and microorganisms into the environment [24].

In environmental studies, it is important to understand the life time of chemicals used in agriculture and their impact on the environment, preventing their build up to toxic levels [25]. Chemicals such as pesticides and insecticides are harmful, not only to the target pests and insects, but also to humans, other mammals and fish. There has been much focused research on bioremediation techniques to detoxify contaminated environments using aerobic

microorganisms. These aerobic microorganisms utilise pesticides and insecticides as a source of carbon, nitrogen and phosphates, breaking down the complex molecules to a usable source of energy which is fed back into the TCA cycle (**figure 1.2.2.1**) [26]. BOD could be used as a tool to monitor the rate of pesticide and insecticide breakdown by bacteria [25].
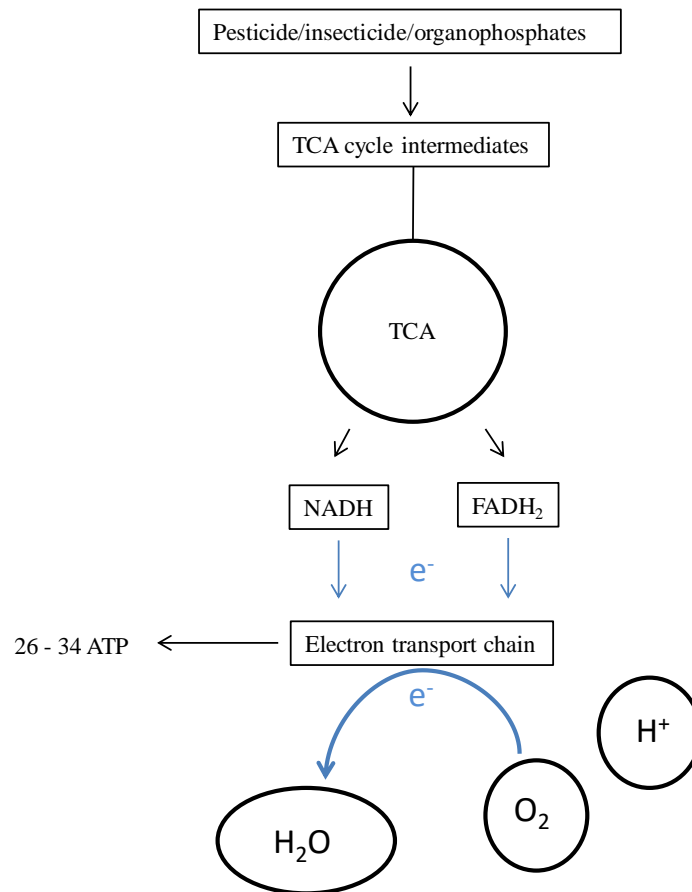
Figure 1.2.2.1 A simplified diagram of the aerobic metabolism of pesticides/insecticides/organophosphates by microorganisms [26].

1.2.3 Current biochemical oxygen demand assay in the market

1.2.3.1 Photometric methodology

The international standard water quality determination is also known as the closed bottle test which is based on the Winkler's method [27]. Samples are placed into a closed bottle and

stored in the dark at 20 °C for 5 days. Dissolved oxygen level is measured and compared between the control sample (without incubation) and the test sample (after incubation) with the Winkler's method. The Winkler's method is a 5 stages chemical reaction (**figure 1.2.3.1.1**) procedure that first fixates the dissolved oxygen in the solution which culminates in production of iodine in the solution with a yellow brown colour (often a starch indicator is used to enhance the colour change). The iodine is then titrated with sodium thiosulfate to produce sodium iodide which is a clear solution. Finally the amount of sodium thiosulfate required to titrate the sodium iodide is used to calculate the oxygen dissolved in the sample solution at the point of oxygen fixation.

Stage 1 $\quad\quad MnSO_4 + 2KOH \rightarrow Mn(OH)_2 + K_2SO_4$

Stage 2 $\quad\quad 4Mn(OH)_2 + O_2 + 2H_2O \rightarrow 4Mn(OH)_3$

Stage 3 $\quad\quad 2Mn(OH)_3 + 3H_2SO_4 \rightarrow Mn_2(SO_4)_3 + 6H_2O$

Stage 4 $\quad\quad Mn_2(SO_4)_3 + 2KI \rightarrow 2MnSO_4 + K_2SO_4 + I_2$

Stage 5 $\quad\quad 2Na_2S_2O_3 + I_2 \rightarrow Na_2S_4O_6 + 2NaI$
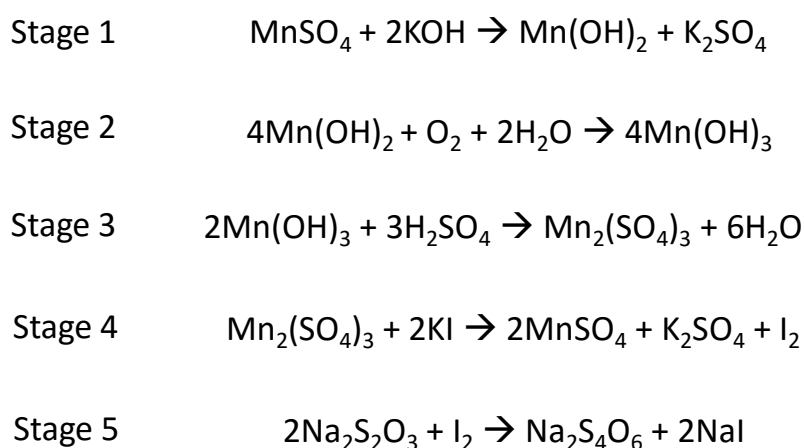
Figure 1.2.3.1.1 The 5 stage chemical reactions in the Winkler methodology.

However, because of the limited nutrient and oxygen supply that can be sealed in the bottle for the 5 to 7 days incubation, the range of measurement is narrow, 0 to 6 mg/L [27]. In addition, due to this low sensitivity, the assay takes 5 days and sometimes longer [23, 28]. The long incubation period required means it is impossible to get immediate result limiting the application of the assay. Also because of the 5 day minimum incubation period the assay can not match the high throughput demands of hospital or food industry uses. The assay is also reported to be very inaccurate with a 20% variability [27]. It also requires protective

clothing for sample preparations and laboratory equipment to perform the final reading, seriously restricting the portability of the assay. Moreover, this is an end point assay drawing comparison between the oxygen level at day 5 and a sample at time point 0. This does not meet the technological requirements for pharmaceutical and medical research industries for a real time BOD assay, or the field base work necessary in environmental studies. There are some automated machines that have been designed to help minimising the error introduced by the multiple step assays, however this exacerbates the issues in lack of portability. Attempts have been made to improve the accuracy on this BOD assay by adaptation with manometric method [28], photometric method using alternative dye kits (such as Hach Lange LCK554 and 555) and measurements using spectrophotometry [27], and electrochemical probe [29-31] (Clark's electrode) instead of using iodine.

1.2.3.2 Manometric methods

The manometric BOD method was developed in 1948 by Caldwell and Langelier [27]. The measurement is conducted by placing the microorganisms with nutrient broth in a sealed bottle connected to a manometer. As the microorganisms metabolise the nutrients, oxygen is consumed and carbon dioxide is produced. The carbon dioxide produced during metabolism is absorbed by a sodium hydroxide pellet know as an absorber within the bottle. The decreased in pressure is measured by the manometer as the oxygen is consumed [32] (**figure 1.2.3.2.1**). The advantage of this assay compare to the standard BOD_5 assay, is the result can be obtained throughout the test [32]. It also allows detection using samples with higher cell density as the amount of oxygen that is trapped in the bottle is larger [27]. However, the standard test duration like the Winkler method is 5 days, thus too slow for high throughput industrial uses. In addition, the large amount of oxygen that is trapped in the bottle also make the sensitivity of the assay very low [27].
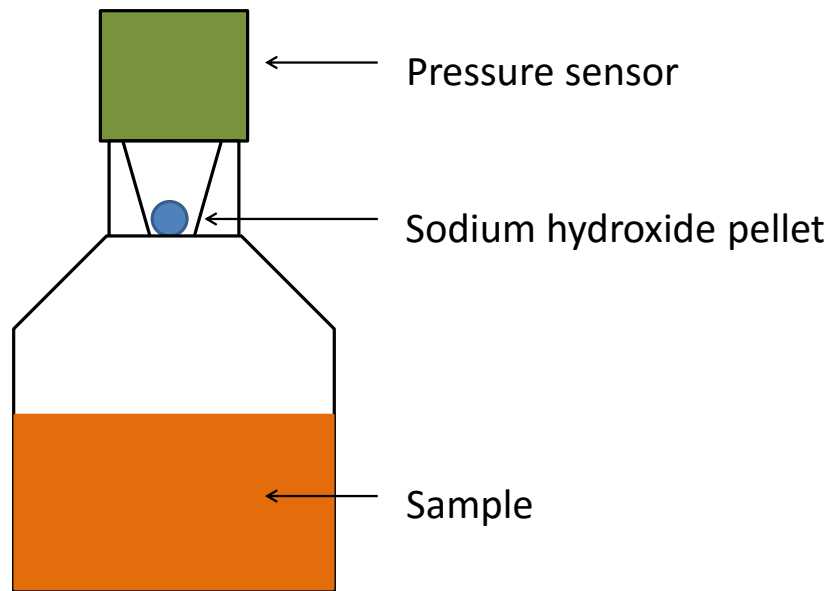
Figure 1.2.3.2.1 A diagram of a manometric methods bottle [28].

1.2.3.3 Optical sensor

The Optical dissolved oxygen sensor based BOD assay is based on the use of fluorescence quenching [33]. A fluorescent dye is usually trapped in a gas-permeable membrane at the tip of the sensor. Ruthenium complexes are the most commonly used as the intensity of the fluorescence is at a one to one ratio with O_2 molecules present [34, 35]. Light at a specific excitation wavelength is applied to the dye causing it to fluoresce, however the resultant fluorescence is inversely proportional to the concentration of oxygen present. The intensity or the lifetime of the fluorescence is then detected by a photodiode allowing calculation of oxygen concentration present in the sample [34, 35]. These probes require less maintenance than an electrochemical electrode, and unlike electrochemical systems the Optical sensor does not consume any oxygen [35]. However, there are many potential influence factors, e.g. temperature variations, pH, metal ions and oxidation processes [36]. Long term aging (instability) of the trapped luminescent chemical would also cause variation in the readings and require re-calibration [37]. Membrane fouling is also a big issue for this type of

membrane reliant sensor, as microorganisms, e.g. bacteria, like to grow on the membrane which is very difficult to clean. This would affect the membrane's performance and lifetime [38].
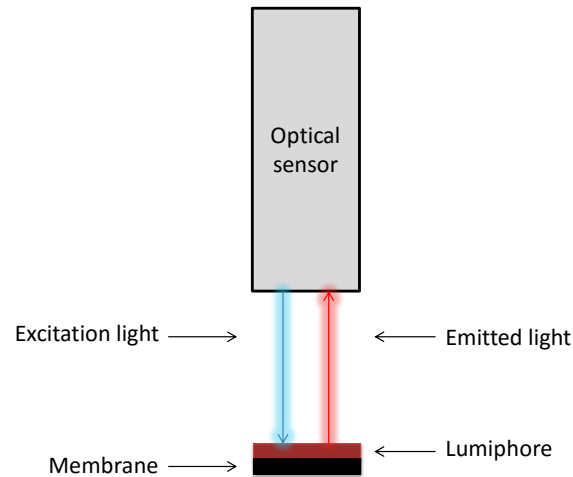
1.2.3.3.1 Simplified graphical representation of the optical sensor.

1.2.3.4 Clark's electrode

The Clark type electrode allows for direct measurement of oxygen concentration usually via the use of a silver/silver chloride anode and a platinum or gold cathode. A reaction chamber holds the sample for measurement and is separated from the electrodes by a polyethylene or Teflon membrane, allowing the diffusion of only oxygen from the reaction solution into a saturated KCl solution in which the electrodes are bathed [29-31] (**figure 1.2.3.4.1**). The system is calibrated by measurement of the current generated using a 100% saturated O_2 buffer and a 0% saturated O_2 buffer. For measurement of oxygen consumption a sample can be loaded into the reaction chamber and the initial current measured giving a percentage O_2 saturation of the solution. The current generated can be measured over time thus allowing the

measurement of oxygen consumption. The measurement range is normally between 0 to 20 mg/l with an error of ± 0.03 mg/l, an error of up to 0.15% [39].
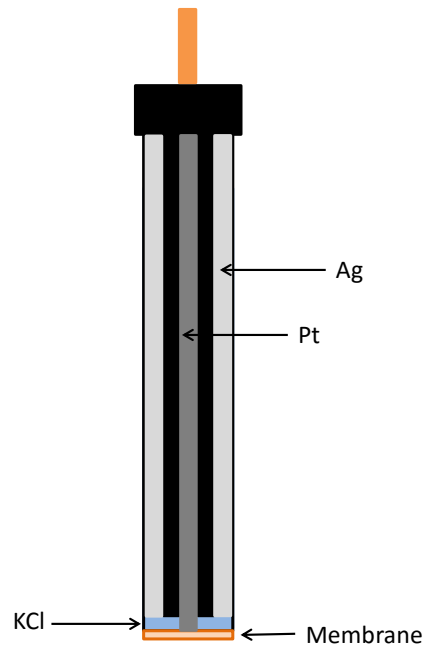
Figure 1.2.3.4.1 Simplified graphical representation of the Clark's electrode.

The Clark electrode while being a useful tool in field and laboratory testing and allowing continual measurement of O_2 does have some serious limitations. The system is dependent on O_2 diffusion across a semi-permeable membrane which requires maintenance and limits the use of the electrode in certain conditions, for example where oil or algae may be present and the sample may block the membrane. Also calibration can be complicated as it requires the temperature to remain constant and for 100% and 0% O_2 dissolved solutions to be prepared and set up to give the percentage range of the electrode. These calibration solutions can be confirmed by the use of spectrophotometry. However, this is a time consuming process in the laboratory and not be very adaptable to the field environment [40].

1.2.3.5 Summary.

Due to the current limitation of BOD technology, BOD assays are not currently applied in many sectors. Further development of BOD technology is required in order for the technology to be a useful analytical tool in other sectors. The requirements for development of new BOD assays are the combination of the following points; (1) rapid – measurements that could be made in seconds to provide real time/close to real time readings to meet industrial high throughput demands, (2) accurate – reliable and reproducible results to cut down labour intensiveness and time, (3) sensitive – requiring small sample sizes, especially in biological and environmental work, where sample size may be an issue, (4) simple – both in terms of practical use and to increase accuracy by limiting interference with the sample, and (5) portable – ideal for field based studies, such as in environmental studies or hospitals. The current BOD methodologies in the market and the focus of current BOD research have been based around these 5 requirements. However, none of the BOD methodologies currently in the market covers all these essential criteria.

1.3 Electrochemical sensor

Research into electrochemical sensors, especially electrochemical biosensors, is a field that has and is continuously expanding. Full or partial electrochemical sensor and biosensors are wildly used in many sectors, including food e.g. sugar [9], environmental e.g. pH, oxygen [8] and health care sectors e.g. glucose [41] and cholesterol [42]. In recent years, many "reagentless systems" have been undergoing development [43]. In these "reagentless systems", reactions take place at the electrode surface by immobilising an analyte and a selective interface in close proximity or integrated with a transducer as working electrode [44]. This approach can be use directly, no interface, or indirectly, with a selective interface which is called the mediator. The "reagentless systems" do not require the end user to add in

any reagents before using the system, which allows them to be cost effective, rapid, reliable and simple to operate [8-10]. Due to these factors popular demand is driving research for ever more, new and electrochemical based sensors boosting their continual development. Research is focused on improving selectivity giving even more accurate results, pushing the boundary of detection limits to improve sensitivity, thus reducing sample size requirements, and response time for reduced assay interference.

1.3.1 Use of mediator in electrochemical biosensors

An electrochemical mediator is defined as electroactive species which is added to a reduction-oxidation (redox) system and acts as an "electron shuttle" to provide redox coupling between the electrode and analyte [45] (**figure 1.3.1.1**). There are several characteristics for an "ideal" electrochemical mediator: (1) to have a reversible or quasireversible behaviour; (2) a low (close to 0 V) redox potential to avoid interference from other electrochemically active species in samples; (3) fast electron transfer; (4) solubility in the electrochemical media; (5) stable in both oxidised and reduced forms to sustain the adopted experimental condition; and (6) should have no interactions with the analyte in a manner which would alter the redox potential [46].
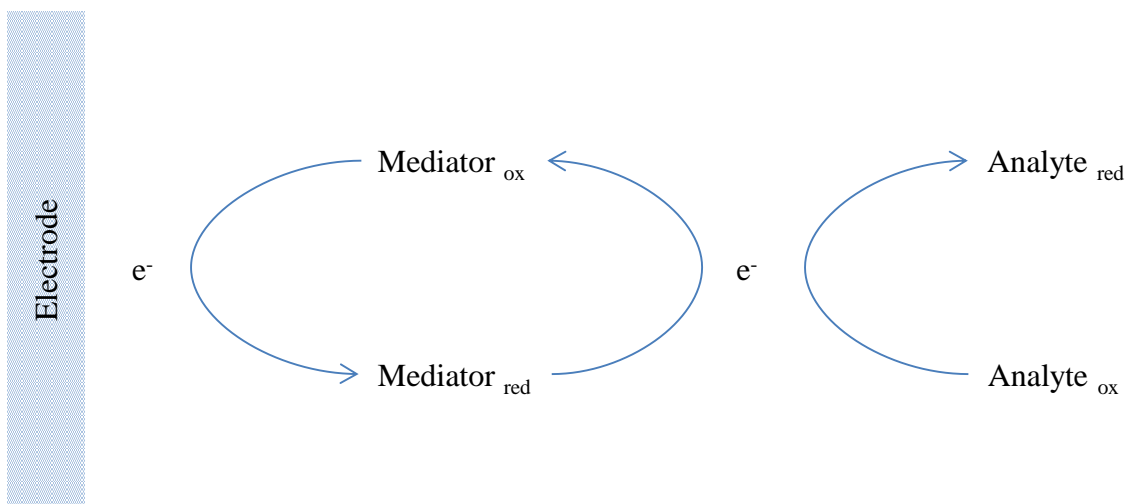
Figure 1.3.1.1 Electrochemical mediator acting as an "electron shuttle" between electrode and analyte.

Electrochemical mediators are particularly important in electrochemical biosensors because they allow the sensor to function at a lower working redox potential. By reducing the working potential range, it is possible to avoid interference from common metabolites in biological samples, such as uric acid, ascorbic acid, and glutathione. These molecules can also undergo redox and mask the electrochemical signal [44]. More importantly, with the fast redox kinetic, the use of electrochemical mediator also helps facilitate the electron transfer process [45]. Structurally similar mediators, that differ by side chain functional groups only, will have similar formal potential. However, depending on if the side chain functional group is electron donating (such as methyl groups) or electron withdrawing (such as sulfate group), the formal potential will shift either more negatively or positively, respectively [45]. Some commonly used mediators and their redox potential versus saturated calomel reference electrode (SCE) are listed below (**table 1.3.1.2**) [44]. In addition, working at a potential closer to 0 V reduces the risk of disturbing the cell membrane potential when analysing biological samples [47].

Table 1.3.1.2 List of commonly used mediators with their redox potential.

Mediator	Redox potential (versus SCE) mV
1,1-dimethyl ferrocene	100
Ferrocene	165
$[Fe(CN)_6]^{4-}$	180
N-ethyl phenazene	−172

1.3.2 Electrochemical mechanism

The usual mediator base electrochemical sensors mechanisms follow a mixture of electrochemical (E) and chemical (C) steps [48-50]. One of the most common combinations is the E-C-E mechanism [51, 52]. For example, the electrochemical sensor for the determination of Sudan I (1-(phenylazo)-2-naphthol) uses multiwall carbon nanotube-modified glassy carbon electrode (MWCNT/GCE), and functions via an E-C-E mechanism [53]. This E-C-E mechanism is a 4 electron 4 proton process where Sudan I is electrochemically reduced to hydrazol compound (E_1), a 2 electron 2 proton reaction. This develops into a very rapid chemical reaction (C) leading to the production of an electroactive substance (α-amino naphthol quinoneimine). This electroactive substance then undergoes a second 2 electron 2 proton electrochemical reaction (E_2). This E-C-E reaction is summarised in **figure 1.3.2.1**.
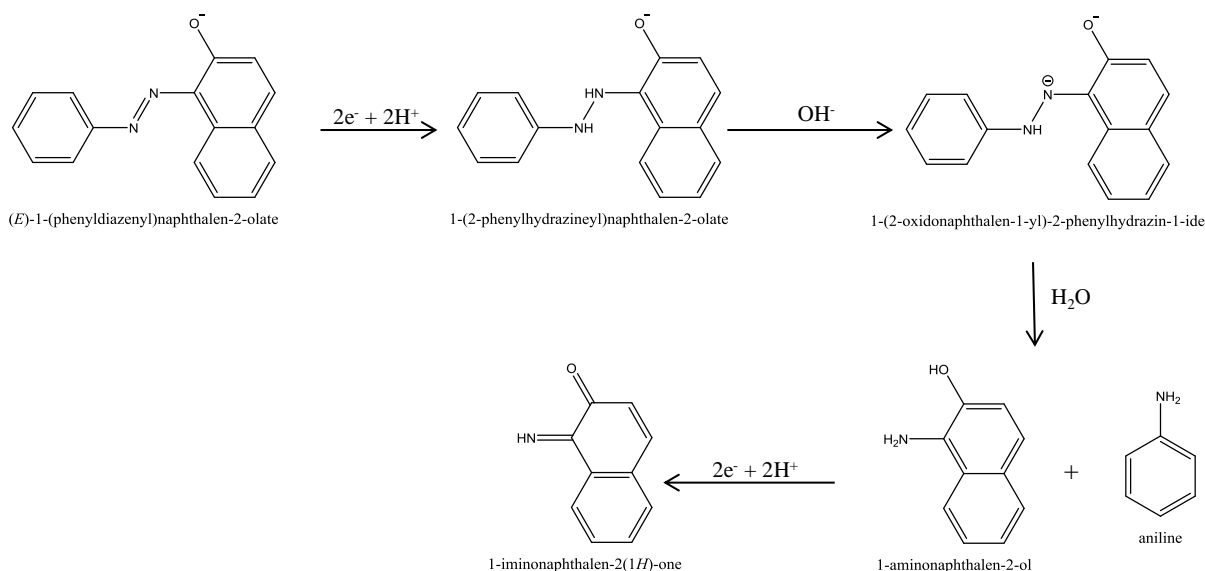
Figure 1.3.2.1 Summary of the E-C-E electrochemical reaction mechanism of Sudan 1 dye.

Other combinations of electrochemical reaction mechanism also occur, such as that of first generation glucose biosensor [54]. In this first generation glucose biosensors, glucose oxidase (FAD) is reduced by glucose in a chemical process (C_1) to form glucose oxidase ($FADH_2$) and gluconolactone. Glucose oxidase ($FADH_2$) in a second chemical reaction (C_2) reduces Oxygen (O_2) to form Glucose oxidase (FAD) and hydrogen peroxide (H_2O_2). Finally, using a platinum electrode with an applied potential of +0.6V (vs Ag/AgCl) an electrochemically (E_1) step oxidise the hydrogen peroxide to form O_2, hydrogen gas (H_2) and $2e^-$, The glucose biosensor electrochemical reaction mechanism is a chemical-chemical-electrochemical (C-C-E) mechanism. Figure 1.3.2.2 summarises the C-C-E mechanism of first generation glucose biosensor.
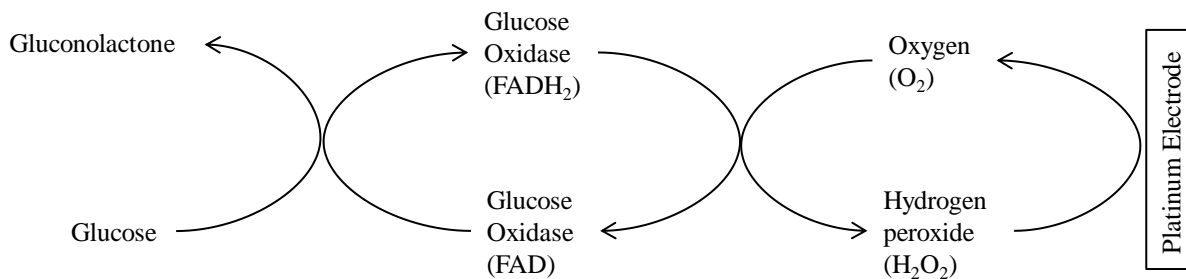
Figure 1.3.2.2 Schematic representation of the C-C-E electrochemical reaction mechanism of first generation glucose biosensor

The electrochemical reaction mechanism of an electrochemical sensor differs for each system, and understanding the electrochemical reaction mechanism allow further improvement of the system to be achieved. Taking the above example of the first generation glucose biosensors, the limiting factor of the system is the systems dependence on oxygen. Oxygen tension is 1 order of magnitude lower than physiological glucose level. Therefore, to improve the accuracy of glucose biosensors, the second generation glucose biosensors were developed, exploiting further the understanding of the C-C-E mechanism by removal of the oxygen dependent step [54]. The first mediator based glucose biosensor was produced, using a mediator to act as the electron acceptor in place of oxygen. **Figure 1.3.2.3** summarises the C-C-E mechanism of second generation glucose biosensor.
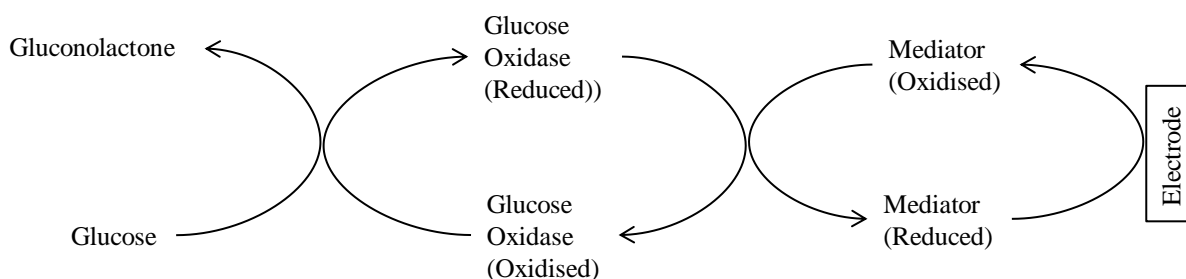
Figure 1.3.2.3 Schematic representation of the C-C-E electrochemical reaction mechanism of second generation glucose biosensor

However, in second generation glucose biosensor, oxygen still remains an influence factor which could compete with the mediator leading to low accuracy, this is especially apparent when glucose level is low. To overcome this issue, current trend in glucose biosensor development has been focused on changing the electrochemical reaction mechanism by removing the oxygen influencing step (and the mediator step) entirely, heading towards a reagentless glucose biosensor. Currently no third generation glucose biosensors have been developed [54], but research has been focused on an electrochemical reaction mechanism which is E-C based (**figure 1.3.2.4**). Several different concepts have been tested where the glucose oxidase enzyme is directly immobilised onto the electrode to act as direct transfer of electrons, missing a chemical step where the electrons are transferred either to oxygen or mediator. This third generation glucose biosensor could potentially be highly selective to glucose without interference from oxygen.

Gluconolactone

Glucose Oxidase

Electrode

Glucose

Glucose oxidase immobilised electrode
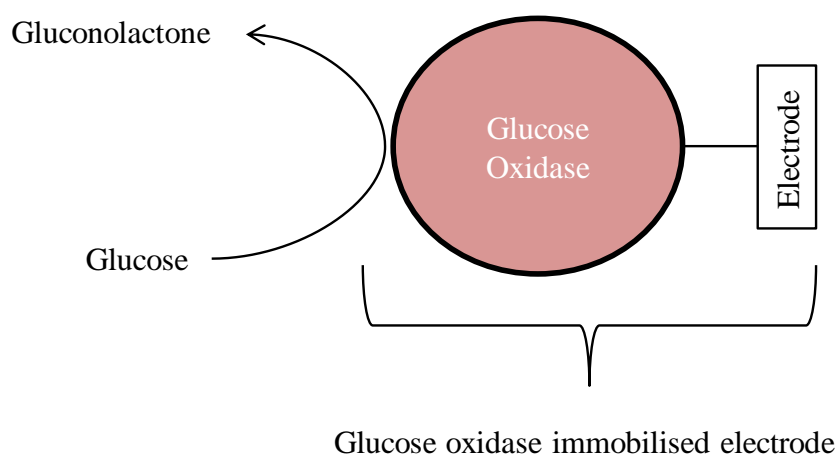
Figure 1.3.2.4 Schematic representation of the C-E electrochemical reaction mechanism of the trend in glucose biosensor development

Therefore, to develop a BOD electrochemical biosensor, it is important to understand the electrochemical reaction mechanism taking place so that improvements could be made to achieve a BOD sensor that is sensitive, selective and rapid.

1.3.3 Developing electrochemical based electrochemical oxygen sensor

There have been many attempts in development of electrochemical BOD sensors, and most of these sensors are focused on developing a system for high throughput analysis. There is the microbial fuel cell system, which uses a two compartment system separated by a proton exchange membrane (**figure 1.3.3.1**) [55]. The anode compartment (negative electrode), the anaerobic compartment, contains anaerobic microorganisms which degrade organic matter and generate electrons and protons. The protons will pass through the proton exchange membrane from the anode to the cathode compartment (positive electrode aerobic compartment), whereas electrons generated will pass from the anode to the cathode through an external electrical circuit. At the cathode end, oxygen is electrochemically reduced to water. The electrons travelling through the external circuit are measured as current, and this measurement is proportional to the biochemical oxygen demand of the system. This newly improved method greatly cuts down the analysis time from the standard 5 day BOD_5 assay, and can be conducted is as little as 30 mins. More importantly, the data obtained is in good correlation ($r^2 = 0.999$) with data obtained from the standard BOD_5 method [56].
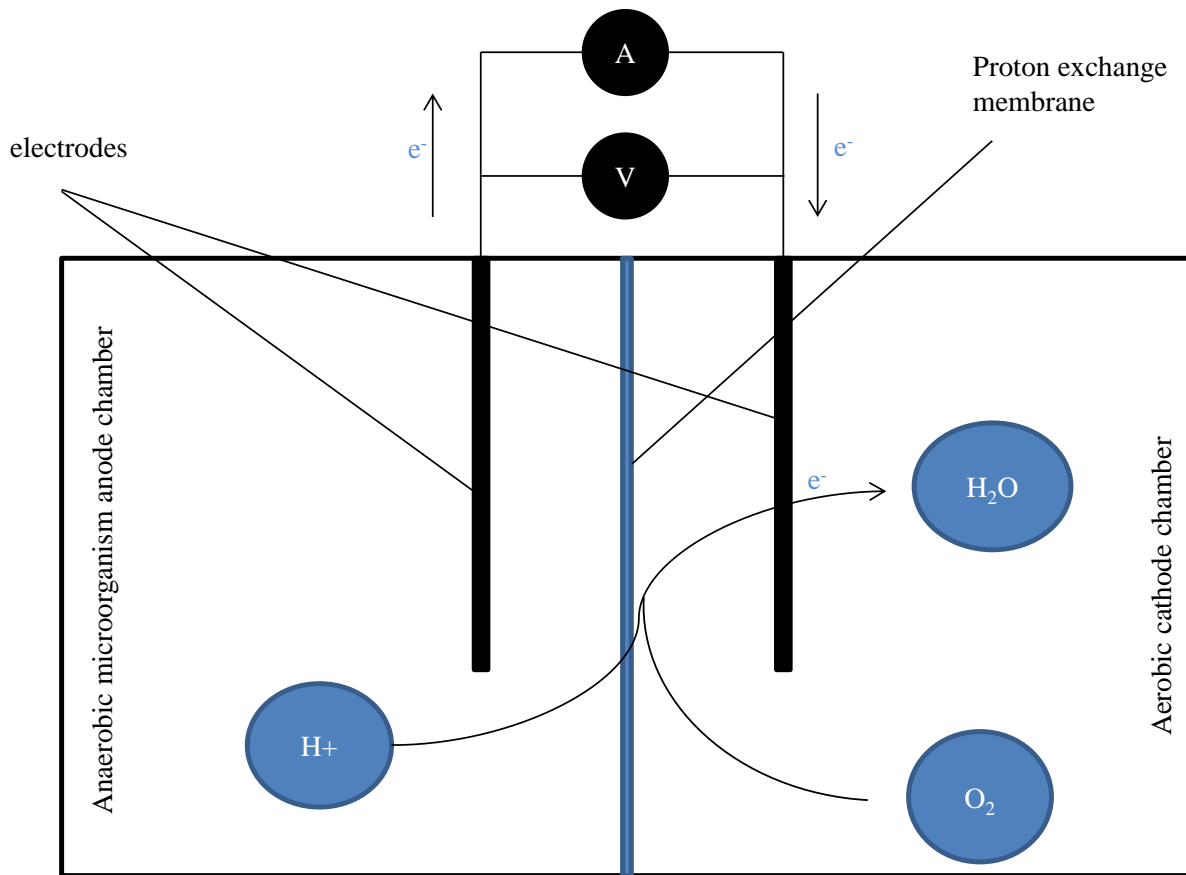
Figure 1.3.3.1 Schematic of the microbial fuel cell BOD sensor [55].

In addition to the microbial fuel cell system, electrochemical BOD systems using redox mediators were also developed. A ferricyanide mediated BOD assay was developed in the last decade [57-60]. The principal on which the assay functions, is to incubate samples in a deoxygenated environment with ferricyanide. In such an environment, instead of oxygen, cells are forced to use ferricyanide (in the oxidised form) as substitute for the terminal electron acceptor in the aerobic metabolic pathway into ferrocyanide (reduced form) [61]. Samples are then incubated for a fixed period of time, depending on the assay parameters and the cell sample type, sometimes up to 6 hours [62]. Following the incubation period the sample is analysed by either chronoamperometry [61, 62] or linear sweep voltammetry for determination of the concentration of ferrocyanide (the form having undergone reduction)

which is a direct indication of BOD as it indicates the concentration of the oxygen the cells would have consumed [62].

There are currently still some limitations with this assay system. Measurements cannot be taken as whole samples, only the supernatant is used for actual detection, therefore the assay allows an end point measurement only, with the same limitations as discussed previously for example with the BOD_5 assay. Also, it is really only suitable to the laboratory environment due to equipment requirements. The assay requires incubating cells in relatively high concentration, for example 250 mM ferricyanide from Pasco's study [61], and 55 mM ferricyanide from Morris's study [63], for prolonged incubation periods between 1 and 6 hours. Studies have shown low concentration of ferricyanide stimulates cell proliferation [64, 65], however high concentration inhibit cell proliferation [64] the result of which may affect reliability of results. This effect on cell proliferation is just one example of how the assay procedure and chemicals could affect the physiological statues of microorganisms or mammalian cells. There are potentially more physiological effects, however currently more studies in to this are required. In addition, as incubation time and the required concentration of ferricyanide varies dependent on cell types and concentration, optimisation of the assay is required before performing the assay on each different sample type.

1.3.4 Biological applications in electrochemical sensor development

The current research in electrochemical sensors, in the biological setting, have been focused on improving the compatibility of the assay with whole cell analysis [66]. Studies have been mainly focused on bacterial (prokaryotic cells) models because the redox machinery is situated on the cell membrane which is easy to access. Whereas, for eukaryotic cells, where the major redox machinery, are situated on the mitochondria membrane inside the cell.

Approaches to form interfaces to improve cell-to-electrode attachment and electron transfer vary greatly between prokaryote and eukaryote cell types. Approaches used in prokaryote cell, cell-to-electrode interfaces include: (i) altering the anode surface charge by ammonium treatment to make the anode surface positively charged. This increases compatiblity with the overall negative charge of the cell surface membrane in microbial fuel cell systems [67]. The result being increased efficiency by an order of magnitude of electron transfer, between the bacteria and the anode, aided by bacterial attachment to the anode surface. (ii) Use of electrochemical mediators for electron shuttling in microbial fuel cells [68]. (iii) Use of electroactive linkers attached directly to specific redox enzymes from the cell surface membrane of the bacteria to the electrode [69]. Eukaryote cell-to-electrode interface is more challenging because the redox mechanism is within the cell, and not located on the cell surface membrane. Therefore, cell-to-electrode interface methodologies have been focused on using electroactive linkers, such as synthetic ion channels and carbon nanotubes, that are directly inserted into the cell membrane. There are several challenges to this method, the main challenge is to insert these synthetic electroactive linkers without killing the cell [70].

1.4 Conclusion

There are many different types of approaches used for metabolic rate based assays currently available in the market place, and under development. The direct measurement of production of electrons based system, MTT, is mainly used in the biomedical research sector as viability assay [16, 18]. However, this is a time consuming and labour intensive process, which provides only ratiometric results relative to control samples which also have to be prepared. In addition, the assay requires a high number of replicates to produce reliable results due to the complicated manual protocol including sample washing for example. Each step in the

protocol has the potential to introduce errors into results. Due to these many replicates and the need for control samples each experiment requires many sample cultures adding to the labour intensiveness. Also due to it being an end point assay it is not possible to take multiple measurements from a single sample for example an hourly measurement of a drugs influence on a sample cell culture. For this type of experiment multiple samples would have to be produced for controls and replicates, plus all of these would need to be multiplied by the number of time points required to be tested. All of these factors result in this being a relatively time, labour, and cost inefficient process, and for this reason particularly in the medical sector there is high demand for a new system.

A developing alternative system to MTT that also directly measurements production of electrons, is a solution based ferricyanide-mediated electrochemical assay [61]. This has not currently been applied to the medical and medical research sectors yet. This assay offers potentially far higher accuracy comparatively to the MTT system, as it allows for the actual measurement of electron production. By measuring electrons production directly it no longer relies on a ratiometric approach as used with MTT. The protocol of the ferricyanide-mediated assay has far less manual steps involved, which could reduces the potential for errors through laboratory techniques. However, the prolong incubation of live samples with high concentration of ferricyanide causes some negative effects. Ferricyanide is known to affect cell proliferation [64, 65] which has lowered the credibility of experiments. Plus the removal of oxygen and ensuring it is sealed of the live cell samples during incubation may create a technical challenge for example in the use of 96 well plates. In the use of cytotoxicity assay, as the incubation time is required, only mid, (hours), to long, (days) term effects of drugs/toxic can be measured. The prolong incubation with mediator also makes it an end point assay, with the same disadvantages as exhibited with the MTT assay. Therefore a large

amount of live samples is required if the ferricyanide-mediated electrochemical assay is employed as cytotoxicity assay in biomedical research. To solve this problem would need the development of a non-end point assay.

Current in the market, there are some assays available based on the indirect measurement of metabolic rate, measuring BOD. Both the Clark type electrode system and the optical sensor offer a non-invasive, non-end point measurement of dissolved oxygen and have been used in medical research [71, 72]. The main advantage of these assays is that they can continuous run taking multiple readings, and record responses to stimuli over time as a result of changes to BOD. However, the reliance of the system on a semi-permeable membrane, limits detection rates to the rate of oxygen diffusion, and both systems are prone to membrane fouling. There is a delayed response to dissolved oxygen level in the sample due to the oxygen diffusion through the membrane. The systems cannot be used directly in samples containing cells unless they are adhesive cell lines, as they could clog the membrane, reducing or stopping oxygen diffusion through the membrane. The result of membrane fouling is a false reduction of dissolved oxygen concentration reading, or unknown change to diffusion rate. On top of everything the cost of the systems are also quite expensive, and involve frequency maintenance (change of membrane and cleaning) and calibrations.

The food and sewage industries require waste water processing to avoid environmental contamination, and in general this is managed using the standard BOD_5 assay. BOD_5 as discussed, involves the sealing of a sample into an airtight container with a carbon dioxide eliminating element (usually a sodium hydroxide pellet), and the measurement of pressure change within the container due to cellular oxygen consumption, thus BOD. By elimination of the carbon dioxide gas released by cellular respiration and incubation in the dark the assay is

made very specific to oxygen consumption. Whilst sample sizing is none prohibitive of the use of BOD_5 assay in this case there is a requirement for large sample volumes and long incubation periods due to low sensitivity. Long incubation periods however require the use of laboratory space as sample need to be incubated in the dark for between 5 and 7 days, thus the system has no potential for portability in the current state. Whilst specific to oxygen consumption, there are many steps for oxygen fixation and sample preparation for colorimetric measurements at the end of the incubation period, which introduces potential for error and reducing accuracy. Inaccuracy is also introduced due to the sample being sealed for a prolonged period which as oxygen is reduced due to consumption may affect cellular metabolic rate thus introducing errors to results. If not for the problems of membrane fouling the Clark type electrode and the optical sensor would be a viable option for waste water management, as it is easier to be developed into automated system.

What is really needed for all industries currently using assays to measure cellular metabolism is to produce a system that effectively combines the advantages of each of the systems discussed. A cost effective, time efficient, rapid, simple and portable system would allow much improvement to current methodologies and open up potential new avenues for use where current system restrictions prohibit the use of assays. To achieve this research should focus on an electrochemical solution. Electrochemical sensors are capable of detection down to single electron exchanged reaction, instead of detecting in a ratiometric manor. The addition of a mediator would also facilitate the electron transfer in the system to increase sensitivity. It can also lower the working potential to minimise chances of interference by electroactive components in the sample, and disturbance of the membrane potential of the living cells in the sample. Immobilisation on to a working electrode would allow for a quicker sample preparation, more biocompatible, highly sensitive and cost effective system.

Immobilisation would also allow for a non-end point assay which as discussed is a major disadvantage for example of the MTT assay. Removal of the reliance of a membrane which has been shown to introduce disadvantages as seen in the Clark type electrode and the optical sensors systems would be greatly beneficial.

1.5 PhD Aim

The aim of this project is to develop an electrochemical system with the combined properties of fast, cost effective, practical and accurate, for the measurement of cellular metabolic rate. This will be accomplished either by direct measurement of the electron production or indirect measurement of the oxygen consumption. The initial focus of the project would be the identification of the ideal electrochemical mediator. System development would include proof of concept, mediator identification, practical application exploration, and finally system optimisation through mediator immobilisation.

1.6 References

1.   Cui, L., J. Wu, and H. Ju, *Electrochemical sensing of heavy metal ions with inorganic, organic and bio-materials.* Biosensors and Bioelectronics, 2015. **63**: p. 276-286.

2.   Ikeda, T., F. Matsushita, and M. Senda, *Amperometric fructose sensor based on direct bioelectrocatalysis.* Biosensors and Bioelectronics, 1991. **6**(4): p. 299-304.

3.   Gilmartin, M.A.T. and J.P. Hart, *Rapid detection of paracetamol using a disposable, surface-modified screen-printed carbon electrode.* Analyst, 1994. **119**(11): p. 2431-2437.

4.   Cinti, S., et al., *Cholesterol biosensor based on inkjet-printed Prussian blue nanoparticle-modified screen-printed electrodes.* Sensors and Actuators B: Chemical, 2015. **221**: p. 187-190.

5.   Gilmartin, M.A.T. and J.P. Hart, *Novel, reagentless, amperometric biosensor for uric acid based on a chemically modified screen-printed carbon electrode coated with cellulose acetate and uricase.* Analyst, 1994. **119**(5): p. 833-840.

6.   Taleat, Z., A. Khoshroo, and M. Mazloum-Ardakani, *Screen-printed electrodes for biosensing: a review (2008–2013).* Microchimica Acta, 2014. **181**(9-10): p. 865-891.

7.   Xu, H., et al. *A glucose oxidase sensor based on screen-printed carbon electrodes modified by polypyrrole*. in *Engineering in Medicine and Biology Society, 2005. IEEE-EMBS 2005. 27th Annual International Conference of the*. 2006. IEEE.

8.   Wang, J. and K. Rogers, *Electrochemical sensors for environmental monitoring: a review of recent technology*. 1995: Citeseer.

9.   Yang, J., *Electrochemical sensing for food quality and safety*. 2013, THE UNIVERSITY OF WISCONSIN-MADISON.

10.   *Electrochemical Sensors and Biosensors.* International Journal of Electrochemistry, 2011. **2011**.

11.   Pitman, K., M. Raud, and T. Kikas, *Biochemical oxygen demand sensor arrays.* Agronomy Research, 2015. **13**(2): p. 382-395.

12. Beckett, B.S., *Biology: A Modern Introduction*. 1986: Oxford University Press.

13. Rich, P., *The molecular machinery of Keilin's respiratory chain.* Biochemical Society Transactions, 2003. **31**(6): p. 1095-1105.

14. Berg, J.M., J.L. Tymoczko, and L. Stryer, *Biochemistry. 5th*. 2002, New York: WH Freeman.

15. Uzman, A., *Molecular biology of the cell (4th ed.): Alberts, B., Johnson, A., Lewis, J., Raff, M., Roberts, K., and Walter, P.* Biochemistry and Molecular Biology Education, 2003. **31**(4): p. 212-214.

16. Yip, N., et al., *Disulfiram modulated ROS–MAPK and NFκB pathways and targeted breast cancer cells with cancer stem cell-like properties.* British journal of cancer, 2011. **104**(10): p. 1564-1574.

17. Molina-Molina, J.-M., et al., *In vitro study on the agonistic and antagonistic activities of bisphenol-S and other bisphenol-A congeners and derivatives via nuclear receptors.* Toxicology and applied pharmacology, 2013. **272**(1): p. 127-136.

18. Fotakis, G. and J.A. Timbrell, *In vitro cytotoxicity assays: comparison of LDH, neutral red, MTT and protein assay in hepatoma cell lines following exposure to cadmium chloride.* Toxicology letters, 2006. **160**(2): p. 171-177.

19. Berridge, M.V. and A.S. Tan, *The protein kinase C inhibitor, calphostin C, inhibits succinate-dependent mitochondrial reduction of MTT by a mechanism that does not involve protein kinase C.* Biochemical and biophysical research communications, 1992. **185**(3): p. 806-811.

20. Sittampalam, G.S., et al., *Assay Guidance Manual.* 2004.

21. Martin, D.S., *The Oxygen Consumption of Escherichia Coli during the Lag and Logarithmic Phases of Growth.* J Gen Physiol, 1932. **15**(6): p. 691-708.

22. Fisher, K.C. and F.H. Armstrong, *The oxygen consumption concerned with growth in E. coli and the effect of sulfathiazole and N-propyl carbamate on it.* Fed Proc, 1946. **5**(1): p. 27.

23. Liu, J. and B. Mattiasson, *Microbial BOD sensors for wastewater analysis.* Water Research, 2002. **36**(15): p. 3786-3802.

24.   Low, E.W. and H.A. Chase, *Reducing production of excess biomass during wastewater treatment.* Water Research, 1999. **33**(5): p. 1119-1132.

25.   Aislabie, J.M., N.K. Richards, and H.L. Boul, *Microbial degradation of DDT and its residues—A review.* New Zealand Journal of Agricultural Research, 1997. **40**(2): p. 269-282.

26.   Matsumura, F., *Biodegradation of Pesticides*. 2012: Springer US.

27.   Jouanneau, S., et al., *Methods for assessing biochemical oxygen demand (BOD): A review.* Water Research, 2014. **49**: p. 62-82.

28.   Jouanneau, S., et al., *Methods for assessing biochemical oxygen demand (BOD): a review.* Water research, 2014. **49**: p. 62-82.

29.   Clark, L.C., Jr. and C. Lyons, *Electrode systems for continuous monitoring in cardiovascular surgery.* Ann N Y Acad Sci, 1962. **102**: p. 29-45.

30.   Kahn, J.S., *Construction of a simple and sensitive clark-type electrode for measurement of oxygen concentration.* Analytical Biochemistry, 1964. **9**(3): p. 389-391.

31.   Friese, P., *A new type of Clark oxygen electrode.* Journal of Electroanalytical Chemistry and Interfacial Electrochemistry, 1980. **106**: p. 409-412.

32.   Roppola, K., et al., *Comparison study of manometric respirometric test and common chemical methods in the determination of BOD 7 in a pulp and paper mill's wastewaters.* Journal of Analytical Methods in Chemistry, 2006. **2006**.

33.   Tai, H., et al., *A Review of Measurement Methods of Dissolved Oxygen in Water*, in *Computer and Computing Technologies in Agriculture V*. 2012, Springer. p. 569-576.

34.   McDonagh, C., et al., *Phase fluorometric dissolved oxygen sensor.* Sensors and Actuators B: Chemical, 2001. **74**(1–3): p. 124-130.

35.   Quaranta, M., S.M. Borisov, and I. Klimant, *Indicators for optical oxygen sensors.* Bioanalytical Reviews, 2012. **4**(2-4): p. 115-157.

36.   Henderson, R., et al., *Fluorescence as a potential monitoring tool for recycled water systems: A review.* Water research, 2009. **43**(4): p. 863-881.

37.   Bell, S. and F. Dunand, *A Comparison of Amperometric and Optical Dissolved Oxygen Sensors in Power and Industrial Water Applications at Low Oxygen Levels (< 5 µg· kg−).* Power Plant Chemistry, 2010. **12**: p. 296-303.

38.   Lindblom, T., *Qualitative Comparision of Optical and Electrochemical Sensors for Measuring Dissolved Oxygen in Bioreactors.* 2009.

39.   Tai, H., et al., *A review of measurement methods of dissolved oxygen in water*, in *Computer and Computing Technologies in Agriculture V*. 2011, Springer. p. 569-576.

40.   Wise, R.R. and A.W. Naylor, *Calibration and use of a Clark-type oxygen electrode from 5 to 45 C.* Analytical biochemistry, 1985. **146**(1): p. 260-264.

41.   Louie, R.F., et al., *Point-of-Care Glucose Testing.* Archives of Pathology & Laboratory Medicine, 2000. **124**(2): p. 257-266.

42.   Lesmana, T., et al. *Dual glucose/cholesterol meter applications based on FPGA platform*. in *Next-Generation Electronics (ISNE), 2013 IEEE International Symposium on*. 2013.

43.   Leech, D. and K. Feerick, *Biosensor warning devices: reagentless detection of modulators of Laccase activity.* Electroanalysis, 2000. **12**(16): p. 1339-1342.

44.   Chaubey, A. and B.D. Malhotra, *Mediated biosensors.* Biosensors and Bioelectronics, 2002. **17**(6–7): p. 441-456.

45.   Fultz, M.L. and R.A. Durst, *Mediator compounds for the electrochemical study of biological redox systems: a compilation.* Analytica Chimica Acta, 1982. **140**(1): p. 1-18.

46.   delle Noci, S., et al., *Electrochemical Kinetic Characterization of Redox Mediated Glucose Oxidase Reactions: A Simplified Approach.* Electroanalysis, 2008. **20**(2): p. 163-169.

47.   Haberl, S., et al., *Cell membrane electroporation-Part 2: the applications.* Electrical Insulation Magazine, IEEE, 2013. **29**(1): p. 29-37.

48.   Feldberg, S.W. and L. Jeftic, *Nuances of the ECE mechanism. IV. Theory of cyclic voltammetry and chronoamperometry and the electrochemical reduction of hexacyanochromate(III).* The Journal of Physical Chemistry, 1972. **76**(17): p. 2439-2446.

49.   Nematollahi, D. and Z. Forooghi, *ECEC and ECE-Type Mechanisms in Electrochemical Oxidation of 4-Substituted Catechols in the Presence of 4-Hydroxy-6-methyl-2-pyrone.* Electroanalysis, 2003. **15**(20): p. 1639-1644.

50.   Compton, R.G. and C.E. Banks, *Understanding Voltammetry*. 2007: World Scientific.

51.   Svir, I., et al., *Theoretical and experimental study of the ECE mechanism at microring electrodes.* Journal of Electroanalytical Chemistry, 2005. **578**(2): p. 289-299.

52.   Yip, N.C., et al., *Real-time electrocatalytic sensing of cellular respiration.* Biosens Bioelectron, 2014. **57**: p. 303-9.

53.   Yang, D., L. Zhu, and X. Jiang, *Electrochemical reaction mechanism and determination of Sudan I at a multi wall carbon nanotubes modified glassy carbon electrode.* Journal of Electroanalytical Chemistry, 2010. **640**(1): p. 17-22.

54.   Wang, J., *Electrochemical glucose biosensors.* Chemical reviews, 2008. **108**(2): p. 814-825.

55.   Grzebyk, M. and G. Poźniak, *Microbial fuel cells (MFCs) with interpolymer cation exchange membranes.* Separation and Purification Technology, 2005. **41**(3): p. 321-328.

56.   Kim, B.H., et al., *Novel BOD (biological oxygen demand) sensor using mediator-less microbial fuel cell.* Biotechnology letters, 2003. **25**(7): p. 541-545.

57.   Jordan, M.A., et al., *A sensitive ferricyanide-mediated biochemical oxygen demand assay for analysis of wastewater treatment plant influents and treated effluents.* Water Research, 2013. **47**(2): p. 841-849.

58.   Jordan, M.A., et al., *A ferricyanide-mediated activated sludge bioassay for fast determination of the biochemical oxygen demand of wastewaters.* Water Research, 2010. **44**(20): p. 5981-5988.

59.   Catterall, K., et al., *The use of microorganisms with broad range substrate utilisation for the ferricyanide-mediated rapid determination of biochemical oxygen demand.* Talanta, 2001. **55**(6): p. 1187-1194.

60. Catterall, K., et al., *Development of a rapid ferricyanide-mediated assay for biochemical oxygen demand using a mixed microbial consortium.* Analytical chemistry, 2003. **75**(11): p. 2584-2590.

61. Pasco, N., et al., *MICREDOX®—development of a ferricyanide-mediated rapid biochemical oxygen demand method using an immobilised Proteus vulgaris biocomponent.* Biosensors and Bioelectronics, 2004. **20**(3): p. 524-532.

62. Jordan, M.A., D.T. Welsh, and P.R. Teasdale, *Ubiquity of activated sludge ferricyanide-mediated BOD methods: A comparison of sludge seeds across wastewater treatment plants.* Talanta, 2014. **125**: p. 293-300.

63. Morris, K., et al., *Ferricyanide mediated biochemical oxygen demand – development of a rapid biochemical oxygen demand assay.* Analytica Chimica Acta, 2001. **442**(1): p. 129-139.

64. Sun, I.L., et al., *Transmembrane redox in control of cell growth Stimulation of HeLa cell growth by ferricyanide and insulin.* Experimental Cell Research, 1985. **156**(2): p. 528-536.

65. Alcaín, F.J., et al., *Ascorbate Free Radical Stimulates the Growth of a Human Promyelocytic Leukemia Cell Line.* Cancer Research, 1990. **50**(18): p. 5887-5891.

66. Du, J., C. Catania, and G.C. Bazan, *Modification of Abiotic–Biotic Interfaces with Small Molecules and Nanomaterials for Improved Bioelectronics.* Chemistry of Materials, 2014. **26**(1): p. 686-697.

67. Cheng, S. and B.E. Logan, *Ammonia treatment of carbon cloth anodes to enhance power generation of microbial fuel cells.* Electrochemistry Communications, 2007. **9**(3): p. 492-496.

68. Kim, N., et al., *Effect of initial carbon sources on the performance of microbial fuel cells containing Proteus vulgaris.* Biotechnol Bioeng, 2000. **70**(1): p. 109-14.

69. Amir, L., et al., *Surface display of a redox enzyme and its site-specific wiring to gold electrodes.* J Am Chem Soc, 2013. **135**(1): p. 70-3.

70. Ajo-Franklin, C.M. and A. Noy, *Crossing Over: Nanostructures that Move Electrons and Ions across Cellular Membranes.* Advanced Materials, 2015. **27**(38): p. 5797-5804.

71.   Sin, A., et al., *The Design and Fabrication of Three-Chamber Microscale Cell Culture Analog Devices with Integrated Dissolved Oxygen Sensors.* Biotechnology Progress, 2004. **20**(1): p. 338-345.

72.   Wagner, B.A., S. Venkataraman, and G.R. Buettner, *The Rate of Oxygen Utilization by Cells.* Free radical biology & medicine, 2011. **51**(3): p. 700-712.

Chapter 2

Techniques

2.1 Electrochemical techniques

The basic principal of electrochemical analytics relevant to this project, involves the application of a known potential (E), and measurement of the resultant current. The current is influenced by electrochemical reactive species in a conductive medium completing a circuit.

2.1.1 Electroanalytical Techniques

A typical electroanalytical setup consists of a three-electrode cell, and the applied voltage is controlled by a potentiostat, a simplified diagram can be seen in **figure 2.1.1** [1]. A potential is applied at the working electrode to enable electrochemical reactions of interest to occur. The reference electrode monitors the potential delivered to the working electrode, which then feeds back this information to the potentiostat [2]. The potentiostat measures any difference (iR) in the potential that is delivered to the working electrode and makes adjustments to the output until the desired potential is fed to the working electrode, this mechanism is termed feedback [3]. The two common reference electrodes used for electroanalytical studies described in this thesis include saturated calomel (SCE) and silver-silver chloride (Ag/AgCl) electrodes [4].
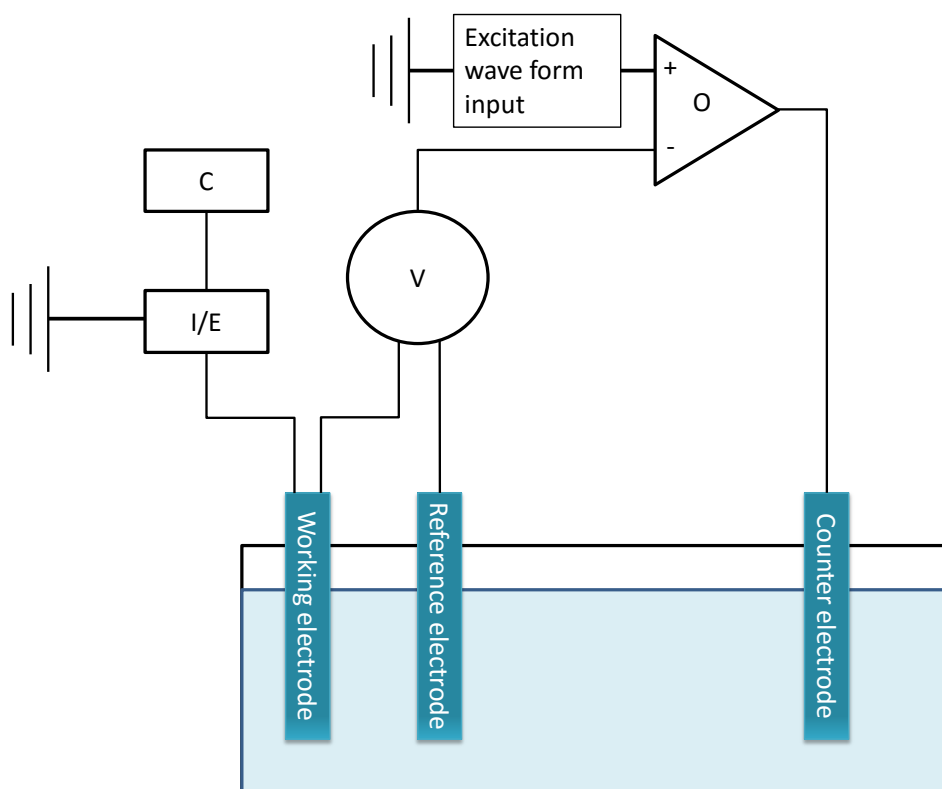
Figure 2.1.1 A simplified diagram of a 3 electrode potentiostat system. (O) is the operational amplifier, (V) is the electrometer, (I/E) is the current to voltage convertor and (C) is the data acquisition system [1].

In a SCE, there are 2 fritted compartments (**figure 2.1.2**). The inner fritted compartment contains mercury which is in contact with a pool or a paste of calomel (Hg_2Cl_2) and potassium chloride (KCl) mixture. Usually a platinum wire is embedded into the mercury to complete the external circuit. A fritted junction is located at the end of the inner compartment to allow contact of saturated KCl in the outer compartment to complete the circuit. The redox reaction of the electrode is show in **equation 2.1[2]**.

$$Hg_2Cl_2 + e^- \leftrightarrow 2Hg + 2Cl^- \qquad \textbf{(Equation 2.1)}$$
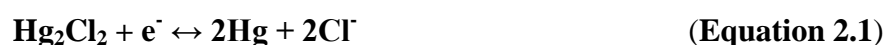
This reaction has a potential of 0.241 V compared to a standard hydrogen electrode which is 0 V.
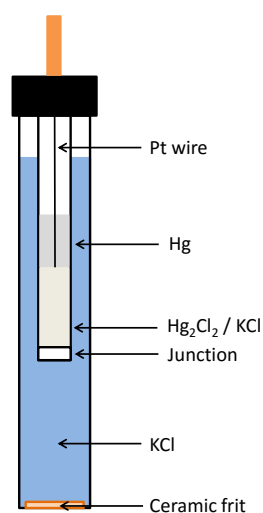
Figure 2.1.2 A diagram of a saturated calomel electrode.

In a Ag/AgCl electrode, a silver rod is coated with silver chloride and soaked in saturated KCl solution (**figure 2.1.3**). The half cell redox reaction is shown in **equation 2.2[2]**.

$$\textbf{AgCl(s) + e}^- \leftrightarrow \textbf{Ag(s) + Cl}^- \qquad\qquad (\textbf{Equation 2.2})$$

The reaction has a known 0.222 V potential compared to a standard hydrogen electrode.
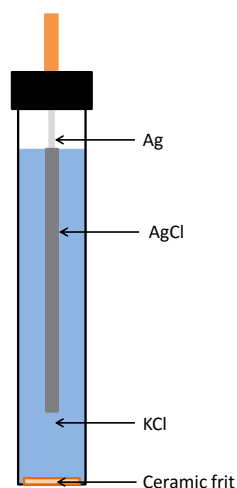
Figure 2.1.3 A diagram of a silver-silver chloride elecrode.

2.1.2 Linear sweep voltammetry using microelectrode

Linear sweep voltammetry (LSV) is conducted similarly to cyclic voltammetry (CV) (**section 2.1.3**), with two major differences; (1) the potential is applied in one direction only, over time (**figure 2.1.2.1**) and (2) linear sweep voltammetry can be conducted using microelectrodes or macroelectrodes, the former was used in this project. Initially the potential is set at a level where the targeted electrochemical species cannot be oxidised or reduced (**figure 2.1.2.2,** 0 to 0.2 V). A scan rate is then set where the potential is increased or decreased over time, measured in volts per second (Vs^{-1}). As the sweep is performed it will reach a point where a faradaic current (**figure 2.1.2.2,** 0.2 to 0.5 V) is generated as a result of an electrochemical reduction or oxidation reaction of the targeted electrochemical species taking place at the electrode surface.

Microelectrodes are defined as electrodes with critical dimensions in the micrometer/nanometer range (falling in the range of 0.1 to 50µm), and is comparable to or

smaller than the diffusion layer thickness [5]. A smaller diffusion layer thickness ensures a higher mass transport diffusion rate, see **figure 2.1.2.3**. The diffusion layer around the macroelectrode is planar and the microelectrode is hemispherical. As a result, there is an increase in concentration gradient around the microelectrode, and therefore the diffusion layer is confined around the microelectrode. Whereas, the concentration gradient around the macroelectrode is spread throughout the plane, leading to an extension of the diffusion layer to the surrounding bulk solution to achieve a similar concentration gradient needed for mass transport [5]. When a microelectrode is used for LSV, due to the increased diffusion gradient generated in the proximity of the electrode surface, mass transport rates are sufficient to keep up with the rate of the redox reaction taking place. This is an important property of microelectrodes used in linear sweep voltammetry, whereby removing the diffusion limitation from the electrochemical system, the peak current reaches a steady state [6]. This steady state voltammetry method is convenient for determining the amounts of oxidised and reduced forms of the electroactive species within the solution [7]. The difference between the anodic and cathodic steady state current plateau shows a proportional representation of the total amount of mediator in the system, by measuring the difference of each relative to 0 current you can determine the proportion of the mediator that is in the oxidised and reduced form (**figure 2.1.2.4**).
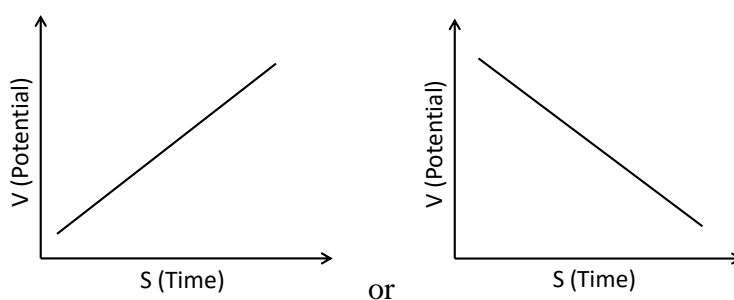
Figure 2.1.2.1 Typical representation of an linear sweep voltammetry excitation waveforms.
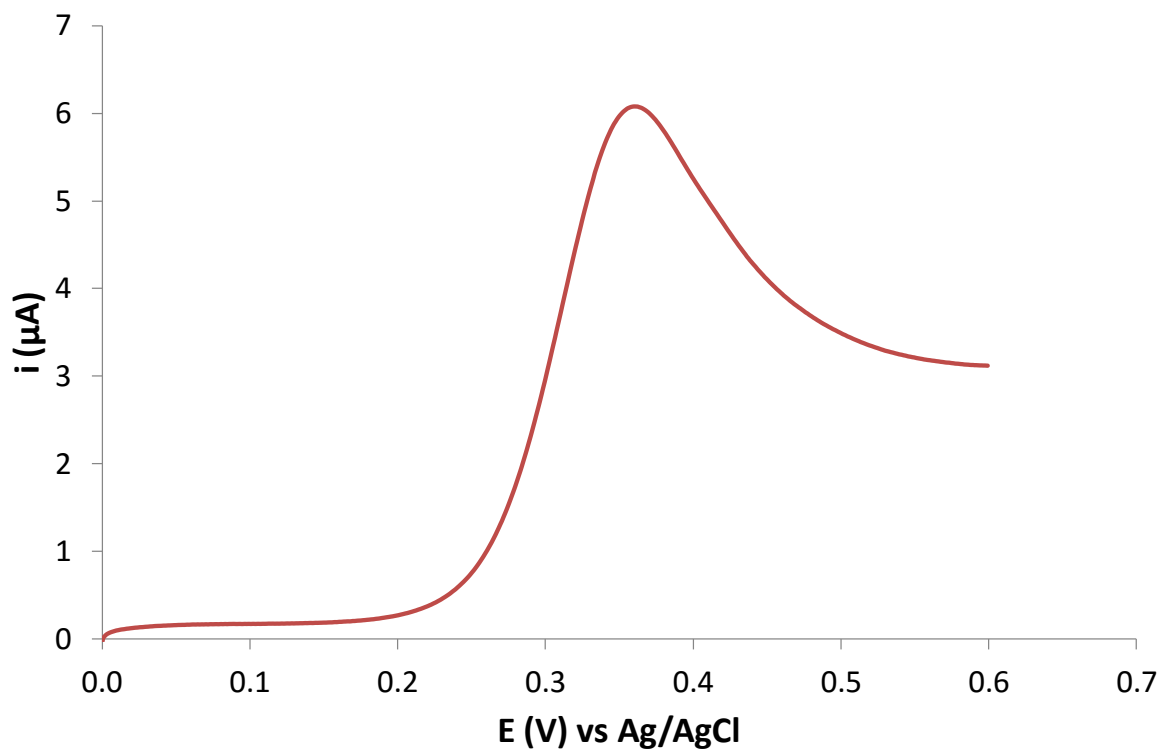
Figure 2.1.2.2 Typical linear sweep voltammetry data with a macroelectrode.
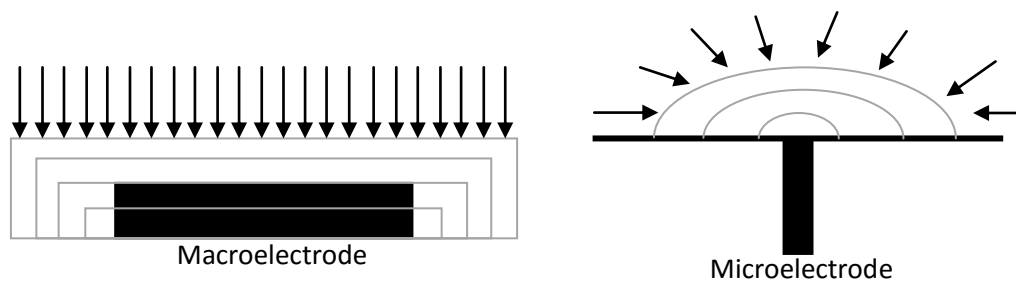
Macroelectrode

Microelectrode

Figure 2.1.2.3: The diffusion layer around the macroelectrode is planar and the microelectrode is hemispherical. The population of electroactive species affecting the microelectrode exceeds the macroelectrode.
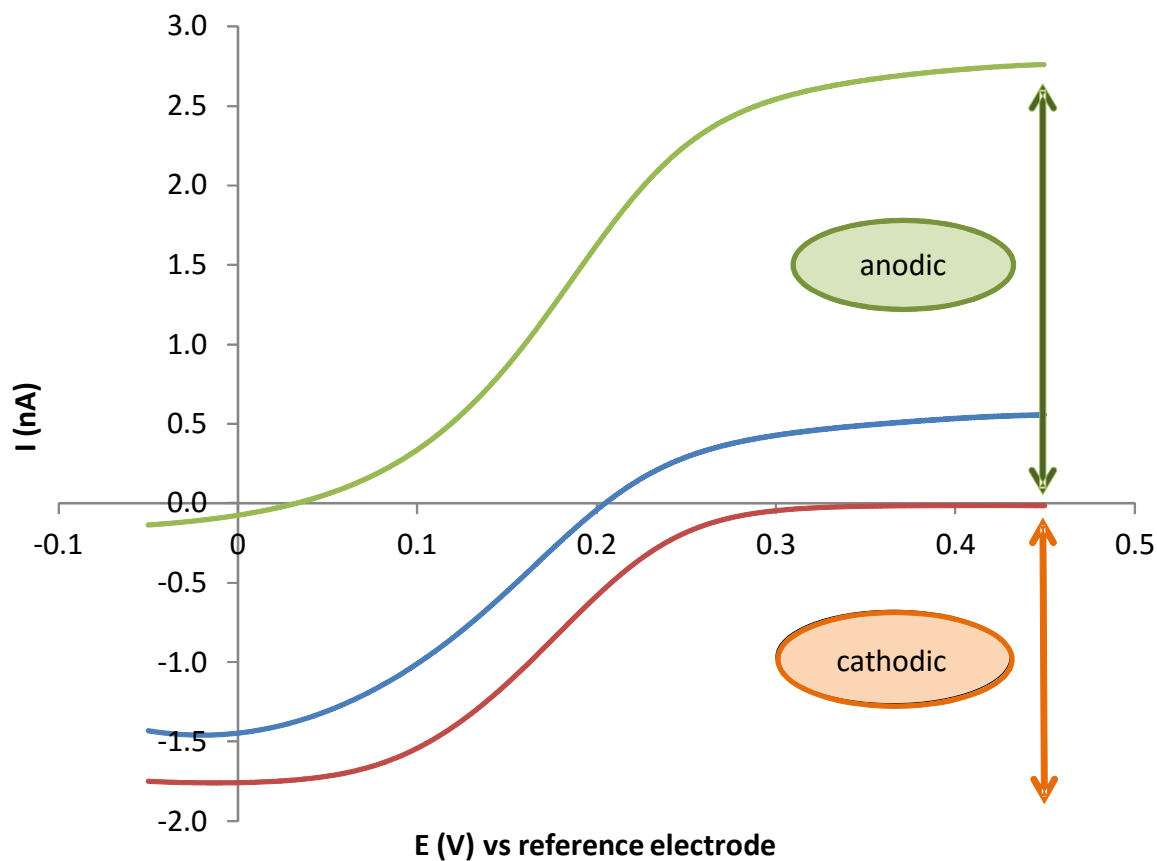
Figure 2.1.2.4: A typical experimental response for linear sweep voltammetry showing 3 different results.

2.1.3 Cyclic Voltammetry using macroelectrode

Cyclic Voltammetry (CV) consists of a cycling potential in a forward direction until reaching a switching potential, at which point, the potential is reversed. This is carried out at a set scan rate (**section 2.1.2**) and is summarised in **figure 2.1.3.1** [8].
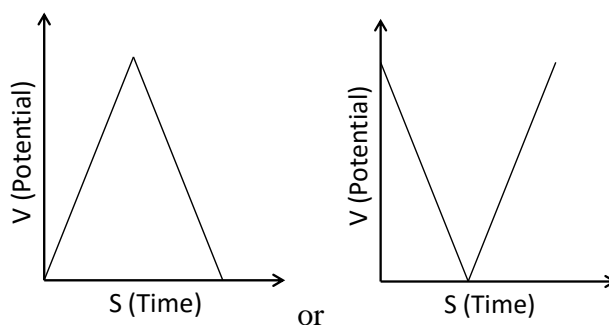
Figure 2.1.3.1: A typical representation of an excitation waveform

The data is acquired and plotted as the resulting current versus the potential, as summarised in **figure 2.1.3.2**. The reaction is determined as reversible when the ΔE_p is close to or less than 0.059V/n at 25 °C [9], and any deviation greater than 0.059V/n would indicate a loss of reversibility in the reaction. This value is obtained from **equation 2.1**, where n is the number of electrons in the redox reaction [10]. Reversibility is also demonstrated when the anodic and cathodic currents are the same, see **equation 2.2**. In addition, a redox couple is reversible when the formal reduction potential (E^0) lies midway between E_{pa} and E_{pc} (**equation 2.3**) [10]. At the formal reduction potential, the mediator should be half in oxidised form and half in reduced form on the working electrode surface.
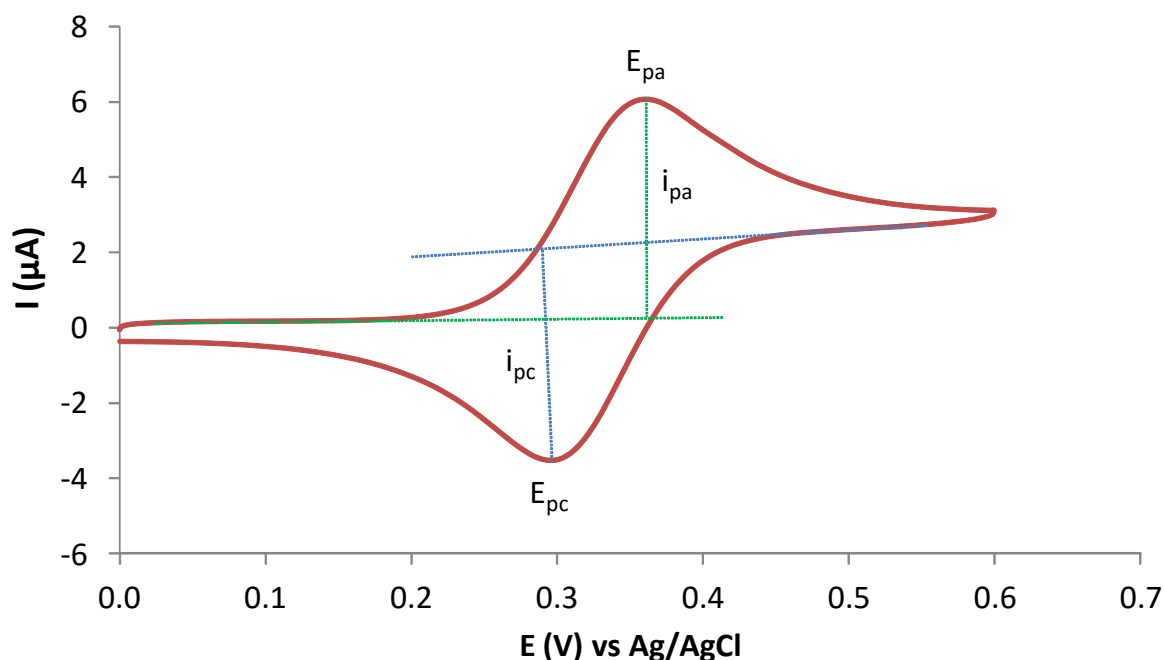
Figure 2.1.3.2: A typical experimental response for cyclic voltammetry.

$$\Delta Ep = Epa - Epc = 0.059V/n \qquad \textbf{(Equation 2.1)}$$

$$I_{pa}/i_{pc} = 1 \qquad \textbf{(Equation 2.2)}$$

$$E^0 = (Epa + Epc)/2 \qquad \textbf{(Equation 2.3)}$$

There are two factors, faradic current and capacitance, which contribute to the observed current in a cyclic voltammagram. Peak current is proportional to the concentration of the analyte being studied. The faradic current is the current generated through a chemical redox reaction. The capacitance current is a result of the charging of the 'double layer' (**figure 2.1.3.3**) in which the inner layer, known as the inner Helmholtz plane (IHP) runs parallel to the working electrode. The IHP is composed of a monolayer of orientated solvent molecules, and absorbed neutral and unsolvated ions. The outer layer, known as the outer Helmholtz

43

plane (OHP), is physically separated by the barrier formed by the IHP. The OHP is made up of solvated ions. The region beyond this 'double layer' is known as the 'diffusion layer', and the solvated ions in this region are arranged accordingly to the electrostatic interactions between them. Solvated ions that are further away from the electrode surface have greater entropy, forming the bulk solution, which is no longer affected by the electrode [11].
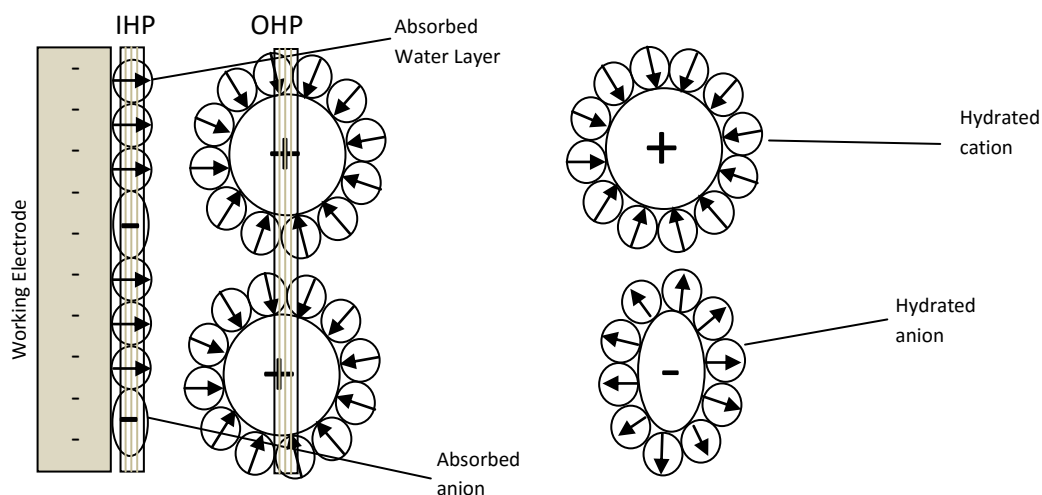
Figure 2.1.3.3: Model of double layer

The peak currents for a reversible system is calculated using the Randles-Sevick equation, where the i_p is the peak current (A), n is the number of electrons, A is the surface area of the electrode (cm^2), D is the diffusion coefficient ($cm^2 s^{-1}$), C^0 is the concentration of the ions of interest in the bulk solution (mol cm^{-3}) and v is the scan rate (Vs^{-1}), see **equation 2.4** [9].

$$i_p = (2.69 \times 10^5) n^{3/2} A D^{1/2} C^0 v^{1/2}$$ (**Equation 2.4**)

The peak current for an irreversible system could also be calculated using **equation 2.5** [12], where α is the transfer coefficient and n_a is the number of electrons in the rate limiting step are introduced into **equation 2.4**.

$$ip = (2.69 \times 10^5) n (\alpha n_a)^{1/2} A D^{1/2} C^0 v^{1/2} \quad\quad\quad \textbf{(equation 2.5)}$$

2.1.4 Amperometry in stirring solution

Amperometry is a technique that applies a fixed potential that will generate an oxidation or reduction faradaic current from the electroactive compound of interest in a solution whilst stirring at a fixed rate (**figure 2.1.4.1 i**). By stirring, the rate of mass transport is increased sufficiently to keep up with the rate of electron transfer, and so a steady state current can be maintained (**figure 2.1.4.1 ii**). As the solution is stirring, there is a constant feed of fresh analyte to the electrodes therefore the limit of the current becomes the concentration of the analyte. As the concentration of analyte is increased the current generated is increased. In this project, amperometry was used as a technique to synthesise a reagent for another experiment rather than an analytical technique.
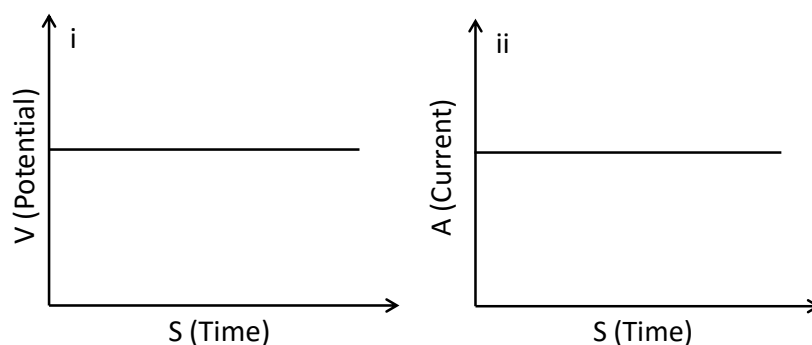
Figure 2.1.4.1 (i) A typical representation of an excitation waveform. **(ii)** A typical experimental response for amperometry.

2.2 Screen printing

The basic principle of screen printing for electrochemistry purposes is to push a conductive ink (for example carbon, graphite or silver) through a mesh that has been layered with a pattern of illustration[13-15]. **Figure 2.2.1 (i)** is a plan view diagrammatic example of screen printing although there are techniques which would flood the whole surface of the mesh with ink also. As the squeegee moves in the direction show it pushes the ink and the mesh into contact with the substrate surface where the exposed sections of the pattern allow for the ink to be forced through (**figure 2.2.1(ii)**). Where the ink is forced through the mesh the ink adheres to the substrate surface resulting in the printed pattern on the substrate (**figure 2.2.1(iii)**). Conductive ink is often mixed with mediators and/or enzymes for printing the working electrodes depending on the function of the system [16, 17].
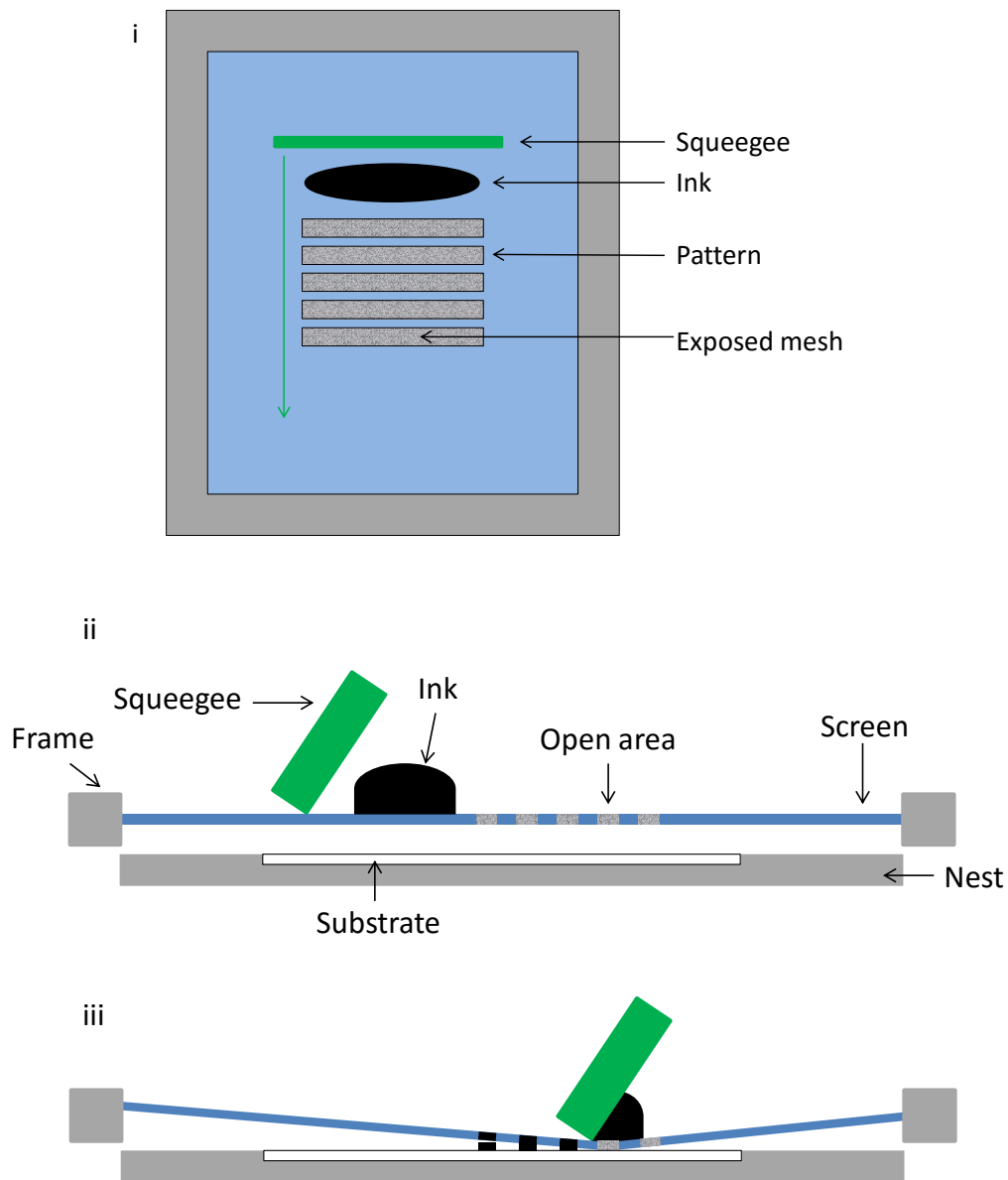
Figure 2.2.1 (i) An example of the plan view of the screen. **(ii)** The side view of the screen in **(i)**. **(iii)** Graphic explanation of how the ink is pushed through the screen by the squeegee **[13-15]**.

2.3 Optical density

A UV/visible spectrophotometer was used to determine cell culture density for this project by measuring the optical density (OD) of the samples. The concept of the spectrophotometer is

drawn in **figure 2.3.1**[18]. A light source, e.g. UV lamp shines light through the light dispersion device where the wavelengths of light are dispersed. The light is then passed through a slit which allows the device to control the wavelength of light that is transmitted to the sample cuvette. Light passes through the sample and is detected after transmission through the sample. The decrease in light density detected after transmission through the sample gives a reading of light absorption. When used for measuring cell density, the machine is zeroed by using a cuvette containing only the culture medium but no cells. As cell number increases in the sample cuvette the medium become cloudier, therefore allowing less light through and subsequently less light is detected after transmission through sample cuvette. The reading is often referred to as absorbance, however cells are mostly transparent, therefore it is more accurately described that the turbidity of the sample solution is measured. A 1 OD sample was taken and the actual cell number was counted using a hemocytometer. From the actual cell number calculation it can be determined the cell count in each sample according to the OD reading.
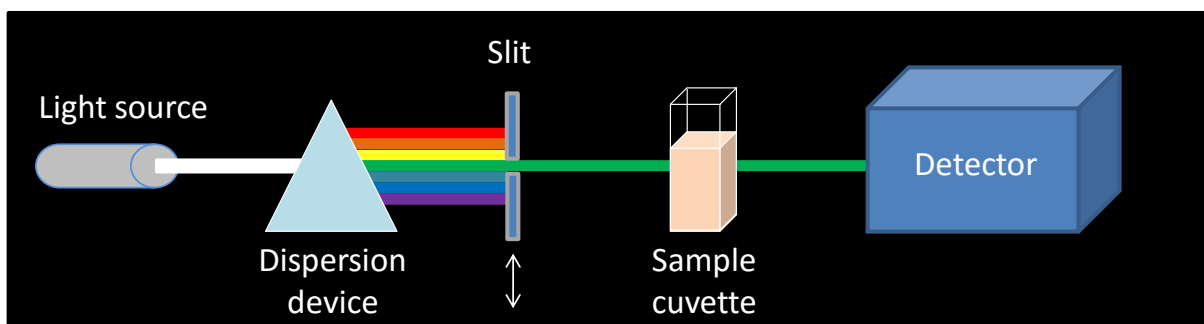
Figure 2.3.1 A simplified diagrammatic explanation of how a UV/visible spectrophotometer works [18].

2.4 Liquid Chromatography Electrospray Ionisation Mass Spectrometry

Liquid Chromatography Electrospray Ionisation Mass Spectrometry (LC-ESI-MS) was conducted using an Alliance e2695 (Waters Limited) liquid chromatography (LC) instrument directly coupled to a Xevo-G2-XS-ToF (Waters Limited) mass spectrometer (MS). The LC instrument is used in the injection of samples that are not volatile enough for gas chromatography (GC) coupling [19]. In addition, the LC serves as a pump for delivering a solvent for the delivery of the injected sample for electrospray ionisation (ESI).

ESI technique uses electrical energy to assist in the ionisation of the sample injected in the solvent [20]. The injected sample and delivered solvent is forced through a fine metal capillary that is at a high potential relative to the wall of the unit. The solution exiting the capillary tube tip is sprayed out, with the assistance of dry nitrogen gas used as a nebuliser gas, as extremely small charged droplets. The droplets are charged at the same polarity as the voltage applied to the capillary, in this experiment, a positive voltage is applied to the ESI capillary. With the aid of a secondary source of heated dry nitrogen gas (desolvation gas), the droplets of solvent exiting the capillary tube tip vaporises and becomes smaller in radius and the surface charge density increases. As the surface charged density of the droplet increases from solvent vaporisation, the charged droplet will reach a critical point where the sample ions at the droplet surface are ejected into a gas phase, which is then sampled by the sampling cone down a time-of-flight (ToF) analyser. The sample ions formed during ESI could exist in several forms. Sample ions could exist as the molecular charged ion $[M]^+$, hydrogen adduct $[M+H]^+$, solvent adducts $[M+S]^+$, salt adducts $[M+salt]^+$ and/or combination of adduct formation $[M+S+salt]^+$ [21]. The events taking place by ESI technique is diagrammatically depicted in **figure 2.4.1.**
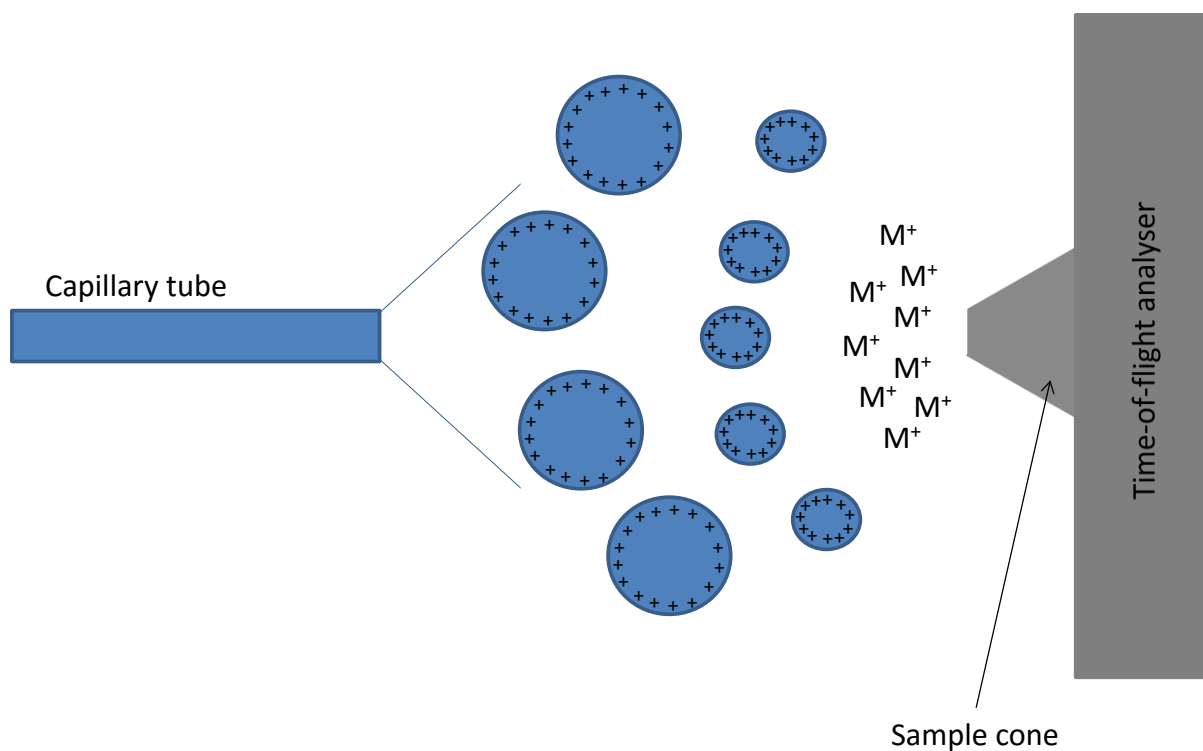
Figure 2.4.1 Ionisation of samples by electrospray ionisation. M$^+$ are the sample ions ejected from the charged droplets.

The charged ions enter the time-of-flight (ToF) mass analyser through the sampling cone. The ToF region of the mass spectrometer is under vacuum, as the ions enter the ToF, it enters through a series of ion optics. The ion optics are responsible for applying a fixed energy which accelerates the ions at the same energy down a flight tube in a straight line. The ions then travel through the flight tube and reach the detector in the order of increasing mass [22, 23], see **figure 2.4.2** for a diagrammatic representation of the events in a ToF analyser. The data is then recorded by a computer and displayed as mass (m) to charge (z) ratio (m/z).
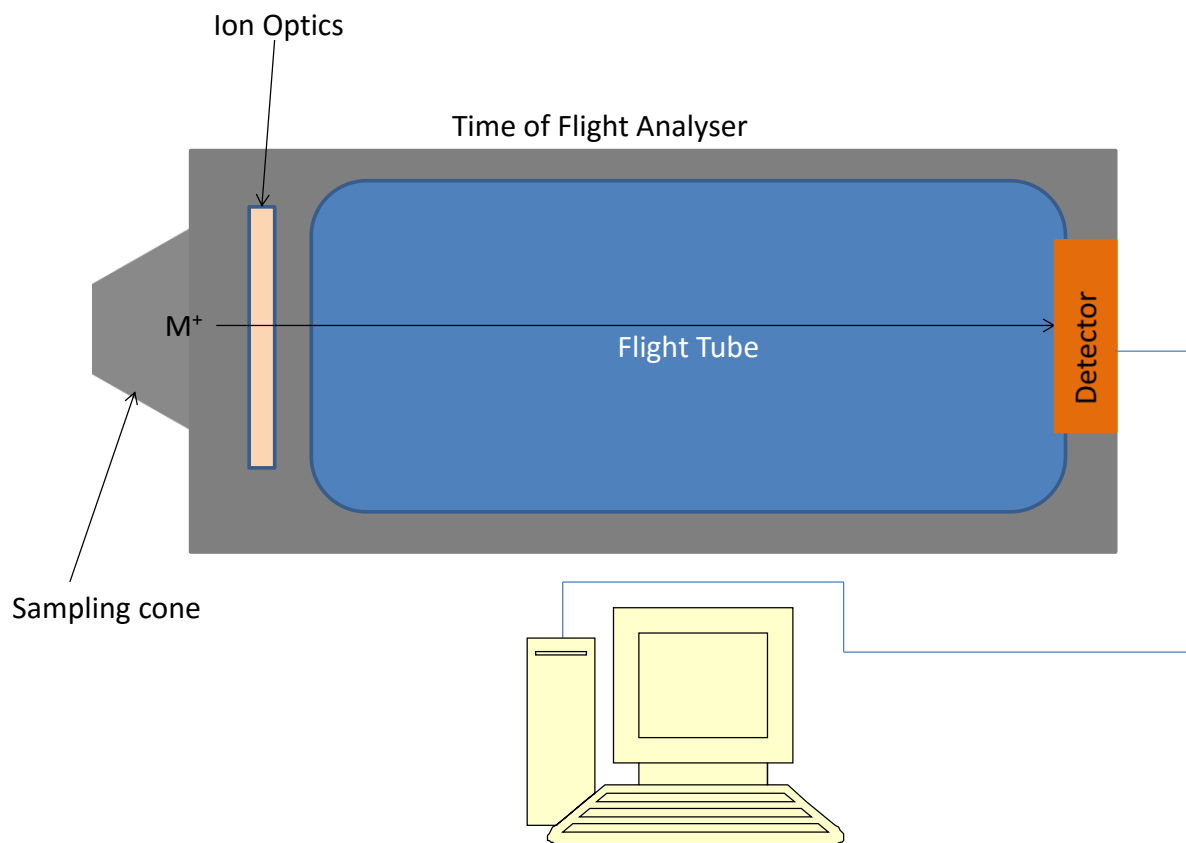
Figure 2.4.2 Diagrammatic representation of events taking place inside a Time of Flight Analyser.

2.5 References

1. *Electrode Kinetics*, in *Understanding Voltammetry*. 2011, IMPERIAL COLLEGE PRESS. p. 35-76.

2. Ives, D.J.G. and G.J. Janz, *Reference electrodes, theory and practice*. 1961, New York: Academic Press.

3. Gilmartin, M.A.T., Hart J.P., Patton, D.T., *Prototype, solid-phase, glucose biosensor.* Analyst, 1995. **120**: p. 1973-1981.

4. Kissinger, P.T.a.H., W.R., *Laboratory Techniques in Electroanalytical Chemistry.* Marcel Dekker, 1984. **Chapter 3**(New York).

5. Xie, X., D. Stueben, and Z. Berner, *The Application of Microelectrodes for the Measurements of Trace Metals in Water.* Analytical Letters, 2005. **38**(14): p. 2281-2300.

6. Davies, T.J. and R.G. Compton, *The cyclic and linear sweep voltammetry of regular and random arrays of microdisc electrodes: Theory.* Journal of Electroanalytical Chemistry, 2005. **585**(1): p. 63-82.

7. Morris, K., et al., *Ferricyanide mediated biochemical oxygen demand – development of a rapid biochemical oxygen demand assay.* Analytica Chimica Acta, 2001. **442**(1): p. 129-139.

8. Kissinger, P.T.a.H., W.R., *Cyclic Voltammetry.* Journal of Chemical Education, 1983. **60**(9): p. 702-706.

9. Mabbott, G.A., *An introduction to cyclic voltammetry.* Journal of Chemical Education, 1983. **60**(9): p. 697.

10. Wring, S.A. and J.P. Hart, *Chemically modified, carbon-based electrodes and their application as electrochemical sensors for the analysis of biologically important compounds. A review.* Analyst, 1992. **117**(8): p. 1215-1229.

11. Fry, A.J., *Synthetic organic electrochemistry.* Second Edition John Wiley & Sons, 1989. **Chapter 1**: p. 38-42.

12. Dryhurst, G., et al., *Laboratory techniques in electroanalytical chemistry.* Marcel Dekker, New York, 1984.

13. Hyun, W.J., et al., *High-Resolution Patterning of Graphene by Screen Printing with a Silicon Stencil for Highly Flexible Printed Electronics.* Advanced Materials, 2015. **27**(1): p. 109-115.

14. Khaleel, H.R., A.I. Abbosh, and H.M. Al-Rizzo, *Design, fabrication, and testing of flexible antennas*. 2013: INTECH Open Access Publisher.

15. Aleeva, Y. and B. Pignataro, *Recent advances in upscalable wet methods and ink formulations for printed electronics.* Journal of Materials Chemistry C, 2014. **2**(32): p. 6436-6453.

16. Smolander, M., et al., *Development of a printable laccase-based biocathode for fuel cell applications.* Enzyme and Microbial Technology, 2008. **43**(2): p. 93-102.

17. Albareda-Sirvent, M., A. Merkoçi, and S. Alegret, *Configurations used in the design of screen-printed enzymatic biosensors. A review.* Sensors and Actuators B: Chemical, 2000. **69**(1–2): p. 153-163.

18. Widdel, F., *Theory and measurement of bacterial growth.*

19. Niessen, W.M.A., *Liquid Chromatography: Mass Spectrometry, Second Edition*. 1998: Taylor & Francis.

20. Ho, C.S., et al., *Electrospray Ionisation Mass Spectrometry: Principles and Clinical Applications.* The Clinical Biochemist Reviews, 2003. **24**(1): p. 3-12.

21. Kebarle, P. and U.H. Verkerk, *Electrospray: From ions in solution to ions in the gas phase, what we know now.* Mass Spectrometry Reviews, 2009. **28**(6): p. 898-917.

22. Hvistendahl, G., *E. Constantin and A. Schnell. Mass spectrometry. Ellis Horwood Series in Analytical Chemistry, Ellis Horwood Limited, London. 1990. 184 pp. £48.50 (hardcover, ISBN 0-13-555525-6) and £16.95 (paperback, ISBN 0-13-553363-5).* Organic Mass Spectrometry, 1992. **27**(10): p. 1163-1164.

23. Wiley, W.C. and I.H. McLaren, *Time-of-Flight Mass Spectrometer with Improved Resolution.* Review of Scientific Instruments, 1955. **26**(12): p. 1150-1157.

Chapter 3

The study of electrochemical biosystems for cellular sensing

3.1 Introduction

3.1.1 Justification of choice of mediators - Ferrocene carboxylic acid (FcA) and ferri/ferro-cyanide (FCN^{3-}/ FCN^{4-})

In biological systems, many biological compounds show irreversible redox behaviour characteristic of slow heterogenous electron transfer at the electrode surface [1]. To study these electrochemical behaviours, electrochemical mediators (ECM) are used to promote the electron transfer process, acting as an "electron shuttle" to provide redox coupling between the electrode and redox species of interest. An ideal ECM should meet several essential requirements to fulfil the role as an "electron shuttle". Firstly, an ECM should be highly stable under the experimental conditions, is non-cytotoxic, does not interfere with cellular behaviour, and should play a 'spectator role' in the observation and reporting of cellular signalling. An ECM does not undergo changes during the electron transfer, since any changes would compromise repeatability and reliability of the system. The ECM should have reversible behaviour, defined as absolute self-regeneration of the system allowing reproducibility and reliability of the experiment, without alterations to the experimental environment. The ECM redox potential should be lower than the other common electrochemically active molecule in the biological medium, e.g. zinc, magnesium, that can interfere due to being electrochemically active in the same potential window. Finally, an ECM should have a lower redox potential than the electrochemically active components that

are being studied, to maximise specific sensitivity tuned to detect, report and present an absolute finding [2].

Iron-based ECMs are of particular interest, this is because iron plays an essential role in cellular biology, especially in cellular survival [3, 4]. The role of iron in cellular biology includes promoting cell proliferation [5], formation of haemoglobin [6], regulating intra-cellular reactive oxygen species (ROS) level [7], and more importantly iron in the heme group of cytochrome c, and iron-sulphur proteins play an important role in the transport of electrons through the electron transport chain [8]. In mammalian cells, a family of cytoplasmic membrane ferrireductase, such as duodenal cytochrome B (Dcytb) [9], stromal cell-derived receptor 2 (SCDR2) [10] and six transmembrane epithelial antigen of the prostate (STEAP) [11] are capable in reducing extra-cellular free iron. These ferrireductases helps regulating iron intake [3, 9] and have a downstream effect on intra-cellular ROS level [12, 13] through reducing extra-cellular Fe^{3+} to Fe^{2+}. ROS plays an important role as a secondary cell signalling messenger [14], such as its contradicting role in the control of cell proliferation [14] and ROS-mitogen-activated protein kinase (MAPK) pathway induced apoptosis (programmed cell death) [15]. Therefore, from a cell biology perspective, it is vital information to profile and monitor intracellular ROS levels to decipher when ROS levels become signalling for cell proliferation or for programming cell death. In addition to profiling and monitoring of ROS through studying ferrireductase, it may be possible through developing surface bound ECM, to electrochemically control the activity of these ferrireductases and control cell proliferation or cell death. This could potentially be medically beneficial, such as cancer related studies [16], to control the death of cancer cells.

FcA and FCN^{3-}/ FCN^{4-} [17, 18] are of particular interest due to their fast electron exchange, thus minimising competitive interference with oxygen, and also fulfil the requirements of an ideal ECM for biological studies. FcA was one of the earliest developed and characterised ECM for use in early glucose detection [19, 20]. It is non-cytotoxic at mM concentration [21] compared to other ferrocene derivatives and has the highest mediator performance index in bacterial studies [22]. Mediator performance index, ΔImax/K_M ratio, is defined as the enzyme-mediator interaction and determines the performance of the electron acceptor. In addition, the solubility of FcA in water plays a crucial role in its mediator performance index. FcA is slightly more soluble in water than ferrocene making it compatible for biological studies. However, ferrocene dicarboxylic acid (FcDA) and ferroceneboracic acid (FBA) are highly water soluble, which would cause a significant decrease in the mediator concentration at the near-cell membrane space leading to poorer mediator performance. Moreover, FDA and FBA, acid groups are highly effective electron-acceptors and could possibly facilitate electron transfer between the enzyme and itself [22]. Therefore, FcA, is a good candidate for this study because it fulfils all the requirements of an ideal ECM for biological studies. In addition, FcA has a carboxylic acid functional group which makes it ideal for performing surface chemistry, for example N,N'-Dicyclohexylcarbodiimide (DCC) coupling or 1-Ethyl-3-(3-dimethylaminopropyl) carbodiimide (EDC) coupling, in order to synthesize a surface bound ECM system, e.g. Self Assembled Monolayers (SAM) [23] (**figure 3.1.1.1**).
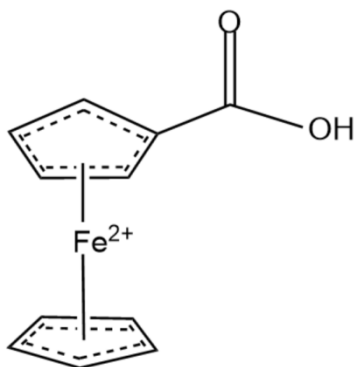
Figure 3.1.1.1 Chemical structure of FcA

Another well studied mediator, FCN^{3-}/ FCN^{4-} (**figure 3.1.1.2**) are highly water soluble iron-based derivatives which has been studied for its electrochemical catalytic properties and used in biological assays [24, 25], especially for enabling glucose detection. This well developed glucose detection system had demonstrated that FCN is a good electron acceptor, therefore capable in accepting electrons from reduced glucose oxidase and report to the system [25]. More importantly, FCN^{3-}/ FCN^{4-} could be used in these cellular studies at high concentrations (mM levels) and does not exhibit toxicity to cells. Therefore, FCN^{3-}/ FCN^{4-} is a good candidate and compatible with biological studies. FCN^{3-} has also been developed into a ferricyanide mediated biological oxygen demand system (FM-BOD) [26, 27], where FCN was shown to be able to replace oxygen as the terminal electron acceptor during glucose metabolism [28-30]. FCN^{3-} is reduced to FCN^{4-} as a replacement of oxygen in the role of terminal electron acceptor during glucose metabolism in cells incubated in oxygen depleted environment for a prolonged period. The concentration of FCN^{3-} reduced to FCN^{4-} was then measured by linear sweep voltammetry [31] and chronoamperogram [27, 32] using microelectrodes. Moreover, this highly water-soluble feature of FCN^{3-}/ FCN^{4-} makes it difficult to pass through the cell plasma membrane, and therefore, ideal for use as an extracellular ECM [33].
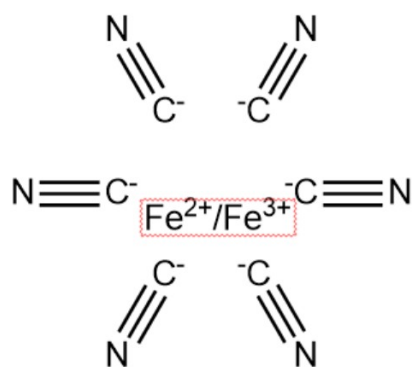
Figure 3.1.1.2 Chemical structure of FCN^{3-}/ FCN^{4-}

3.1.2 Biological model

A biological model that could act as biocatalysts, that could produce extra-cellular electrons, was required to test out the theory and compare the mediator's electro-catalytic properties. Aerobic bacteria, *Escherichia coli (E. coli) DH5-α* was used as a model for preliminary optimisation of the system. During aerobic metabolism, every molecule of glucose metabolised by the bacteria produces 24 electrons (**figure 3.1.2**) [34]. This rich source of electrons is ideal for testing the ability of live cells to chemically reduce FcA and FCN^{3-}. In addition, *E. coli* reproduce at a much faster rate than mammalian cell lines, thus they provide a better system for refining the electrochemical method before testing in mammalian cell lines in future studies. The metabolic machinery in bacteria is more accessible, as most of them are located on the cell membrane [35] therefore the ECM does not need to diffuse in and out of the cell to access the generated electron pool. Whereas in eukaryote models, most of the metabolic machinery is found within the cell (the mitochondria) making it difficult to access. Moreover, studies on *E. coli* models are well defined, and serve to provide a backbone for the migration onto mammalian cell work.
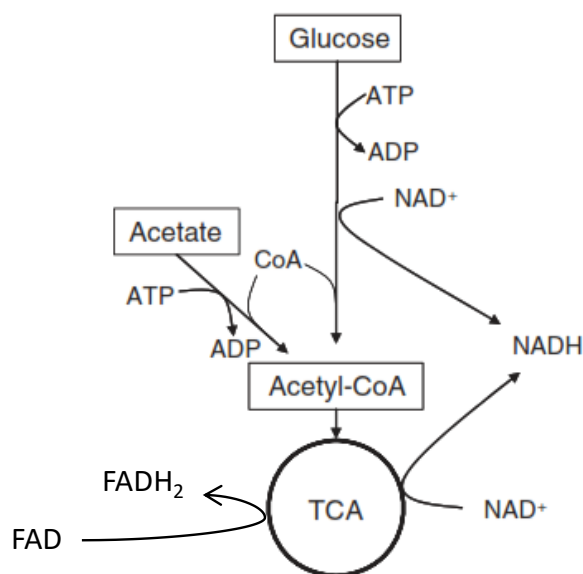
Figure 3.1.2 Glucose is metabolised in *E.coli* via the glycolysis and tricarboxylic acid cycle (TCA) to produce 24 electrons [34].

3.1.3 Electron transfer from *E.coli* to ECM

The role of a biological electrochemical mediator is to capture electrons released by the biological organism which is acting as a reduction catalyst. In summary the route to sensing external electron transfer is to start with an ECM that is in the reduced form which is then electrochemically oxidised to mediator $_{(Ox)}$. The oxidised mediator diffuses to the cell and interacts with its metabolic machinery where it is reduced (mediator $_{(Red)}$), and then diffuses to the electrode where it is subsequently oxidised again (**figure 3.1.3.1**). The mediator was first electrochemically oxidised, then chemically reduced by the catalyst in this case *E.coli*, and finally electrochemically oxidised by the system, this is referred to as the E-C-E mechanism (See **section 1.3.2** for more detail). This leads to an enhancement in the oxidation current and decrease in the reduction current obtained, because the magnitude of the peak current is governed by the iron concentration as explained by the Randles-Sevcik equation

[36] (See **section 4.5.2** for more detail). **Figure 3.1.3.2** shows a diagrammatic depiction of the events that take place during a CV study [37].
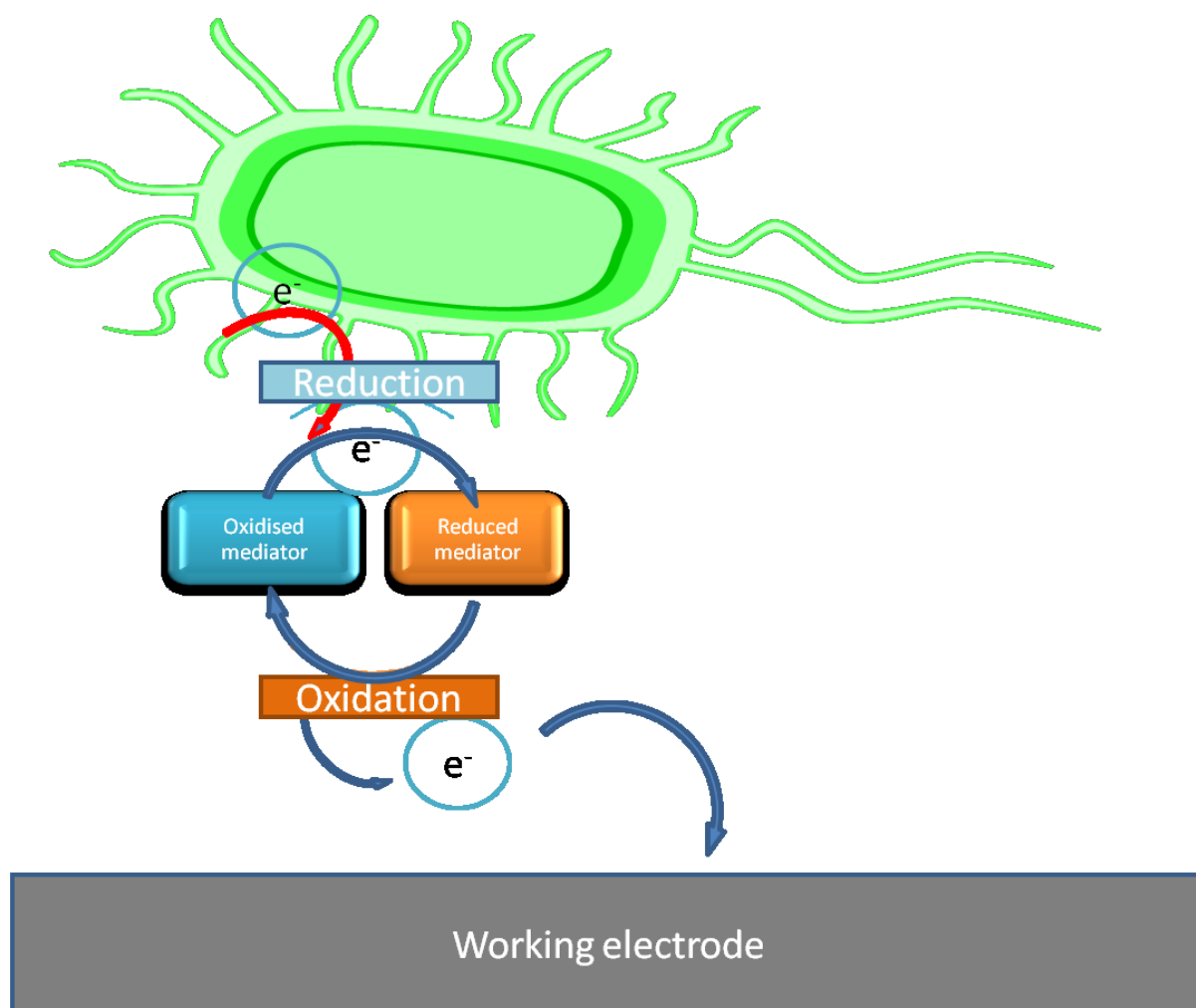
Figure 3.1.3.1 Schematic diagram of bioelectrocatalysm of mediator.
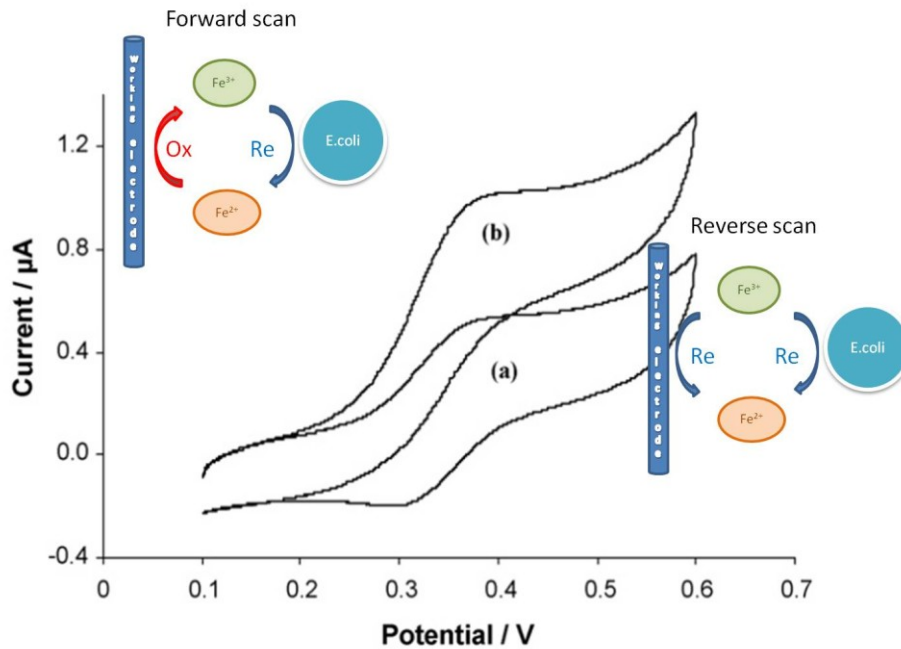
Figure 3.1.3.2 Voltammogram modified from Jamal (2009) [37] (a) show the cyclic voltammetry of ECM in the absence of *E.coli*, and (b) in the presence of *E.coli*.

3.1.4 *E.coli* metabolic rate

The rate at which *E.coli* produce electrons is proportional to the glucose metabolic rate [34]. The factors that could possibly affect metabolic rate of *E.coli* includes; (1) Growing phase of *E.coli* [38]; (2) Temperature [39]; (3) Nutrient availability [40] and (4) Oxygen availability [41]. The effects of these factors require investigating so that we could optimise the electrochemical assay.

In a fresh *E.coli* sub-culture, the growth rate of cells is low, this is defined as a lag phase [38]. The cells then enters the exponential phase defined as the rapid increase of cell culture population [38]. When the cells have reached certain saturation, due to the limitation of oxygen and nutrient available in solution, cell growth will reach a stationary phase. In the stationary phase, cell viability decreases [38]. It was important to determine the *E.coli* growth

curve/timeline which would allow accurate identification of the optimal time point to harvest the cells when they are most efficiently producing electrons. By investigating the above it was envisaged that we could optimize the system to detect the bioelectrochemical catalytic effect of the cells as previously hypothesized.

3.2 Aim

The aim of the work described in this chapter was to assess the suitability of the mediators FCN^{4-} and FcA to facilitate electron transfer from a model cell. Additionally, it would allow us to determine the most appropriate mediator to develop into a surface immobilised mediator sensing system in later studies.

3.3 Objectives

The objectives of chapter 3 were to test both mediators in a biological system and see if the cellular reduction capacity could be monitored in real-time and to establish which mediator is more sensitive for detection electron transfer from cells.

1) Test if FcA and FCN^{4-} can be used as a reporter mediators for a real-time bioelectrochemical metabolic rate sensing system.

2) Compare the sensitivities of the two mediators.

3.4 Methods and materials

3.4.1 Chemicals

All reagents were purchased from Sigma-Aldrich, apart from LB broth was purchased from Fisher Scientific. Phosphate buffer saline (PBS) was prepared by mixing 50 mM K_2HPO_4 and 0.1 M KCl solution with 50 mM KH_2PO_4 and 0.1 M KCl solution until the solution reaches

pH 7.3. PBS was then autoclaved, sealed in glass bottles and then stored in a cool dark place until used.

3.4.2 *Escherichia coli* DH5-α culture before optimisation

E. coli DH5-α was stored on LB agar plates at 4 °C. *E. coli* were sub-cultured in liquid LB broth medium the day before the experiment was performed. The LB broth was allowed to grow for 18 hours at 37 °C on a shaker at 200 rpm in conical flasks. Bacteria were sub-cultured at 1:5 dilution in fresh LB broth in conical flasks and incubated at 37 °C on a shaker for 5 hours. Bacteria were subsequently harvested by centrifugation at 3261 g and washed twice in 10 ml of sterile PBS before finally re-suspending in PBS. Cell density measurements were performed at $OD_{600\ nm}$ using a Cecil CE1020 UV spectrometer. The cell suspension was kept on ice for up to 5 hours until cells were needed for assaying.

3.4.3 Electrochemical measurements (Cyclic voltammatry (CV))

An electrochemical cell consisting of a Saturated Calomel reference Electrode (SCE), 3 mm diameter glassy carbon working electrode and platinum counter electrode were used in the cyclic voltammetric studies. A Gamry 600 potentiostat with data acquisition software was used for electrochemistry experiments. All electrodes were rinsed with acetone and high quality deionised water in between CVs. The glassy carbon electrode was polished with 50 nm alumina powder for 5 min prior to each CV being performed. Cyclic voltammetric studies were performed on solutions of 2 mM ferrocene carboxylic acid (FcA) or potassium hexacyanoferrate(II) trihydrate (FCN^{4-}) in PBS, with/without 0.5 mM of glucose and with/without 1 OD of *E.coli*. The voltammograms were recorded using an initiating potential of -0.2 V with a switching potential of 0.6 V and an end potential of -0.2 V while using FcA as mediator. The voltammograms were recorded using an initiating potential of -0.1 V with a

switching potential of 0.45 V and an end potential of -0.1 V while using FCN^{4-} as mediator. All CVs were performed at 5 mV sec^{-1} scan rate.

3.4.4 Electrochemical measurements (Linear sweep voltammatry (LSV))

An electrochemical cell consisting of an Ag/AgCl reference electrode, 0.3 μm platinum working electrode and platinum counter electrode were used in the cyclic voltammetric studies. A Gamry 600 potentiostat with data acquisition software was used for electrochemistry experiments. All electrodes were rinsed with acetone and high quality deionised water in between LSVs. The working micro platinum electrode was polished with 50 nm alumina powder for 5 min prior to each LSV being performed. Linear swipe voltammetric studies were performed on solutions containing 2 mM potassium ferricyanide(III) (FCN^{3-}) in PBS, with/without 10 mM of glucose and with/without 2 OD of *E.coli*. The voltammograms were recorded using an initiating potential of -0.05 V and an end potential of -0.05 V at scan rate 100 mVsec^{-1}.

3.4.5 Electrochemical oxidation of FcA

A three electrodes system, consisting of an Ag/AgCl reference electrode, carbon sheet as working electrode and a platinum counter electrode were used in the electrochemical oxidising FcA process. The electrochemical cell was placed on a magnetic stirrer. 2 mM of FcA in PBS was placed inside the cell and chronoamperometry was ran at a potential of 0.45V for 10 hours.

3.4.6 Growth rate study of solid to liquid medium sub-culture of *E.coli*

A colony of stocked *E.coli* (on agar plate) was scooped and placed into a flask of 200 ml LB broth. The flask was then incubated at 37°C on shaker for the length of the experiment. Samples were taken from the flask and cell density measurements were performed at $OD_{600\,nm}$ using a Cecil CE1020 UV spectrometer every hour (0 to 11 hours).

3.4.7 Growth rate study of liquid to liquid medium sub-culture of *E.coli*

Solid to liquid sub-culturing was performed (See **section 3.4.6**) and the sub-culture was incubated at 37°C on shaker overnight. 10 ml, 20 ml and 50 ml of the overnight culture were then put into a fresh flask of 200 ml LB broth and incubated at 37°C on shaker for the length of the experiment. Samples were taken from the flask and cell density measurements were performed at $OD_{600\,nm}$ using a Cecil CE1020 UV spectrometer every 30 minutes for up to five hours.

3.4.8 Growth rate study between conical flasks and baffled flasks culture of *E.coli*

A solid to liquid medium sub-culture of *E.coli* was performed as described in **section 3.4.6**. The overnight culture was diluted in 1 to 21 ratio of fresh LB broth in conical flasks or baffled flasks and incubate at 37°C on shaker for the length of the experiment. Cell density measurements were taken every 30 minutes for baffled flask cultures at $OD_{600\,nm}$ using a Cecil CE1020 UV spectrometer. Cell density of measurement of concial flask cultures were taken after 0, 0.5, 1, 1.5, 2, 3, 4, 5, 6, 7, hours of incubation.

3.4.9 Glucose consumtion rate study of *E.coli* during resuscitation incubation period

A solid to liquid medium sub-culture of *E.coli* was performed as described in **section 3.4.6**. Overnight culture were then sub-cultured at 1:21 dilution in fresh LB broth in baffled flasks and incubated at 37 °C on a shaker for 2 hours. Bacteria were subsequently harvested by centrifugation at 3261 g and washed twice in 10 ml of sterile PBS before finally re-suspending in PBS. Cell density measurements were performed at $OD_{600\ nm}$ using a Cecil CE1020 UV spectrometer. The cell suspension was kept on ice for the length of experiment. After stored on ice for 0, 1, 2, 3, 4, and 5 hours, 2 OD of *E.coli* were diluted in 10 ml of PBS containing 10 mM of glucose and incubated at 37 °C on a shaker for 1 hour. Glucose concentration of the resuscitation cultures were measured before and after the incubation using a Accu-chek active blood glucose meter.

3.4.10 Mass spectrometry analysis of FcA

1mg/ml of FcA was prepared in HPLC grade methanol, and further diluted 1:1000 in HPLC grade methanol, to make a final concentration of 1ug/ml of FcA. 1ul of the 1ug/ml FcA was manually injected into the LC-MS (Waters Limited Synapt G2S TOF-MS using Waters Limited nanoAcquity systems as the LC system running HPLC grade methanol as mobile phase). The analysis was conducted using electrospray (ESI) ionisation technique in negative ionisation mode. Data analysis was conducted using Waters Limited Masslynx 4.1.

3.5 Results and discussion

3.5.1 Cell samples preparation

Cell samples preparation protocol was obtained from previous master student's project. The stock *E.coli* DH5-α was stored at 4 °C on agar plate (**figure 3.5.1.1 i**). The stock was sub-

cultured into LB broth and incubated at 37 °C over night (**figure 3.5.1.1 ii)**. The overnight culture was then sub-culture into fresh LB broth in a 1 in 5 dilutions and re-incubate for 5 hours on the day of experiment (**figure 3.5.1.1 iii)**. This step of LB to LB sub-culturing would further stimulate the growth of *E.coli* by introducing fresh nutrients from the broth, therefore ensuring the culture would enter the exponential growth phase. This is important because cells in exponential growth phase is when cell metabolism is at its peak, and therefore, would have a higher degree of electron transfer [38]. The cells were then collected by centrifugation, and to ensure that no LB broth was left in the sample, samples were washed in PBS twice and finally re-suspended in PBS and stored on ice for duration of the experiment (**figure 3.5.1.1 iv)**. Residual LB broth was removed through thorough PBS wash because complex medium may contain electrochemically active components which could out compete and interfere with our ECM and/or produce unexpected redox peaks. To resuscitate the cells from ice, an appropriate amount of sample was taken off of ice and incubated at 37 °C for 30 minutes with glucose (**figure 3.5.1.1 v)**. Finally, the resurrected cells were mixed with FcA/FCN^{4-} in PBS to perform the CV experiments (**figure 3.5.1.1 vi)**.
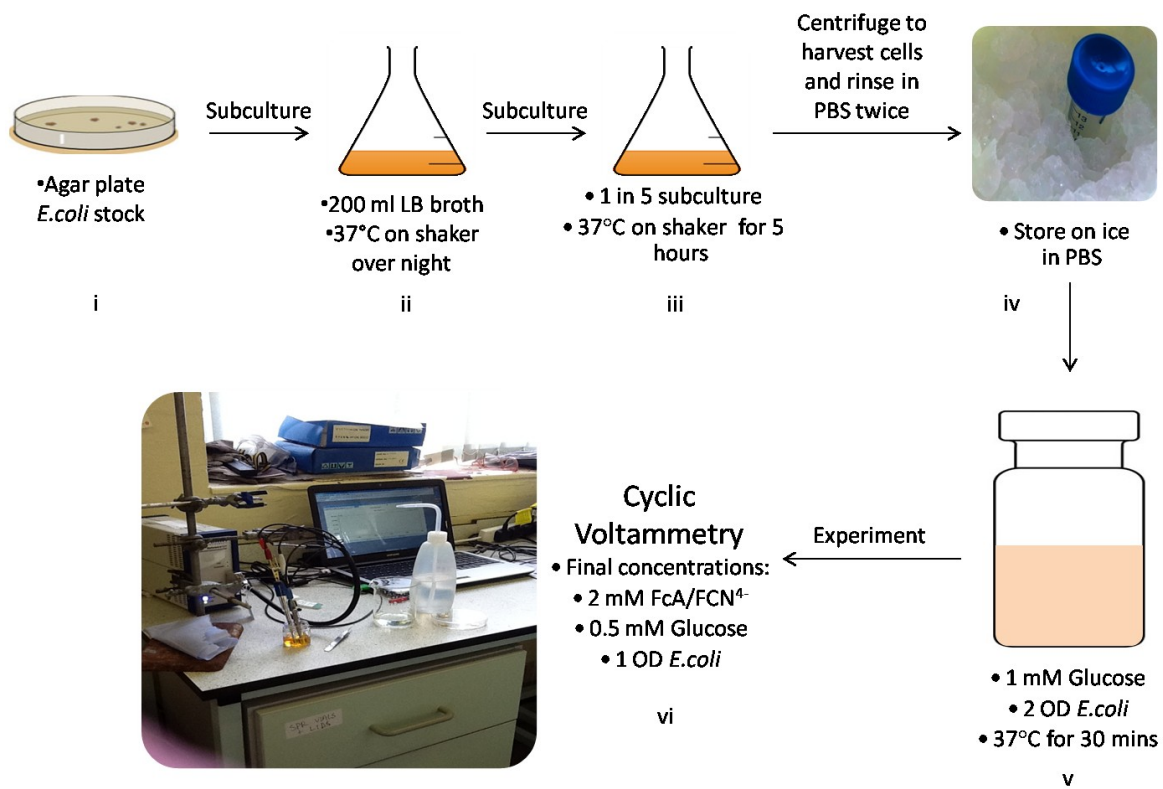
Figure 3.5.1.1 Summary of cyclic voltammetry experimental sample preparation process.

3.5.2 Monitoring electron transfer from *E.coli* via FcA and FCN^{4-}

Samples were prepared as described in **section 3.5.1**, (A) Controls were FcA / FCN^{4-} in PBS alone (n=4/3), (B) FcA/FCN^{4-} with added 0.5 mM glucose (n=5/3), and experimental sample (C) FcA/FCN^{4-} was added to a 0.5 mM glucose solution and 1 OD of live *E.coli* (n=5/3), then CVs were performed. **Figure 3.5.2.1** and **3.5.2.2** show typical CVs obtained with a three electrode system consisting saturated calomel reference electrode (SCE), platinum counter electrode and a 3mm glossy carbon working electrode with solutions of 2 mM FcA or FCN^{4-} as the mediator. All CVs were performed at a slow scan rate, 5 mV s^{-1}, because we expected the rate of electron transfer from the cells to be relatively slow[42]. Consequently if a cyclic voltammogram was recorded at fast scan rates the electron transfer from the cells may well be missed. A summary of the anodic and cathodic peak currents obtained from cyclic voltammograms at approximately 245 mV and 193 mV taken from FcA CVs (**Figure 3.5.2.1**)

are plotted in **figure 3.5.2.3** and **figure 3.5.2.4**. Summary of i_{pa} around 155 mV and i_{pc} around

99 mV taken from FCN^{4-} CVs (**Figure 3.5.2.2**) are plotted in **figure 3.5.2.5** and **figure**

3.5.2.6. From the preliminary CV data, no differences was observed between samples

containing mediators in PBS alone, mediators and glucose in PBS and mediator with glucose

and *E.coli*. Note that an extra oxidation peak was observed in the CV of FcA at around 287

mV, this will be discussed later (please see **chapter 4**). We hypothesised that we would see a

catalytic enhancement in the oxidation signal of the reporter mediator due to cellular

reduction, however, this was not the case.
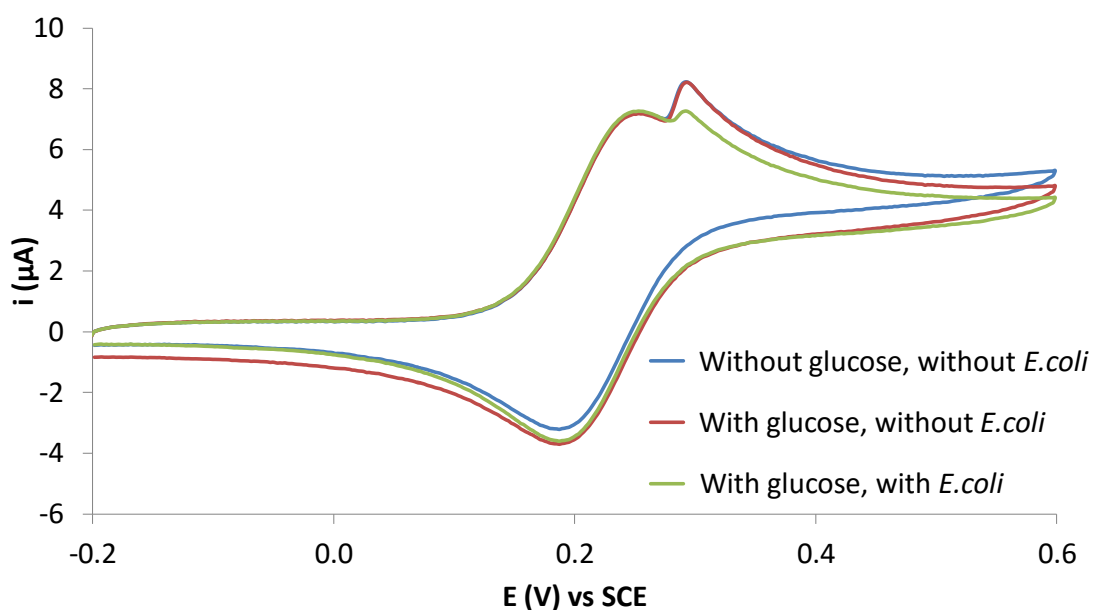
Figure 3.5.2.1 Typical cyclic voltammograms recorded with a GC working electrode using

PBS solutions containing 2 mM FcA, 0.5 mM glucose and 1 OD of *E.coli*. All CVs were

performed at scan rate 5 mVs^{-1}.
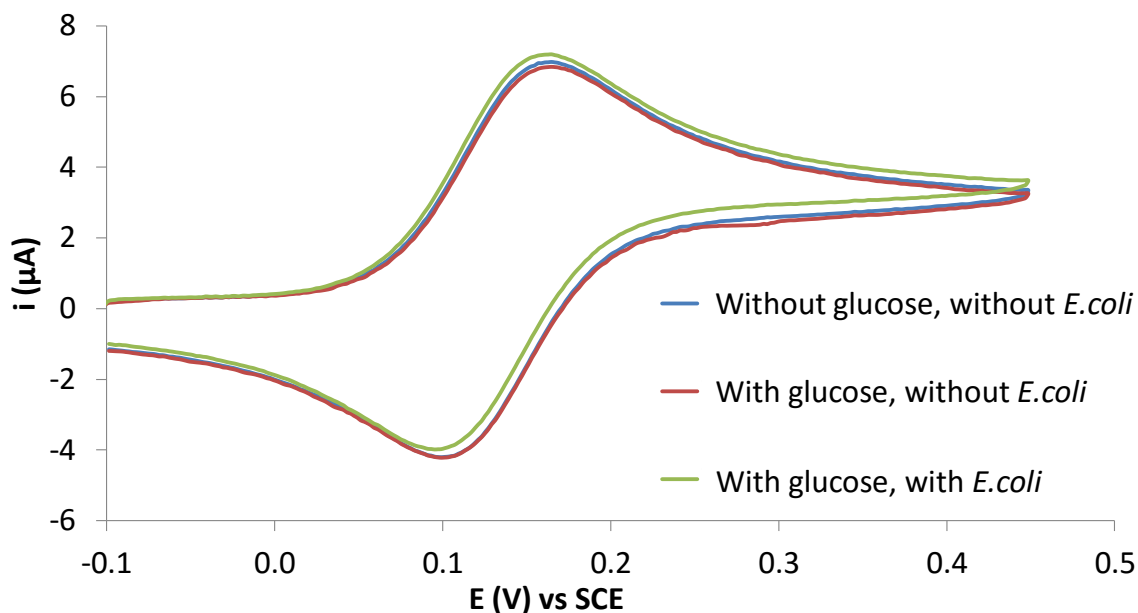
Figure 3.5.2.2 Typical cyclic voltammograms recorded with a GC working electrode using PBS solutions containing 2 mM FCN^{4-}, 0.5 mM glucose and 1 OD of *E.coli*. All CVs were performed at scan rate 5 mV s^{-1}.
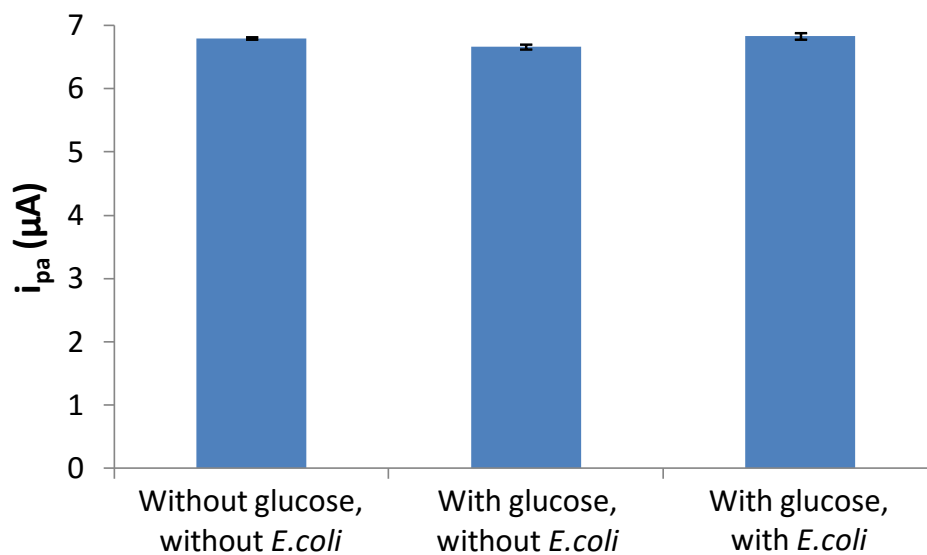
Figure 3.5.2.3 A histogram of the mean i_{pa} obtained from the cyclic voltammograms shown in **figure 3.5.2.1**. (n=4-5, ± 1 SD)
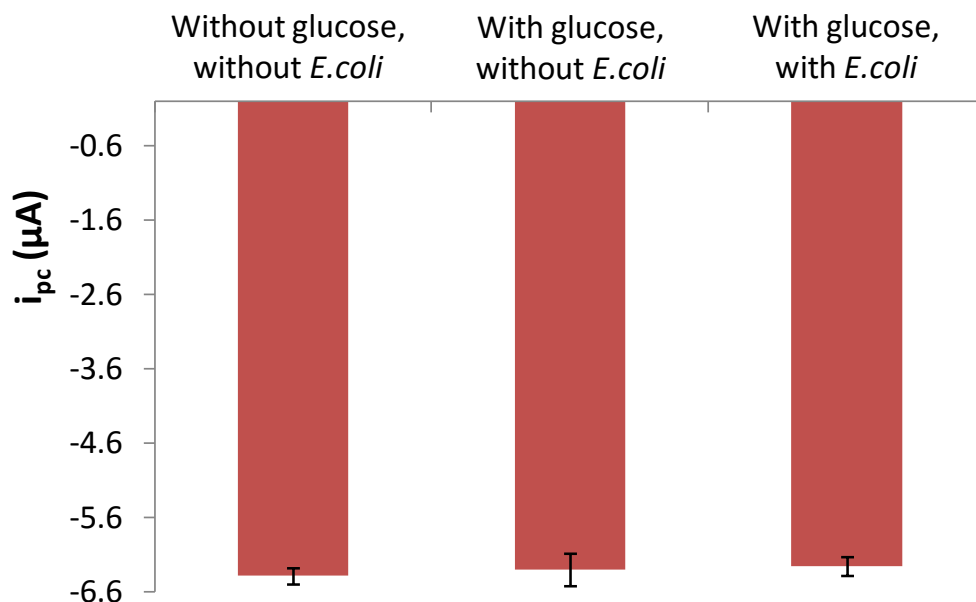
Figure 3.5.2.4 A histogram of the mean i_{pc} obtained from the cyclic voltammograms shown

in **figure 3.5.2.1**. (n=4-5, ± 1 SD)
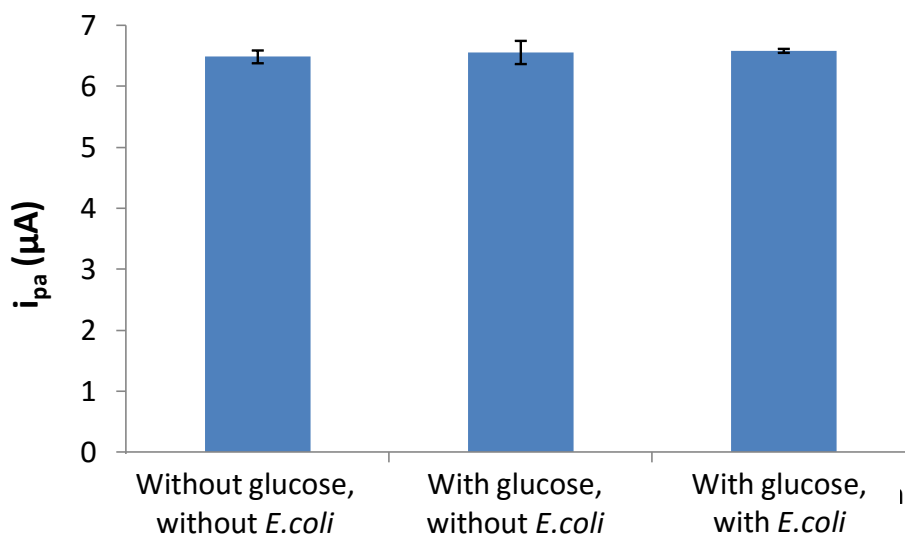
Figure 3.5.2.5 A histogram of the mean i_{pa} obtained from the cyclic voltammograms shown

in **figure 3.5.2.2**. (n=3-4, ± 1 SD)
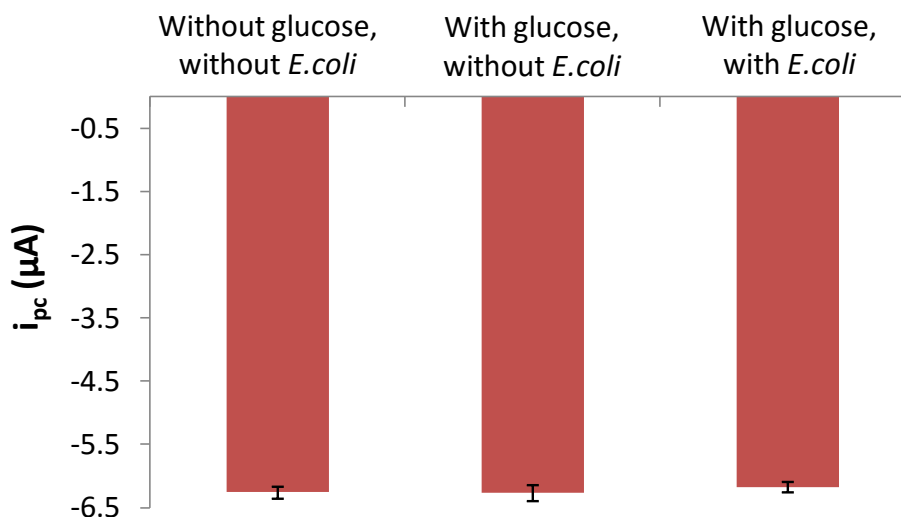
Figure 3.5.2.6 A histogram of the mean i_{pc} obtained from the cyclic voltammograms shown in **figure 3.5.2.2**. (n=3-4, ± 1 SD)

The data does not show any classical external electron transfer from the cells as depicted in **figure 3.1.3.2**, we envisaged this could be due to the low number of electrons being expelled and therefore cyclic voltammetry at a macro-electrode was not sensitive enough to measure the external electron transfer. Therefore an investigation into *E.coli* external electron transfer was performed with an established method based on linear sweep voltammetry using microelectrodes. It would be expected that this method would generate a steady state voltammogram and allows quantitation of the amount of mediator reduced by the cells over the extended incubation period [31]. *E.coli* cultures were prepared the same way as described in **section 3.5.1.1** except in process (v) **(figure 3.5.1.1)**, FCN^{3-} was added into the resuscitation incubation and the incubation time was extended to one hour. The reasoning behind this was that the mediator was in the oxidised form, therefore incubating it with *E.coli* cells would allow more time for the cells to produce sufficient electrons and subsequently lead to a higher rate of electrons transfer from the cell to the mediator. The whole

resuscitation incubated sample was then examined using linear sweep voltammetry (LSV) with a 0.3 μm diameter platinum micro working electrode (**figure 3.5.2.7)** in order to measure if any FCN^{3-} was reduced to FCN^{4-} by the *E.coli*. Note: anodic current is proportional to the bulk concentration of FCN^{4}, whereas, the cathodic current is proportional to the bulk concentration of FCN^{3-}. The results demonstrated that in the absence of *E.coli*, FCN^{3-} was stable in the oxidized form at 37 °C for one hour, because no *E.coli* was present to reduce FCN^{3-} to FCN^{4-}. Whereas, when *E.coli* was cultured with 10 mM of glucose, according to the anodic to cathodic ratio, about 96 % of FCN^{3-} in the solution was reduced to FCN^{4-}. In the presence of *E.coli*, but absence of glucose, only around 28 % of FCN^{3-} was reduced. This is possibly due to base-line metabolism of glucose pre-stored within the *E.coli* while it was in culture prior to conducting the experiment. The LSV data show the *E.coli* cells were actively reducing the mediator, while the CV data did not. This is possibly because the LSV is measuring bulk changes in concentration of FCN^{3-} to FCN^{4-}, whereas in CV experiment we were monitoring real time changes in FCN^{3-} reduction. This may suggest the CV experiments were not sensitive enough to measure FCN^{3-} reduction by cells in a real-time manner. Moreover, it may be possible the *E.coli* cells used in these experiments were not in optimal condition, therefore, further optimization of cellular work was needed.
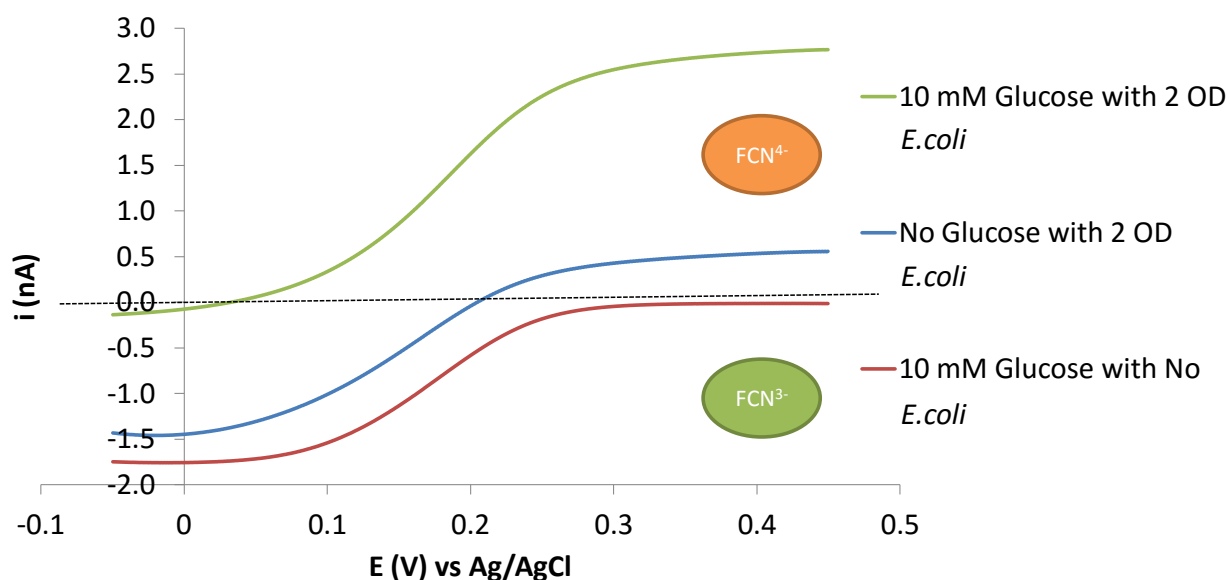
Figure 3.5.2.7 LSV showing the ratio of FCN^{3-}/FCN^{4-} in the different experimental conditions (black line) *E.coli* with 10m M glucose, (blue line) *E.coli* without glucose, and (red line) 10 mM glucose and no *E.coli.* LSV was scanned from -0.05 to 0.45 V at scan rate 100 mV s^{-1}.

FcA was purchased in the reduced form and therefore to replicate the LSV experiment we attempted to electrochemically oxidise all FcA via chronoamperometry using carbon sheet on stirrer and holding the potential at 0.45 V (**figure 3.5.2.8 i)**.However, the oxidised form of FcA did not appear stable and precipitated from solution (**figure 3.5.2.8 ii and iii)**.
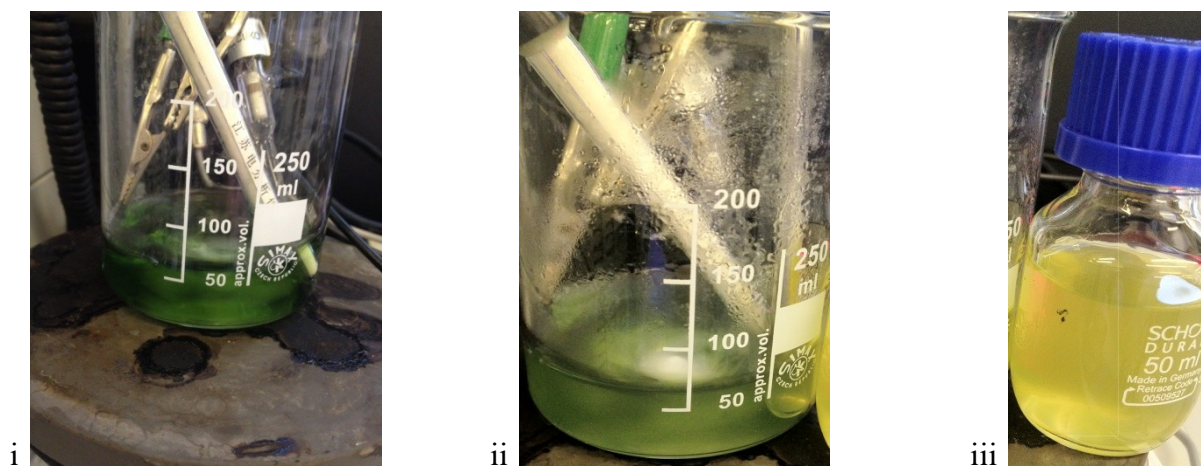
Figure 3.5.2.8 (i) After 10 hours on chronoamprometry, FcA turned green into ferricinium. **(ii)** Precipitation observed. **(iii)** 10 hours electrochemically oxidised FcA after storing at 4 °C over night.

The concept of developing an FcA and/or FCN^{3-}/FCN^{4-} mediated real time biological metabolic rate measuring system should be feasible which was confirmed by the LSV study. One of the factors that could have lead to the failure in the macro-electrode based system, using *E.coli* as our model, could be that the cells were harvested not at its peak metabolic state (exponential growth rate) leading to low levels of external electron transfer. Therefore, cell culture condition needed further optimisation. In addition, an extra oxidation peak was observed in the CVs obtained from FcA at approximately 287 mV, this requires further investigation.

3.5.3 Cell culture condition optimisation

The *E.coli* sample preparation protocol in the preliminary studies (**section 3.5.1**), was obtained from previous master student. This protocol may not be refined for our work as suggested by our preliminary studies result not showing any detection of electrochemical catalytic event in the system. This pointed to the possibility that our cell condition could be one of the contributing factors. Therefore, a series of cell culture condition optimization experiments were performed.

The protocol was broken down and investigated step by step from the very beginning. The first step of *E.coli* sample preparation was sub-culturing the stock *E.coli* from solid to liquid medium (**Figure 3.5.1.1 (ii))**. The growth curve of solid to liquid medium sub-culture was investigated. All *E.coli* growth rate studies were conducted by indirectly measuring cell density (optical density (OD)) using UV spectrometer reading at 600 nm. *E.coli* were sub-cultured from solid medium (agar plate) to liquid medium (liquid broth (LB)), and incubated at 37 °C on a shaker. OD measurements were taken every hour. The data **(figure 3.5.3.1)** shows when *E.coli* was sub-cultured from solid agar to LB medium, there is a 6 hours lag phase period, where the bacterial growth is relatively slowly. After 6 hours in culture, *E.coli* growth enters an exponential growth rate lasting approximately 2-3 hours, where the bacteria grow rapidly. The bacterial growth then enters a stationary phase after 10 hours of culture, where there is very little growth (n=3, ± 1 SD). A possible reason for the long lag phase of *E.coli* could be due to the cells needing to adapt from one growing condition (solid agar) to another growing condition (LB). We conclude from this that the agar to liquid broth medium culture was not an ideal way to time precisely for when experiments should be conducted at the optimal growth condition. Therefore LB to LB culturing was studied, for which we hypothesized that this would remove the adaptation factor and shorten the lag phase.
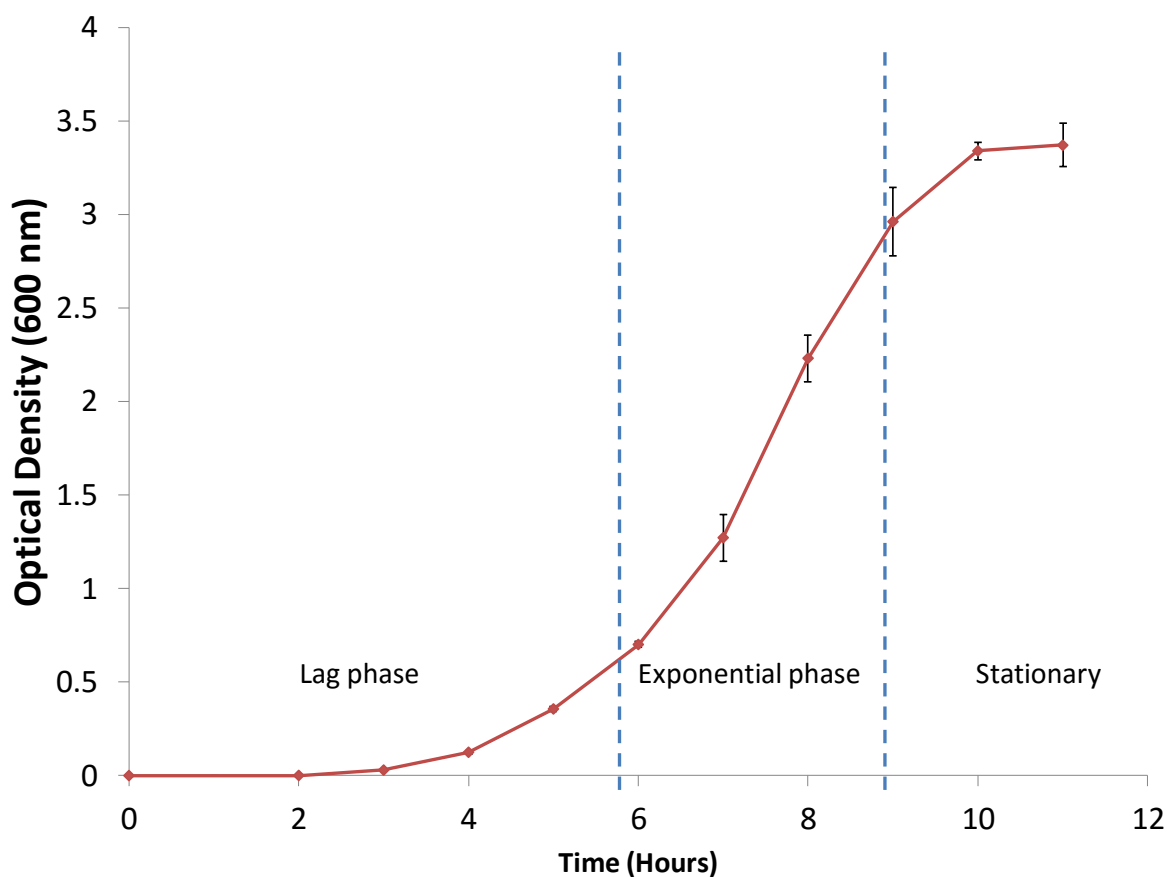
Figure 3.5.3.1 The growth pattern of *E.coli* when sub-cultured from solid agar to liquid broth (LB) medium. This Figure shows the growth rate of *E.coli* presented as OD over time in hours (n=3, ± 1 SD).

LB to LB culturing experiment was conducted to determine the optimal sub-culture dilution, since nutrient content is a limiting factor for bacterial growth, finding the balance between cell numbers and nutrient availability is vital. The nutrient concentration with regards to time is influenced by the bacterial cell density within the culturing medium [43]. *E.coli* cells were sub-cultured solid to liquid medium overnight to allow the culture to reach the maximum cell density. On day two, 10, 20 and 50 ml of cells from the confluent flask were diluted in 200 ml of fresh liquid medium. Growth rate studies (**figure 3.5.3.2**) of the 3 dilution cultures showed 10 in 200 ml dilutions was the optimal sub-culturing dilution as the growth curve was the

steepest. This means the 10 in 200 ml dilution sub-cultured cells were growing at the most optimal rate out of the 3 dilutions studied.
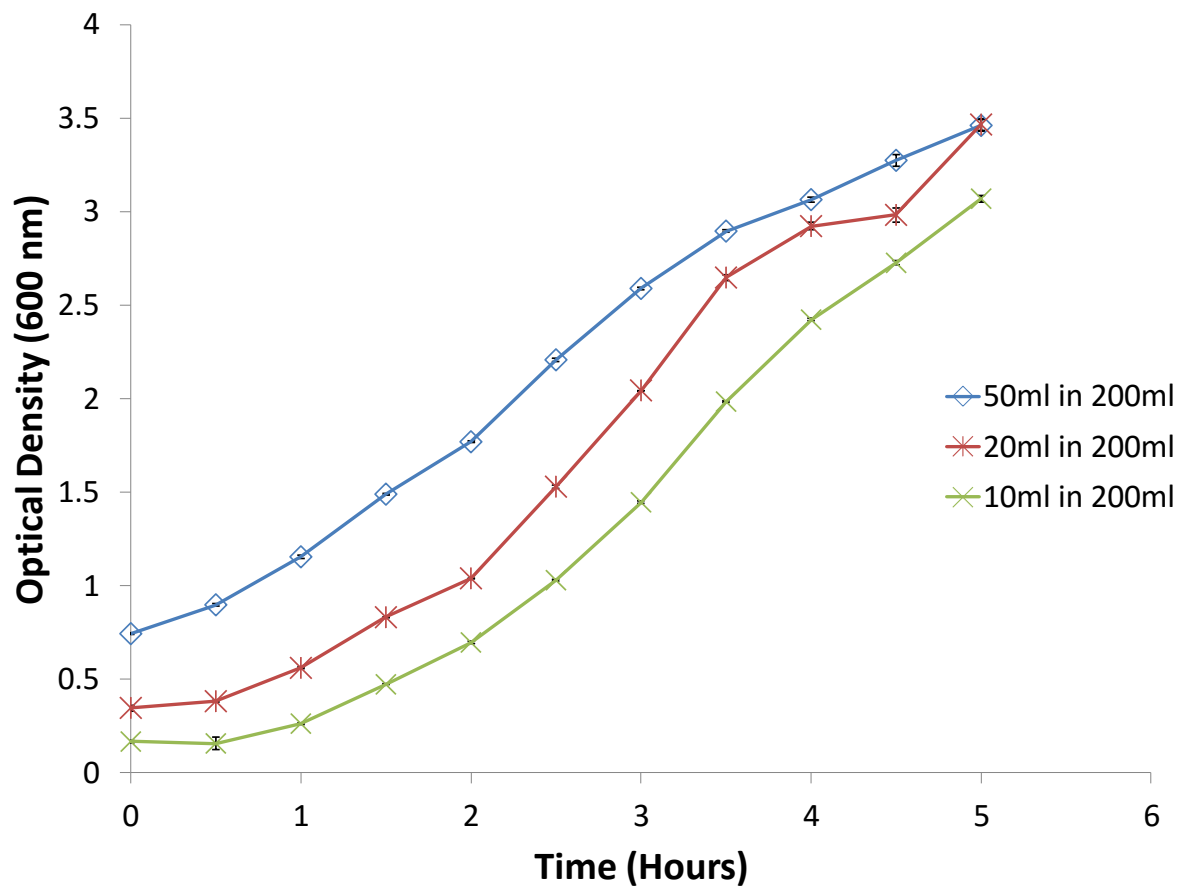
Figure 3.5.3.2 Growth rate study of LB to LB culturing of *E*.coli. The growth pattern of *E.coli*, sub-culturing stationary phase bacteria into freshly prepared LB medium, at different dilution factors; (blue) 50 ml stationary phase bacterial solution: 200 ml fresh LB medium, (red) 20ml stationary phase bacterial solution: 200 ml fresh LB medium, and (green) 10 ml stationary phase bacterial solution: 200 ml fresh LB medium. *E.coli* sub-cultured at dilution factor 10 ml stationary phase bacterial solution: 200 ml fresh LB medium (green) showed the steepest gradient, and therefore, a faster exponential growth rate compared to the other dilution factors (blue and red) (n=3, ± 1 SD).

Oxygen availability is also one of the major factors affecting growth rates of *E.coli*, therefore, a comparison study of culturing *E.coli* in conical flasks and baffled flasks was performed. The typical bacterial culturing conical flasks (**figure 3.5.3.3 i)** were used in previous studies. Baffled flask in **figure 3.5.3.3 ii** is another type of bacterial culturing flasks which are specific for aerobic bacterial culturing [43]. The baffle indents of the baffled flasks folds culture medium and increases oxygen level in the medium. In theory, the more availability of oxygen should increase aerobic bacterial proliferation. The data **(figure 3.5.3.4)** suggested that cultures grown in baffled flasks have a higher proliferation rate and higher maximum cell density. This is because the baffled flasks, alongside with culturing on a shaker, the shaking movement of the medium hitting the baffle of the baffled flask are suggested to higher oxygen availability into the culture solution during incubation [43].

Figure 3.5.3.3 Picture of **(i)** concial flask and **(ii)** baffled flask.
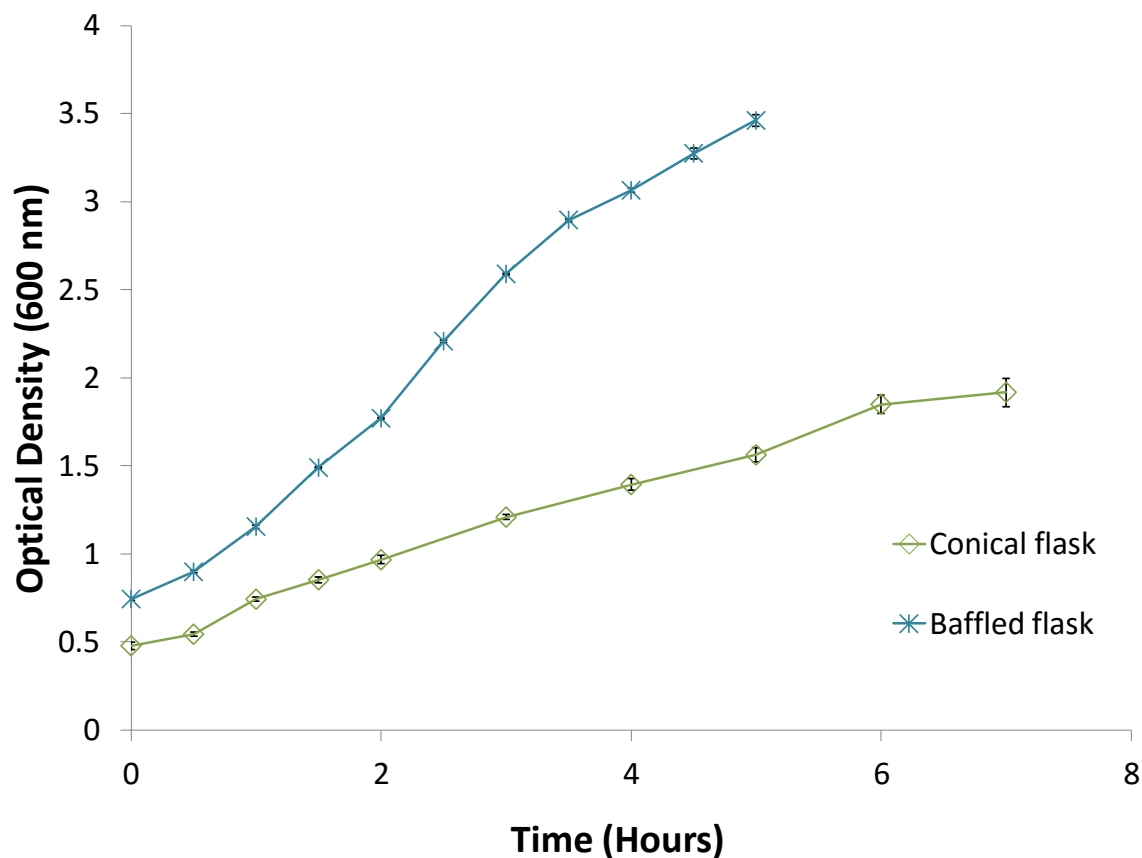
Figure 3.5.3.4 Growth rate study of *E.coli* using different culture flasks. The growth rate of *E.coli* cultured in conical flasks and baffled flasks was studied using the liquid to liquid culturing technique, and at dilution factor 10 ml stationary phase bacterial solution: 200 ml fresh LB medium. *E.coli* cultured in baffled flasks (blue) showed steeper gradient exponential growth rate than when cultured in conical flasks (green) (n=3, ± 1 SD).

During the resuscitation incubation process of sample preparation **(figure 3.5.1.1 v)**, *E.coli* was re-suspended in PBS and glucose only. PBS was used, as complex media like LB broth could potentially contain electrochemically active species which could produce unexpected peaks and interfere with the reading. To ensure the *E.coli* had sufficient resources for glucose metabolism, glucose was added into the culture. An investigation was performed to determine if 1mM of glucose, as directed in the original protocol (**figure 3.5.1.1**), was sufficient nutrient

to sustain 2 OD of *E.coli* cells during the 1 hour resuscitation incubation and the period of the electrochemistry experiments **(figure 3.5.3.5)**. The cell culture method **(figure 3.5.1.1, process i through iii)**, was adjusted as follows; LB to LB sub-culturing was performed in baffled flasks, diluted 1 in 21 and incubated at 37°C on a shaker for 2 hours. The cells were then harvested and washed in PBS twice then stored on ice in PBS (**figure 3.5.1.1,** process vi). An aliquot of 10 ml of cells at 2 OD cell density treated with 10 mM glucose was taken and put through the resuscitation procedure after storing on ice for different time periods. The glucose concentrations in the samples were measured before and after resuscitation incubation. The results of these glucose measurements **(figure 3.5.3.5)** show that 2 OD /ml of *E.coli* consumed on average 1.6 mM (SD=±0.2, n=3) glucose in one hour. This demonstrated that 1 mM of glucose was insufficient in the resuscitation incubation process suggested in the original method. Moreover cell density measurements were taken before and after the one hour resuscitation incubation showing no change from the original 2 OD after 1 hour **(data not shown)**. The cell density correlates to the number of cells however gives no measurement of cell respiration, which is related to the cell glucose consumption. As the cell density remains unchanged we can therefore use the glucose consumption rate of the cells after different periods being stored on ice to measure how this affects the cells viability. The data **(figure 3.5.3.5)** shows that there were no differences in the glucose consumption rate of *E.coli* during resuscitation incubation when stored on ice for up to 5 hours, thus suggesting *E.coli* cell viability is unaffected by storage on ice for up to 5 hours. Therefore, *E coli* electrochemical experiments reported hereafter are only stored for under the maximum storage time of 5 hours. The optimized method is summarized in (**Figure 3.5.3.6.**).
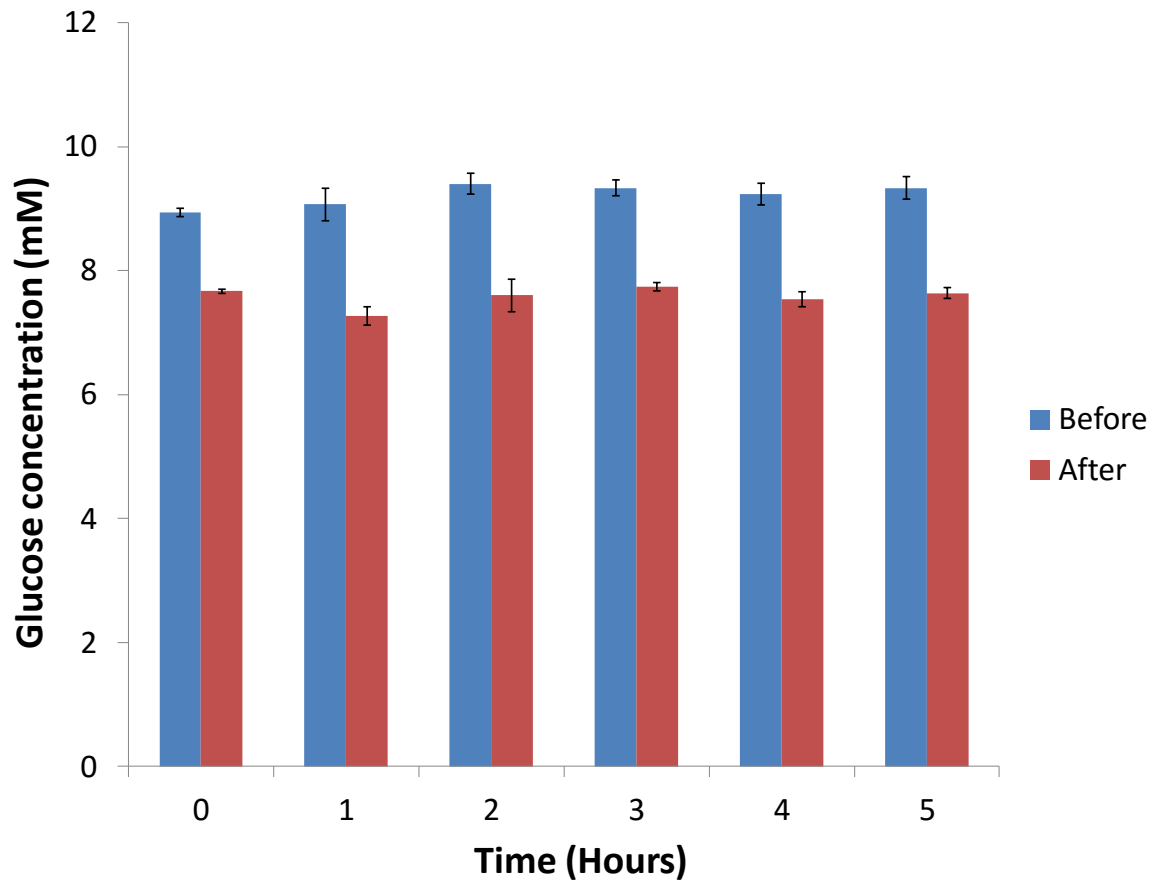
Figure 3.5.3.5 Glucose concentration study. *E.coli* was stored on ice for different period of time, and upon resuscitation from ice, 10 mM glucose was added and the glucose concentration was measured (blue). The *E.coli* was then cultured in an incubator at 37 °C for 1 hour, and then a final glucose concentration was measure (red). The results showed *E.coli* can be resurrected and viability is unaffected after up to 5 hours storage on ice, with metabolic capacity equivalent to cells not stored on ice.(n=3, ±=SE)
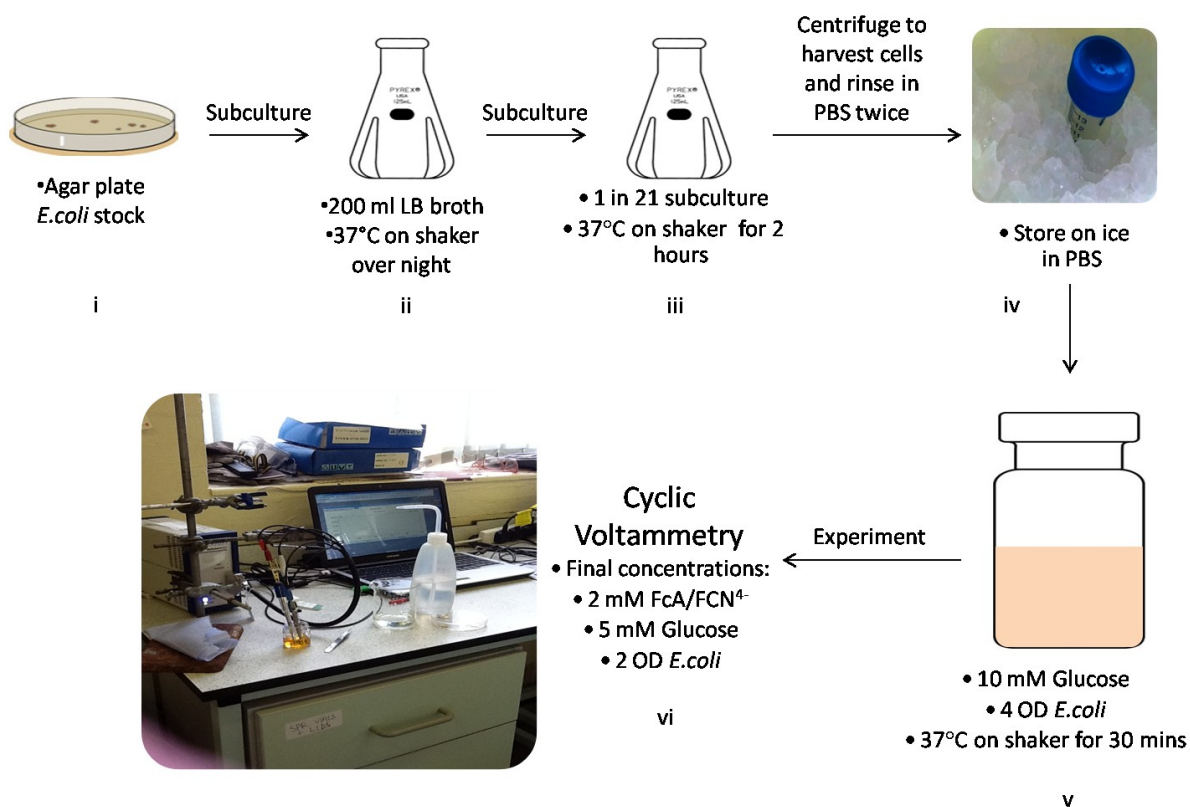
Figure 3.5.3.6 Summary of optimised cyclic voltammetry experimental sample preparation

process.

In summary, the series of cell culture optimisation experiments conducted are as follows; (1) growth curve of the *E.coli* in solid to liquid medium sub-culture; (2) optimal liquid to liquid medium sub-culture dilution were established; (3) oxygen supply during cell culture was maximised; (4) glucose supply for cell culture in length of incubation was optimised; and (5) maximum length of time that sample can be stored on ice was established. These optimisation experiments ensure that the *E.coli* samples are producing electrons at their maximal rate during the electrochemical assay. This should maximise the chance for our electrochemical system to detect any catalytic effects.

3.5.4 Purity of FcA

In the preliminary studies **(section 3.5.2)**, an extra oxidation peak of FcA appeared in the CV studies at approximately 287 mV **(figure 3.5.2.1).** One possible reason for this post-oxidation peak could be explained by reactant absorption on the working electrode [44]. However the overall CV behavior does not fit into the theory of reactant absorption. A pre-reduction peak should appear if there is strong reactant absorption of the mediator on the working electrode [45], and this was not observed.

Another possibility for causing the post-oxidation peak could be due to contamination of the mediator with something that displays non-reversible electrochemical behaviour. To confirm if this was the case, mass spectrometry analysis was performed to check for contaminants in the mediator. Data obtained from negative electrospray ionisation mass spectrometry analysis confirmed the FcA used in these studies was greater than 97% pure as stated in the specification document from Sigma-Aldrich **(figure 3.5.4.1).**

Lydia Yip FcA
msynesi_827 221 (3.035) Cm (217:223-167:199)   1: TOF MS ES-
228.7   1.50e7
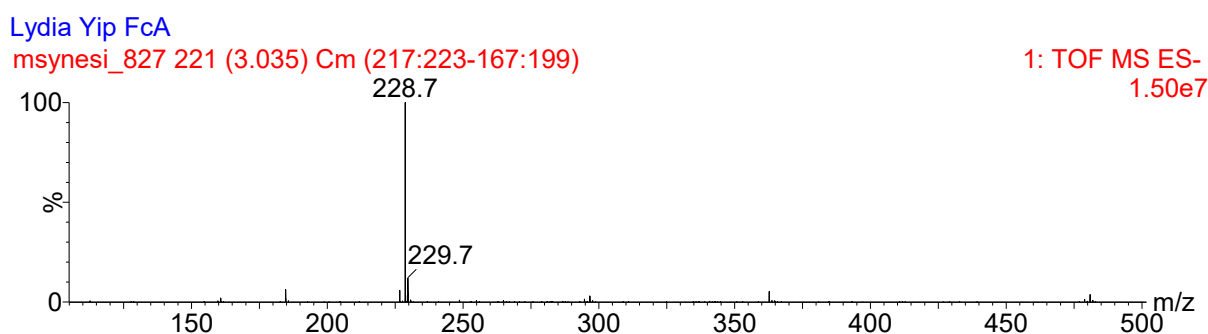
Figure 3.5.4.1 Mass spectrometry data conducted in negative electrospray ionisation.

3.6 Conclusion

In this chapter, preliminary CV studies were conducted on the both FCN^{4-} and FcA mediated systems, but, no catalytic event was detected. However, LSV experiments demonstrated the actual system should be working because the *E.coli* cells were actively reducing the bulk

FCN^{3-} to FCN^{4-}. This suggests the *E.coli* cells were actively metabolising, and their metabolim is detectable. It is possibly the CV experiments did not work but LSV experiments worked because the cell culture condition and the sensitivity of the system was not high enough. In addition, a post oxidation peak was observed in the CV obtained from FcA at 287 mV vs SCE reference electrode. It is unclear at the point why there is a post oxidation peak found in FcA but not in FCN. The next chapter, Chapter 4, will look at and fully investigate into the theory of the post oxidation peak. More importantly, break through advancement into FcA-based biosensor.

3.7 References

1.   Fultz, M.L. and R.A. Durst, *Mediator compounds for the electrochemical study of biological redox systems: a compilation.* Analytica Chimica Acta, 1982. **140**(1): p. 1-18.

2.   delle Noci, S., et al., *Electrochemical Kinetic Characterization of Redox Mediated Glucose Oxidase Reactions: A Simplified Approach.* Electroanalysis, 2008. **20**(2): p. 163-169.

3.   Lane, D.J.R., et al., *Cellular iron uptake, trafficking and metabolism: Key molecules and mechanisms and their roles in disease.* Biochimica et Biophysica Acta (BBA) - Molecular Cell Research, 2015. **1853**(5): p. 1130-1144.

4.   Lasocki, S., T. Gaillard, and E. Rineau, *Iron is essential for living!* Crit Care, 2014. **18**(6).

5.   Steegmann-Olmedillas, J.L., *The role of iron in tumour cell proliferation.* Clin Transl Oncol, 2011. **13**(2): p. 71-6.

6.   Wong, S.Y., *Colorimetric determination of iron and hemoglobin in blood. II.* Journal of Biological Chemistry, 1928. **77**(2): p. 409-412.

7.   Stohs, S.J. and D. Bagchi, *Oxidative mechanisms in the toxicity of metal ions.* Free Radic Biol Med, 1995. **18**(2): p. 321-36.

8.   Rich, P., *The molecular machinery of Keilin's respiratory chain.* Biochemical Society Transactions, 2003. **31**(6): p. 1095-1105.

9.   McKie, A.T., et al., *An iron-regulated ferric reductase associated with the absorption of dietary iron.* Science, 2001. **291**(5509): p. 1755-9.

10.   Vargas, J.D., et al., *Stromal cell-derived receptor 2 and cytochrome b561 are functional ferric reductases.* Biochim Biophys Acta, 2003. **1651**(1-2): p. 116-23.

11.   Gauss, G.H., et al., *The crystal structure of six-transmembrane epithelial antigen of the prostate 4 (Steap4), a ferri/cuprireductase, suggests a novel interdomain flavin-binding site.* J Biol Chem, 2013. **288**(28): p. 20668-82.

12. Jin, Y., et al., *STAMP2 increases oxidative stress and is critical for prostate cancer.* EMBO Molecular Medicine, 2015. **7**(3): p. 315-331.

13. Zhou, J., et al., *Steap4 Plays a Critical Role in Osteoclastogenesis in Vitro by Regulating Cellular Iron/Reactive Oxygen Species (ROS) Levels and cAMP Response Element-binding Protein (CREB) Activation.* J Biol Chem, 2013. **288**(42): p. 30064-74.

14. Sauer, H., M. Wartenberg, and J. Hescheler, *Reactive oxygen species as intracellular messengers during cell growth and differentiation.* Cell Physiol Biochem, 2001. **11**(4): p. 173-86.

15. Yip, N., et al., *Disulfiram modulated ROS–MAPK and NFκB pathways and targeted breast cancer cells with cancer stem cell-like properties.* British journal of cancer, 2011. **104**(10): p. 1564-1574.

16. Hsieh, H.-C., et al., *ROS-induced toxicity: exposure of 3T3, RAW264.7, and MCF7 cells to superparamagnetic iron oxide nanoparticles results in cell death by mitochondria-dependent apoptosis.* Journal of Nanoparticle Research, 2015. **17**(2): p. 1-14.

17. Cass, A.E., et al., *Ferrocene-mediated enzyme electrode for amperometric determination of glucose.* Anal Chem, 1984. **56**(4): p. 667-71.

18. Frew, J.E. and H.A. Hill, *Electrochemical biosensors.* Anal Chem, 1987. **59**(15): p. 933A-944A.

19. Wang, J., *Electrochemical glucose biosensors.* Chem Rev, 2008. **108**(2): p. 814-25.

20. Cass, A.E.G., et al., *Ferrocene-mediated enzyme electrode for amperometric determination of glucose.* Anal Chem, 1984. **56**(4): p. 667-671.

21. Pinto, A., et al., *Modification with Organometallic Compounds Improves Crossing of the Blood–Brain Barrier of [Leu5]-Enkephalin Derivatives in an In Vitro Model System.* ChemBioChem, 2009. **10**(11): p. 1852-1860.

22. Ponamoreva, O., et al., *Efficiency of bioelectrocatalytic oxidation of ethanol by whole cells and membrane fractions of <i>Gluconobacter Oxydans bacteria in the presence of*

mediators of ferrocene series. Russian Journal of Electrochemistry, 2010. **46**(12): p. 1408-1413.

23. LYONS, M.E., *Magnetic field effects in ferrocenealkane thiol self assembled monolayer modified electrodes.* 2010.

24. Catterall, K., et al., *Development of a Rapid Ferricyanide-Mediated Assay for Biochemical Oxygen Demand Using a Mixed Microbial Consortium.* Anal Chem, 2003. **75**(11): p. 2584-2590.

25. Wang, J., *Glucose biosensors: 40 years of advances and challenges.* Electroanalysis, 2001. **13**(12): p. 983.

26. Pasco, N., et al., *MICREDOX®—development of a ferricyanide-mediated rapid biochemical oxygen demand method using an immobilised Proteus vulgaris biocomponent.* Biosensors and Bioelectronics, 2004. **20**(3): p. 524-532.

27. Catterall, K., et al., *Development of a rapid ferricyanide-mediated assay for biochemical oxygen demand using a mixed microbial consortium.* Analytical chemistry, 2003. **75**(11): p. 2584-2590.

28. Yoshida, N., et al., *A mediator-type biosensor as a new approach to biochemical oxygen demand estimation.* Analyst, 2000. **125**(12): p. 2280-2284.

29. Yoshida, N., et al., *Improvement of a mediator-type biochemical oxygen demand sensor for on-site measurement.* Journal of biotechnology, 2001. **88**(3): p. 269-275.

30. Pasco, N., et al., *Biochemical mediator demand–a novel rapid alternative for measuring biochemical oxygen demand.* Applied Microbiology and Biotechnology, 2000. **53**(5): p. 613-618.

31. Rawson, F.J., A.J. Downard, and K.H. Baronian, *Electrochemical detection of intracellular and cell membrane redox systems in Saccharomyces cerevisiae.* Sci. Rep., 2014. **4**.

32.   Catterall, K., et al., *The use of microorganisms with broad range substrate utilisation for the ferricyanide-mediated rapid determination of biochemical oxygen demand.* Talanta, 2001. **55**(6): p. 1187-1194.

33.   Koley, D. and A.J. Bard, *Triton X-100 concentration effects on membrane permeability of a single HeLa cell by scanning electrochemical microscopy (SECM).* Proceedings of the National Academy of Sciences, 2010. **107**(39): p. 16783-16787.

34.   Wang, Y.F., et al., *Escherichia coli-catalyzed bioelectrochemical oxidation of acetate in the presence of mediators.* Bioelectrochemistry, 2006. **69**(1): p. 74-81.

35.   Pereira, I.A.C., et al., *A comparative genomic analysis of energy metabolism in sulfate reducing bacteria and archaea.* Frontiers in Microbiology, 2011. **2**.

36.   Oldham, K.B., *Analytical expressions for the reversible Randles-Sevcik function.* Journal of Electroanalytical Chemistry and Interfacial Electrochemistry, 1979. **105**(2): p. 373-375.

37.   Jamal, M., et al., *A stable and selective electrochemical biosensor for the liver enzyme alanine aminotransferase (ALT).* Biosensors and Bioelectronics, 2009. **24**(9): p. 2926-2930.

38.   Monon, J., *The growth of bacterial cultures.* Selected Papers in Molecular Biology by Jacques Monod, 2012: p. 139.

39.   Marr, A.G., J.L. Ingraham, and C.L. Squires, *EFFECT OF THE TEMPERATURE OF GROWTH OF ESCHERICHIA COLI ON THE FORMATION OF β-GALACTOSIDASE.* Journal of Bacteriology, 1964. **87**(2): p. 356-362.

40.   Shehata, T.E. and A.G. Marr, *Effect of Nutrient Concentration on the Growth of Escherichia coli.* Journal of Bacteriology, 1971. **107**(1): p. 210-216.

41.   Andersen, K.B. and K. von Meyenburg, *Are growth rates of Escherichia coli in batch cultures limited by respiration?* Journal of Bacteriology, 1980. **144**(1): p. 114-123.

42.   Hirst, J., *Elucidating the mechanisms of coupled electron transfer and catalytic reactions by protein film voltammetry.* Biochimica et Biophysica Acta (BBA) - Bioenergetics, 2006. **1757**(4): p. 225-239.

43.   Clark, G.J. and M.E. Bushell, *Oxygen limitation can induce microbial secondary metabolite formation: investigations with miniature electrodes in shaker and bioreactor culture.* Microbiology, 1995. **141**(3): p. 663-669.

44.   Wopschall, R.H. and I. Shain, *Effects of adsorption of electroactive species in stationary electrode polarography.* Analytical Chemistry, 1967. **39**(13): p. 1514-1527.

45.   Compton, R.G. and C.E. Banks, *Understanding Voltammetry*. 2011: Imperial College Press.

Chapter 4

Development of the bio-oxygen demand measuring system

Chapter 4 is based upon an article entitled:

"Real-time electrocatalytic sensing of cellular respiration" Nga-Chi Yip, Frankie J Rawson, Chi Wai Tsang, Paula M Mendes. Biosensors and Bioelectronics, 2014, 57, 303-9 [1]

Abstract: *In the present work we develop a real-time electrochemical mediator assay to enable the assessment of cell numbers and chemical toxicity. This allowed us to monitor metabolism down to a single cell in a low cost easy to use rapid assay which is not possible with current technology. The developed assay was based on the determination of oxygen. This was made possible via the use of electrochemical mediator ferrocene carboxylic acid (FcA). The FcA showed distinctive catalytic properties in interacting with reactive oxygen species generated from oxygen when compared to ferrocene methanol (FcMeOH). A deeper insight into the chemistry controlling this behaviour is provided. The behaviour is then taken advantage of to develop a cellular aerobic respiration assay. We describe the properties of the FcA system to detect, in real-time, the oxygen consumption of Escherichia coli DH5α (E. coli). We demonstrated that the FcA-based oxygen assay is highly sensitive, and using a population of cells, oxygen consumption rates could be calculated down to a single cell level. More importantly, the*

results can be accomplished in minutes, considerably outperforming current commercially available biooxygen demand assays. The developed assay is expected to have a significant impact in diverse fields and industries, ranging from environmental toxicology through to pharmaceutical and agrochemical industries.

Chapter 4 is also based upon a patent entitled:

"Oxygene sensor comprising a ferrocene compound." Patent publication

number WO2015036612 A1[2].

Abstract: *The invention relates to a ferrocene carboxylic containing assay system which may include a cellulose acetate membrane containing ferrocene. The assay is used to detect the presence of aerobic micelles in various substances based on the demand for oxygen. Individual cellscan be located on an electrode and oxygen demand can be calculated for individual biocompatible cells.*

4.1 Background - Choosing the mediator

In an electrochemical cell, the oxygen reduction reaction happens at potentials from 0 V or lower [3]. In aqueous electrolyte such as PBS, the O_2 molecules are reduced via two pathways which include a 2 or 4 electron pathway [4]. Regardless of which pathway the O_2 was being reduced, in an alkaline aqueous environment, the reduced O_2 (O_2^-) would always react with surrounding H_2O molecules and produces HO_2^- and OH^-. Combining these points, from chapter 3 **section 3.5.2**, the CVs of FcA were started at potential 0 V in an aqueous electrolyte (PBS) with a slight alkaline (pH 7.3) environment. It is suggested that as the CVs are conducted these reactive oxygen species (ROS), namely HO_2^- and OH^- were generated in the system. Both HO_2^- and OH^- are strong reducing agents [5]. We hypothesised that the ROS generated in the system react with the electrochemically oxidised FcA and cause the unexpected oxidation peak. In this Chapter, we further investigate the E-C-E mechanism as mentioned in **section 3.1.3**.

Cassidy's study [3] has also observed similar catalytic behavior in FcA and 1,1'-ferrocene dicarboxylate (FcDA).According to Cassidy's paper both FcA and FcDA also have the E-C-E superoxide catalytic properties [3]. So it is possible other ferrocene derivatives may also exhibit similar properties. The catalytic property of these ferrocene derivatives will differ to varying degrees as they have different functional groups. As suggested by Batterjee's study[6], the functional groups "steric bulk" shielding and the electron withdrawing effect would result in changes to the redox kinetics. These may affect the normal non-catalytic redox peak and catalytic oxidation peak location, normal redox kinetic and the electrochemical catalytic kinetics. All these factors need to be investigated and understood in order to select the most appropriate mediator to further develop the system.

Ferrocenemethanol (FcMeOH) was selected to perform parallel electrochemical and electrochemical catalytic property studies along with FcA. FcMeOH was selected for a number of reasons; 1) As FcMeOH is also a ferrocene derivative, therefore, it may also have O_2 electrochemical catalytic property ; 2) As the functional group of FcMeOH is a carbonyl group short compare to FcA (see **figure 4.1.1**), this can be use to test if Batterjee's suggestion [6] regarding the electron withdrawing effect is correct. We hypothesize that FcMeOH, due to the lack of this carbonyl group compared to FcA, has a lower "steric bulk", and therefore should have less electron withdrawing effect. This would result in FcMeOH having a lower redox potential. Data from Cassidy's study on FcDA, which has an additional carboxylic acid group compared to FcA (see **figure 4.1.1**), will be pooled with data from FcA and FcMeOH studies to help us understand the different effect of the functional groups on the electrochemical and electrochemical catalytic properties of the mediators. The best mediator for the system can then be selected using the criteria of lowest redox potential and quickest kinetics. These properties combined should provide the greatest sensitivity while also reducing the risk of the electrochemical process disturbing the cell's normal membrane potential [7].
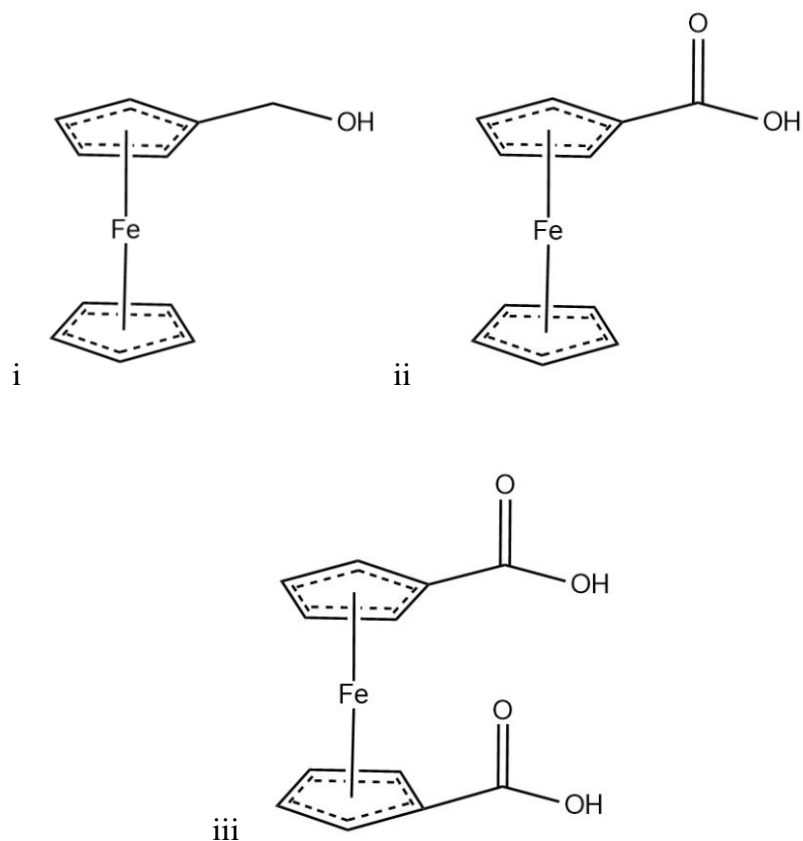
Figure 4.1.1 Chemical structures of (i) ferrocenemethanol, (ii) ferrocene carboxylic acid and (iii) ferrocene dicarboxylic acid.

4.2 Aim

The aim of this section of work was to investigate the electrochemical properties of the chosen mediators. This would also help to aid our understanding of how different functional groups affect the mediators' electrochemical behaviour. More importantly, it provides vital information for selecting the most suitable mediator for testing the concept on biological models, and explores the potential usage of the system.

4.3 Objectives

The objectives are as follows;

1) To confirm the post oxidation peak in CVs obtained from FcA is due to the catalytic reaction with ROS.

2) To confirm if FcMeOH has catalytic property towards superoxides.

3) To investigate the electrochemical properties of FcA and FcMeOH.

4) To investigate the electrochemical catalytic properties of FcA and FcMeOH.

5) To compare data obtained from objectives 2 and 3 and data from Cassidy's report involving FcDA and select the most suitable mediator.

6) To test the system on biological models.

Objective 1

CVs were conducted on oxygenated and de-oxygenated (nitrogen degassed) 2 mM FcA solutions to confirm if the post peak is caused by oxygen.

A preliminary scan rate study was performed with oxygenated FcA solutions and a plot summary drawn up of the post peak. Data was put into a current functional plot to confirm if the rate limiting step is a chemical one.

Objective 2

Ascertain the viability of using FcMeOH as a test mediator offering catalytic properties towards superoxides. This is determined by conducting CV tests with FcMeOH as mediator

in oxygenated and nitrogen purged de-oxygenated solutions as was conducted in **section 4.5.1** with FcA as mediator.

Objective 3

Scan rate study of FcA and FcMeOH to investigate the basic electrochemical properties of the mediators.

Objective 4

Perform and compare scan rate studies of deoxygenated and oxygenated solutions with FcA and FcMeOH as mediators and to use the disappearance of the catalytic peak to compare the catalytic kinetics of each mediator.

Objective 5

Combine data from FcA and FcMeOH studies in objectives 2 and 3 and data of FcDA from Cassidy's report to select the most suitable mediator using criteria as discussed for further development.

Objective 6

Put the system into practical use by investigating biological models, e.g. *E.coli*, fresh water samples and mammalian cells.

4.4 Methods and materials

4.4.1 Chemicals

LB broth was purchased from Fisher and ferrocene methanol was purchased from Acros Organics. All other reagents were purchased from Sigma–Aldrich. All solutions prepared were oxygenated by being exposed to air in atmospheric conditions. There was no artificial oxidation of the solution performed. Phosphate buffer saline (PBS) was prepared by mixing 50 mM K_2HPO_4 and 0.1 M KCl solution with 50 mM KH_2PO_4 and 0.1 M KCl solution until the solution reaches pH 7.3. PBS was then autoclaved and sealed in glass bottles then stored in a cool dark place until used.

4.4.2 *Escherichia coli* DH5-α culture

E. coli DH5-α was stored on LB agar plates at 4 °C. *E. coli* were sub-cultured in liquid LB broth medium the day before the experiment was performed. The LB broth was allowed to grow for 18 hours at 37 °C on a shaker at 200 rpm in baffled flasks. Bacteria were sub-cultured at 1:21 dilution in fresh LB broth in baffled flasks and incubated at 37 °C on a shaker for 2 hours. Bacteria were subsequently harvested by centrifugation at 3261 g and washed twice in 10 ml of sterile PBS before finally re-suspending in PBS. Cell density measurements were performed at $OD_{600 \, nm}$ using a Cecil CE1020 UV spectrometer. The cell suspension was kept on ice for up to 5 hours until cells were needed for assaying.

4.4.3 Electrochemical measurements

An electrochemical cell consisting of a Ag/AgCl reference electrode, 3 mm diameter glassy carbon working electrode and platinum counter electrode were used in the cyclic voltammetric studies. A Gamry 600 potentiostat with data acquisition software was used for electrochemistry experiments. The glassy carbon electrode was polished with 50 nm

alumina powder for 5 min prior to each CV being performed. Cyclic voltammetric studies were performed on solutions of 2 mM ferrocene carboxylic acid (FcA) and ferrocene methanol (FcMeOH) in PBS. The voltammograms were recorded using an initiating potential of 0 V with a switching potential of 0.6 V and an end potential of 0 V. CVs in the absence of *E. coli* and fresh water samples cells were generated at scan rates from 5 to 2000 mV s^{-1} for FcA and FcMeOH in the presence of air (oxygenated). Additionally, cyclic voltammetry was performed on deoxygenated solutions containing FcMeOH and FcA that were purged of oxygen with oxygen free nitrogen, at scan rates of 5–40 mV s^{-1} and 5 mV s^{-1}, respectively.

4.4.4 Electrochemical determination of bacterial cell numbers

Before each assay, 0.5, 1, 1.5, 2, 2.5, 3, 3.5, and 4 OD of *E. coli* were pre-incubated with 10 mM of glucose in PBS at 37 °C on a shaker in conical flasks for 30 minutes. These solutions were then diluted by half. FcA was then added to give a final concentration of 2 mM and cyclic voltammograms (CVs) were recorded at 5mVs^{-1}.

4.4.5 Cytotoxicity measurements

A 5 ml stock solution containing *E. coli* (4 OD) was prepared in PBS, containing 10 mM glucose as the growth substrate and HPLC grade ethanol at a final concentrations of 0, 2.5, 5, 10 and 12.5%, v/v. This *E. coli* suspension was then incubated in a shaking incubator at 37 °C for 1 hour. Optical density (OD) measurements were taken before and after incubation to verify if any cellular growth occurred during the 1 h incubation. For electrochemical interrogation, a 3.5 ml sample of the incubated *E.coli* suspension was added to 3.5 ml of 4 mM FcA in PBS. This gave a final working assay concentration used in cyclic voltammetric studies of *E. coli* at 2 OD and FcA at a concentration of 2 mM. Cyclic

voltammetry was then performed at a scan rate of 5mVs^{-1}. For agar plate growth assays, the *E. coli* suspension was diluted to 1:1000, 1:100,000, 1:500,000 and 1:1,000,000 prior to seeding onto the agar plates. These agar plates were then incubated for 20 h at 37 °C followed by colony counts after the incubation period.

4.4.6 Fresh water sample testing

Algae rich fresh water samples were collected from two different water sources, namely from a canal and from a stream (Vale water). None living organism controls (acellular controls) were prepared by filtering the water samples through a 0.5 μm filter. 3.5 ml of each sample was mixed with 3.5 ml of 4 mM FcA giving a final concentration of 2 mM FcA. Cyclic voltammetry was then performed at a scan rate of 5 mV s^{-1}.

4.5 Results and discussion

4.5.1 Catalysis of superoxide

Two experiments were conducted to confirm the post oxidation peak of FcA CVs were electro-catalytic peaks. The first experiment, a scan rate study was conducted on 2 mM of FcA in PBS. The summary of the post oxidation peak currents of FcA would confirm if the rate limiting step in the system is a chemical-chemical step or an electrochemical step in two ways. Firstly, the scan rate studies show that the post-oxidation peak current of FcA decrease as the scan rate increase (**figure 4.5.1.1**). Secondly, plotting the post-oxidation peak current of FcA in a current functional plot (**figure 4.5.1.2**), demonstrates that the FcA post-oxidation peak is not under diffusion control but indicates that the rate limiting step is a relatively slow chemical step. This is because the data line is linear with a gradient [8].
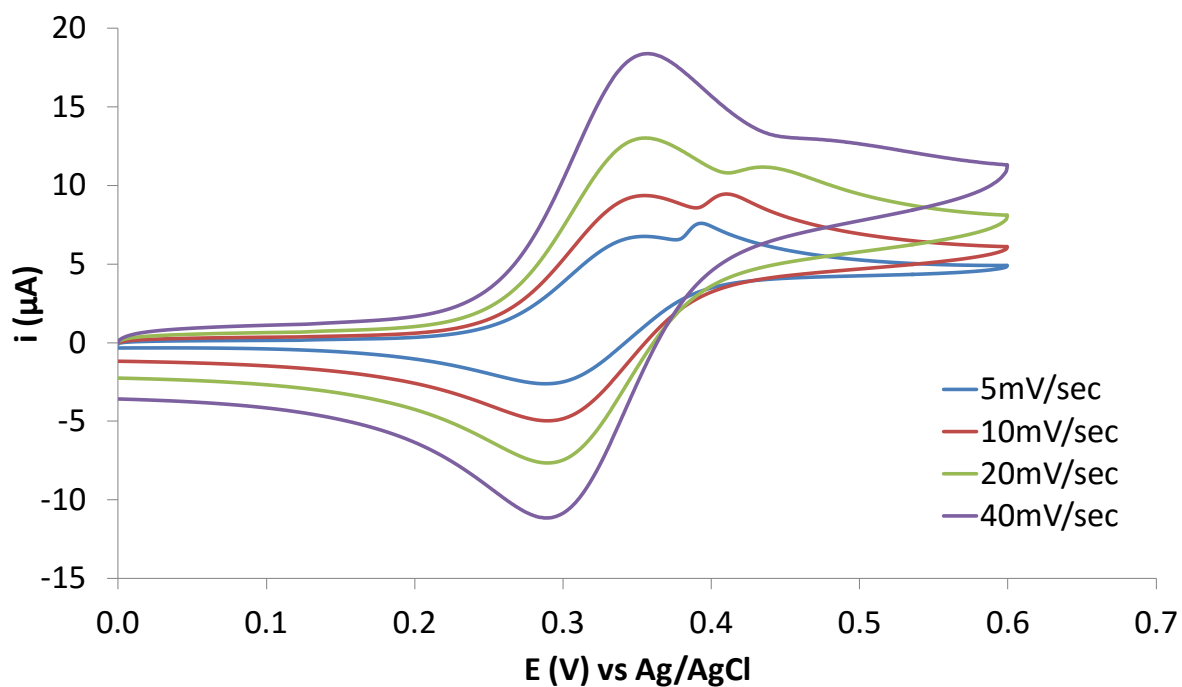
Figure 4.5.1.1 Cyclic voltammogram showing the FcA post-oxidation peak current decrease

with the increase in scan rate.
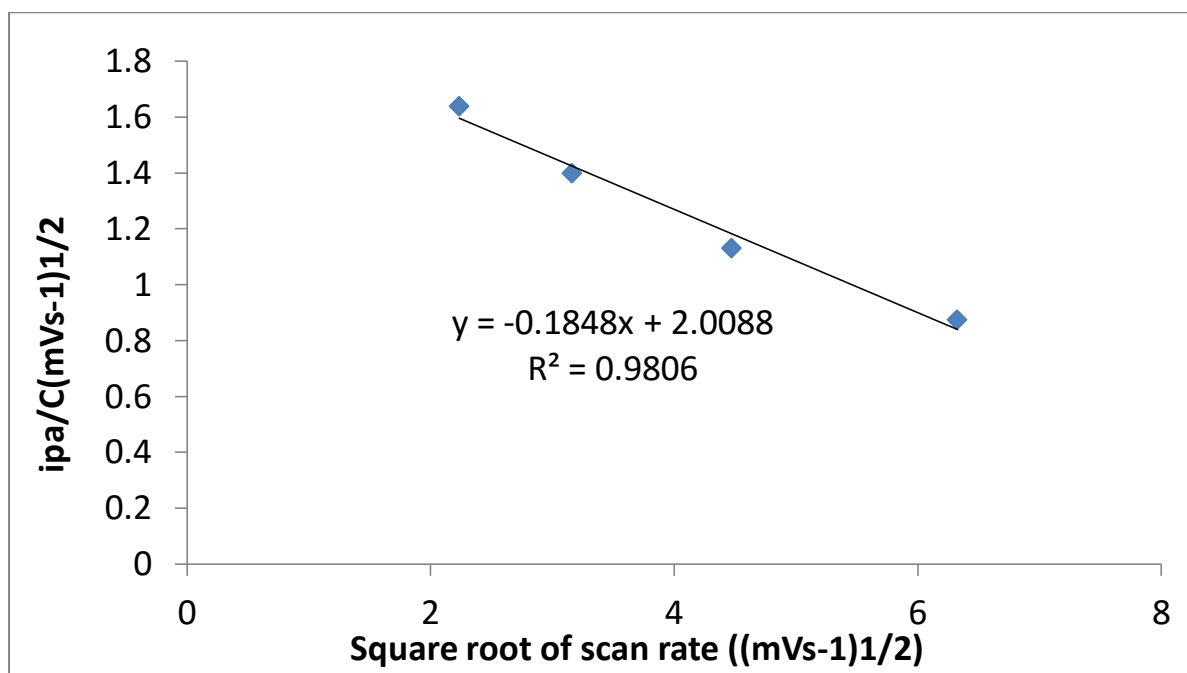
Figure 4.5.1.2 Current function plot of FcA post-oxidation peak. This FcA post-oxidation

peak is not under diffusion control because the line is linear with a gradient.

In the second experiments, CVs were conducted with nitrogen purged and non-purged FcA samples (**figure 4.5.1.3**). If the post oxidation peak of FcA was an O_2 catalytic peak, removing oxygen from the samples should also remove the post oxidation peak. The data shows purging of samples with nitrogen, removing all oxygen by displacing with nitrogen in solution, removes the post-oxidation peak.

Figure 4.5.1.3 Typical cyclic voltammograms recorded from PBS solutions containing

2 mM FcA in the absence of air (deoxygenated) and the presence

of air (oxygenated).

Revisiting the data shown in the preliminary studies **section 3.5.2**, and the additional data from the scan rate studies of FcA and oxygen containing vs nitrogen purged sample studies, there is evidence that the FcA post-oxidation peak is directly related to the concentration of dissolved oxygen in the samples. In **figure 3.5.2.1**, the FcA post-oxidation peak current of samples containing *E.coli* is dramatically smaller than in samples that do not contain *E.coli*. This smaller post-oxidation peak can be explained as a result of *E.coli* consumption of

oxygen in aerobic metabolism during the period of experiment. Therefore, the source of superoxide is decreased, resulting in a smaller post-oxidation peak.

4.5.2 Confirmation of FcMeOH catalytic property

Before conducting electrochemical characterisation experiment of FcA and FcMeOH, it was important to confirm FcMeOH also displays the superoxide catalytic property as seen in FcA and FcDA [3]. Therefore, CVs were performed on oxygenated and deoxygenated solutions of PBS containing 2 mM FcMeOH. Typical CVs obtained are shown in **figure 4.5.2.1**. Data shows that FcMeHO has a decreased i_{pa} in deoxygenated solutions compared to oxygenated solutions. This confirmed that FcMeHO does have superoxide catalytic properties due to the same mechanism explained earlier, and shows the same convoluted O_2 catalytic peak that has been observed in other FcDA study [3].
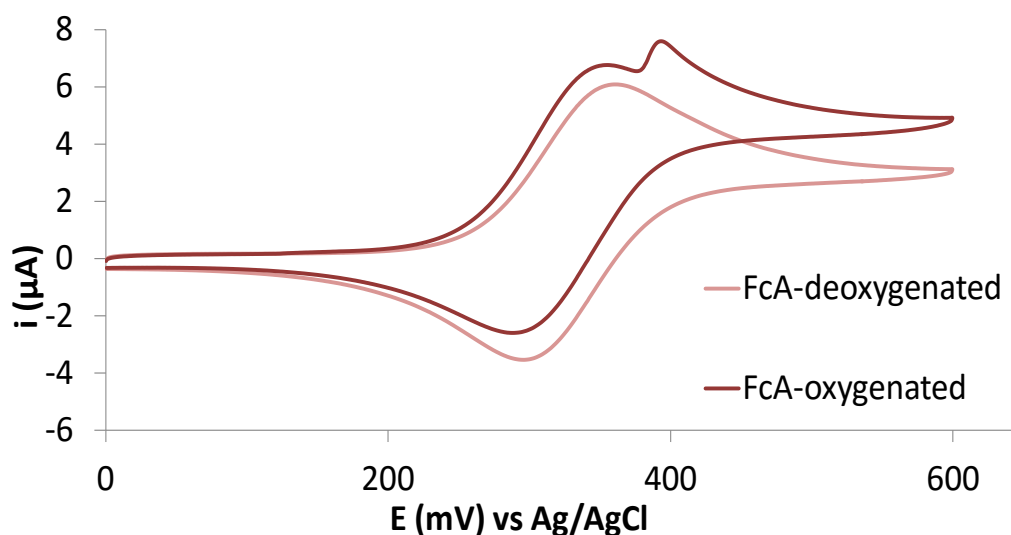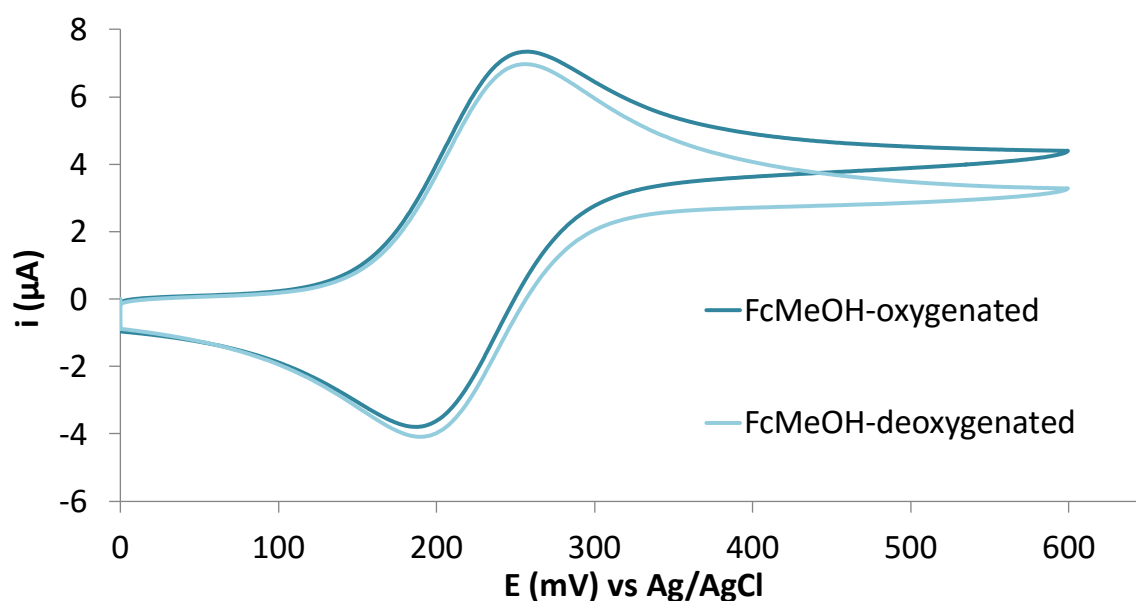

Figure 4.5.2.1 Typical cyclic voltammograms recorded from PBS solutions containing 2 mM FcMeOH in the absence of air (deoxygenated) and the presence of air (oxygenated).

4.5.3 Electrochemical characterisation

Following confirmation FcMeOH does have the superoxide catalytic property; Data for both CVs obtained from oxygenated and deoxygenated 2 mM FcA (**figure 4.5.1.3**) and FcMeOH (**figure 4.5.2.1**) were put together for comparison (**figure 4.5.3.1**). The overall electrochemical characterisation studies were then conducted.
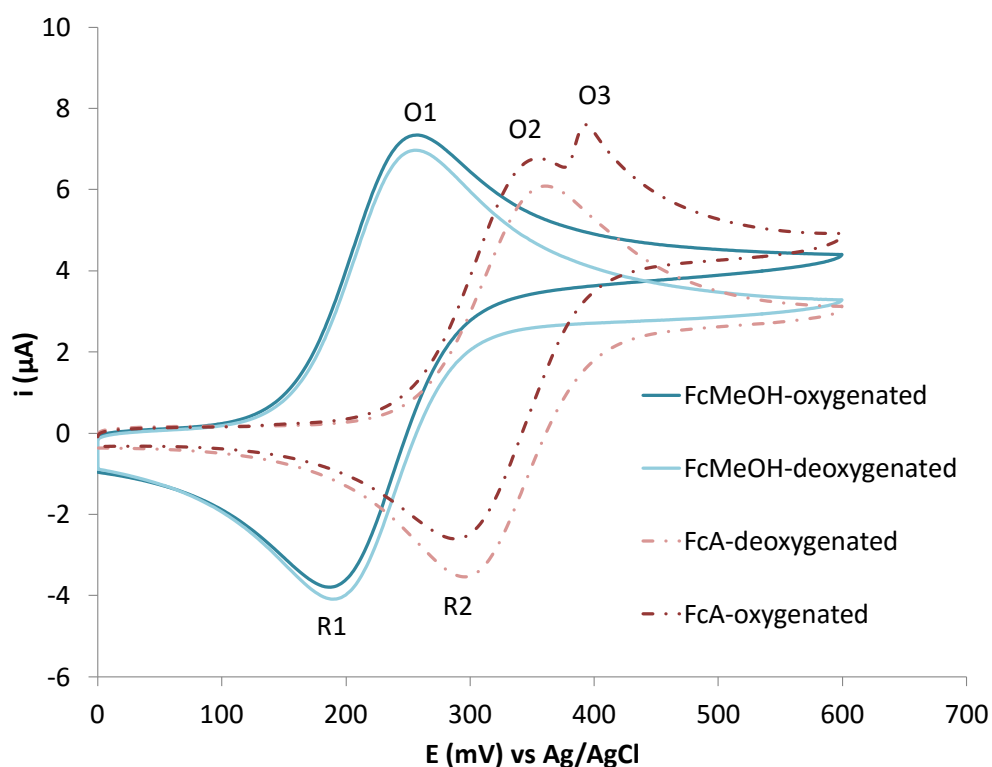
Figure 4.5.3.1 Summary of cyclic voltammograms recorded from PBS solutions containing2 mM FcMeOH (**figure 4.5.2.1**) and FcA (**figure 4.5.1.3**) in the absence of air (deoxygenated) and the presence of air (oxygenated).

There is a major difference between the CVs recorded from solutions containing FcA and FcMeOH in the presence of air. When CVs were generated in the presence of oxygen and FcMeOH only one oxidation peak was obtained at a mean peak potential of 257 mV (**figure 4.5.3.1** O1). However, when CVs were recorded in the presence of FcA and oxygen two

oxidation peaks were observed (**figure 4.5.3.1** O2 and O3) at mean peak potentials of 352 mV and 394 mV. The mean separation in peak potential (ΔE_p) for FcA and FcMeOH is 66 mV ($\pm 1SD=1.572$) and 70 mV ($\pm 1SD=4.561$), respectively. The values for the mean oxidation peak current over reduction peak current (i_{pa}/i_{pc}) are 0.993 ($\pm 1SD=0.022$) and 0.997 ($\pm 1SD=0.007$), respectively. These values indicate that both FcA and FcMeOH are displaying a quasi-reversible electrochemical behavior [9, 10]. The mean peak potential (E_p) values for FcMeOH are 257 mV ($\pm 1SD=3.194$) for the oxidation peak and 187 mV ($\pm 1SD=1.518$) for the reduction peak, whereas in the case of FcA, they are 353 mV ($\pm 1SD=0.643$) for the oxidation peak and 287 mV ($\pm 1SD=1.692$) for the reduction peak. These values for FcMeOH and FcA are similar to the values reported in the literature[9]. Additionally, a second oxidation peak is observed at approximately 394 mV ($\pm 1SD=1.510$), which is slightly higher than 317 mV reported in Cassidy's study [3] and is likely due to the use of different electrolytes. From Cassidy's report, i_{pa} of FcDA is around 368 mV versus SCE which is equivalent to 413 mV versus Ag/AgCl [11]. This study showed FcMeOH requires much less energy to trigger the electrochemical redox event than FcA and FcDA (See **figure 4.5.3.1**) as highlighted by the lower peak potential values. This would be advantageous to an electrochemical bio-oxygen demand assay, since the applied potential for the cyclic voltammteric scans would be lower, and therefore, lowering the risk of influencing cellular membrane potential [7], thereby avoiding perturbations of cells metabolism induced by electronic fields. Additionally, it minimises the possibility of encountering problems with interfering species.

We suggest that the difference in behavior observed for FcA, FcMeOH and FcDA (from Cassidy's report) [3] in terms of the position of peak potentials is caused by the different functional groups. FcA contains 1 carbonyl group, FcDA contains 2 carbonyl groups and

FcMeOH contains 1 hydroxyl group. The electron withdrawing effect of the carbonyl group adjacent to the cyclopentadienyl ring would lead to lowering the electron density around the iron (Fe^{2+}) center, meaning the ferrocene requires a larger over-potential to be oxidized and evidence for this behavior has been reported by others for different ferrocene derivatives[12, 13]. This would decrease the ability of the Fe^{2+} to lose electrons, therefore, as observed, a higher potential is required to electrochemically oxidize FcDA compared to FcA, and even higher compared to FcMeOH, resulting in FcMeOH having a lower redox potential than FcA (figure 4.5.3.1) and FcDA [12, 13].

A scan rate study was performed with solutions of FcMeOH and FcA and typical peak current obtained at the varying scan rates are plotted in figure 4.5.3.2. The peak currents for both FcA (▲) and FcMeOH (◆) are proportional to the square root of the scan rate. This well-known behavior indicates that the peak current is under diffusion control. We also noted that at higher scan rates the electrochemical O_2 peak (figure 4.5.3.1 peak O3) observed for FcA is no longer present. We were interested in ascertaining the rate of diffusion of the mediators as this can influence the sensitivity of the system. Using the Randles-Sevcik equation ($i_p=(2.69x10^5)n^{3/2}AD^{1/2}Cv^{1/2}$), the diffusion coefficient (D) of FcMeOH and FcA were calculated from 5 mVs^{-1} oxidation peak data (Peak O1 and O2 from figure 4.5.3.1). The diffusion coefficient for FcMeOH (D=7.87 x 10^{-7} cm^{2}s^{-1}) is similar to that reported in the literature (D=2.50 x 10^{-7} cm^{2}s^{-1}) [14]. Whereas, the diffusion coefficient for FcA (D=7.08 x 10^{-7} cm^{2}s^{-1}) is a magnitude smaller than reported in literature (D=4.30 × 10^{-6} cm^{2}s^{-1}) [10]. It is not a surprise that the diffusion coefficient for FcMeOH and FcA obtained in our study are not identical to those reported in the literature, since the viscosity of the room temperature ionic liquids used would greatly influence the diffusion coefficient of the mediator[14]. We show that FcMeOH has a faster diffusion coefficient than FcA in

106

our study, which could be explained by the fact that FcMeOH (Mw=216.06 g mol^{-1}) is a smaller molecule than FcA (Mw=274.05 g mol^{-1}).

At this stage, data was suggesting that FcMeOH was the most ideal mediator, as it has the lowest redox potential among FcA and FcDA [3] along with a faster diffusion rate than FcA. It should provide the most sensitive system of the three mediators with the lowest risk of interference.
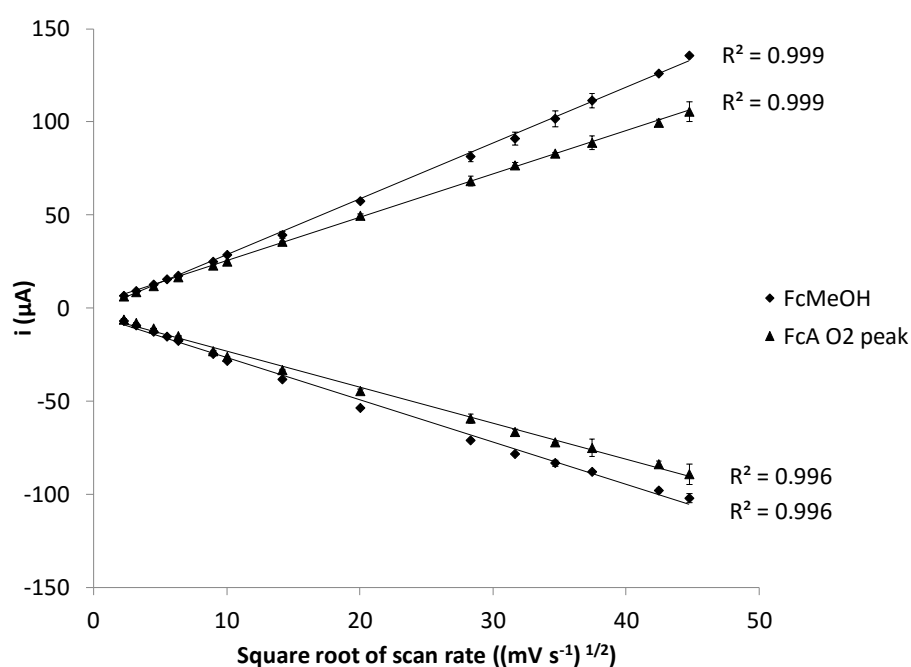
Figure 4.5.3.2 Plot of oxidation and reduction peak currents versus square root of scan rate from CVs obtained for FcA (see **figure 4.5.3.1** O2) and FcMeOH (see **figure 4.5.3.1** O1) at varying scan rates.

4.5.4 Further confirmation of locations of O$_2$ catalytic peak and investigation of catalytic kinetics

The magnitude of peak current for FcMeOH (**figure 4.5.3.1** O1) and FcA (**figure 4.5.3.1** O3) is dependent on the presence of oxygen. This was shown by comparing the oxidation

peak current obtained from CVs scaled with FcMeOH solution in the presence (**figure 4.5.3.1** O1-oxygenated, mean = 6.75 µA, ±1SD = 0.037) and absence (**figure 4.5.3.1** O1-deoxygenated, mean = 6.48 µA, ±1SD = 0.053) of oxygen. This comparison showed that CVs recorded in the presence of oxygen resulted in an increase in the magnitude of the O1 peak of approximately 200 nA and the equivalent decrease in the reduction peak occurred (**figure 4.5.3.1**). The magnitude of the oxidation peak current measured from CVs recorded with solutions of FcMeOH which can be attributed to oxygen, is equal to the difference between the peak current obtained in the presence and absence of oxygen. We conclude that any current generated which is associated with the presence of O_2 is convoluted with the normal FcMeOH electrochemistry. Additionally, results from the current function plots for FcMeOH (**figure 4.5.4.1**) also supports this proposition as the correlation coefficients obtained at low scan rates prior to subtracting the deoxygenated peak ($R^2 = 0.965$) lies between the deoxygenated correlation coefficient value of $R^2 = 0.752$ and O_2 electrocatalytic current correlation coefficient value of $R^2 = 0.982$. However, when cyclic voltammetry was performed with solutions of FcA in a deoxygenated solution, the O3 peak current associated with the presence of oxygen (**figure 4.5.3.1** O3) was no longer observed. We conclude that the O3 peak (**figure 4.5.3.1**) observed in the CV recorded in the presence of FcA arises from the existence of oxygen in the assay solution. For simplicity the current that is attributed to the presence of oxygen is termed the O_2 electrocatalytic current.
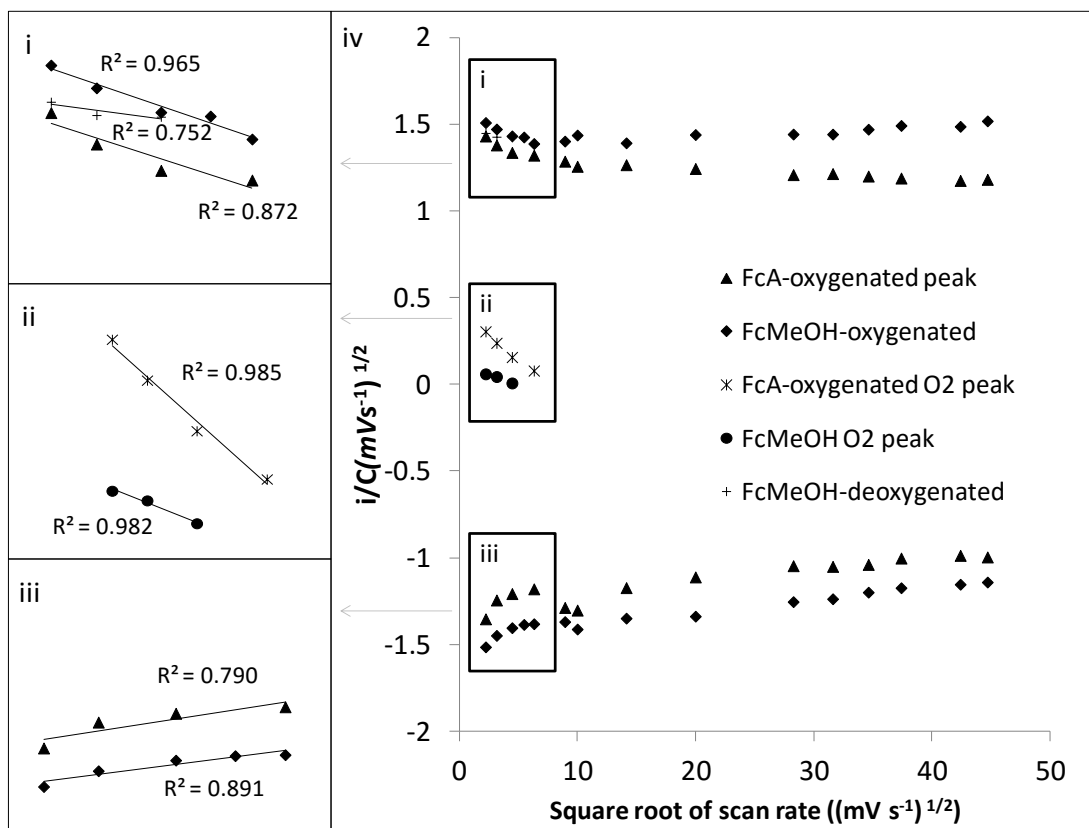
Figure 4.5.4.1 Current functional plot of i_{pa} and i_{pc} for FcA and FcMeOH; peak currents obtained from cyclic voltammograms recorded from solutions of FcMeOH-oxygenated ◆, FcMeOH-deoxygenated +, non-electrocatalytic FcA-oxygenated (**figure 4.5.3.1** O2) ▲, FcA-oxygenated O_2 electrocatalytic peak * (**figure 4.5.3.1** O3), difference between peak currents obtained for FcMeOH-oxygenated and FcMeOH-deoxygenated which termed the electrocatalytic O_2 peak ● < 20 mV s^{-1}). Insets represent current values at lower scan rates.

In order to understand the mechanistic control and provide further evidence that electrocatalysm was occurring via the mechanism proposed. Investigations into the kinetics of the reaction were performed using cyclic voltammograms of the FcA and FcMeOH at varying scan rates in both oxygenated and deoxygenated solutions. Peak currents obtained from cyclic voltammograms performed at varying scan rates were then plotted into a current functional plot (**figure 4.5.4.1**). At higher scan rates there is no relationship with current

function (**figure 4.5.4.1 iv**). This lack of relationship at relatively fast scan rates is indicative of a diffusion limited process and supports the data obtained in **figure 4.5.3.2**. However, when we analyze the plot at slower scan rates there is a deviation from this behavior when oxygen is present both for FcA and FcMeOH (**figure 4.5.4.1 i, ii, and iii**) and is indicative of an electrocatalytic process [15].

In the absence of oxygen, the current function plot for FcMeOH (<20 mV s^{-1}) yields a correlation coefficient value of $R^2=0.752$ (**figure 4.5.4.1 i**), suggesting the current is diffusion limited as expected for a simple 1 electron transfer event. On the other hand, in the presence of oxygen the electrocatalytic current obtained for FcMeOH (attained by subtracting the peak current obtained in the presence of oxygen minus the peak current obtained in the absence of oxygen) is directly correlated to scan rate in the current function plot with a correlation coefficient value of $R^2=0.982$, indicative of a non-diffusion limited process (**figure 4.5.4.1 ii**). This relative large correlation provides supporting evidence that the electrocatalysis is occurring via the proposed E-C-E mechanism and we attribute this deviation to a slow chemical step which is rate limiting.

The correlation coefficient values obtained for current function plot for the non-electrocatalytic FcA peak (**figure 4.5.3.1** O2) in the presence of oxygen yields a relatively low correlation coefficient value of $R^2=0.872$ at low scan rates (**figure 4.5.4.1 i**). This indicates that the peak current even at slower scan rates (<40mV s^{-1}) is under diffusion control as expected for a simple 1 electron transfer redox process. Moreover, the current function values obtained for the electrocatalytic O_2 peak for FcA (**figure 4.5.4.1 ii**) yield a correlation coefficient of $R^2=0.985$ indicating the current is under non-diffusion control and we suggest this arises due to this peak representing the electrocatalytic oxidation. This

deviation from diffusion controlled behavior is attributed to the chemical step being rate limiting which is similar behavior to that observed with FcMeOH. Consequently, oxidation peak O2 (**figure 4.5.3.1**) is largely non-catalytic current arising from the redox events of the FcA alone whereas the electrocatalytic O_2 peak (**figure 4.5.3.1** O3) represents the electrocatalytic oxidation of superoxide.

The proposed mechanism for O_2 electrocatalytic current with FcA and FcMeOH is attributed to the oxygen which is electrochemically reduced at 0 V forming a superoxide anion (O_2^-) and is supported by Cassidy[3]. This conclusion is elucidated by the fact that on removal of the oxygen there is a decrease in current observed with FcMeOH (**figure 4.5.3.1**) and removal of the electrocatalytic O_2 peak in CVs obtained for FcA. The O_2^- subsequently chemically oxidises water forming the reactive oxygen species hydroxyperoxyl (HO_2^-) and a hydroxyl ion (OH^-). As we scan through the voltammogram in a forward direction the Fc is electrochemically oxidised to Fc^+. We suggest the OH^- and HO_2^- generated chemically reduce Fc^+ to Fc and at the same time the chemically reduced mediator would be once again electrochemically oxidised. This leads to a catalytic enhancement in the magnitude of the oxidation peak current as the concentration of reduced Fc is increased in the presence of oxygen. Moreover, it is well understood that peak current is proportional to concentration of redox molecules under investigation and explains why in deoxygenated solutions we see a decrease in the electrocatalytic peak oxidation current for FcMeOH and FcA. The mechanism we propose is an electrochemical-chemical-electrochemical (E-C-E) system. It can be presumed that the chemical steps must be relatively slow because with increasing scan rate there is no increase in the observed O_2 electrocatalytic current above 20 mVs^{-1} for FcMeOH, and 40 mV s^{-1} for FcA. We suggest that the reason for this difference is because the rate at which the chemical step occurs is slower with the FcMeOH than the FcA. This is

also supported by **figure 4.5.4.2** in which we show the actual charge transfer coefficient for the electrocatalytic oxidation is fast for the FcA when compared to FcMeOH. Consequently, FcA produces a larger electrocatalytic current under the same condition. On the other hand, according to Cassidy's study of FcDA, it was suggested that FcDA has an even faster electrocatalytic kinetics toward superoxides than FcA. This is because the O_2 electrocatalytic current of FcDA does not disappear even at scan rate 100 mV s^{-1} [3].

This behavior of the O_2 electrocatalytic peak for FcA is de-convoluted, whilst for FcMeOH it is convoluted, and occurs at higher potentials than the simple non-electrocatalytic current for the FcA which could also be explained by the different functional groups. This difference is caused by the fact that after the Fc is oxidized into Fc$^+$, the Fe^{3+} centre interacts with the surrounding OH$^-$ and HO$_2^-$. These findings suggest that the Fe^{3+} centre is instantaneously reduced by the reactive oxygen species forming an adduct, wherein the carbonyl group on the FcA makes the adduct relatively stable. This causes a further lowering of the electron density of the iron centre when compared to FcA alone. As a result, an even higher oxidation peak potential is needed to oxidise FcA resulting in the separation of the O_2 electrocatalytic peak. On the other hand, the FcMeOH adduct is not stabilized and instantaneously oxidises. Therefore, the catalytic signal seen for FcMeOH is not separate from the normal FcMeOH signal when compared with the FcA.

The oxidation peak potential of FcMeOH (**figure 4.5.3.1** O1) and FcA (**figure 4.5.3.1** O2 and O3) obtained from cyclic voltammograms performed in the presence of oxygen were plotted against logarithm of scan rate (**figure 4.5.4.2**). As seen from the figure, there were no changes in oxidation peak potential for scan rates up to about 100 mVs^{-1} in the case of FcMeOH (**figure 4.5.4.2** FcMeOH O1 peak) and FcA non-electrocatalytic peak (**figure**

4.5.4.2 FcA O2 peak). For scan rates beyond 100 mVs^{-1}, both peak potentials mentioned changed linearly with log of scan rate with correlation coefficient values of R^2=0.937 and R^2=0.955 for FcA-oxygenated non-catalytic peak (**figure 4.5.4.2** FcA O2 peak) and FcMeOH-oxygenated (**figure 4.5.4.2** FcMeOH O1 peak). On the other hand, the FcA electrocatalytic peak (**figure 4.5.4.2** FcA O3 peak) yielded a correlation coefficient value of R^2=0.964 from very low scan rates (5mVs^{-1} to 40 mVs^{-1}). These observations indicated FcMeOH (**figure 4.5.4.2** FcMeOH O1 peak) and FcA-non-electrocatalytic peak (**figure 4.5.4.2** FcA O2 peak) were quasi-reversible over the scan rate range of 5 to 100 mVs^{-1} and irreversible beyond 100 mVs^{-1}. Whereas in the case of the FcA electrocatalytic process (**figure 4.5.4.2** FcA O3 peak) is irreversible from 5-40 mV s^{-1}.

By comparing the graphical lines for the irreversible behavior we can ascertain that the electrocatalytic current for FcMeOH is convoluted with the non-electrocatalytic current. We can calculate the charge transfer coefficients (αn_a) for the various peaks by using **equation 4.1** in which, $\Delta E_{pa}/\Delta \log v$ is equivalent to the gradient of the plots obtained in **figure 4.5.4.2**.

Equation 4.1

$$\frac{\Delta Epa}{\Delta log v} = \frac{2.3RT}{2\alpha na F}$$

In which Epa (V) is the oxidation peak potential, v is scan rate in mV s^{-1}, n_a is the number of electrons in the rate determining step and α is the charge transfer coefficient in which with increasing faster charge transfer process. R is the standard gas constant, T is the standard temperature in Kelvin at 25°C.

The charge transfer coefficient value of 0.28 was obtained for the FcA non-electrocatalytic peak. In contrast, the FcA electrocatalytic peak (**figure 4.5.4.2** FcA O3 peak) has an α value of 0.77 for one electron. This indicates two electrons are involved in this oxidation. However, due to the nature of FcMeOH electrocatalytic peak and non- electrocatalytic peak being convoluted, the FcMeOH electrocatalytic peak potential just simply cannot be extract for the α value calculation.
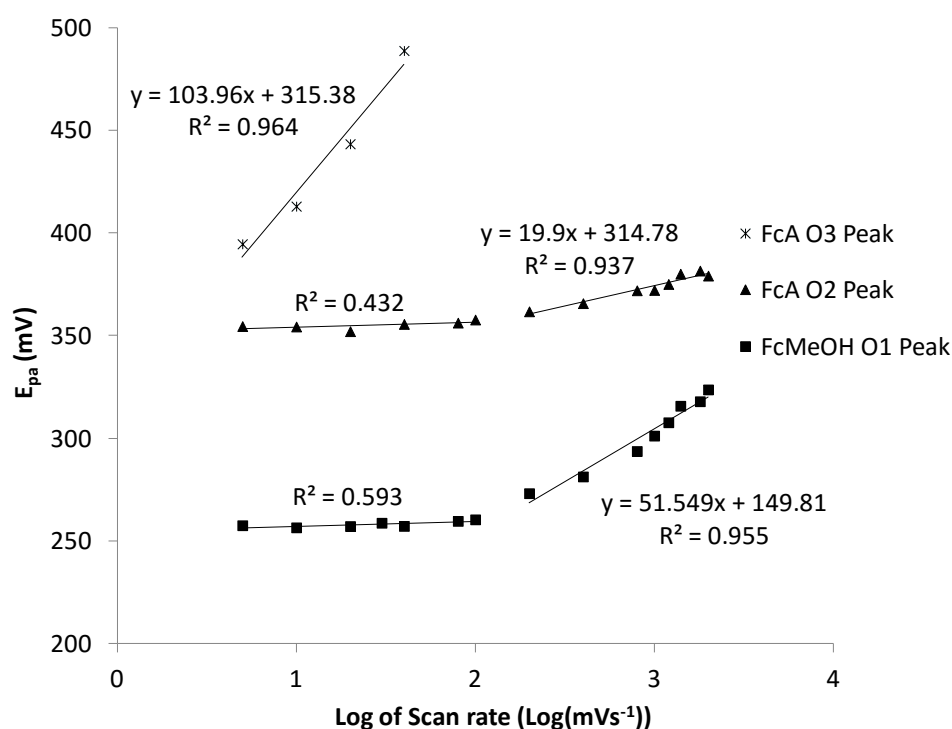

Figure 4.5.4.2. Oxidation peak potential versus logarithm of scan rate measured for FcMeOH-oxygenated, FcA-oxygenated.

Combining the data discussed for FcA, FcMeOH and Cassidy's report on FcDA, FcA was specifically chosen for the next part of our study for the following reasons: Despite FcMeOH having the lowest E_{pa} making it the most favourable mediator in a biological

system, the slower chemical electron transfer kinetics in the reduction of FcMeOH in the presence of oxygen would make the system less sensitive. FcDA has the fastest catalytic redox kinetics with the superoxide but also has the highest E_{pa}. This is the least favourable because a high potential could disturb the cellular membrane potential [7]. FcA has a unique and separate electrocatalytic O_2 peak, which is favourable, because this would simplify the system of study. In the absence of a unique and separate electrocatalytic O_2 peak, two CV studies are conducted in the presence of and absence of oxygen in order to obtain the electrocatalytic signal. In the case of FcA, a single CV can be recorded from which the electrocatalytic O_2 peak is directly measured.

4.5.5 Testing on biological model

E. coli (strain DH5α) was used to characterise the ability of FcA to monitor cellular respiration via oxygen concentration. Optical density measurements were calibrated by determining the *E. coli* cell numbers, using a haemocytometer, in 1 ml of 1 OD solution. According to the counting, it was about 54,441,260.7 cells in 1 ml of a 1 OD suspension. This was followed by serial dilution of the stock *E. coli* solution to the appropriate concentrations in PBS. The cell solution was subsequently pre-incubated with 10 mM of glucose then mixed to a final concentration of 2 mM FcA. Two consecutive cyclic voltammograms were performed on solutions containing varying numbers of cells (0, 0.25, 0.5, 1.75, 1, 1.25, 1.5, 1.75 and 2 OD) and **figure 4.5.5.1** summarises the first of the two consecutive cyclic voltammograms conducted to demonstrate the magnitude of the FcA electrocatalytic O_2 peak. As expected, an increase in *E. coli* concentration in the system leads to an increase in oxygen consumption, and therefore, a decrease in the electrocatalytic O_2 peak current (**figure 4.5.5.1 (i)**). In addition, the decrease in the electrocatalytic O_2 peak current is directly proportional to the increase in *E. coli* cell numbers (**figure 4.5.5.1 (ii)**).

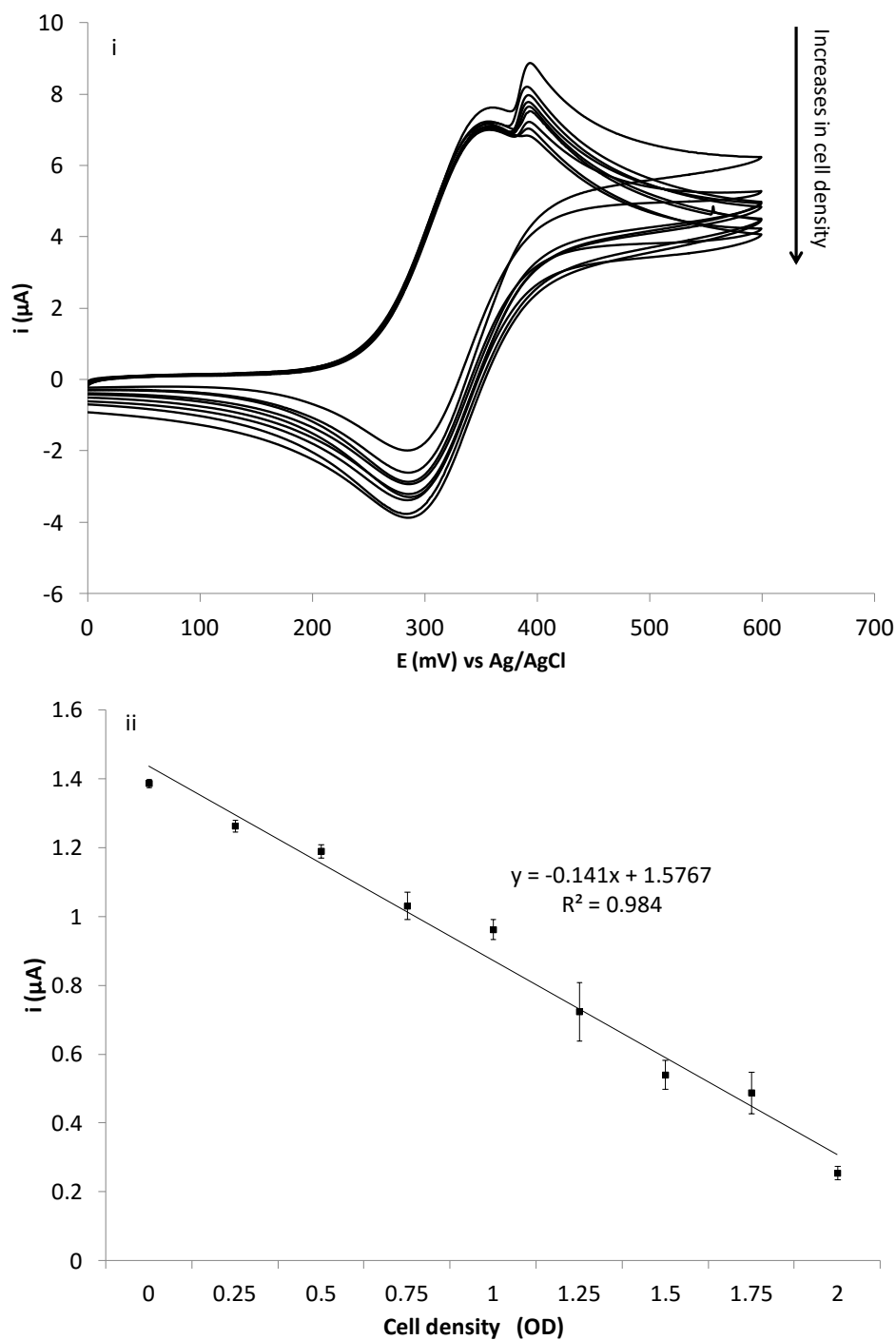**Figure 4.5.5.1 (i)** Shows typical CVs obtained for the first of the two cycles for solutions

containing different *E. coli* concentration of 0, 0.25, 0.5, 0.75, 1, 1.25, 1.5, 1.75, and 2 OD

with 2 mM FcA. **(ii)** Shows a plot of OD_{600mn} vs. electrocatalytic O_2 peak current obtained

from cyclic voltammograms in (**i**) All CVs were performed at a scan rate of

$5 \ mVs^{-1}$. (n=8, ±1SE)

During the assay the *E. coli* would be continuously consuming oxygen, and this could be monitored in near real-time by measuring the change in the catalytic peak current between two consecutive cycles. The electrocatalytic O_2 peak current generated on the first cycle and the second cycle is exactly one cyclic voltammetric scan apart at a fixed scan rate of 5 mVs^{-1}. A plot of the electrocatalytic O_2 peak current documented from the two cycles at the varying cell concentrations can be observed **figure 4.5.5.2 (i)**. Assay solutions containing higher cell numbers resulted in a larger difference in the magnitude of the current between the cycles. It is also worth mentioning that there is always an 18% drop in the magnitude of the electrocatalytic O_2 peak observed between the first and second cyclic voltammetric cycle in the control study (cyclic voltammetry conducted in the absence of *E. coli*). This indicates that oxygen from the atmosphere cannot dissolve into solution at sufficient rates to replenish electrochemically consumed oxygen. It will therefore not interfere with measurement of O_2 in cellular assays. Therefore, any current decrease measured that was greater than 18% between the first and second electrocatalytic O_2 peak can be assigned to oxygen consumption by the *E.coli*. Moreover, a decrease in the peak current obtained for the electrocatalytic O_2 peak between the two cyclic voltammetric cycles is directly proportional to the increase in *E.coli* cell numbers (**figure 4.5.5.2 (ii)**). Using Eq. (2), the oxygen consumption rate down to a single cell level (cells per second) was calculated to be approximately 1.12×10^{-17} moles s^{-1} cell^{-1}, which is similar to the values published in the literature (4.31×10^{-20} mole s^{-1} cell^{-1}) for *E. coli* strain K-12 [16]. The difference in oxygen consumption rate observed in our study using *E. coli* strain DH5-α and the K-12 strain is likely due to the difference in metabolic demands between the two *E. coli* strains and the different culture conditions resulting in the cells being at different stages of the growth cycle. In addition, the experimental setup, the method of measurement and the experimental condition between this study and in the literature are very different. Therefore, the accuracy

and sensitivity between the different measuring methods and the conditions of the cells at the point of measurement will cause variations. More importantly, in this study, we demonstrated for the first time the simplicity and the accuracy and sensitivity of the FcA-mediated system.

Equation 4.2

(i)

$$O_2 \text{ consumption } (moles \ cell^{-1} \ s^{-1}) = \frac{(moles \ of \ O_2 \ from \ 1st \ cycle \ \times X) - moles \ of \ O_2 \ from \ 2nd \ cycle}{time \ (s) \ \times number \ of \ cells}$$

(ii)

$$moles \ of \ O_2 \ from \ each \ cycle \ = \left(\frac{i_p}{(2.99 \ x \ 10^5) n (\propto n_a)^{1/2} A D^{1/2} v^{1/2}} \right) \times volume \ in \ cm^3$$

Where: X = percentage of current drop between 2 cycles due to the limitation of oxygen diffusion to the electrode. This percentage drop varies with different electrolytes, and is obtained by doing a non-living organism control e.g. filtering the samples; i_p = the peak current (A); n = the number of electrons; α = the transfer coefficient (See **section 4.5.4**); n_a = the number of electrons in the rate limiting step; A = the surface area of the electrode (cm^2); D = the diffusion coefficient $(cm^2 s^{-1})$ calculated from the non-electrocatalytic FcA peak (**figure 4.5.3.1** O1) using the Randles-Sevcik equation for reversible system (See **section 4.5.3**); v = the scan rate (Vs^{-1}).
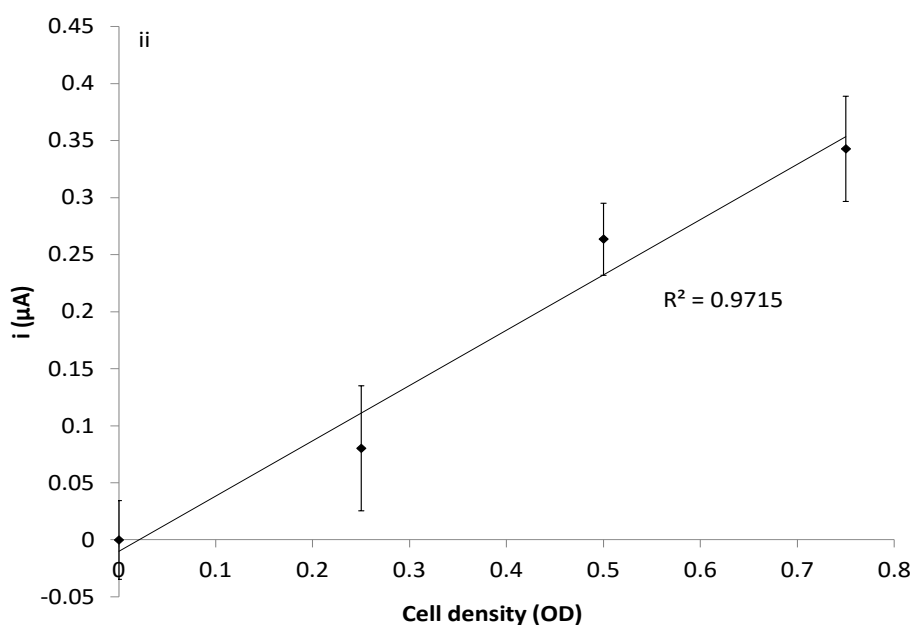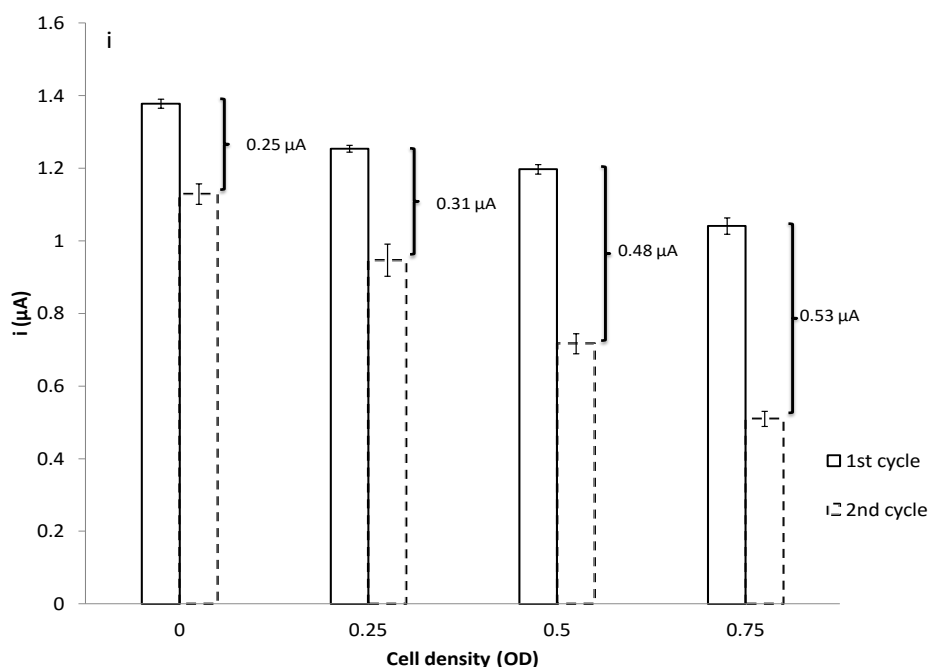
Figure 4.5.5.2 (i) A histogram of the magnitude of the mean electrocatalytic O_2 peak current obtained from the cyclic voltammogram on the first cycle and second cycle (0, 0.25, 0.5, and 0.75 OD). **(ii)** Summarizes the first and second electrocatalytic O_2 peak i_{pa} difference minus 18% (negative control – cyclic voltammetry studies conducted in the absence of *E. coli*), calculated as the limitation in the rate of oxygen dissolving into the system, (n=5, ±1SE). In addition to the detection of oxygen consumption, we have also

shown our system to be compatible in the measurement of oxygen increase in solution (see **section 4.5.7**).

4.5.6 Electrochemical cytotoxicity assay

To confirm FcA-mediated system can accurately report on the metabolic rate of cells and to demonstrate the wide capabilities of the developed assay the FcA was used to detect the toxicity of a model toxin ethanol. Cyclic voltammetry studies were conducted using a fixed number of *E. coli* (4 OD) and incubated with different concentrations of ethanol (0, 2.5, 5, 10, and 12.5% (v/v)) and 2 mM FcA. Ethanol was used because it is cytotoxic to *E. coli* through the disruption of plasma membrane [17]. It is hypothesized that an increase in ethanol concentration would lead to a decrease in the number of viable cells. Consequently, this would lead to a decrease in oxygen consumption and therefore an increase in the generated electrocatalytic O_2 peak current. In addition, a control was performed in which the optical density of *E. coli* was measured post-incubation with ethanol to ensure the same number of cells were still present prior to performing cyclic voltammetric studies to confirm any difference was not due to bulk changes in cells density. Moreover, our electrochemistry assay results for analyzing the toxic effects that ethanol had on the cells were compared to a standard viable agar plate method of toxicity testing to enable validation of our system.

The electrocatalytic O_2 peak currents generated in CVs in the presence of ethanol and cells are summarized in **figure 4.5.6.1 i**. In the presence of relatively high ethanol concentrations, a decrease in oxygen consumption and consequently increase in the electrocatalytic O_2 peak current was observed. As expected the magnitude of the peak current was inversely proportional to increase in ethanol content. A complete loss in oxygen consumption was determined at 12.5% (v/v) ethanol, indicating that no respiring cells remain since the

electrocatalytic O_2 peak current of the negative control (cyclic voltammetry studies in the absence of cells) is approximately the same as cell incubated with 12.5% (v/v) ethanol. In addition, the number of respiring cells was confirmed by the growth assay (**figure 4.5.6.1 ii**) with the increase in ethanol concentration, there was a decrease in viable cells numbers and a complete loss in cell viability at 12.5% (v/v) ethanol concentration matching the electrochemistry results. Moreover, the optical density study confirms the number of cells pre- and post- ethanol incubation was consistent, see **figure 4.5.6.1 iii**. This further demonstrated the biological compatibility and sensitivity of the FcA-mediated system. Moreover, a key advantage of toxicity assay developed was that it is much more rapid compared to the standard plate viability assay which takes 24 hours to perform compared to seconds with the our electrochemical methods. In addition, our system reports sub-lethal toxicity which is missed by the plate viability assay as we see that there is no significant difference at concentrations of ethanol obtained equal to and below 10%. This is because over the 24 hours period the cells can recover from the lower concentration and therefore the sub-lethal toxicity is missed which is reported by the electrochemistry assay. This is important and demonstrates a key advantage of our toxicity assay as pharmaceutical companies are interested in avoiding sub-lethal toxicity. The developed electrochemical method (**figure 4.5.6.1 i**) is also more precise than the plate viability assay as indicated by the much larger standard error bars (**figure 4.5.6.1 ii**).
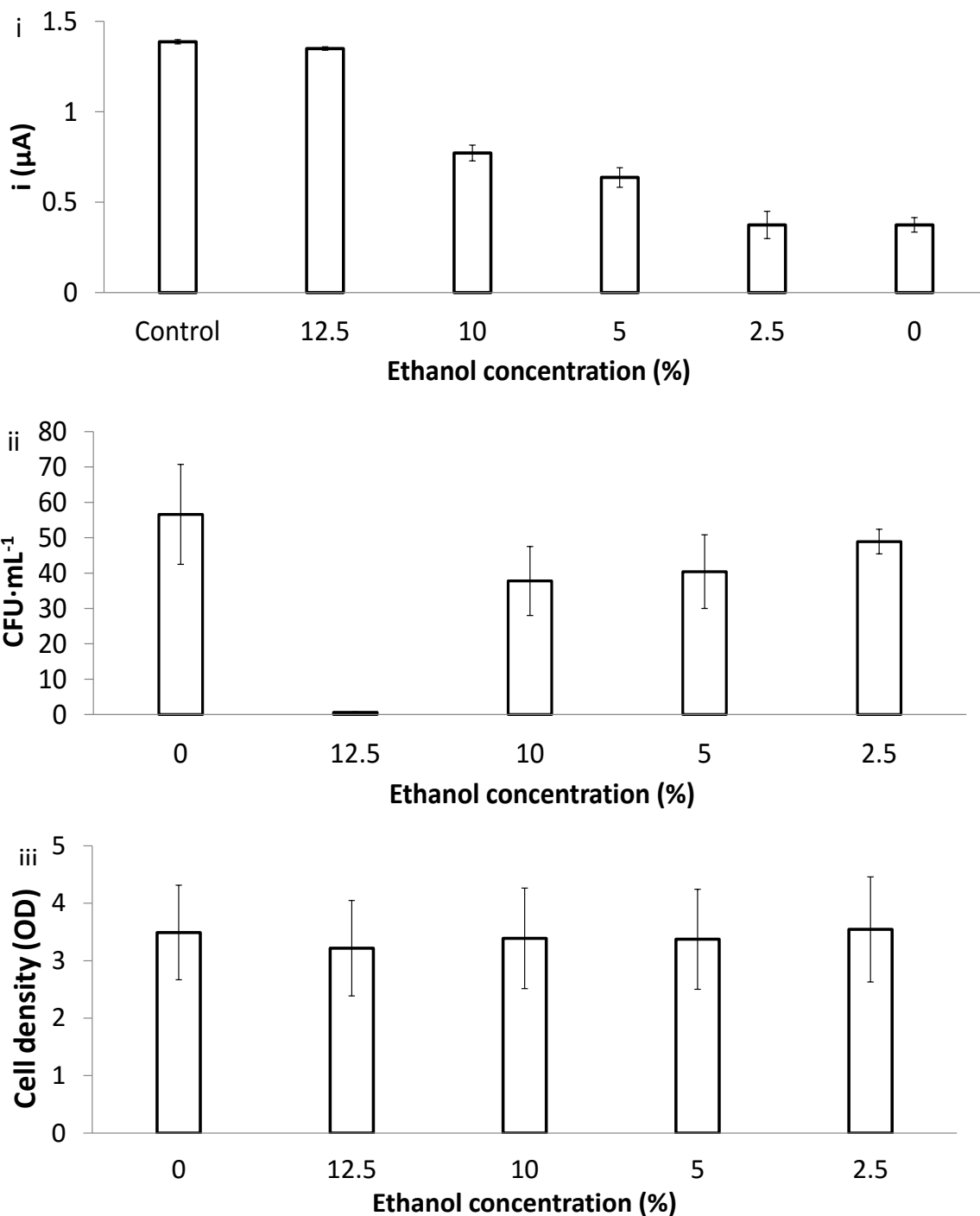
Figure 4.5.6.1 (i) Summarises the magnitude of the mean electrocatalytic O_2 peak current difference between the first and second cyclic voltammetric cycles for solutions of cells at 4 OD at varying concentrations of ethanol (0, 2.5, 5, 10, or 12.5% (v/v)). A cyclic voltammogram was conducted in the absence of *E. coli* which acted as a negative control (n=5, ±1SE). (**ii**) Summarise the mean colony counts post-ethanol incubation of same batch

of cells used in the cyclic voltammetry study (n=14-16, ±1SE). (**iii**) Summarises the mean optical density measured by UV spectrophotometer at 600 nm post-ethanol incubation of the same batch of cells used for cyclic voltammetry studies and agar plate bacterial growth assay, (n=5, ±1SE).

4.5.7 Measurement of oxygen production in samples

In order to investigate further the applicability of the developed FcA mediated oxygen demand assay for multiple applications, experiments were performed with Algae-rich fresh water samples. These were collected from nearby natural water resources, namely from a canal and from a stream (Vale water). A sample of the water sources were filtered to remove all living organisms and decaying matter, serving as acellular controls. This allowed us to obtain the standard percentage current drop due to the limitation of oxygen diffusion in different electrolyte environments. From simple observation, the water sample collected from the canal appears a darker shade of green than the water sample from the Vale (**figure 4.5.7.1 i**), suggesting that the former had higher algae content. After filtration, both water samples became clear (**figure 4.5.7.1 ii**). CVs were generated for acellular controls and raw water samples from the canal and Vale stream and the O2 electrocatalytic peak currents were measured. A summary of the current changes and percentage current changes between the two cyclic voltammetric cycles for both raw samples and control samples are plotted in **figure 4.5.7.2**. Using **Equation 4.2** part ii, the electrocatalytic O2 peak current of the first cycle can be used to calculate the overall oxygen contained in the sample. For the Vale and canal water samples a total oxygen concentration of 341.6 µM and 351.3 µM was calculated, respectively. Interestingly, during the time frame of the 2 consecutive cyclic voltammteric scans being performed on the raw environmental water samples, the oxygen

content increased which was opposite to result observed with *E.coli* solutions. In the case of *E.coli* samples, the cells were consuming oxygen in the solution therefore the decrease of the electrocatalytic O2 peak at the second cycle is greater when comparing to the acellular controls. That is if one calculates the percentage change in current between the first cycle from the second cycle of acellular control, and then subtract the equivalent percentage change calculated from the *E. coli* working sample at OD 0.75, a relative negative change when compared to the acellular control of approximately of -33% is calculated (18%-51%=-33% values obtained from **figure 4.5.5.1 ii**). The value of -33% represents an oxygen consumption. For the case of the raw water samples obtained from the Vale and canal an approximate relative change, when working samples were compared to acellular controls, of +14% and +18% were calculated, respectively. The larger value obtained for the canal sample of 18% is indicative of a high algae content as previously observed by a deeper green colour of the sample. Algae are capable of photosynthesizing and producing oxygen and consequently this experimentally proves the canal water had a higher algae content than the Vale water. In this study, the electrocatalytic O2 peak obtained from the second CV generated in the presence of the raw algae rich water samples showed a relatively much smaller decrease in the current when comparing it to the acellular controls. This indicates that there is an increase in oxygen content over time for the raw water samples. By inputting the data into **Equation 4.3**, where X is defined as in **Equation 4.2 i**, an increase in oxygen level of 2.522×10^{-9} moles s^{-1} and 3.422×10^{-9} moles s^{-1} was obtained from the vale and canal water, respectively. These experiments demonstrated that FcA mediated oxygen demand assay can also be used for detecting increases in oxygen content in solution over time, not just for detecting oxygen consumption.
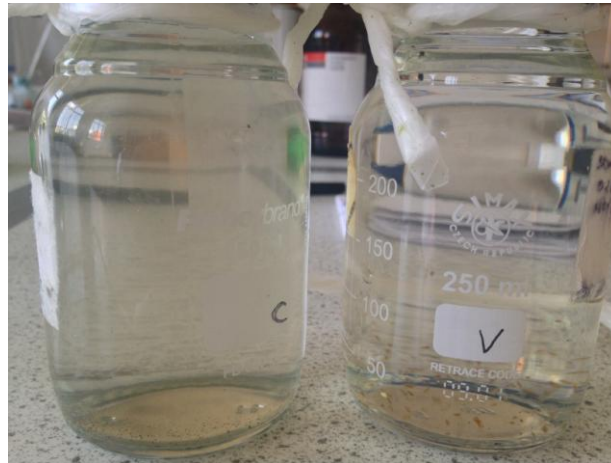
	Canal water sample	Vale water sample
i		
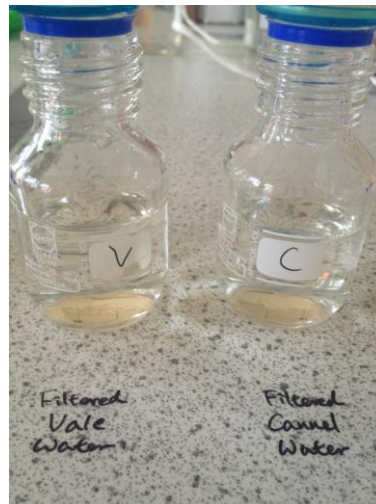
ii

Figure 4.5.7.1 (i) Image of water sample collected from canal and the stream (Vale water).

Showing water sample collected from the canal has a darker grade of green. **(ii)** Image of

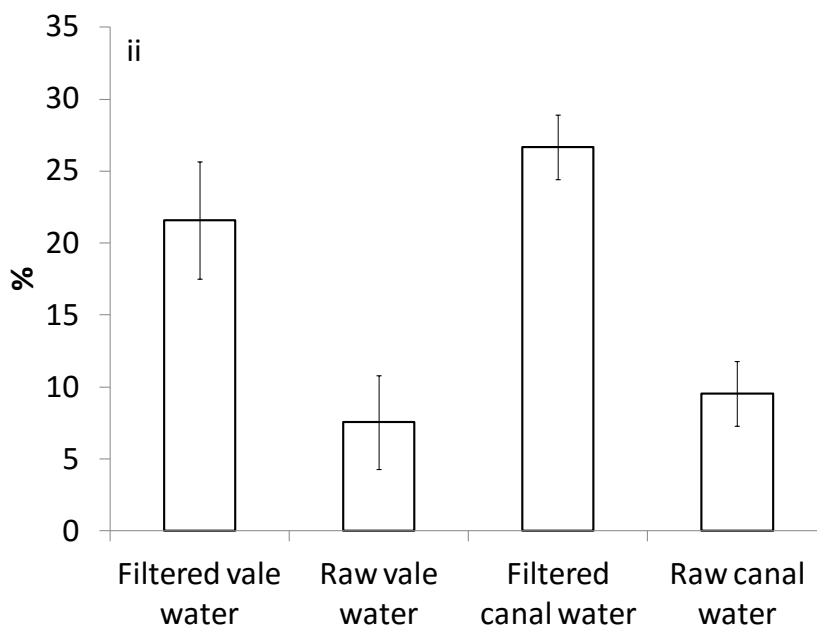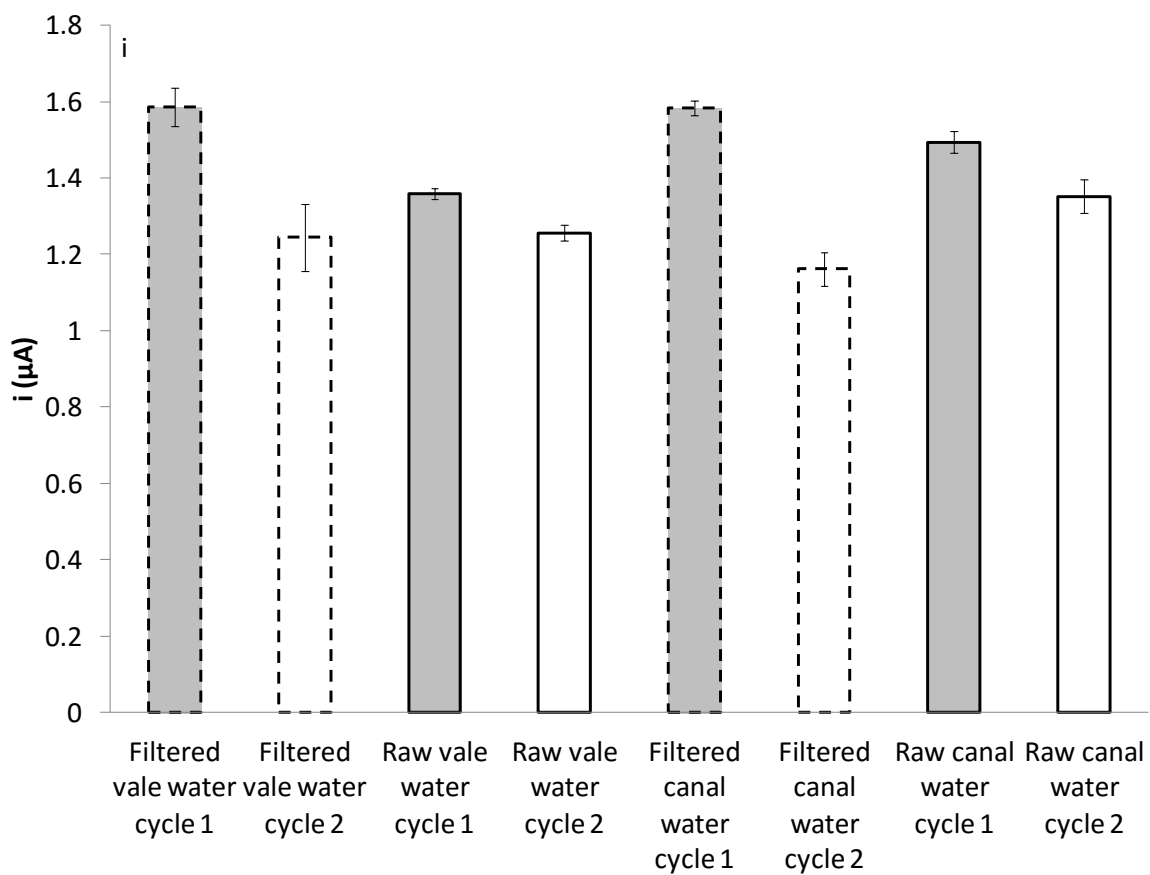both water sample after being filtered.

Figure 4.5.7.2 (i) shows a histogram of the magnitude of the mean electrocatalytic O_2 peak

current obtained from the cyclic voltammograms on the first cycle and second cycle

(Filtered and raw Vale/canal water samples (n=3)). **(ii)** shows a histogram of the mean

percentage electrocatalytic O_2 peak current drop between first cycle and second cycle in the cyclic voltammogram (Water control (n=2), filtered and raw Vale/canal water samples (n=3)) ($\pm$1SD).

Equation 4.3

$$O_2 \ increase \ (moles \ s^{-1}) = \frac{(moles \ of \ O_2 \ from \ 1st \ cycle \ \times X) - moles \ of \ O_2 \ from \ 2nd \ cycle}{time \ (s)}$$

4.6 Conclusion

In this chapter, a full investigation of FcA and FcMeOH electrochemical properties and their ability to electrocatalytically report on oxygen concentration via its interaction with OH^- and HO_2^- was conducted. Data were compared with FcDA data from Cassidy's study and the most suitable mediator was selected. The ability of FcA to monitor oxygen was taken advantage of to develop a rapid cellular respiration assay which could be monitored in near real-time, faster than any current comparable biochemical oxygen demand (BOD) assay. This assay was shown to be able to report accurately on the cell numbers present and was adapted to be used as a rapid toxicity assay on the *E.coli* model. Additionally, data showed that the oxygen demand assay developed can be used in a complex water environment to determine total oxygen concentration and shows that the method is sensitive to oxygen increases also. It is envisaged [2] that the developed assay has potential to impact on fields and industries ranging from environmental toxicology through to pharmaceutical and agrochemical industries as demonstrated by the shortening of a commercially available bio-oxygen demand assay down to minutes rather than 5 days.

The next step is to increase the sensitivity of the assay and further develop the assay into more application compatible system, e.g. mammalian cell, hand held system.

4.7 References

1. Yip, N.C., et al., *Real-time electrocatalytic sensing of cellular respiration.* Biosens Bioelectron, 2014. **57**: p. 303-9.

2. YIP, N.C., F.J. RAWSON, and P. MENDES, *Oxygene sensor comprising a ferrocene compound*. 2015, Google Patents.

3. Cassidy, J., et al., *Note on the voltammetry of ferrocene carboxylate in aqueous solution.* Electrochemistry Communications, 1999. **1**(2): p. 69-71.

4. Song, C. and J. Zhang, *Electrocatalytic Oxygen Reduction Reaction*, in *PEM Fuel Cell Electrocatalysts and Catalyst Layers*, J. Zhang, Editor. 2008, Springer London. p. 89-134.

5. Earley, J.E. and T. Fealey, *Hydroxide ion as a reducing agent for cations containing three ruthenium atoms in nonintegral oxidation states.* Inorganic Chemistry, 1973. **12**(2): p. 323-327.

6. Batterjee, S.M., et al., *The electrochemistry of some ferrocene derivatives: redox potential and substituent effects.* Applied Organometallic Chemistry, 2003. **17**(5): p. 291-297.

7. Haberl, S., et al., *Cell membrane electroporation-Part 2: the applications.* Electrical Insulation Magazine, IEEE, 2013. **29**(1): p. 29-37.

8. Moiroux, J. and P.J. Elving, *Mechanistic aspects of the electrochemical oxidation of dihydronicotinamide adenine dinucleotide (NADH).* Journal of the American Chemical Society, 1980. **102**(21): p. 6533-6538.

9. Laschi, S., et al., *Enzyme-amplified electrochemical hybridization assay based on PNA, LNA and DNA probe-modified micro-magnetic beads.* Bioelectrochemistry, 2009. **76**(1): p. 214-220.

10. Nie, Z., et al., *Electrochemical sensing in paper-based microfluidic devices.* Lab on a Chip, 2010. **10**(4): p. 477-483.

11. Scott, R.A. and C.M. Lukehart, *Applications of Physical Methods to Inorganic and Bioinorganic Chemistry*. 2007: Wiley.

12. Wu, X., et al., *Antiplasmodial activity of ferrocenyl chalcones: Investigations into the role of ferrocene.* Eur J Pharm Sci, 2006. **27**(2–3): p. 175-187.

13. Hocek, M., et al., *Ferrocene-Modified Purines as Potential Electrochemical Markers: Synthesis, Crystal Structures, Electrochemistry and Cytostatic Activity of (Ferrocenylethynyl)- and (Ferrocenylethyl)purines.* Chem – Eur J, 2004. **10**(8): p. 2058-2066.

14. Lovelock, K.R., et al., *On the diffusion of ferrocenemethanol in room-temperature ionic liquids: an electrochemical study.* Phys Chem Chem Phys, 2011. **13**(21): p. 10155-64.

15. Nicholson, R.S., *Theory and Application of Cyclic Voltammetry for Measurement of Electrode Reaction Kinetics.* Analytical Chemistry, 1965. **37**(11): p. 1351-1355.

16. Saito, T., et al., *Oxygen consumption of cell suspension in a poly(dimethylsiloxane) (PDMS) microchannel estimated by scanning electrochemical microscopy.* Analyst, 2006. **131**(9): p. 1006-11.

17. Dombek, K.M. and L. Ingram, *Effects of ethanol on the Escherichia coli plasma membrane.* J Bacteriol, 1984. **157**(1): p. 233-239.

Chapter 5

Immobilization of mediator

5.1 Introduction

A detailed account of the invention and development of a ferrocene carboxylic acid (FcA) mediated oxygen demand assay (patent publication number WO2015036612 A1) was documented in Chapter 4. In Chapter 5, we expand on this study looking into the refinement of the FcA-oxygen demand assay into a system which is more user friendly and fit for commercial use. The current system, as described in chapter 4, using dissolved mediator has several disadvantages. Firstly, this method requires a bench top setup consisting of a potentiostat and an electrochemical cell with solution mixing to conduct the experiment. In many areas of work and study this would limit the practicality of employing this system, for example in field based environmental studies where facilities could be limited. Secondly, it has limited practical use on biological cell line studies because it is difficult to ensure sufficient biological cell numbers and mediator, in close proximity to the working electrode area. This is especially the case for adherent biological cell lines (biological cell lines that are not in suspension). It becomes difficult to place the adherent cultured cells close enough to the working electrode in a dissolved mediator system. Cells could either block the mediator as cells could adhere to the electrode, or they adhere to the flask away from the working electrode area. It is possible to force adherent cell lines into solution, but this is not be optimal because this would highly affect adherent cells survival [1, 2]. Adherent cell line survival is highly regulated by cell-matrix adhesion through many pathways [1, 2]. Adherent cell lines would not achieve peak metabolism when they are in suspension, and may behave differently compare to when they are in optimal condition. This would render results from

adherent cell line studies, e.g. drug testing, toxicology studies and cell signalling, invalid. Thirdly, when mediator is dissolved in solution, diffusion becomes one of the rate limiting steps, as the mediator needs to diffuse to the electrode in order for the electrochemistry to happen. Diffusion rate is highly affected by temperature, osmolarity and concentration and a system affected by such environmental conditions could give rise to inconsistent results [3]. It is thus concluded that the way forward is to develop a system removing the disadvantages of dissolved mediator in solution by means of fixation of FcA mediator on a working electrode.

The immobilisation of mediator on electrodes for electrochemical biosensors has become more and more popular since Clarks and Lyons, 1962 [4] for the following reasons. The immobilised mediator becomes a non-diffusion redox station which facilitates electron transfer from mediator to electrode, thus resulting in higher current density and increase signal to noise ratio [5]. The immobilized mediators on the electrode surface allows repeat usage of the electrodes and measurement over prolonged time periods, as no reagent needs to be replaced or replenished [6]. It also allows development into portable chip electrode systems. The immobilisation of mediators allow the systems to work at relatively smaller potential (closer to 0V) and minimises background interference [5]. Mediator immobilisation techniques are widely used by many different types of electrochemical sensors, including glucose [7-9], fructose [10] and cholesterol [11, 12] meters. Common mediator immobilisation methods include, screen printing [7, 8], drop coat and seal/immobilized in a semi-permeable membrane [10, 13] and chemical immobilisation [14, 15].

Screen printed electrodes are widely used in many different electrochemical biosensors, including DNA sensors, aptasensors, immunosensors and enzymatic biosensors [16]. The method is a relatively simple, quick and low cost mix and print procedure. This method reduces the amount of FcA needed by concentrating the FcA on the electrode surface, rather than it being diluted throughout the bulk solution. Screen printing can be used in small batch studies (potentially homemade) with screen-printing machines for research purposes, as well as, industrial scale printing. It also allows flexibility in electrode design, shape, material, and adhesion material [17], and a two or three electrode system can be printed on a small area therefore reducing experimental sample size. Screen printed electrodes have the potential to be easily made into a chip based portable systems [9, 18], and 96 well cell culture plate systems for adhesive cell lines [17]. In addition to all the aforementioned advantages of screen printed electrodes, this method of immobilisation of the FcA requires no chemical modification of the carboxylic acid group. The analyte, FcA, can be simply mixed in a conductive paste and then printed as a thick film onto the substrate. Therefore, no chemical modification is needed thus preserving the single carboxylic acid functional group, identified in chapter 4, to be crucial for the presence of the separate O_2 catalytic peak.

Drop coating analyte onto a screen printed electrode then fixing the analyte with permeable membrane is another method widely used in electrochemical biosensor synthesis [19]. There are a large variety of membranes with different properties which could be used in drop coating. However, there are only a few membranes which are compatible for biosensors, of which must have a non-biofouling environment. Nafion and cellulose acetate are two commonly used membranes which have non-biofouling environments. Nafion is a negatively charged polymer and allows positively charged molecules to pass through while preventing negatively charged molecules repelled by the negatively charged polymers [19]. Whereas,

cellulose acetate is a neutral polymer and will allow both negatively and positively charged molecules to pass through [20]. This neutral polymer is popular among electrochemical biosensors for example cholesterol meter [12], uric acid meter [21] and paracetamol sensor [22]. Cellulose acetate was specifically chosen for this section of work because it would allow charged species of molecules to pass through. This is an important characteristic because the FcA mediator in the system is indirectly measuring oxygen content by directly measuring reactive oxygen species, namely HO_2^- and OH^-. If nafion was to be used, the negative polymers would repel the reactive oxygen species from the mediator which is immobilised under the membrane, therefore a high likelihood of no detection. This method, similar to screen printing, reduces the amount of FcA needed by concentrating the FcA on the electrode surface, rather than it being diluted throughout the bulk solution. A downside of this method is that it relies on the permeability of the membrane, which may affect the accessibility of oxygen to the electrode by introducing another diffusion layer for oxygen between the bulk and electrode.

Self-assembled monolayers (SAM) are used extensively as a bridge between the mediator and electrode in biosensors. It provides a controlled uniformed monolayer on the electrode surface, forming a bridge of fixed distance between the redox centre (mediator) and the electrode [23]. Forming a controlled and uniform monolayer of the surface of the electrode gives two main advantages. Firstly, formation of a controlled and uniform monolayer should give rise to less peak signal variation and secondly there should be less variation between the surfaces of different electrodes produced in the same way relatively for example to drop coating and screen printing. Gold substrate was chosen to synthesise the SAM-ferrocene electrode as this produces a strong thiolate-gold (Au-S) bond when compared to other metals for example silver [24] or copper through absorption [24, 25]. The protocol for synthesis of

the SAM modified electrode is simple and contains few steps and is highly reproducible. The clean substrate is incubated into diluted thiol-SAM solution before rinsing with the same solvent and drying with a gas such as argon [25, 26]. The major disadvantage of immobilisation of FcA by means of SAM modified electrode is that the coupling reaction of the FcA mediator onto a SAM molecule would alter the monocarboxylic acid group. This could lead to the loss of the separated O_2 catalytic peak, as reported in Chapter 4. Also the use of gold as substrate could reduce the effectiveness of the system when used in conjunction with other techniques, such as microscopy and colourimetry.

Diazonium salt is another popular chemical, used as a bridge between substrate and mediator, for electrochemical sensor modified electrodes. It is believed to produce a covalent bond between the diazonium molecule and the substrate being relatively more electrochemically stable than the thiol based bonding [27, 28]. It can also be electrochemically grafted on different materials, including glassy carbon [29], gold [27], indium tin oxide (ITO) [30]. While sharing the same potential chemical downsides as SAM, the biggest advantage of using diazonium is that transparent ITO substrate can be use. This is beneficial because the system could be integrated with other techniques, e.g. microscopy and colourimetry. It may also potentially be more electrochemically stable than SAM surface [27, 28]. The surface synthesis is however, far more complicated than in SAM surface synthesis and relatively less controlled in terms of surface thickness.

5.2 Aim

The aim of this chapter is to further develop FcA mediated oxygen demand assay system by immobilisation of the mediator. The purpose is to improve the sensitivity, user friendliness, portability, and cost effectiveness of the system.

5.3 Objectives

The objectives are as follow;

1. To assess different screen printing approaches, from hand screen printing, in-house screen printing and industrial screen printing.
2. Test the viability of drop coat immobilization of FcA.
3. Investigate SAM and diazonium techniques for chemical immobilisation of the FcA mediator.

Objective 1

Hand screen printing was conducted as a preliminary study for proof of concept for compatible of screen printing and carbon paste ink with the FcA mediated oxygen demand assay. In-house and industrial screen printing was conducted to further optimize/troubleshoot screen printing techniques.

Objective 2

Drop coat technique was investigated as an alternative method for non-chemical immobilisation of the FcA mediator for comparison with screen printing technique.

Objective 3

The two most commonly used techniques for chemical immobilization, SAM and diazonium were assessed to determine the viability of the technique for the FcA-mediated oxygen demand assay system. Gold was used for SAM modified surfaces. Gold and Indium tin oxide (ITO) substrates were used for diazonium surface for comparative purposes, as diazonium can bind strongly to both and ITO has an advantage for being transparent.

5.4 Methods and materials

5.4.1 Chemicals

Carbon graphite paste was purchased from Gwent Electronic Materials Limited, UK. Indium tin oxide (ITO) single-side coated glass was purchased from Delta Technologies Limited, USA. Gold substrates were purchased from George Albert PVD, Germany.10 x PBS, glass slides, were purchased from Fisher Scientific, UK. Sodium Nitrate, FcA, 11-(Ferrocenyl) undecanethiol, cellulose acetate (CA), p-phenylenediamine, 1-dodecanthiol, 11-amino-1-undecanethiol and 4-aminothiophenol were purchased from Sigma Aldrich, UK. Acetone was purchased from VWR, UK. Acetate Film (OHP acetate), paint brush were purchased from Ryman Stationary, UK. Industrial screen printed electrode strips (Part: 9601219 rev. A. Ink Vendor: 1), GSI Technologies, USA. Ferrocene NHS ester was purchased from fivephoton

biochemical. 1, 1'-ferrocene carboxylic acid NHS ester was kindly provided by Dr. Aaron Acton.

5.4.2 Hand screen printing

A 1 x 3 cm hole was cut out from an acetate film and the film was then placed on a glass slide. 10 % w/w FcA was mixed with carbon graphite paste and brushed on the glass slide using the acetate film as a stencil. The printed electrode was placed in an oven at 90 °C for 30 minutes to dry.

5.4.3 In-house screen printing

The DEK 248 screen printer was used to conduct the screen printing. Printing carbon graphite paste alone was used to optimise the printer settings and conditions. Different print gap distances, force and speed were all tested. Chips were then dried at 65 °C for 30 minutes. Images were taken, using a Zeiss Lab.A1 AX10 microscope attached with a Qimaging Micropublisher 3.3 RTV imaging camera, for each chip before and after they were dried.

5.4.4 Gwent Electronic Materials Limited screen printing

In collaboration with Gwent Electronic Materials Limited investigations were performed to troubleshoot the porous issue identified in the carbon paste. The viscosity of the carbon graphite paste and the tension of the screen in the in-house DEK 248 printer was analysed using a Tetko tension meter. Carbon graphite paste was printed on both glass and PET substrates then dried in an oven at 90°C for 30 minutes. Carbon graphite paste adhesion was tests by, a scrape test, using a

spatula to scratch the electrodes printed on both substrates, and a sticky tape test, by applying and removing a strip of sticky tape. A porous test was conducted by putting an adhesive well on the carbon paste and then adding a few drops of PBS into the well. For thoroughness the test was repeated after a further 30 minutes of drying at 90°C.

5.4.5 Drop coat

Industrial screen printed electrode strips (Part: 9601219 rev. A. Ink Vendor: 1) were provided by GSI Technologies. The strip electrodes consist of a 2 mm diameter carbon paste electrode, a carbon counter electrode and a Ag/AgCl reference electrode. A solution of 10 mM FcA in ethanol was dropped onto the carbon working electrodes and allowed to dry at room temperature. After the FcA had dried, 0.5, 0.7 and 1 % w/v of cellulose acetate (CA) was dissolved in 9:1 ratio acetone to water, then dropped on top of the dried FcA. The samples were either placed in an oven to dry for 15 minutes at 65°C or dried in room temperature for 30 minutes.

5.4.6 Cleaning of gold and ITO substrates

Gold and ITO substrates were cleaned by rinsing with ethanol, drying with argon gas and exposed to Ultraviolet ozone for 60 minutes. The substrates were then rinsed and stored in ethanol, and used within 24 hours.

5.4.7 Preparation of SAM surfaces on gold

Cleaned gold substrate was placed in 1 mM of 1-dodecanthiol (DDT), 11-amino-1-undecanethiol (UDT-NH$_2$) or 4-aminothiophenol (phenol-NH$_2$) in ethanol for 24 hours. After 24 hours, SAM-coated gold were rinsed and sonicated for 5 minutes in ethanol before use.

5.4.8 Diazonium-grafting on gold or ITO substrates

Diazonium was grafted on UV-ozone cleaned gold or ITO substrates as described in Rawson, 2013 [31]. A diazonium solution containing 10 mM p-phenylenediamine was mixed with sodium nitrite in a 1:1 ratio in 10 ml of 0.5 M HCl and left on the bench for 3 minutes. The gold or ITO substrate was then connected to the working electrode wire and dipped into the diazonium solution and held at -0.6 V potential for either 10, 20, 25, 30 or 60 seconds. The substrates were then rinsed with water and dried with argon gas, then rinsed again with ethanol and dried with argon gas.

Diazonium-ferrocene (di-Fc) modified surfaces were prepared by incubating the diazonium modified surfaces in 1, 1.2, 2, 3 or 5 mM ferrocene carboxylic N-hydroxysuccinimide ester (FcA-Ester) or 5 mM 1, 1'-ferrocene carboxylic acid NHS ester (FcDA-Ester). Ethanol, dimethylformamide (DMF), and dichloromethane (DCM) were used as solvents and DCM was also used with and without triethylamine (TEA) to aid the grafting reaction, each either overnight or for 24 hours. These diazonium-ferrocene (di-Fc) modified substrate were rinsed and sonicated in ethanol for 5 minutes before use.

5.4.9 Cyclic Voltammetry

All CVs described in Chapter 5 was conducted using three electrode cell, consisting of a working electrode (each of which is the electrode being modified to immobilise the mediator in the respective sections), counter electrode (Pt) and reference electrode (Ag/AgCl). CVs described in hand screen printing, in-house screen printing, and chemical immobilised mediator sections were conducted using a 5 mm diameter Teflon cell. This was to ensure a fixed exposed surface area for CV measurement. All hand screen printed CV work was conducted in 1 x PBS with a scan rate of 5 mVsec^{-1}. All in-house screen printing CV work was conducted in 2 mM FcA in 1 x PBS at 5 mVsec-1 for two consecutive cycles.

Cyclic voltammetry was used for chemical immobilisation section. CVs were conducted, on SAM 11-(Ferrocenyl) undecanethiol modified gold surface and dizonium-ferrocene (di-Fc) modified gold surface for stability investigation. Electrochemical stress was induced by performing 10 consecutive cycles of CV in 1 x PBS at 100 mVsec^{-1} on each sample. The ferrocene peak current obtained from the CVs were plotted and compared.

For the SAM-modified electrode investigation, the electrochemical stability of the thiol-Au bond was determined by measuring the SAM surface concentration difference between SAM-modified surface that has and has not been subjected to electrochemical stress. Electrochemical stress was induced by performing 50 consecutive cycles of CV in 1 x PBS at 100 mVsec^{-1}. The SAM surface concentration was measured by scanning samples from 0 to -1.5 to 0 V at 100 mVsec^{-1} in 0.1 M nitrogen degassed KOH to obtain the desorption peak of

SAM on the gold surface. The concentration of surface SAM was then calculated using **equation 5.1** in **section 5.5.2.1.2.**

Diazonium grafting integrity on gold and ITO surfaces were determined by conducting CV experiments in 1 mM ferricyanide solution in PBS at 100 mVsec^{-1}, scanning from 0.6 V to -0.2 V back to 0.6 V, for 1 cycle. If the diazonium modified surface is stable, the ferricyanide signal would be blocked so no corresponding peak current shown in the CV. The stability of diazonium grafted on gold and ITO surfaces were determined by performing CV using diazoniaum modified surface with and without applying electrochemical stress. The electrode chemical stress was induced in the same way as SAM-modified surfaces.

Diazonium grafted ITO surface storage stability test was conducted by inserting the grafted chip onto the Teflon cell. The chip and Teflon cell were cleaned, by rinsing with water, drying with argon gas, then washing with ethanol and finally drying again using argon gas. 1 x PBS was added to the Teflon cell and 1 CV cycle was run at 100 mVsec^{-1} from 0 to 0.6 and back to 0 V. The chip and Teflon cell were then cleaned using the above method. Then a second CV experiment was conducted in 1 mM ferricyanide solution in PBS run at 100 mVsec^{-1} from 0.6 to -0.2 and back to 0.6 V for 1 cycle. The chip and Teflon cell was cleaned once again, and parafilm was used to protect the Teflon cell from dust. The whole procedure mentioned was conducted on days 0, 1, 3, 5, and 7.

CV experiments done on drop coated industrial printed electrodes were conducted by clamping the individual electrodes to the potentiostat. The printed electrodes were then

dipped into 1 x PBS solution. Two different CV settings were used. The first setting scans from 0 V to 0.6 V and back to 0 V at 5 mVsec^{-1}. The second setting scans from 0 V to 0.6 V and back to 0 V for 25 consecutive cycles at 100 mVsec^{-1}.

5.4.10 Mass Spectrometry

All MS analysis was conducted using an Alliance e2695 liquid chromatography (LC) system directly attached to a Xevo-G2-XS-ToF mass spectrometer. The LC system was used to directly inject the relevant samples and deliver the sample in methanol mobile phase at 100 µl/min, using electrospray ionisation (ESI) technique for MS analysis. The capillary voltage for ESI analysis was set to 3 kV in positive polarity, and the sampling cone voltage was set to 40 V. The source temperature was set to 130 °C, desolvation temperature set to 350 °C. Dry nitrogen gas was used as nebuliser gas (100 L/hr), desolvation gas (800 L/hr) and sample cone gas (60 L/hr).

Samples of FcA-Ester and FcDA-Ester were prepared at 0.5 mg/ml in each of the following solvents, ethanol, tetrahydrofuran (THF), and dimethylformamide (DMF) both with and without 1 mM triethylamine (TEA) additive. MS were performed on samples diluted in ethanol, THF, and DMF without TEA at 0 and 48 hours. MS were performed on samples dilutaed in ethanol with or without TEA at 0, 1, 2, 24 and 48 hours.

5.5 Results and discussion

5.5.1 Screen printing

5.5.1.1 Hand screen printing

Preliminary work was performed to screen print an electrode by hand. A 1 X 3 cm hole was carefully cut out from an acetate film and the film was then placed on a glass slide. 10 % w/w FcA was mixed with carbon graphite paste and brushed on the glass slide using the acetate film as a stencil (**figure 5.5.1.1.1**). The printed electrode was placed in an oven at 90 °C for 30 minutes to dry.
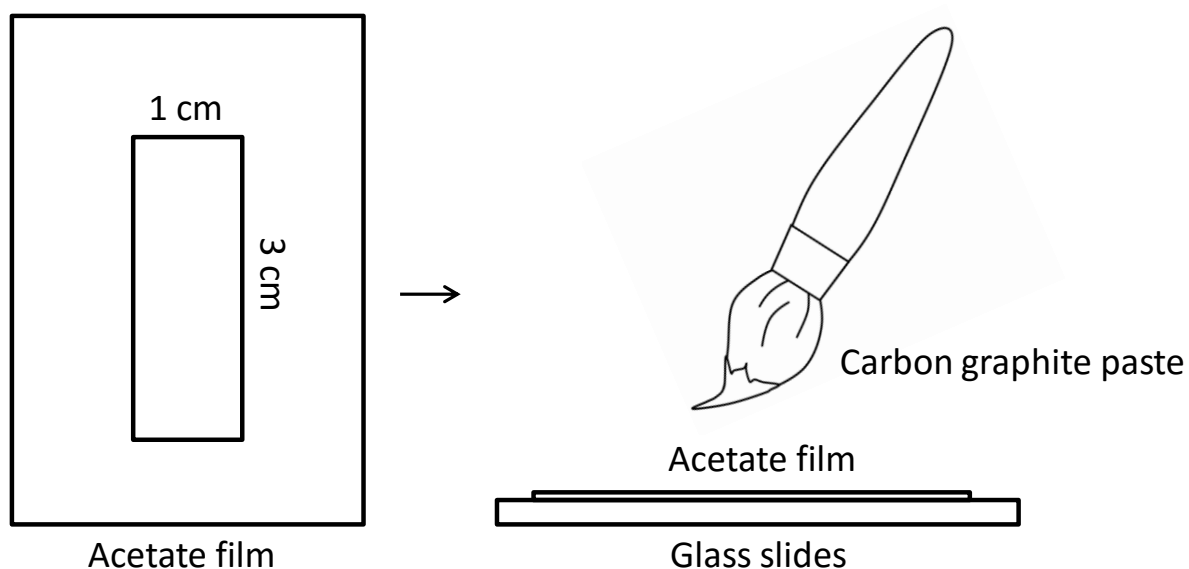

Figure 5.5.1.1.1 Hand screen printing method

Electrodes were then placed into a teflon cell with a 5 mm diameter opening and filled with PBS. CV was then conducted using the electrode in PBS with Pt counter electrode and Ag/AgCl reference electrode at 5 mV sec^{-1}. Carbon graphite paste was chosen as a diluent for

printing the working electrode. It is cheaper than silver paste, more stable while stored in air, and more importantly GC electrodes showed no signal interference when used with FcA, as described in Chapter 4. CV with the hand screen printed carbon paste-FcA electrode shows a second oxidation peak (**figure 5.5.1.1.2** O2), the O_2 catalytic peak, as seen in Chapter 4 (**section 4.5.3**, **figure 4.5.3.1**). This means the carbon paste is not compromising the unique O_2 catalytic property of FcA with HO_2^- and OH^-. The CVs were imported into the Linkfit software to calculate the O_2 catalytic peaks (**figure 5.5.1.1.2** O2), where each peak was analysed five times and a mean value generated. An increase in the peak current, of the O_2 catalytic peak from an average of 1.36 µA (n=2), in the dissolved FcA system, to an average of 9.02 µA (n=2), using hand screen printed system was observed. This could be due to, or a combination of, the following factors; an increase of the actual working concentration of FcA, whereby immobilisation has successfully localised the FcA in the proximity of the electrode. The immobilisation also means the FcA is no longer dissolved in the bulk solution, and therefore it's diffusion factor is eliminated. Additionally, it could also be due to an increase in working area as the solution was soaking through the electrode paste (**figure 5.5.1.1.3**).
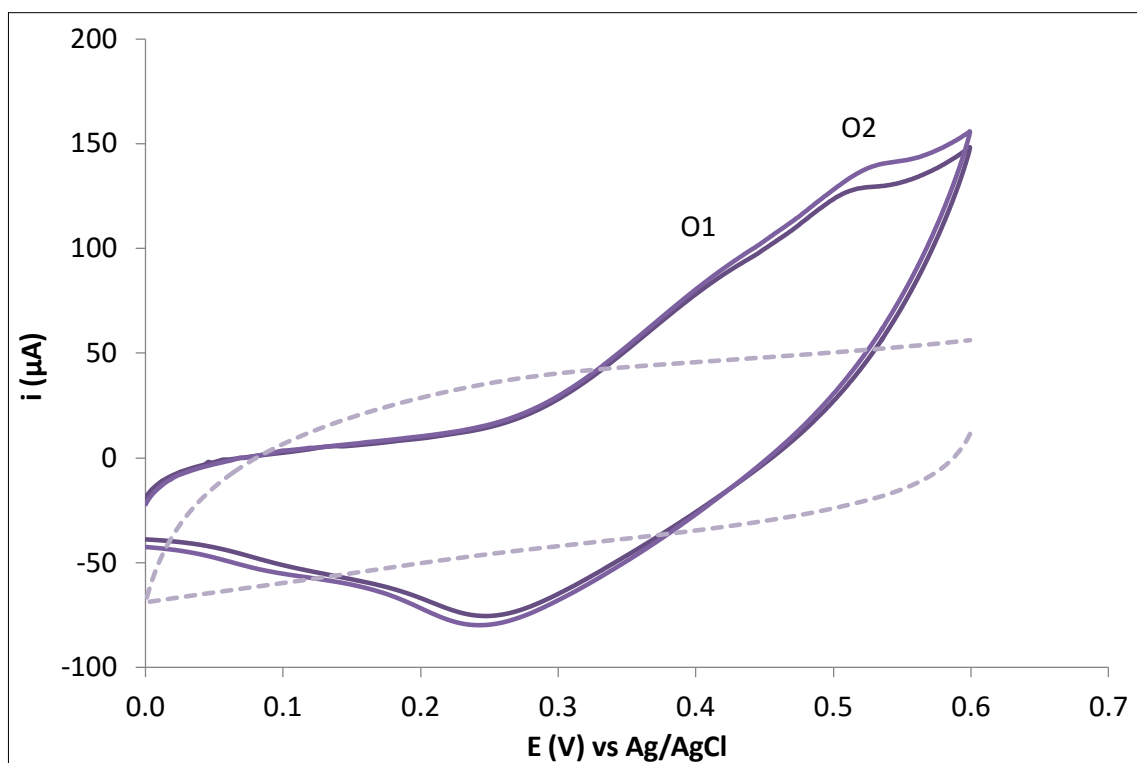
Figure 5.5.1.1.2 Typical cyclic voltammograms recorded with hand screen printed carbon paste (dotted line) and carbon paste-FcA (solid line) working electrodes using PBS solutions. All CVs were performed at a scan rate of 5 mVsec^{-1}. (n=2). Also showing the O1 normal oxidation peak and the O2 O_2 catalytic peak.

Figure 5.5.1.1.3 Photo image of the bottom of the hand screen printed electrode showing PBS solution soaking through the electrode paste.

With the sample solution soaking through the electrode paste, the electrode working area is no longer a 2D area but an unknown, uncontrolled, 3D area including the depth of the electrode. This unknown working electrode area would prevent us from calculating the O_2 concentration by introducing a second variable into **Equation 2 ii in section 4.5.5.** The peak separation however was greatly increased, which could also be due to limitations in the hand screen printing process. The hand printing technique using a simple brush does not create a very smooth surface which may affect the conductivity of the electrode [32]. The poor conductivity would then increase the electron transfer resistance, thus lowering the electron transfer rate resulting in a big variation in ΔE_p [33-35]. In the dissolved FcA system, an E_{pa} was obtained at 352 mV relating to the ferrocene electrochemistry and for O_2 catalytic peak an E_{pa} of 394 mV (**figure 4.5.3.1**). The E_{pc} was approximately 286 mV, resulting an ΔE_p about 66 mV (**figure 4.5.3.1**). In the hand screen printed electrode system, the E_{pc} was approximately 246 mV and E_{pa} was approximately 425 mV, resulting an ΔE_p approximately 179 mV (**figure 5.5.1.1.2**). Microscopy images of the hand screen printed carbon paste-FcA

electrode (**figure 5.5.1.1.4**) had revealed cracks on the electrode surface, confirming the bigger ΔE_p in hand screen printed system was due to the poor printing.

Figure 5.5.1.1.4 20 X microscopy image of 10 % w/w FcA in carbon paste hand print electrode.

In order to confirm that the big peak separation is due to the hand print electrode, another well known mediator was used to repeat the experiment. CV was obtained in 1 mM ferricyanide in PBS using hand printed carbon paste electrode or GC electrode (**figure 5.5.1.1.5**). An increase of ΔE_p from 63 mV (using GC electrode) to 330 mV (using a hand printed electrode) was also observed in the ferricyanide system confirming the hand screen printing has affected the reversibility and causes the peak's shape to not be as pronounced.
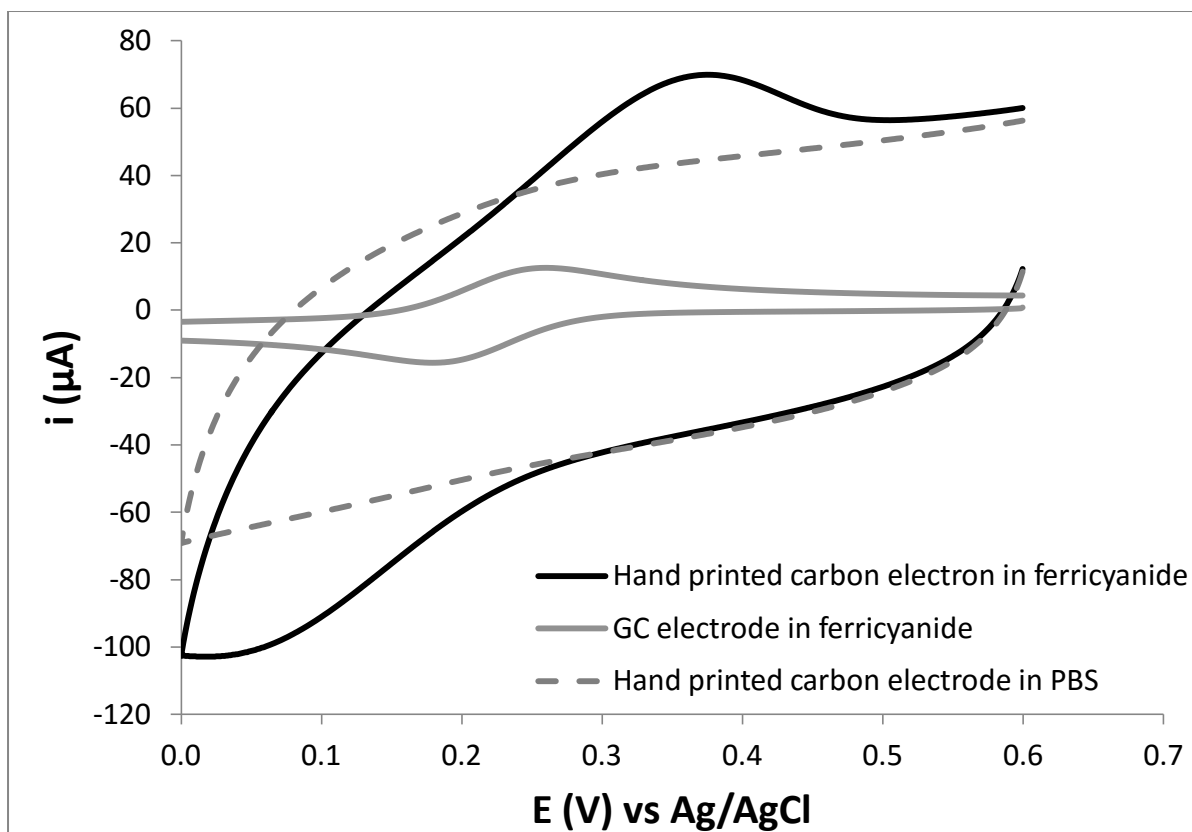
Figure 5.5.1.1.5 Cyclic voltammogram obtained from PBS only (n=2) and 1 mM ferricyanide in PBS (n=3) using a hand printed carbon electrode. As comparison 1 mM ferricyanide in PBS using a GC electrode (n=3)
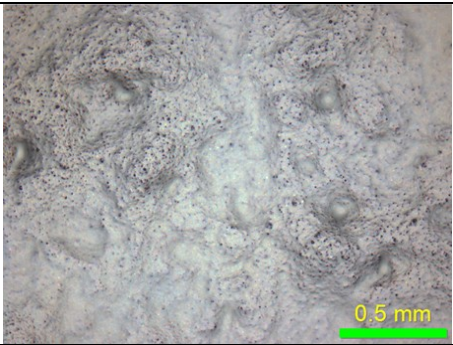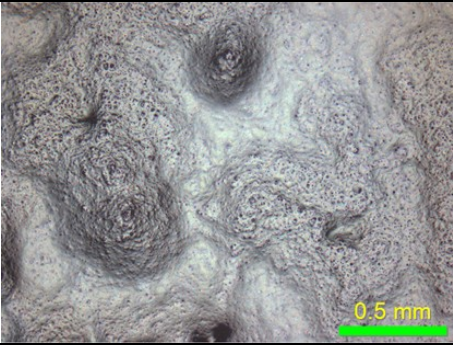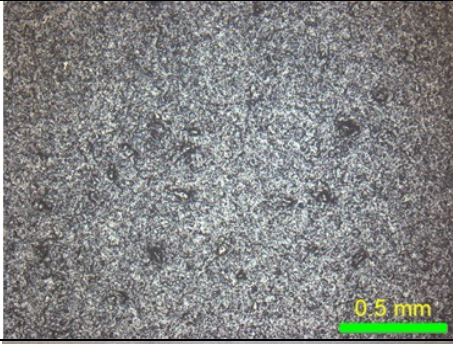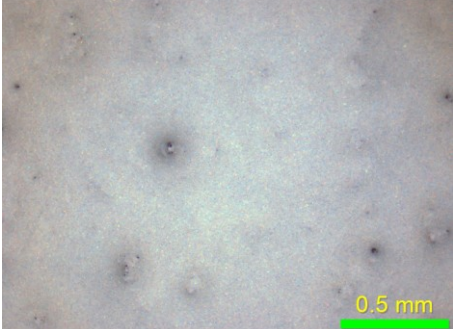
In conclusion, compared to the dissolved FcA system, the hand screen printed carbon paste-FcA electrode system has preserved and enhanced the separated O_2 catalytic peak property of FcA, which is fundamentally crucial for the FcA-mediated bio-oxygen demand measuring system. However the porous carbon paste electrode made the working electrode area unknown, therefore as the reaction is no longer confined to the electrode surface, but throughout the whole printed area, measurements are invalidated by introducing a second variable into **equation 2 ii in section 4.5.5**. In addition, due to limitations of the hand screen printing process, in particular the roughness of the surface, the electrode resistance has

increased therefore decreased the reversibility and made the peak shape not pronounced. The next step to improve the system was to try an in-house screen printer.

5.5.1.2 In-house screen printing

The DEK 248 screen printer was used to conduct the screen printing. The aim of the initial study was to thoroughly test different settings on the screen printer, to achieve a smooth and homogeneous electrode surface. Printing carbon ink alone was used to optimise the printer settings and conditions. Different print gap distances (the distance between the screen and substrate), force (the downward force exerted on the screen by the blade) and speed (how fast the blade moves across the screen) were all tested. Electrodes were then dried at 65 °C for 30 minutes. Images were taken with microscopy for each chip before and after they were dried. **Table 5.5.1.2.1** lists the details of the screen printer settings tested. Microscopy images show how the settings make a difference on the electrode surface when they are wet, and it was noted that inconsistencies were seen across the printed surface even on the same electrode. Microscopy images of all fully dried in-house screen printed electrodes (**figure 5.5.1.2.2**), and hand screen printed electrodes look similar.

Table 5.5.1.2.1 Table of different settings tested on the screen printer and O_2 catalytic peak current obtained from each samples produced by each setting by running CV using the printed samples in 3 mM FcA in PBS at 5 mV sec^{-1}.

Setting:	Image X 5 (wet)	Print Gap (mm)	Force (Kg)	Speed (mm sec^{-1})	O_2 catalytic peak current (µA)
1		2.2	0.65	20	5.91
2		3	2.65	20	6.96
3		2.6	2.65	20	4.42
4		2.6	2.65	10	4.69/4.92
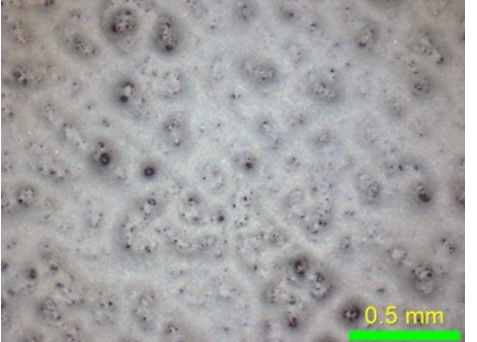
| 5 | | 2.2 | 2.65 | 10 | 4.63/4.71 |

Figure 5.5.1.2.2 Typical image of a dried screen printed carbon electrode.

To ascertain if the in-house screen printing method improved the function of the electrodes, and to find out which in-house screen printer setting was the best, CVs were performed. Each fully dried in-house screen printed carbon paste electrodes was tested in 3 mM FcA in PBS at 5 mV sec^{-1}. Typical CVs of 2 consecutive cycles of the electrodes printed with setting 3 are shown in **figure 5.5.1.2.3,** although results are typical for all the electrodes printed regardless of the screen printing settings. **Figure 5.5.1.2.3** shows the in-house screen printing method has improved the electron transfer rate of the system as the ΔE_p has decreased in range from 71 mV to 87 mV, dependent on the printer setting, compared to 179 mV obtained from the hand printing method. This is comparatively much closer to the ΔE_p of 66 mV obtained using a standard GC electrode (**section 4.5.3**). The O_2 catalytic peak current in the first cycle

showed no differences between the electrodes produced using the various settings on the screen printer except setting 2 (**table 5.5.1.2.1**). However, the O_2 catalytic peak current in the second cycle drops dramatically, ranging from 45 % to 59 %, in all electrodes compared to FcA in solution system, using GC electrode, which was an 18% drop (**figure 5.5.1.2.3**).

As the 3 mM FcA in PBS solution was placed into the electrochemical cell, the solution instantly soaked through the electrode paste (**figure 5.5.1.2.4**). During the first CV cycle, oxygen within the electrode paste and in close proximity to the electrode is consumed. The diffusion rate of oxygen from the bulk solution to the proximity of the electrode (**figure 5.5.1.2.5, diffusion 1**), causes an 18% drop in oxygen concentration in the solution in close proximity to the electrode at room temperature in the second CV cycle. This is as demonstrated in the dissolved FcA system in **chapter 4**. However, in addition to diffusion layer 1, in the in-house screen printed electrode system, an extra diffusion layer is introduced due to the porosity of the electrode paste (**figure 5.5.1.2.5, diffusion 2**). This has introduced an unknown drop in oxygen percentage concentration in close proximity to the electrode and inside the electrode paste. In this case it ranged from 45 % to 59 %, the difference possibly being due to the different thickness of the paste. It shows that the porous property of the electrode has not only invalidated the measurement of oxygen concentration at the first CV cycle, but also completely void the system's ability as an oxygen consumption assay, as the percentage drop of the O_2 catalytic peak current in CV cycle 2 can no longer be accurately reproduced.
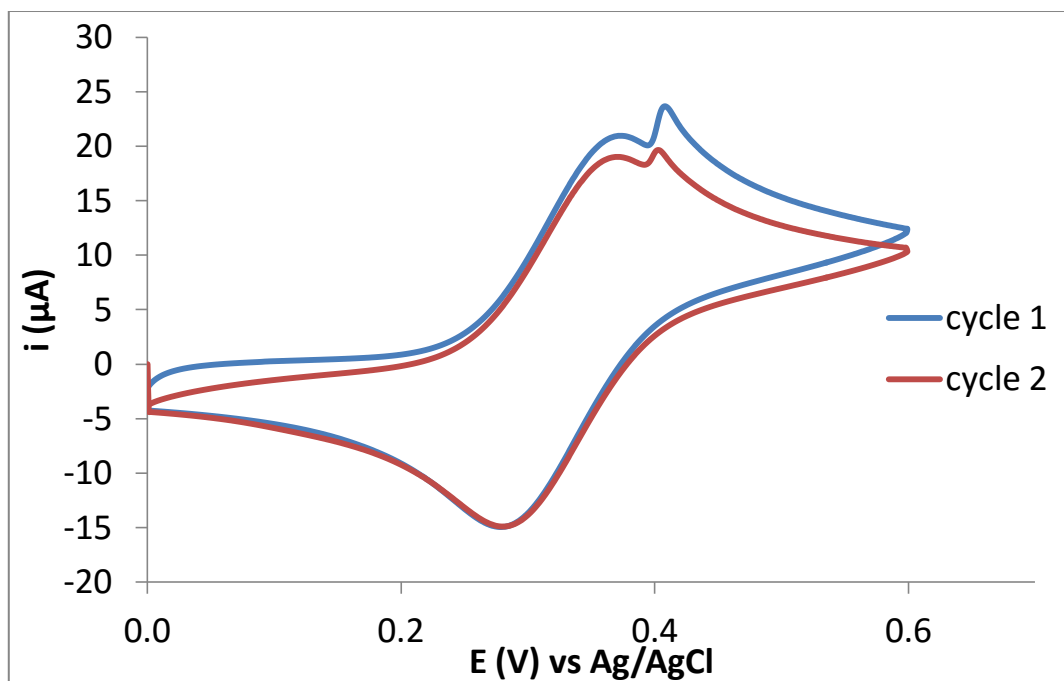
Figure 5.5.1.2.3 Typical two consecutive cyclic voltammograms recorded from 3 mM FcA in

PBS solutions using carbon paste screen printed working electrodes.

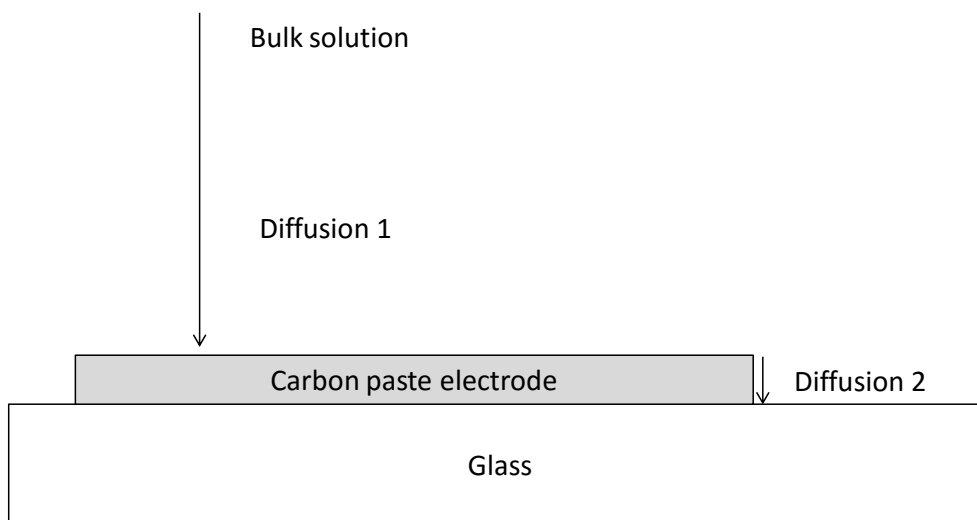**Figure 5.5.1.2.4** Image of PBS solution soaking through the screen printed electrode.

Figure 5.5.1.2.5 The porous carbon paste electrode has created an addition diffusion layer for oxygen.

The in-house screen printing has greatly improved the electron transfer rate of the dissolved mediator system. This was reflected in the decreased of ΔE_p of dissolved FcA in range from 71 mV to 87 mV, which is very closed to using a standard GC electrode which has a ΔE_p of 66 mV at 100 mV sec^{-1}. However, the porous condition of the screen printed electrode has not improved. This is critically affecting the accuracy and function of the FcA-mediated oxygen demand assay which need to be addressed. Therefore, the provider of the carbon paste was consulted and collaborated for a trouble shoot mission.

5.5.1.3 Industrial screen printing (Gwent)

Studies were performed to elucidate why the carbon paste electrode was porous. Viscosity of the screen printing ink affects the shear rate of the ink[36], which is essential for the screen printed electrode quality e.g. thickness and roughness of the printed electrode[37]. Too low viscosity would lead to pinholes and very thin coverage of paste. Too high viscosity may

cause the printed pattern to spread on standing[38]. To ensure the viscosity of the carbon paste was not the reason for the porous electrode, e.g. causing pinholes, a viscosity test was carried out on the supplied carbon paste. The viscosity test was performed using a Searle rotational viscometer, HAAKE viscotester 550 (**figure 5.5.1.3.1**). The carbon paste was placed in the middle of the rotator and spun at a fixed speed while the resistant was measured. The test confirms the viscosity of the carbon paste is within specification set out by the guidelines of Gwent (confidential business information, therefore actual data is not presented), therefore showed that the carbon paste ink was in good condition for screen printing.
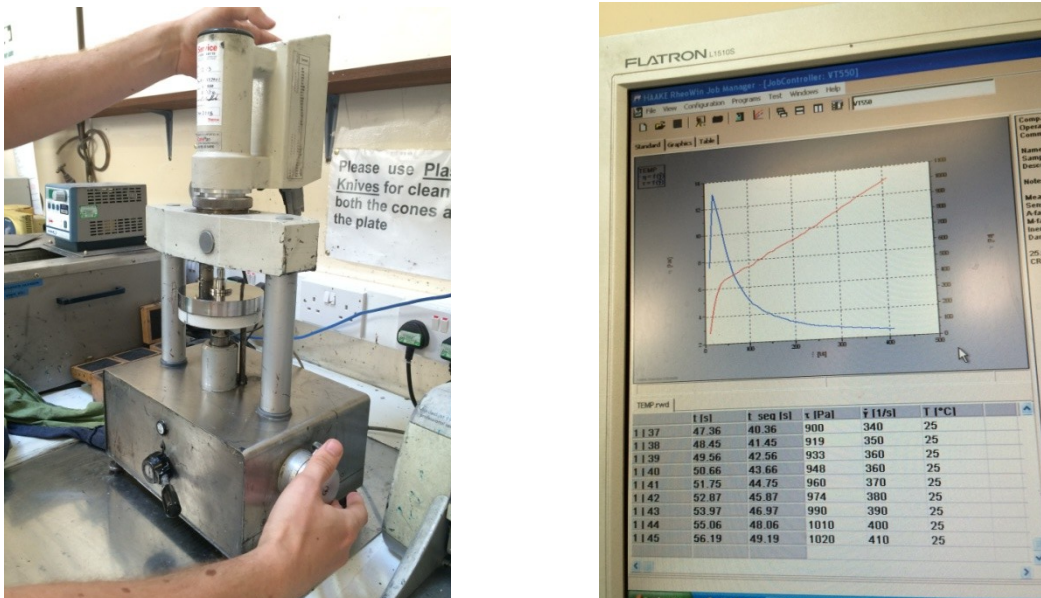

Figure 5.5.1.3.1 Viscosity test carried out by a member of staff.

With increased use, the mesh that makes up the screen used in screen printing become loose, and this loss of tension can result in lateral movement, smudging the printed pattern as the blade pushed along the surface of the screen during printing [39, 40]. Any movement of the

156

screen would cause inconsistencies in the printing process which could affect the function of the electrode, for example incomplete adhesion to the substrate surface due to smudging. To establish if this was the cause of the printed electrode being porous, the tension of the screen in the in-house screen printer was measured using a Tetko tension meter. The tension was found to be within guideline tolerances for a stainless steel mesh screen (15-45 N cm^{-1}) [39], thus confirming the condition of the screen was not the reason the printed electrodes were porous.

Another possible reason for the porous nature of the ink is it's adherence to the base substrate. Wettability plays a vital role in surface adhesion and the subsequent coating efficiency of a media on a substrate, in this case the GC ink [41]. For example a hydrophilic media will have better wettability with a hydrophilic substrate than with a hydrophobic substrate. Ink suppliers do not disclose the nature of the solvent in their inks, therefore the hydrophilicity of the ink is unknown. Polyethylene terephthalate (PET) is a commonly used substrate in screen printing because of its mechanical and chemical properties [42], with a different hydrophilicity compared to glass [43, 44]. Therefore, PET was chosen as an alternative substrate for testing as the differences in hydrophilicity may have improved wettabilty with the carbon paste ink.

Carbon ink was printed on both glass and PET substrates then dried in an oven at 90°C for 30 minutes. Adhesive tests were carried out afterwards. A spatula was used to lightly scrape the electrodes printed on both substrates. The electrodes printed on glass scrapped off a lot easier than the electrodes printed on PET (**figure 5.5.1.3.4**).
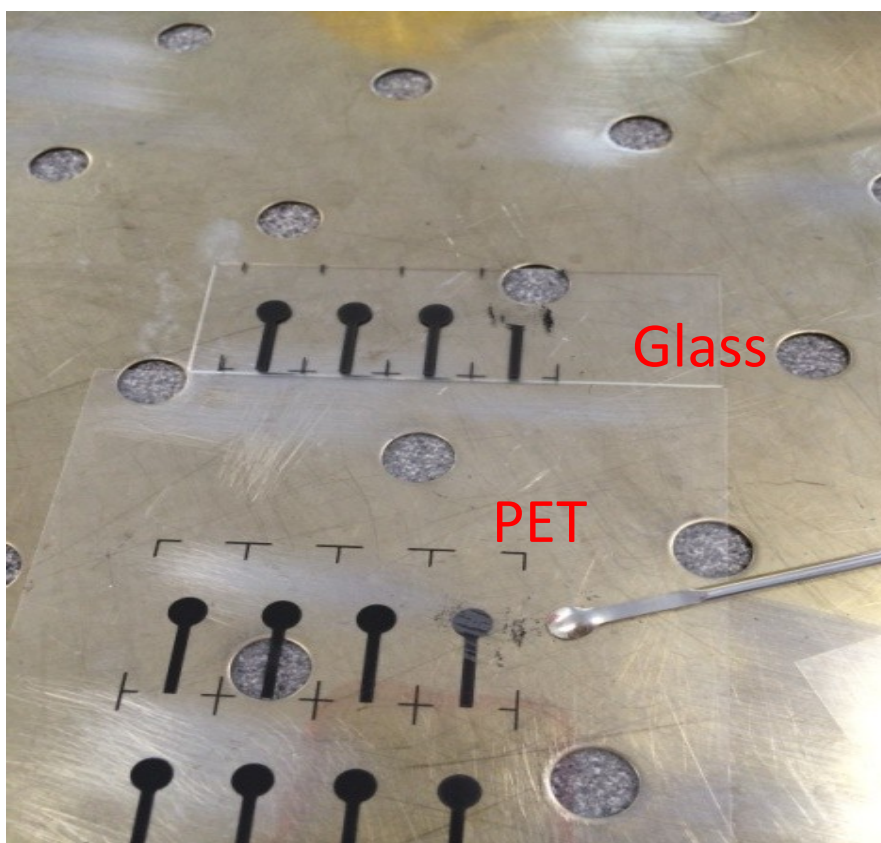
Figure 5.5.1.3.4 Adhesion testing of carbon paste electrodes printed on PET and glass by scrapping with a spatula.

The next adhesion test was carried out by putting sticky tape on the electrodes printed on both substrates and subsequently removing the tape. The electrodes printed on glass substrate were removed almost entirely when the sticky tape was removed, whereas most of the electrodes printed on PET substrate remained intact (**figure 5.5.1.3.5**). Both adhesion tests demonstrated that carbon paste has a much stronger adhesion to PET substrate than glass substrate.
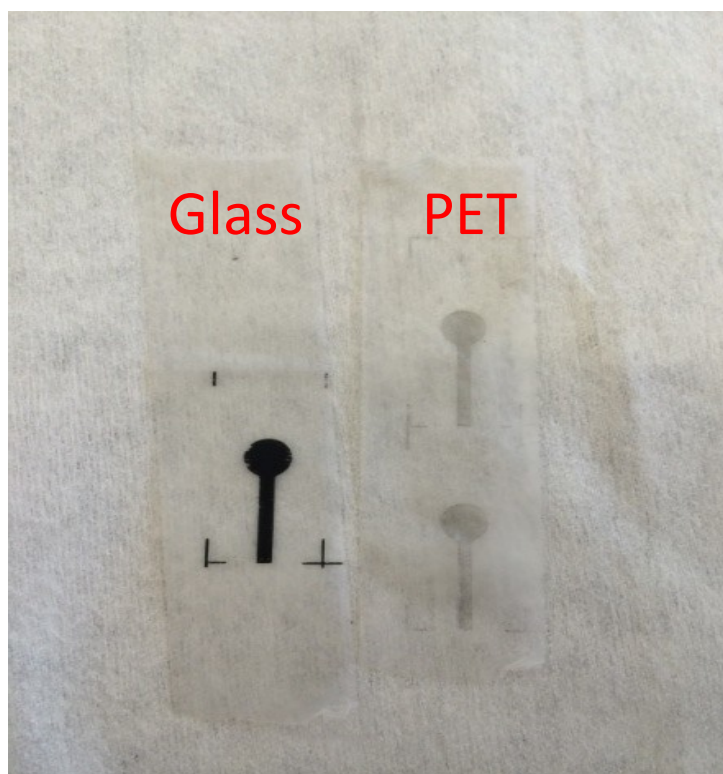
Figure 5.5.1.3.5 Showing the tape which was stuck to and then removed from electrodes

printed on glass and PET substrates.

A DEK 1202 screen printer was used on the day to print the carbon paste on glass and PET surface for comparison. The DEK 1202 screen printer is much smaller and features more simple controls than the DEK 248 previously used, and as such, is ideal for quick troubleshooting and method development purposes. The condition of the blade is absolutely paramount to the successful printing of the electrodes, as a dull or deformed blade edge would not be able to push the ink through the screen evenly and could affect how consistent the printed surface is. This explains why the in-house screen printed electrodes printed on the DEK 248 had inconsistencies across the printed surface (**figure 5.5.1.3.2**). Blade condition is maintained by ensuring the gap between screen and substrate is such that the downward force needed on the blade is as low as possible, thus protecting the blade from any unnecessary

pressure. If the gap is too large and thus the force to high, it could also cause inconsistent printing as the screen can bounce during printing and flick ink or touching back onto the substrate. This explains the mesh like pattern seen on the in-house screen printing on setting 5 (**table 5.5.1.2.1**). The system setting should always be "print then flood", this setting causes the machine to flood a thin layer of ink on the screen after each print. This thin layer of ink is important to prevent any residual ink from drying in the screen mesh where it could affect the next print run. If any mediators or enzymes were mixed into the ink before printing, a mixer should be used to ensure the mediators or enzymes were mixed well into the ink (**figure 5.5.1.3.3**).
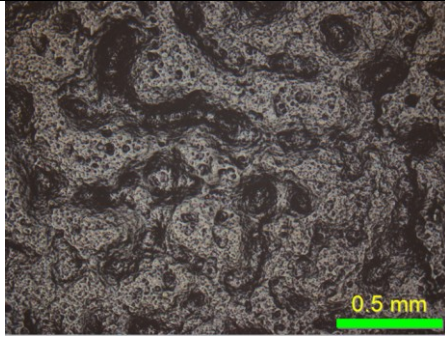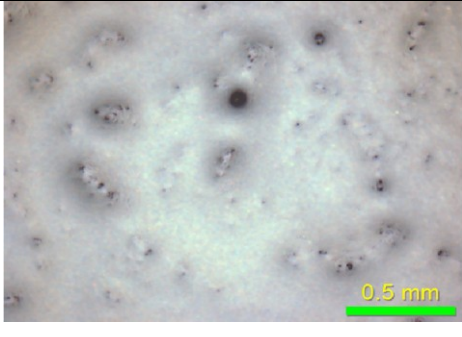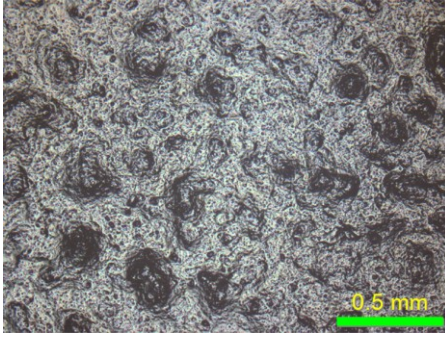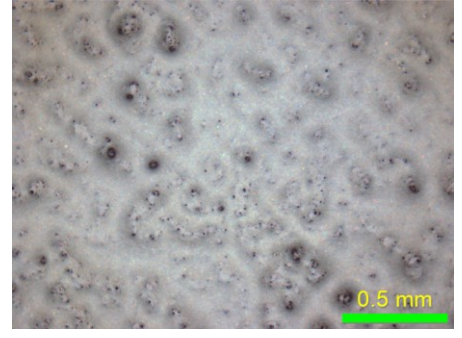
Setting 5	Spot 1	Spot 2
Sample 1		
Sample 2		

Figure 5.5.1.3.2 Microscopy images taken from different sections of the printed electrodes made using the in-house DEK 248. These images show printing inconsistencies.

Figure 5.5.1.3.3 Example of the mixer that is used for blending mediators or enzymes into screen printing ink.

Finally, a porosity test was carried out on electrodes printed on both glass and PET substrates (**figure 5.5.1.3.6**). A waterproof sticker was used to create a well into which a few drops of PBS was placed on both electrodes and left for 3 minutes. The underside of the electrodes were observed after the 3 minute interval and despite better adhesion to PET, PBS was still seen soaked through both electrodes (**figure 5.5.1.3.7**).
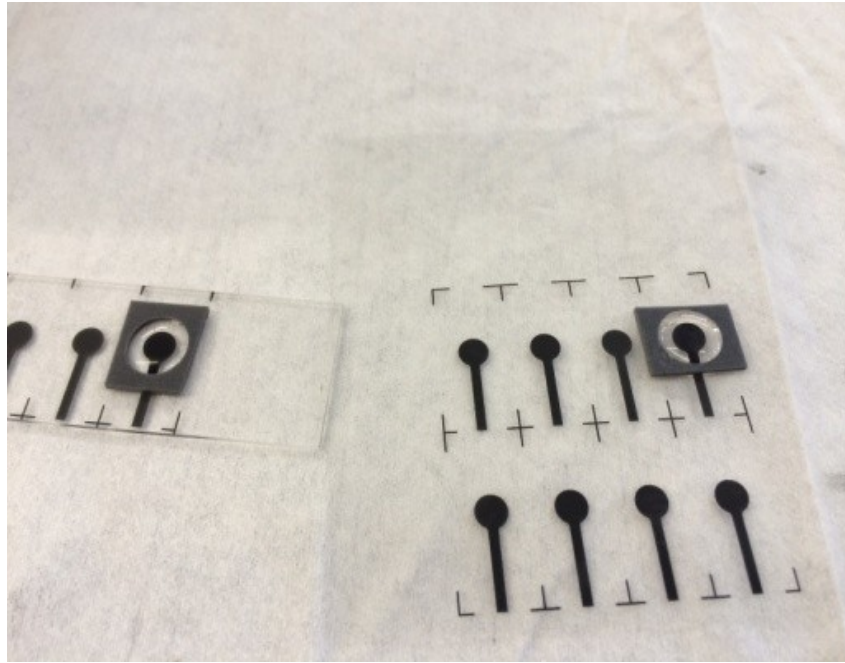
Figure 5.5.1.3.6 Wells were created on top of the carbon paste electrodes printed on both glass and PET substrates.
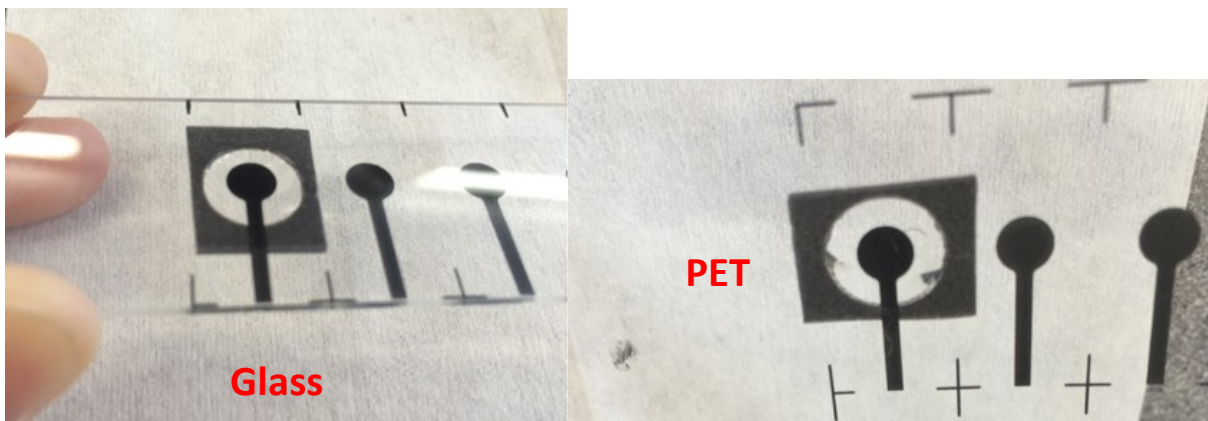

Figure 5.5.1.3.7 Image of the back of the carbon paste electrodes printed on both glass and PET substrates. Both show proof of being porous to PBS as the ink appears wet and darker in colour.

At this point, the only reasons for the electrodes being porous could be a drying problem or the nature of the carbon paste ink. To confirm it was not due to the poor drying, all of the printed electrodes were placed back in the oven for another 30 minutes at 90 °C. The porous test was repeated yielding the same results.

It was concluded that the screen printed electrodes were porous as a result of the nature of the carbon paste ink. The graphite in the ink is formed in sheet like structures that are cross linked throughout the overall structure. By nature the sheet structures would move when in contact with liquid and therefore will be porous. The results are very positive and show the second catalytic O_2 peak and ΔE_p similar to the FcA system in solution. This is all a good indicator that screen printing is a viable option for the production of FcA printed electrodes, however future work is needed to focus on the prevention of the analyte soaking through the porous ink. Much research would be needed in the development of a carbon ink suitable for this project, particularly in respect to the need for multiple cycle CV analysis. Unlike many of the currently commercially available meters e.g. glucose and cholesterol which only have a single CV cycle analysis, and therefore do not suffer the problem of unknown diffusion rate through the carbon paste electrode in the consecutive cycles. Without this multiple CV cycle analysis step the system would not allow the near real time measurement of O_2 consumption. Both the type of carbon powders and pasting liquids have been shown to greatly affect the surface and 3D structure of the resultant carbon paste ink [45], so such development would be a big project in itself. It could involve a very in-depth long term project to develop a non-porous carbon paste electrode without having manufactures to disclose their classified product information and protocols.

5.5.1.4 Drop coating and cellulose acetate membrane

Another option was to use industrially pre-printed carbon electrodes and drop coat FcA on the electrode and seal it with permeable membrane. Industrial screen printed electrode strips (Part: 9601219 rev. A. Ink Vendor: 1) were provided by GSI Technologies. The strip electrodes consist of a 2 mm diameter carbon paste electrode, a carbon counter electrode and a Ag/AgCl reference electrode. A solution of 10 mM FcA in ethanol was dropped onto the carbon working electrodes and allowed to dry (**figure 5.5.1.4.1 i**). After the FcA had dried, 0.5, 0.7 and 1 % w/v of cellulose acetate (CA) was dissolved in 9:1 ratio acetone to water, then dropped on top of the dried FcA. The samples were then placed in an oven to dry for 15 minutes at 65°C. The appearance of cracks on the surface of the membrane was noted following the drying process.

Figure 5.5.1.4.1 Image of electrode after (**i**) 10 mM of FcA in ethanol is dropped and dried on the working electrode and (**ii**) different concentration of CA membrane in 90% acetone dropped on top of the dried FcA.

CVs were conducted on six drop coated electrodes that were prepared using the method above with 1% w/v CA, these are shown in **figure 5.5.1.4.2**. The CVs obtained from all six samples are clearly different in appearance, firstly the i_{pa} and i_{pc} values differ greatly, and secondly there are clear differences in the exhibition of the O_2 catalytic peak. These are probably a result of the irregular cracks on the surface of the electrode. As these irregular cracks allow the sample electrolyte and oxygen to reach the electrode without controlled diffusion through the membrane, depending on how the cracks were formed. As the cracks are formed in an irregular way the resultant CV's data are irreproducible.
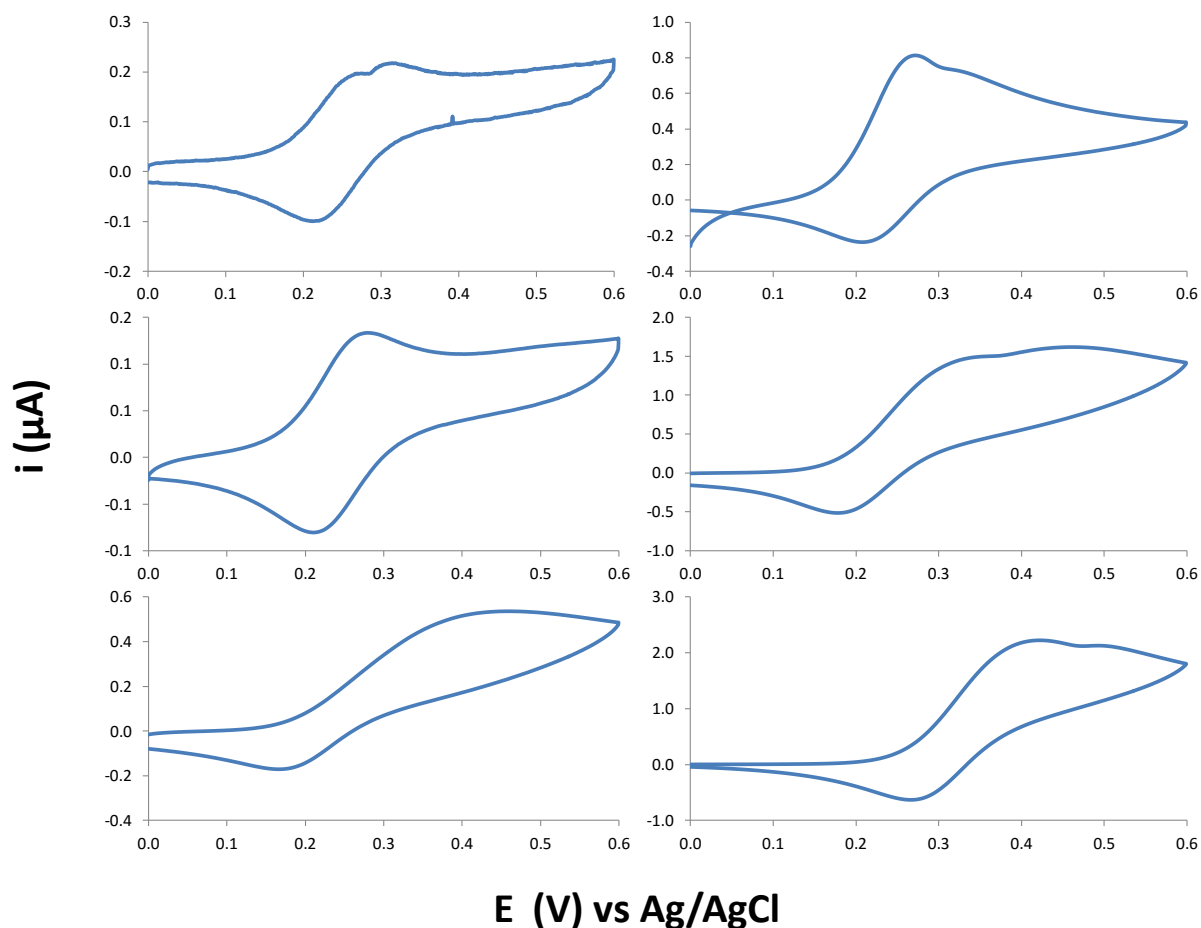
Figure 5.5.1.4.2 CVs obtains from PBS with the FcA and 1% CA membrane drop coated industrial screen printed working carbon electrode.

In an attempt to resolve the issue of the membrane cracking, electrodes were again prepared in the same way as explained above with 0.3, 0.5 and 0.7 % w/v CA membrane, except this time they were dried at room temperature for 30 minutes to avoid cracking. No visible cracks were formed with this method drying at room temperature. However, it was noted that following drop coating with membrane the orange coloured FcA (seen in **figure 5.5.1.4.1 i**) and white CA had mixed forming a yellow spot on the electrode (**figure 5.5.1.4.1 ii**).

CVs were obtained as before, using electrodes with 0.3% 0.5 % and 0.7 % CA membrane, typical CVs are shown in **figure 5.5.1.4.3**. Data suggested that 0.5 % and 0.7 % CA could be too thick for O_2 to diffuse readily through the membrane in the short time period of the CV scan however, 0.3% shows the O_2 catalytic peak **figure 5.5.1.4.3 iii**.
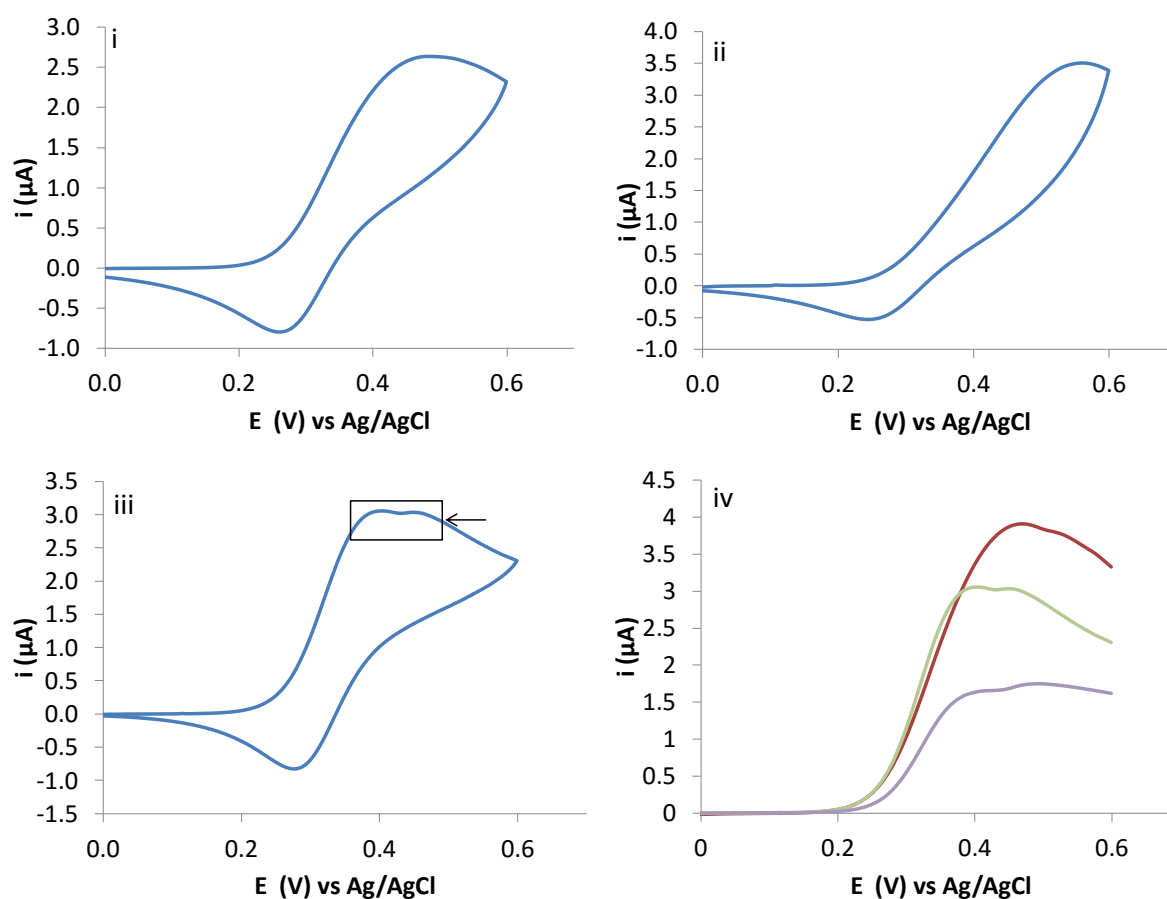

Figure 5.5.1.4.3 Preliminary CVs obtained from PBS using 10mM FcA and CA membrane drop coated electrodes containing **(i)** 0.7 % (n=1), **(ii)** 0.5 % (n=1) and **(iii)** 0.3 % (n=3) CA at 5 mV sec^{-1}, **(iv)** Linear sweep voltammetry of three electrodes as prepared in **(iii)** to show the reproducibility of the O_2 catalytic peak.

Linear sweep voltammetry using electrodes prepared with 0.3 % CA were carried out to test the reproducibility of the results having found this to be the suitable concentration to exhibit the O_2 catalytic peak. Data shown in **figure 5.5.1.4.3 iv**, shows the O_2 catalytic peak is exhibited for each repeat and so results are reproducible. However there are some variations in peak current which can be explained by previous observations. The FcA appeared to dissolve into the droplet of membrane solution, and as the droplet spreads into the electrode the droplet becomes non-uniform. This means there will be minor variations in the concentration of FcA on the actual electrode area which may lead to these minor variations in results shown.

Prior to conducting a scan rate study, an electrode stability test was performed on the 0.3% CA electrodes by running 25 consecutive CV cycles at 100 mVsec^{-1} in PBS, see **figure 5.5.1.4.4**. The data shows the FcA peak current was gradually decreasing over the 25 CV cycles. This suggested that the FcA was slowly leaching from the electrode surface. There are two possible explanations; firstly, the FcA could be leaching through the membrane whilst the CA membrane is still intact. Secondly, the CA membrane could be slowly dissolving into the bulk solution, leading to the FcA leaving the electrode proximity. The latter was subsequently observed to be correct, **figure 5.5.1.4.5** shows a photograph of the 0.3% CA prepared electrode (**i**) pre 25 CV cycles and (**ii**) post 25 CV cycles. In the pre 25 CV cycles electrode, the FcA and CA drop coat can easily be identified as a yellow/orange patch on the working electrode, however this is no longer present post 25 CV cycles. As a result of this loss of the membrane surface over the duration of the CV scan, a scan rate study could not be performed.
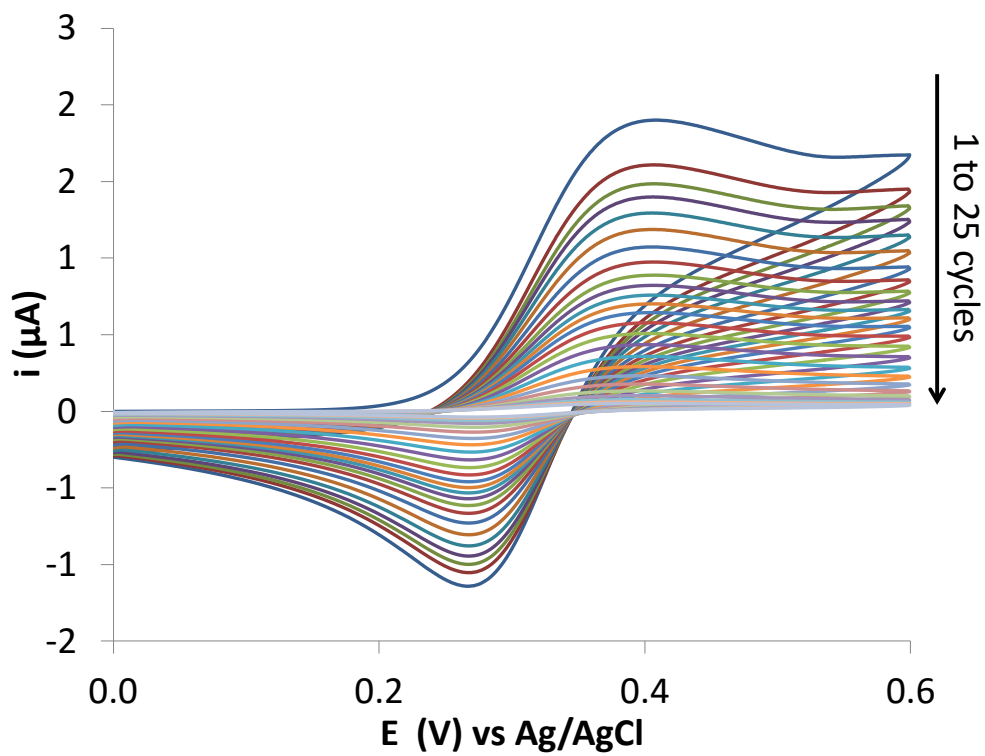
Figure 5.5.1.4.4 Typical CV obtained from PBS using 10 mM FcA and CA membrane drop

coated electrodes containing 0.3 % CA at 100 mV sec^{-1} for 25 cycles. (n=3)

Figure 5.5.1.4.5 Image taken of 10mM FcA and CA membrane drop coated electrode (**i**) before and (**ii**) after 25 cycles of CV in PBS.

The data suggests that drop coat of FcA and oxygen permeable membrane onto an industrially printed electrode could be a solution to the screen printed electrodes being porous. However, the result demonstrated CA membrane is incompatible with the FcA-mediated oxygen demand assay, because the drop coated surface is unstable when conducting electrochemical assays. Therefore, other methods of mediator immobilisation were investigated.

5.5.2 Chemical immobilisation

5.5.2.1 SAM-modified surface

5.5.2.1.1 SAM-Fc modified surface stability study

Self-assembled monolayers (SAM) are commonly used as a bridge between substrate and analyte in modifying electrodes [23]. To ensure the modified surfaces are stable whilst electrochemical assays are conducted, an electrochemical stability test was carried out on SAM bridged modified ferrocene electrodes. If the electrochemical tests show the SAM bridge surfaces are stable under electrochemical influences, it is hereby termed electrochemically stable. Whereas, if the electrochemical tests show the SAM bridge surfaces are unstable under electrochemical influences, it is hereby termed electrochemically unstable. Gold substrate chips were cleaned in the UV-Ozone machine for at least 1 hour before incubating in 1 mM 11-(Ferrocenyl) undecanethiol (UDT-Fc) (**figure 5.5.2.1.1.1**) in ethanol overnight.
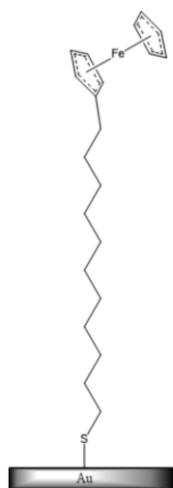

Figure 5.5.2.1.1.1 Structure of 11-(Ferrocenyl)undecanethiol.

Samples were sonicated in ethanol for 5 minutes and dried with argon gas before CVs were run for 10 cycles at 100 mV sec^{-1} (**figure 5.5.2.1.1.2**) (all CVs throughout section 5.5.2 conducted on gold or ITO substrates use a Teflon cell with a 5mm opening except when grafting the diazonium onto the substrate, see **section 5.5.2.2.1**). **Figure 5.5.2.1.1.3** is a summary of redox peak current obtained from **figure 5.5.2.1.1.2** which shows that the ferrocene currents have dramatically reduced within 10 cycles. The decrease of redox peak current suggests that the surface attached ferrocene is not stable during the electrochemical experiment. However, the cause for the reduction in peak current with cycle number and therefore, surface concentration of bound ferrocene could be as a result of 2 factors. Firstly, the thiol bond between the substrate and SAM is not stable and therefore the conjugated alkane thiol and ferrocene molecule comes away from the surface. Secondly, the ferrocene moiety is not stable. Further investigation was required in order to identify the point of instability.
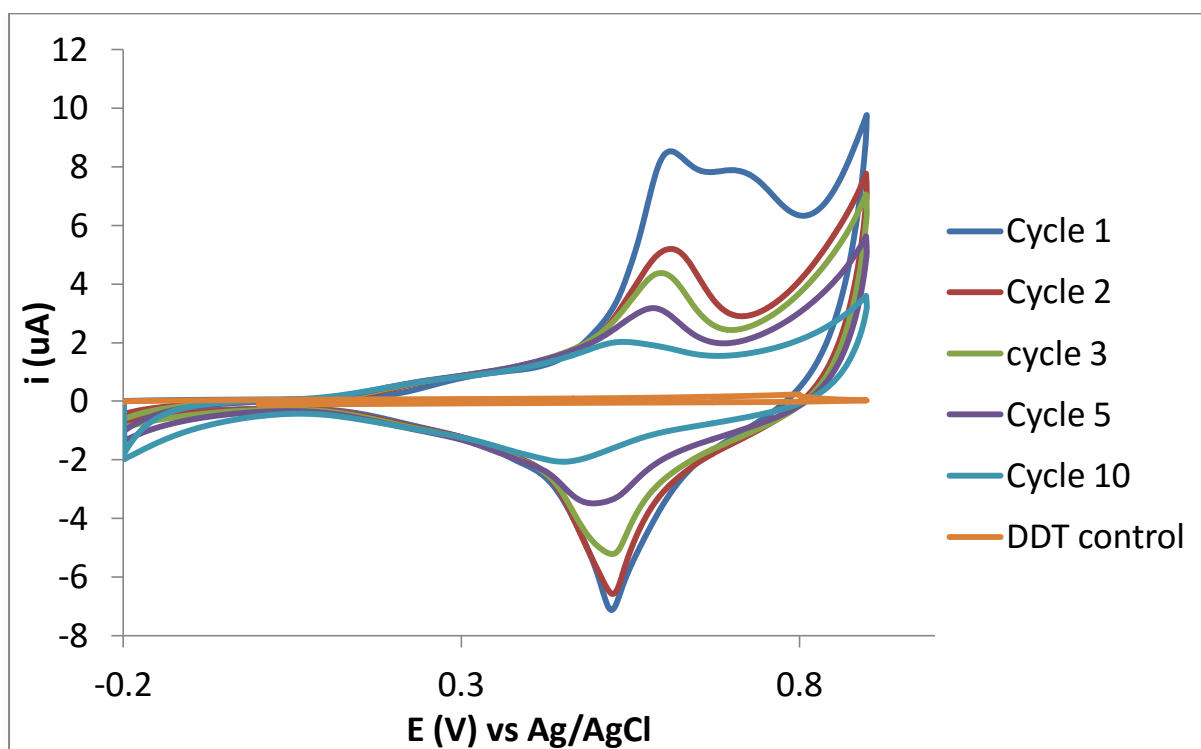

Figure 5.5.2.1.1.2 is a typical CV obtained from 10 cycles of CV of UDT-Fc in PBS. (n=2)
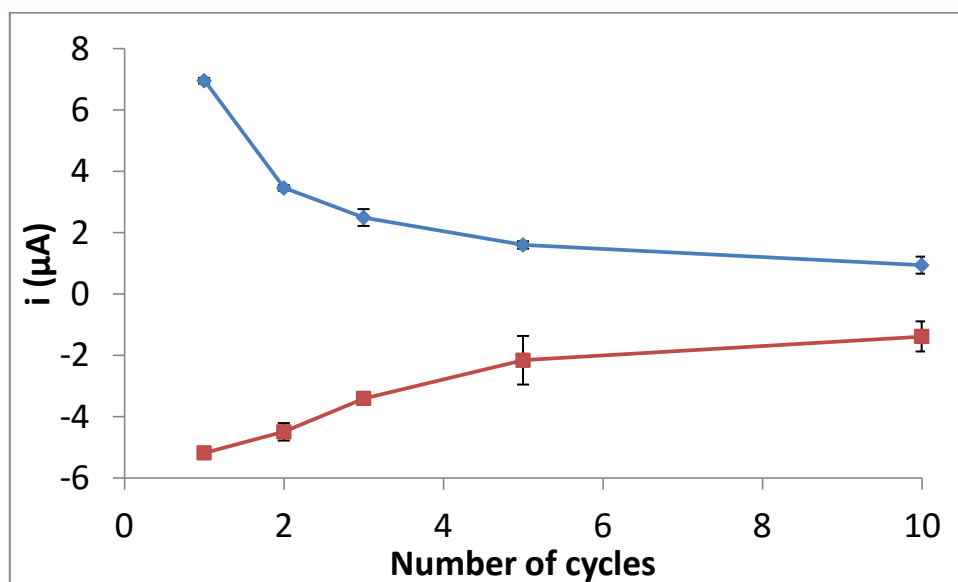
Figure 5.5.2.1.1.3 Summary of redox peak current obtains from **figure 5.5.2.1.1.2**.

5.5.2.1.2 Further investigation into SAM-modified surface stability study

Although the UDT-Fc SAM modified surfaces showed electrochemical instability with a decrease in redox peak current over increasing CV cycles, because the SAM-modified surface synthesis is relatively simple, therefore, further investigation was carried out. Data from **section 5.5.2.1.1** shows that the overall UDT-Fc molecule was not electrochemically stable, however, it is not certain if the electrochemical instability is due to the thiol bond between the alkane chain and the substrate or the alkane chain-Fc bond. Literature shows that diazonium could also be used as a bridge like SAM to synthesis di-Fc surfaces which forms even stronger bonds with the metal substrates [27, 28]. A possible reason for the high diazonium modified surface stability is the delocalisation of electrons in benzene ring structure of the aryl amine. If the benzene ring is the reason for the diazonium modified surface having high stability, it is possible we can still use SAM as the bridge as long as a

benzene ring structured SAM is used. This could potentially result in a chemical immobilisation process that has both advantages of relatively simple preparation offering less error, and yet increased stability for a SAM-Fc surface.

To investigate this possibility, it was necessary to establish if the instability of the original SAM UDT-Fc surfaces was due to the thiol bond or the ferrocene coupling. To investigate this, three different SAM molecule were picked to do a stability test using cyclic voltammetry. 1-dodecanethiol (DDT) (see **figure 5.5.2.1.2.1 i**), 11-amino-1-undecanethiol (UDT-NH$_2$) (see **figure 5.5.2.1.2.1 ii**) and 4-aminothiophenol (phenol-NH$_2$) (see **figure 5.5.2.1.2.1 iii**). UDT-NH$_2$ and phenol-NH$_2$ were chosen to allow investigation of the stabilising effect of the benzene group versus an alkane chain. DDT was chosen as it is very similar to the UDT-NH$_2$ having only a carbon group changed with an amine group, and would be a control to see how the NH$_2$ group affects stability. If the DDT and UDT-NH$_2$ are electrochemically unstable then it would confirm that the thiol bond is the reason the original UDT-Fc (**section 5.5.2.1.1**) surfaces were unstable. If data shows that the thiol-Au bond is stable then the alkane chain-Fc bond must be unstable and causing the decreased ferrocene peak current over multiple cycles. Alternatively if the DDT and UDT-NH$_2$ are found to be electrochemically unstable but the phenol-NH$_2$ is electrochemically stable it confirms that the thiol-Au bond could be being stabilised by the benzene ring.
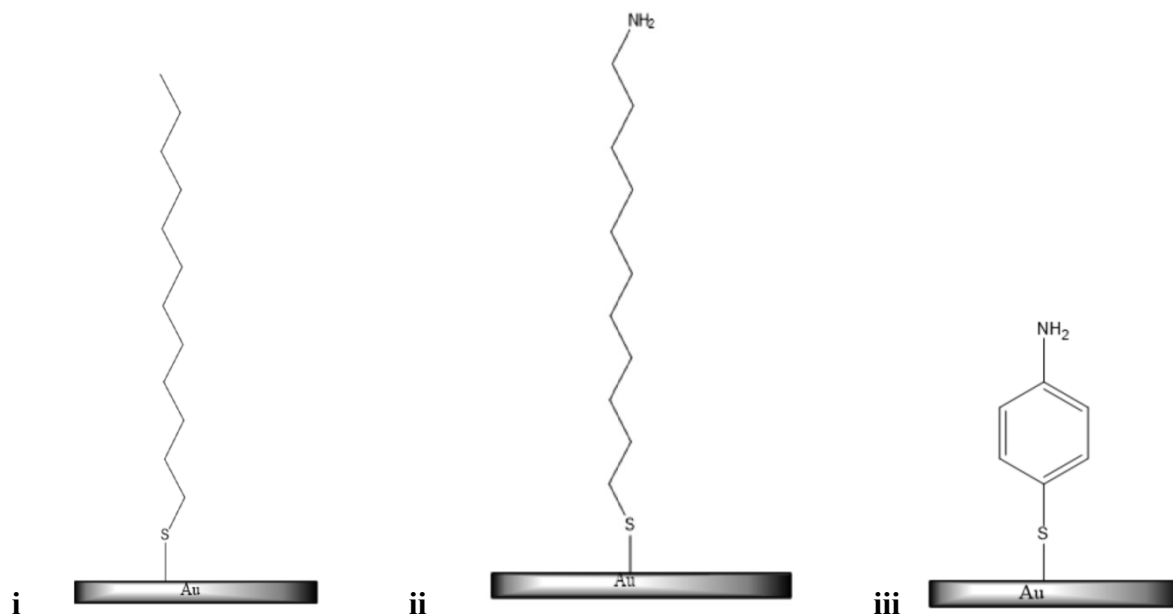
174

Figure 5.5.2.1.2.1 Chemical structure of (**i**) 1-dodecanthiol (DDT), (**ii**) 11-amino-1-undecanethiol (UDT-NH$_2$) and (**iii**) 4-aminothiophenol (phenol-NH$_2$).

To test the electrochemical stability of each SAM molecule, gold substrate chips were cleaned in the UV-Ozone machine for at least 1 hour before incubating in either 1 mM DDT, UDT-NH$_2$, or phenol-NH$_2$ in ethanol for 24 hours. Samples were sonicated in ethanol for 5 minutes and dried with argon gas before CVs (cyclic voltammetry) were performed. CVs were performed from a starting potential of 0 V to -1.5 V finishing at 0 V at 100 mV sec^{-1} in 0.1 M KOH. The extended negative potential would reduce the thiol bond removing all the SAM molecules from the gold substrate chips, and generating a desorption peak [46, 47]. The desorption peak is used to calculate the surface coverage of SAM yielded by 24 hours incubation on gold substrate calculated with **Equation 5.1** [48]. After the CV, samples were cleaned in water then ethanol each time and finally dried with argon gas, before being put back into the same SAM solution and incubated for another 24 hours. After the re-absorption of SAM [47], samples were again sonicated in ethanol for 5 minutes and dried with argon gas

before 50 cycle CVs in PBS solution were run scanning from 0 V to 0.6 V and back to 0 V potential, the same range used when performing the FcA-mediated oxygen demand assay, at 100 mV sec^{-1}. Each sample was then rinsed with water and dried with argon gas, then rinsed with ethanol and dried with argon gas again. Finally, the desorption CV was run again as before to calculate the coverage of SAM on the gold substrate following the 50 cycle CVs. Data from the first desorption CV and second desorption CV could allow for comparison of surface coverage of SAM before and after the 50 cycle CV in PBS was run and give comparison of the electrochemical stability of each DDT, UDT-NH$_2$, and phenol-NH$_2$.

Equation 5.1

$$\Gamma = Q/nFA$$

Where: Γ = surface coverage (mol cm-2), Q= the charge obtained by integrating the desorption peak, n = the number of electrons, F = Faraday constant, A is the electrode area.

Desorption data of DDT, UDT-NH$_2$ and phenol-NH$_2$ prepared gold substrate chips are presented in **figure 5.5.2.1.2.2, figure 5.5.2.1.2.3** and **figure 5.5.2.1.2.4** respectively. CV data is shown in **figure 5.5.2.1.2.2 i, figure 5.5.2.1.2.3 i** and **figure 5.5.2.1.2.4 i**, and finally the summary of DDT, UDT-NH$_2$ and phenol-NH$_2$ surface coverage with and without 50 cycles of CV in PBS are plotted in **figure 5.5.2.1.2.2 ii, figure 5.5.2.1.2.3 ii** and **figure 5.5.2.1.2.4 ii**. The surface coverage of DDT was shown to decrease when we compared the surface coverage before and after the 50 cycles of CV in PBS. This confirms it was the thiol both between UDT-Fc and the gold substrate that was broken in **section 5.5.2.1.1**. UDT- NH$_2$ also shows the surface coverage decreased compare the surface coverage before and after the 50

cycles of CV in PBS. This confirms it was not the amine group affecting the stability of the SAM surface. Finally, phenol-NH$_2$ also demonstrates a surface coverage decrease comparing before and after 50 cycles of CV in PBS. This shows that benzene ring was not the factor contributing to the diazonium modified surfaces' electrochemical stability.
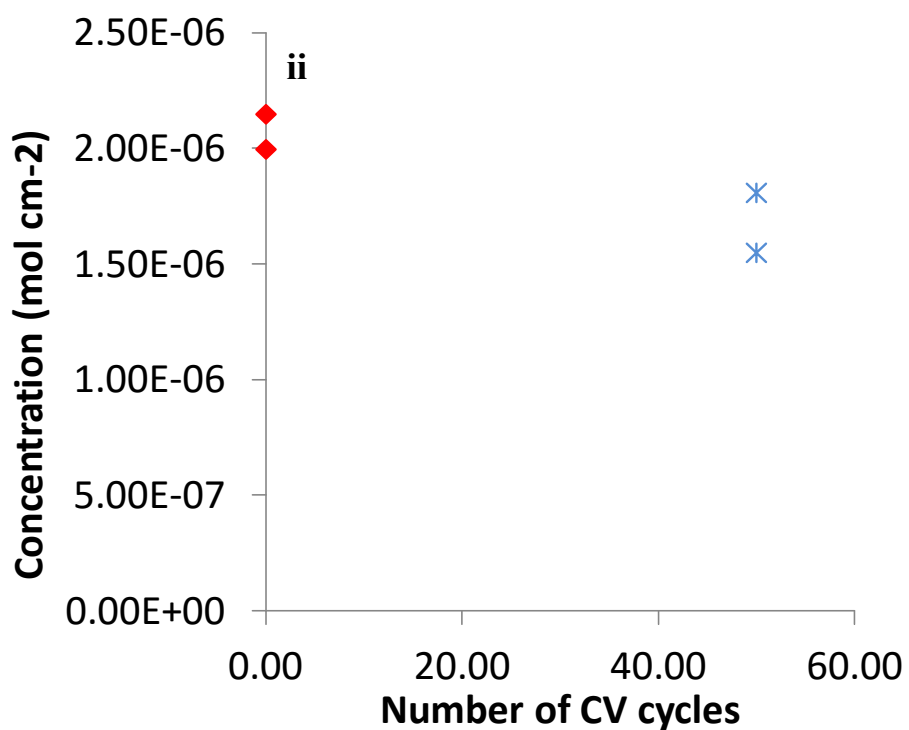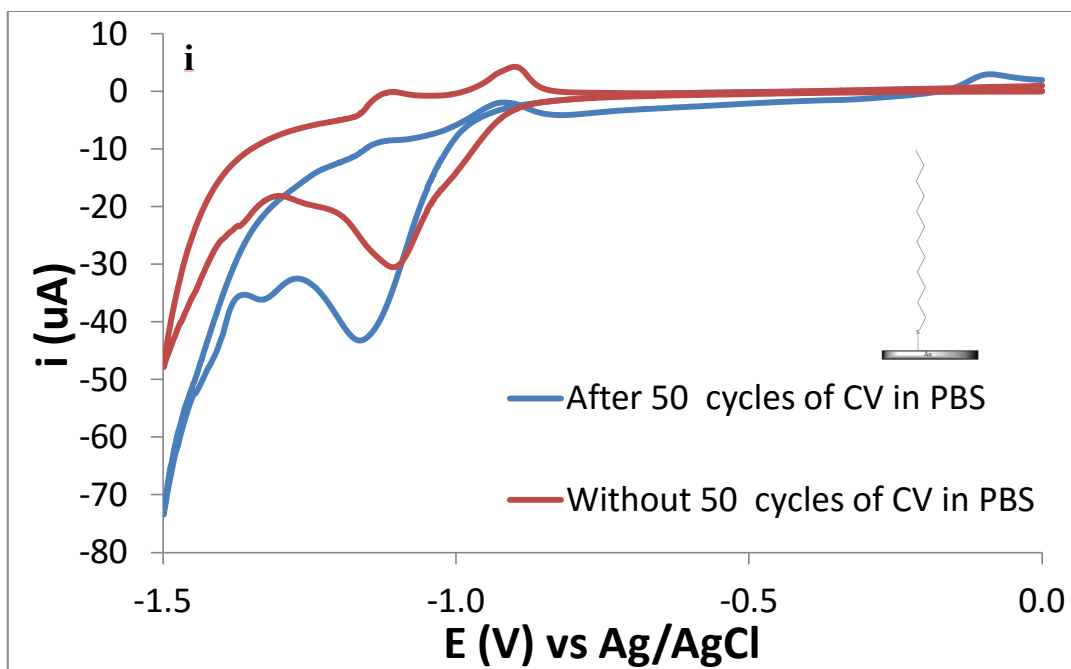
Figure 5.5.2.2.2 (i) Typical CV obtained from DDT modified surface desorption peak in 0.1 M KOH before and after 50 X cycles of CV in PBS. **(ii)** Concentration of DDT present on the electrode surface calculated using data from **figure 5.5.2.2.2 (i)** and **equation 5.1**. (n=2)
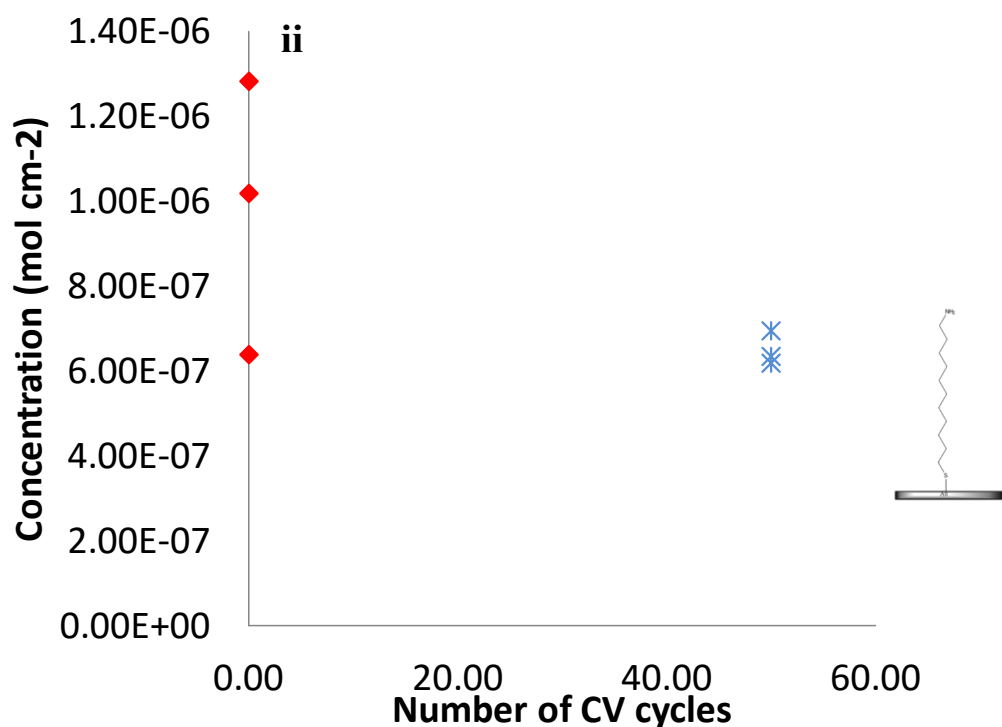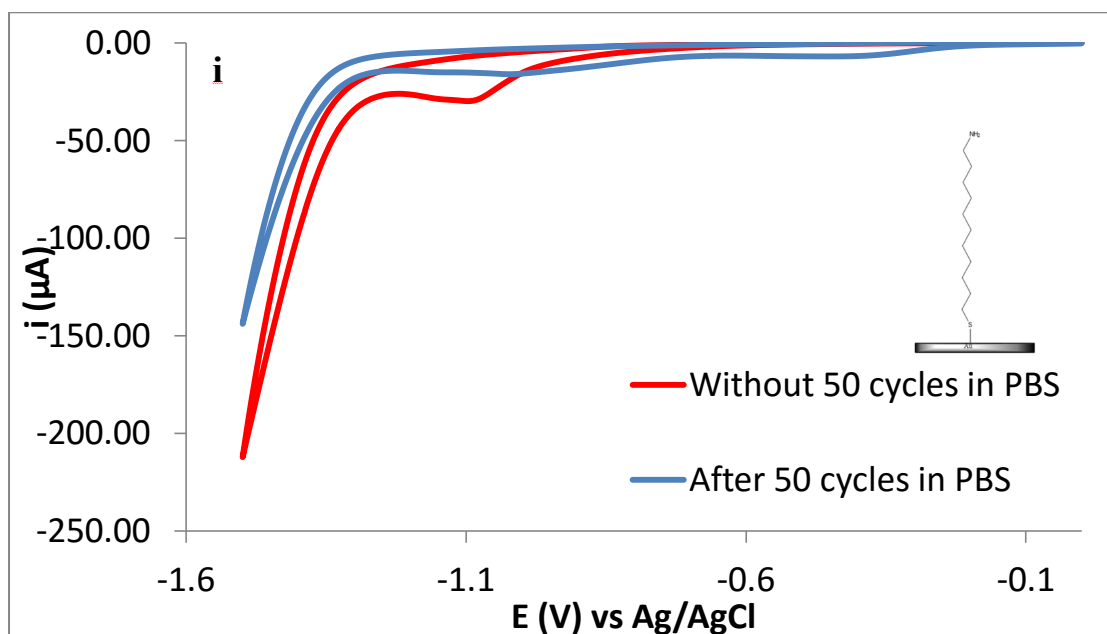
Figure 5.5.2.2.3 (**i**) Typical CV obtained from UDT- NH_2 modified surface desorption peak

in 0.1 M KOH before and after 50 X cycles of CV in PBS. (**ii**) Concentration of UDT- NH_2

present on the electrode surface calculated using data from **figure 5.5.2.2.3** (**i**) and **equation**

5.1. (n=3)

Figure 5.5.2.2.4 (i) Typical CV obtained from Phenol-NH$_2$ modified surface desorption peak in 0.1 M KOH before and after 50 X cycles of CV in PBS. **(ii)** Concentration of UDT- NH$_2$ present on the electrode surface calculated using data from **figure 5.5.2.2.4 (i)** and **equation 5.1**. (n=2)
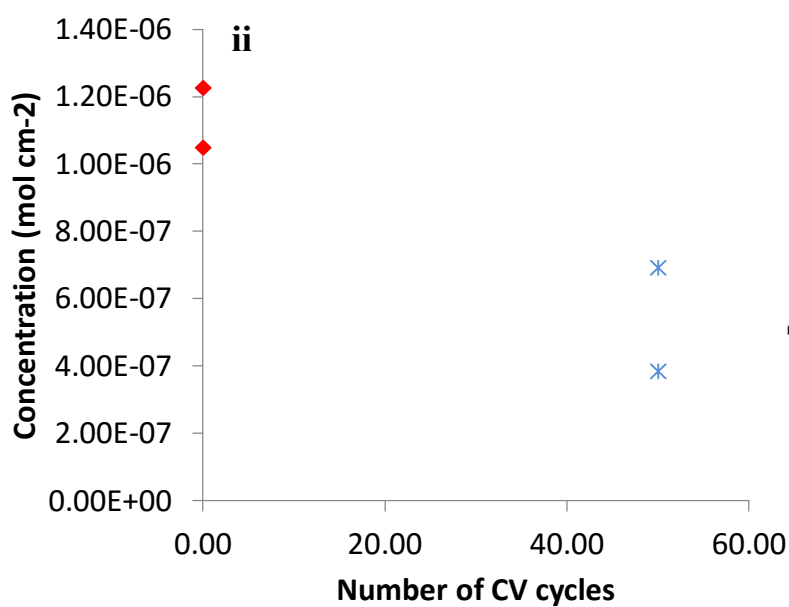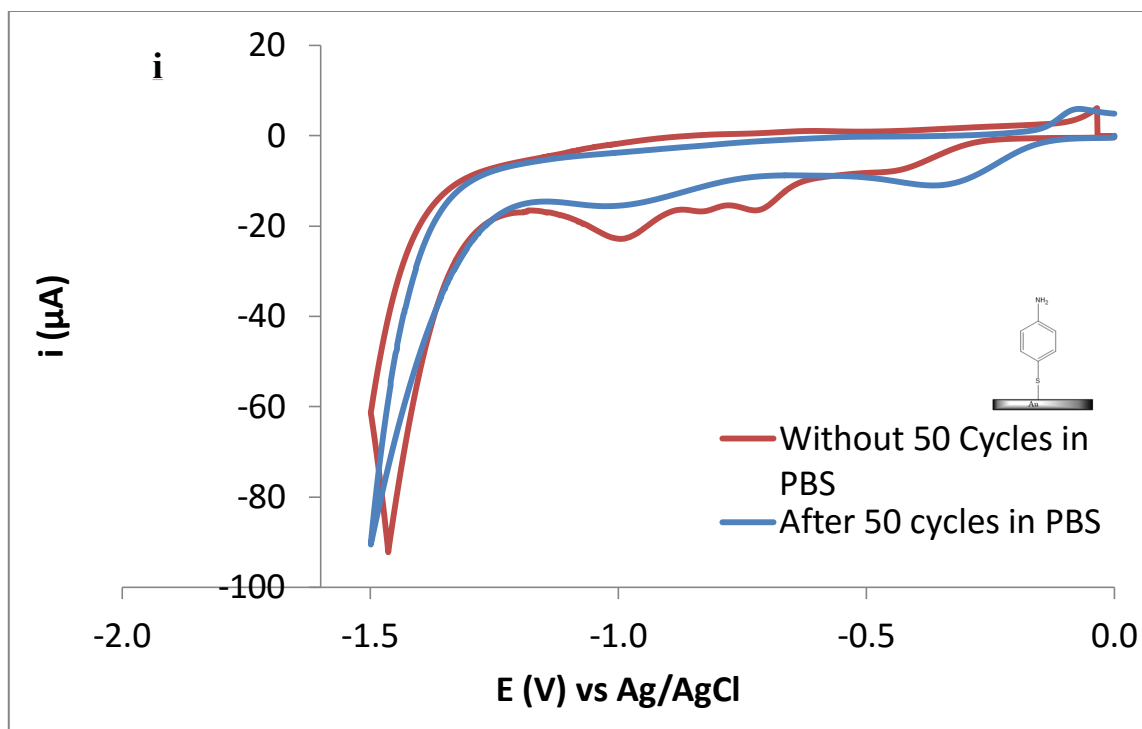
Having investigated further into the electrochemical stability of SAM modified electrode surfaces, it was concluded that the reason for the electrochemical instability of the SAM modified electrode surfaces when applying potential, is that the thiol bond on the gold substrate was being electrochemically oxidised and cleaved [49]. This is supported by the evidence that the phenol-NH_2 SAM (benzene-sulphur-gold bond) was cleaved whereas when bound as aryl-amine (benzene-carbon-gold bond) in the case of diazonium grafting the bond is stable. There are other methods that maybe able to help strengthen the thiol-Au bond. In low pH environment, the thiol-Au would become coordinate bond which is strong than covalent bond in high pH [50]. However, lowering the electrolyte pH would make the system less compatible for biological system, for example mammalian cell lines [51]. In conclusion, at this stage the thiol-gold bond instability at the require working potential needed to run the FcA mediated oxygen demand assay, renders SAM modified surface electrodes unsuitable for FcA immobilisation. For this project, and at this stage, literature suggested investigation would be better focused into testing diazonium as a bridge for FcA immobilisation, due to it having stronger bridge to substrate bonding.

5.5.2.2 Diazonium Modified Surface

5.5.2.2.1 Preliminary diazonium modified surface stability study

Another popular method used to bridge substrate and analyte in modifying electrodes is to use diazonium electrochemical grafting to produce diazonium modified (di) surfaces. The electrochemical stability of this also needed testing to ensure the stability of the grafting for the intended assay conditions. To this end, an aryl amine was grafted on UV-ozone cleaned gold substrate via diazonium electrochemical grafting as described in Rawson, 2013 [31]. 10 mM p-phenylenediamine was mixed with sodium nitrite in a 1:1 ratio in 10 ml of 0.5 M HCl

and left on the bench for 3 minutes (**figure 5.5.2.2.1.1 i**). Substrate chips was then connected

to the working electrode wire and dipped into diazonium and sodium nitrite solution and held

at -0.6 V potential for 10 second (**figure 5.5.2.2.1.1 ii**). Substrate chips were then rinsed with

water and dried with argon gas, then rinsed again with ethanol and dried with argon gas. Di

surfaces were then left in 1 mM ferrocene carboxylic acid NHS ester (FcA-Ester) in ethanol

overnight (**figure 5.5.2.2.1.1 iii**). Diazonium-ferrocene (di-Fc) samples were sonicated in

ethanol for 5 minutes before conducting CV.
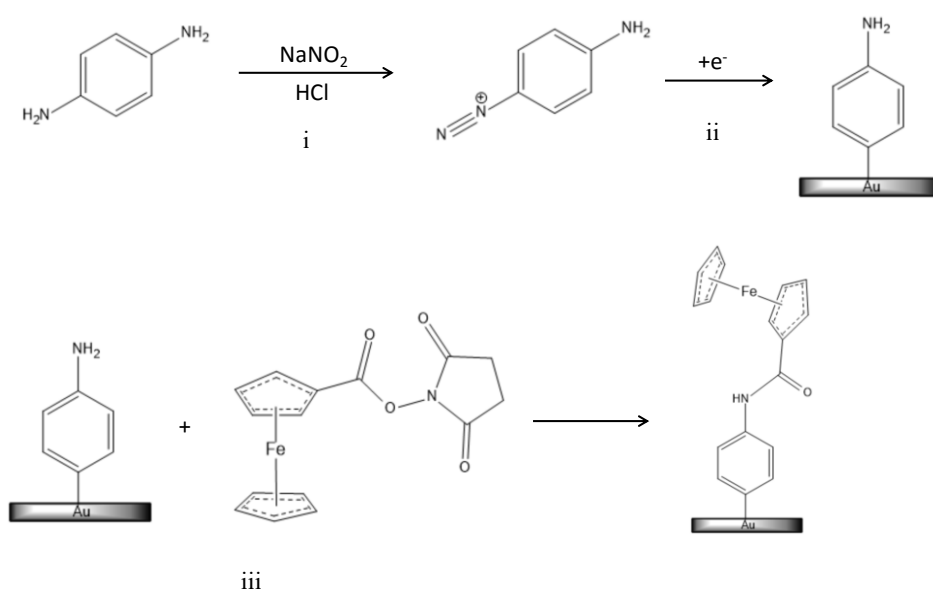
Figure 5.5.2.2.1.1 A diagrammatic explanation of diazonium-ferrocene (di-Fc) surface

synthesis.

Ten consecutive CV were performed with the di-Fc surface in PBS at 100 mV sec^{-1} (**figure

5.5.2.2.1.2**). **Figure 5.5.2.2.1.3** is a summary of the ferrocene redox peak current extracted

from **figure 5.5.2.2.1.2** and the data suggests that di-Fc is stable within the 10 cycles of CV.

However the ferrocene redox current of the di-Fc surface at 572 nA, was significantly smaller

than the UDT-Fc surfaces at 6.96 µA. This is because in comparison to the manufacturer

prepared UDT-Fc which has ferrocene attached to each SAM molecule, there are 2 steps in the process of synthesising the surface that could affect the yield. Both the coverage of diazonium salt and coupling efficient of ferrocene onto the diazonium salt can account for the reduced yield. Optimisation work is required in order to increase the multi-step synthesis yield.

Figure 5.5.2.2.1.2 Ten consecutive cycles of CV conducted in PBS using di-Fc modified electrode.

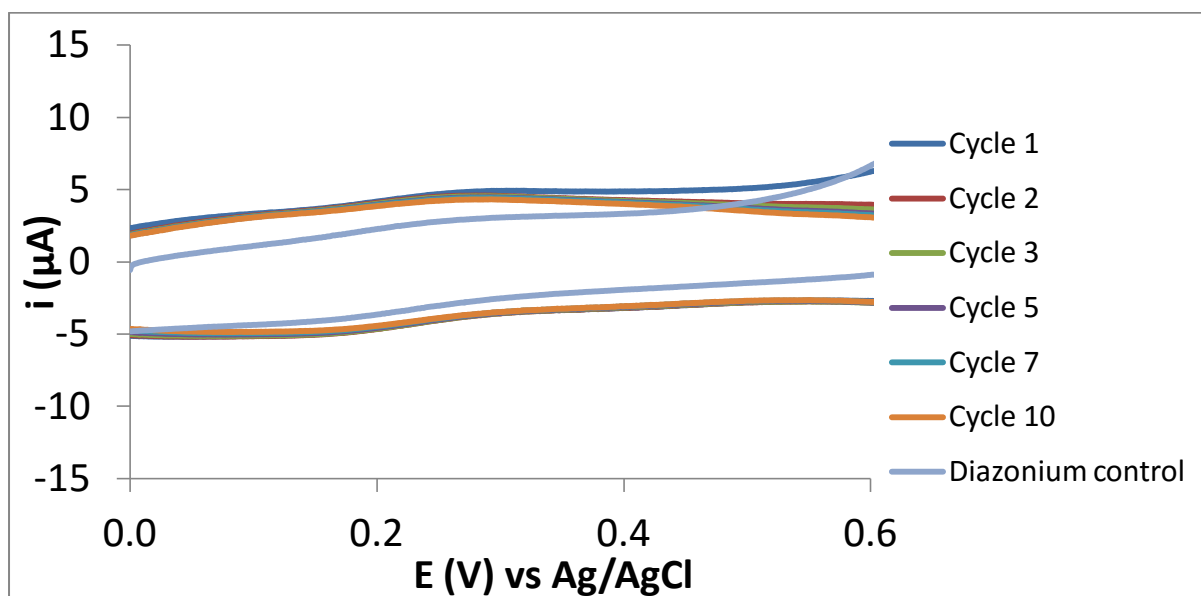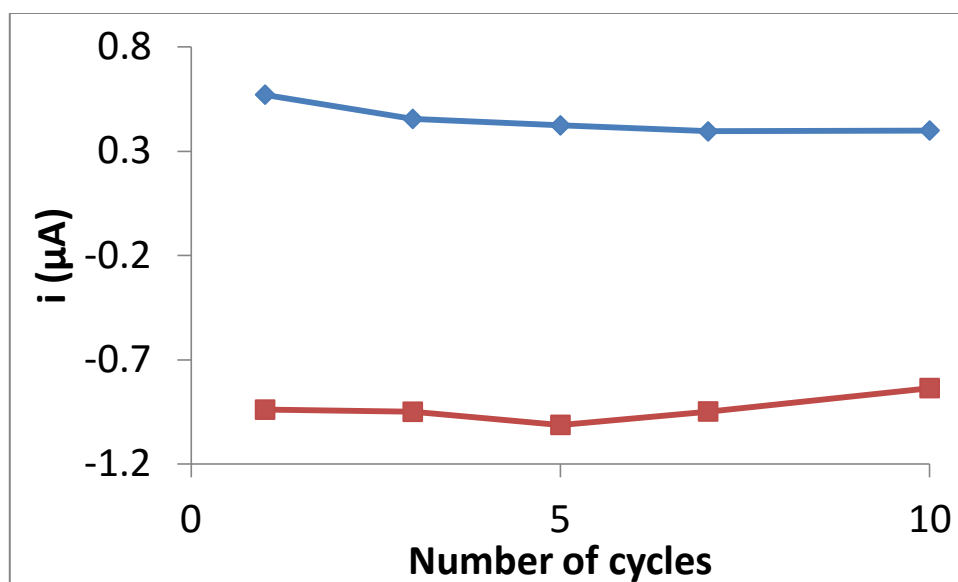**Figure 5.5.2.2.1.3** Plot of ferrocene redox peaks in 10 cycles obtained from **figure 5.5.2.2.1.2**. The blue line shows the oxidation peak and the red line shows the reduction peak current.

5.5.2.2.2 Diazonium grafting optimisation

SAM surface fabrication by its nature produces a single layer coverage of the electrode surface however, comparatively diazonium grafting is much more complex. Many factors for example grafting duration [52], can affect the grafting process which can cause multilayer formation [53, 54]. Formation of multiple layers of excessive thickness of the diazonium as shown in **figure 5.5.2.2.2.1**, could cause blocking of electron transfer from the substrate to the redox centre rendering the electrode useless. Alternatively if the grafting is too thin or incomplete, for example there may be pinholes [30], the amount of mediator that can be coupled onto the surface would be limited and, the system would be vulnerable to interference from any electrochemically active species in the sample. In previous studies 120 s was utilised to graft an aryle amine via electrochemical reduction of the corresponding diazonium on ITO [31] however this is greatly affected by environmental conditions e.g.

temperature. For example, from observation, when sodium nitrite was added into the p-phenylenediamine solution (**figure 5.5.2.2.1.1 i**), the speed of colour change from clear to yellow of the 10 mM p-phenylenediamine was significantly affected by temperature variations in the laboratory. Therefore it was necessary to establish an optimal grafting time for the laboratory environment in which the studies were conducted.
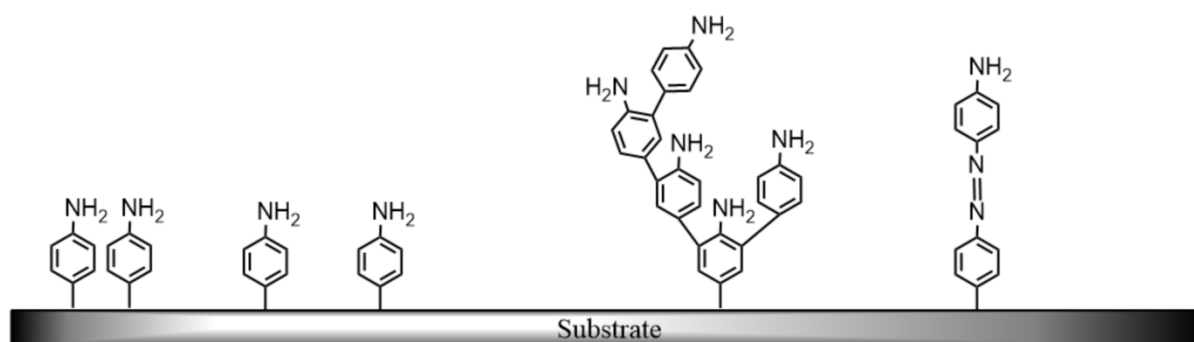
Figure 5.5.2.2.2.1 A diagrammatical representation of examples of diazonium grafting.

An aryl amine was grafted on to gold and ITO substrate via electrochemical diazonium reduction in order to compare the grafting affinity of each substrate. Gold was used to allow comparison between SAMs and aryl amine modified surface via the diazonium immobilisation techniques, however unlike SAM modified surfaces, diazoniums can be grafted on many metals, therefore ITO substrate grafting was also investigated. ITO being transparent offers an advantage over gold substrate as it would allow the system to be integrated for use with other techniques such as microscopy and colourimetry. This could prove highly advantageous for use in biological applications. ITO and gold substrates were cleaned and dipped into p-phenylenediamine solution as described in **section 5.5.2.2.1**. The diazonium was then grafted on the substrates by applying a potential of -0.6 V for 0, 10, 20,

25, 30, and 60 seconds. Samples were rinsed with water and ethanol, before sonicating in ethanol for 5 minutes. The aryl amine modified gold and ITO electrodes were then used to perform CVs using a solution of 1 mM ferricyanide in PBS. The CV was started from a potential of 0.6 V with a switching potential of -0.2 V and an end potential at 0.6 V at 100 mV sec^{-1}. As the grafting time increases, so does the amount of diazonium salt grafted onto the substrate surface [55] until eventually the electrode is completely covered, thus blocking the electrons reaching the ferricyanide in the solution. The ideal grafting time would be the shortest possible time when we observe blockage of electron transfer, meaning complete surface coverage but minimal grafting layer thickness.

Cyclic voltammograms generated for solutions consisting of 1mM ferricyanide using either gold or ITO electrodes modified via electrochemical grafting of diazonium, at electrodes exposed to reduction potentials so facilitate grafting at varying lengths of are presented in **figure 5.5.2.2.2.2 i** and **figure 5.5.2.2.2.3 i**. The summary of i_{pc} of ferricyanide at different grafting times of diazonium on gold and ITO substrates are plotted in **figure 5.5.2.2.2.2 ii** and **figure 5.5.2.2.2.3 ii**. CV data shows that there is no blockage of ferricyanide signals on both substrates at the 0 second control grafting time. It is seen as grafting time increases from 0 to 20 seconds, increased amount of aryl amine are formed on the substrate surface slowing down the transfer of electrons [56], subsequently a decrease in ferricyanide signal is observed. This is also reported in other diazonium modified surfaces [30]. At 30 second grafting time in gold substrate and 25 second on ITO substrate it shows a stable, reliable blockage of ferricyanide signal. This suggested that diazonium has a slight quicker grafting kinetic on ITO compared to gold substrate.

Figure 5.5.2.2.2.2 (**i**) Typical CVs obtained from 1 mM ferricyanide in PBS solution scanned at 100 mV sec^{-1} with diazonium grafted onto gold substrate at 0, 10, 20, 25, 30, and 60 second intervals. (**ii**) Plot summary of i_{pc} of ferricyanide from **Figure 5.5.2.2.2.2 i** (n=3, ±1 SD)
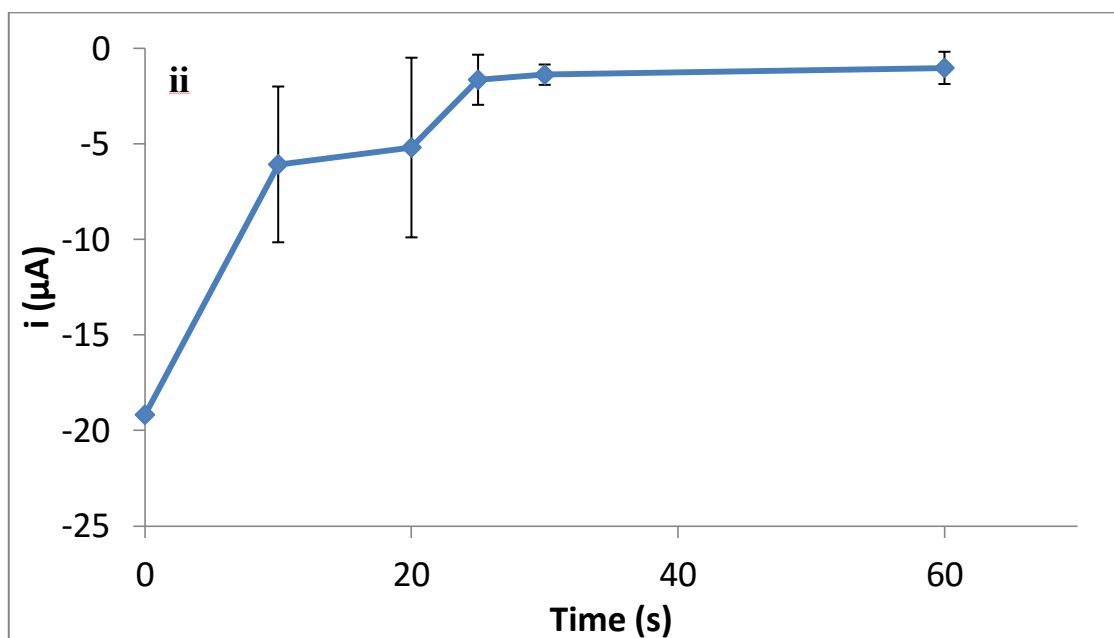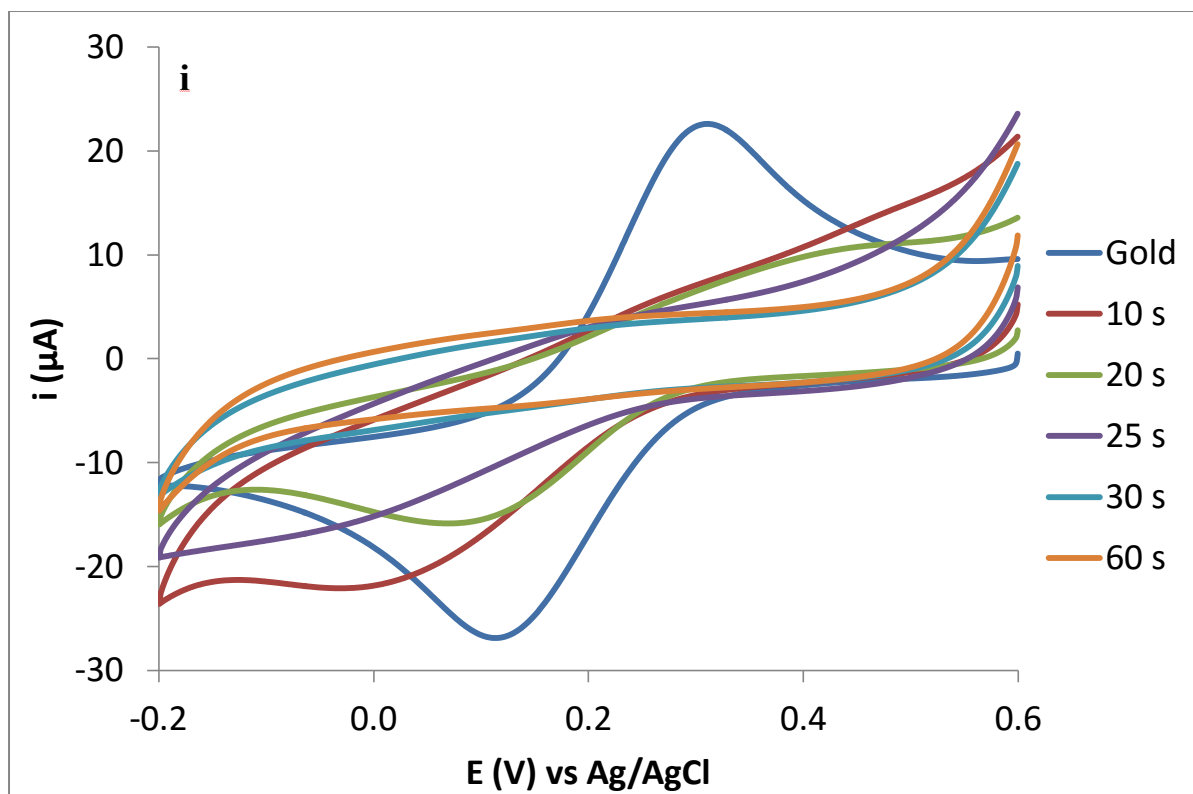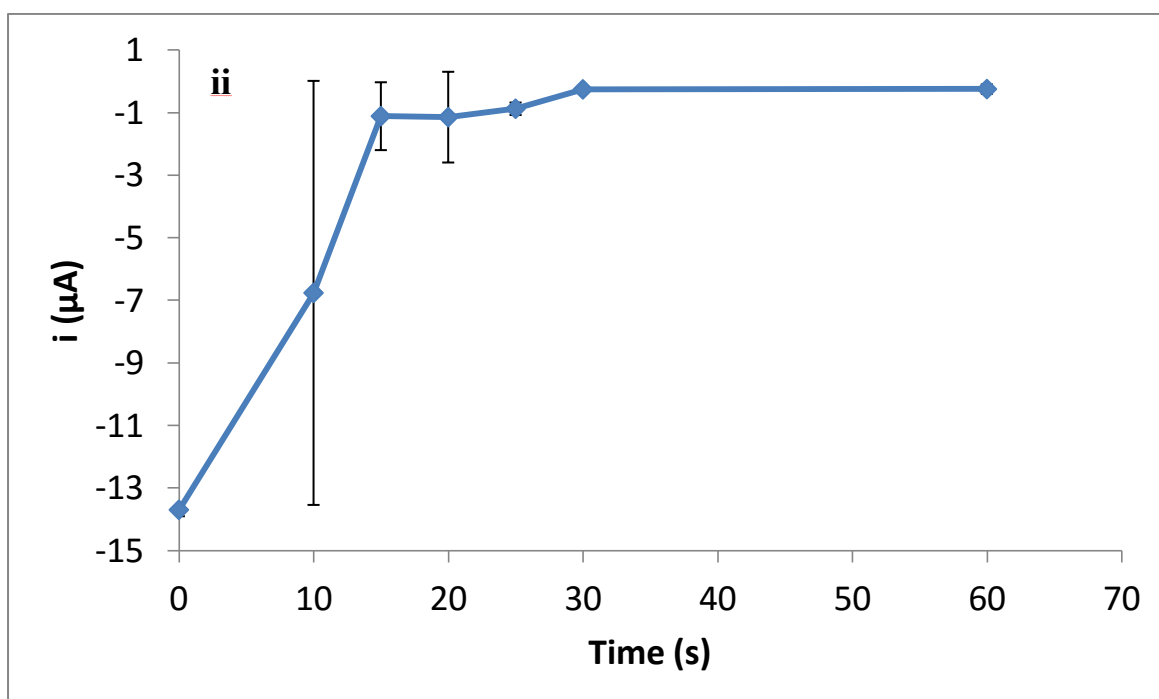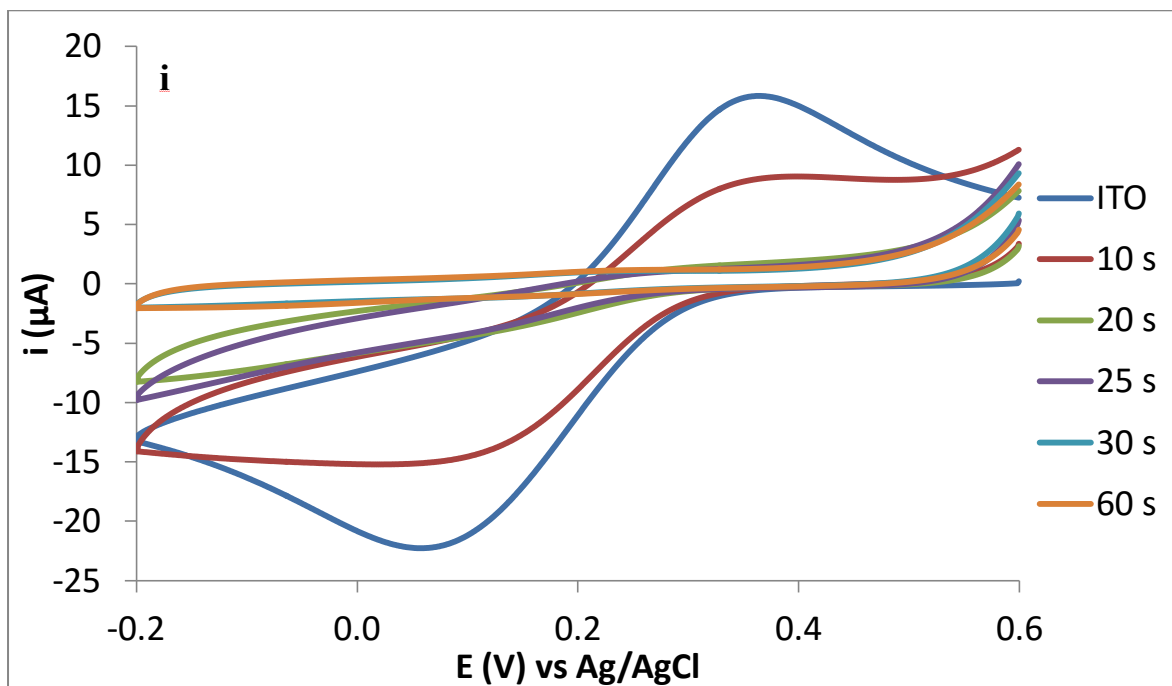
Figure 5.5.2.2.2.3 (**i**) Typical CVs obtained from 1 mM ferricyanide in PBS solution scanned

at 100 mV sec^{-1} with diazonium grafted onto ITO substrate at 0, 10, 20, 25, 30, and 60 second

intervals. (**ii**) Plot summary of i_{pc} of ferricyanide from **Figure 5.5.2.2.2.3 i** (n=3, ±1 SD)

5.5.2.2.3 Diazonium modified surface stability

Having found the optimum grafting time of 30 s and 25 s for gold and ITO substrates respectively a more thorough investigation into the electrochemical stability of the grafting was conducted using CV. As previously discussed in **section 5.5.2.2.1**, data in **figure 5.5.2.2.1.3** shows, the diazonium grafting to be electrochemically stable following 10 cycles of CV with grafting time of 10 s. Using the optimal grafting time, 30s and 25s respectively for gold and ITO diazonium modified substrate chips were prepared and tested with 50 cycles CV running at 0 V to 0.6 V finishing at 0 V in PBS at 100 mV sec^{-1}. Before and after the 50 cycles of CV in PBS was run the coverage of grafted diazonium was tested by CV with 1 mM ferricyanide in PBS as above.

Data shows the diazonium grafted film was stable after 50 cycles of CV in PBS on both gold (**figure 5.5.2.2.3.1**) and ITO (**figure 5.5.2.2.3.2**) substrates. This is clearly visible as the ferricyanide mediated redox reaction was blocked before and after the 50 cycles of CV in PBS was run.
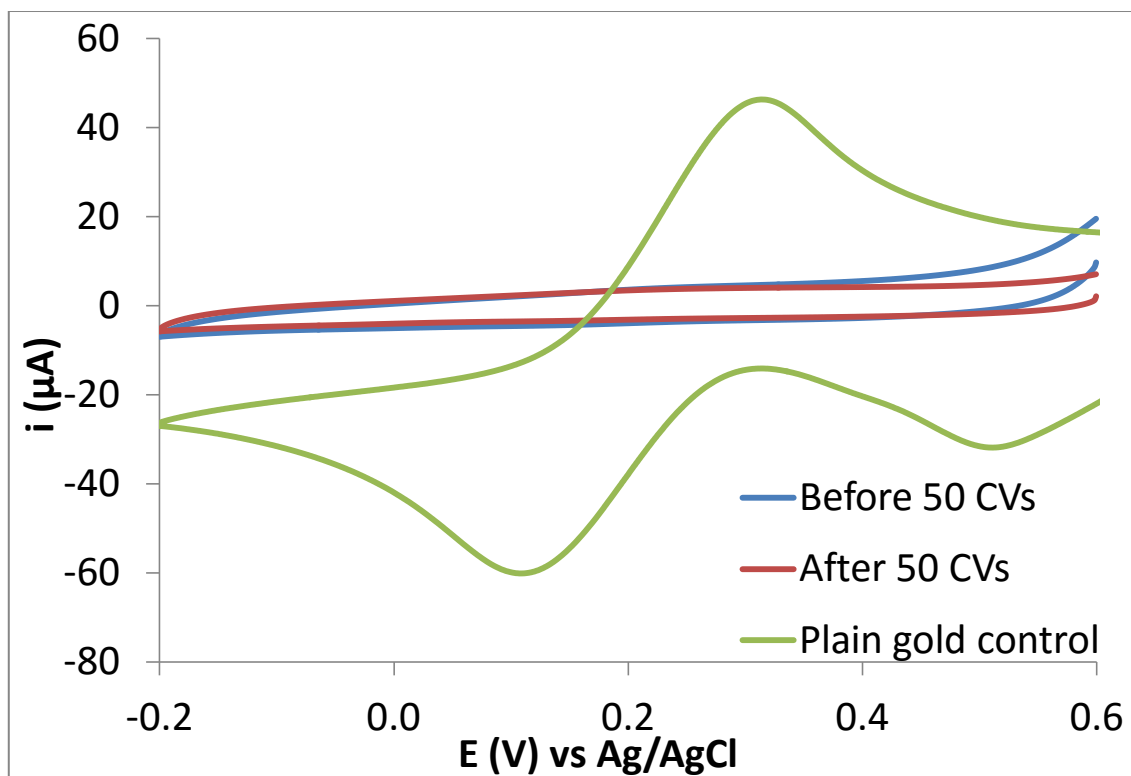
Figure 5.5.2.2.3.1 Typical CVs of 30s grafted diazonium modified gold substrate in 1 mM

ferricyanide. The blue cycle is the CV obtained before running 50 cycles of CVs in PBS, and

the red cycle is the CV obtained after running 50 cycles of CVs in PBS. The green cycle is

the positive control with no diazonium grafted on the gold substrate. (n=3, control n=1)
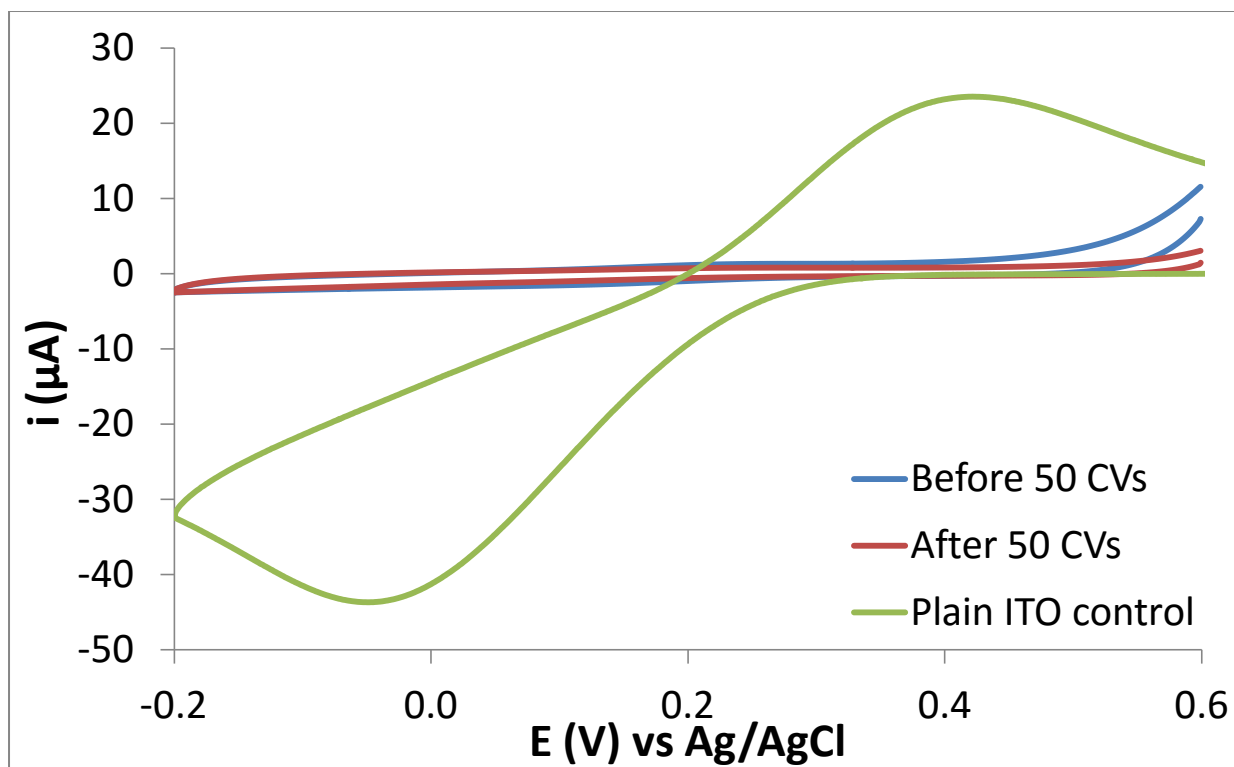
Figure 5.5.2.2.3.2 Typical CVs of 25 s grafted di modified ITO substrate in 1 mM ferricyanide. The blue cycle is the CV obtained before running 50 cycles of CVs in PBS, and the red cycle is the CV obtained after running 50 cycles of CVs in PBS. The green cycle is the positive control with no diazonium grafted on the ITO substrate. (n=3, control n=1)

5.5.2.2.4 Diazonium modified surface storage stability

Following the electrochemical stability study of the aryl amine modified surface, the storage stability was investigated. Storage stability is very important, because after the diazonium modification, FcA has to be coupled onto the diazonium increasing the time taken to synthesise the electrode chips. The storage stability of diazonium modified electrode would directly affect the viability of it as a surface, as it must be stable enough for the duration of the whole di-Fc synthesis process and the subsequent assay work. Also of great importance would be the stability enabling longer term storage of the electrode, for example field work

and production purposes. Previous results show diazonium has similar grafting kinetics on both gold and ITO substrate, as well as, electrochemical stability. Between gold and ITO, ITO is more favourable for biological integration of the system as it is transparent as previously discussed. Therefore, from this point onward, ITO was chosen to be the most optimal substrate to carry on the system development.

Diazonium modified ITO surface was prepared as described earlier in the section with a 25 seconds grafting to maximise coverage. Afterwards the fabricated electrodes were placed in the Teflon cell, and CVs were performed firstly with PBS as negative control to confirm there are no peaks with PBS alone. Afterwards they were rinsed with water and ethanol and finally a CV run 1 mM ferricyanide in PBS. Samples were rinsed with water then ethanol and dried with argon gas. After drying the telfon cell, it was covered with paraffin film and stored in a dry, dark and cool area. The CV run with 1 mM ferricyanide in PBS was repeated after storing in air for intervals of 1, 3, 5, and 7 days (n=5). Typical results are shown in **figure 5.5.2.2.4.1**. All of the samples were shown to be stable on day 0, 1 and 3. One of the samples was shown to be unstable on day 5 and three were not stable on day 7. Therefore, it was concluded that the diazonium grafted film is stable for a maximum of 3 days after grafting if stored in a dry, cool and dark place.
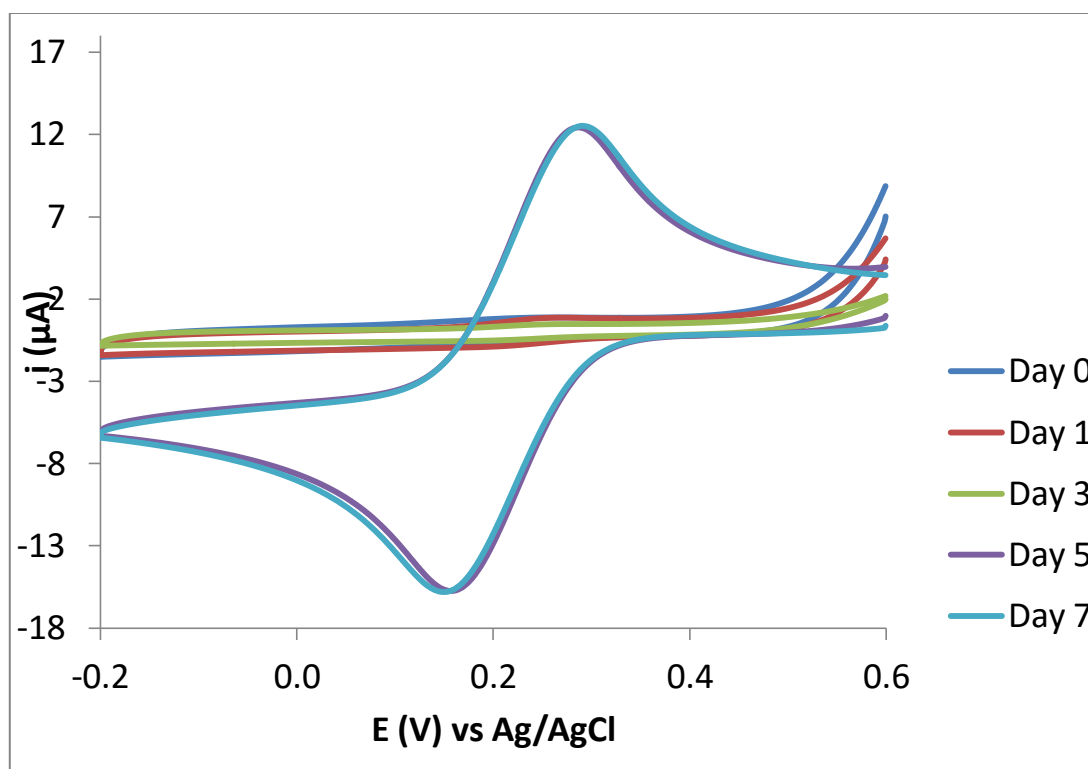
Figure 5.5.2.2.4.1 Typical CV of diaoznium modified surface in 1 mM ferricyanide in PBS

at 100 mV sec^{-1} after being stored in air for 0, 1, 3, 5, 7 days. (n=5)

5.5.2.2.5 Ferrocene coupling

As the optimisation of the bridge, diazonium modified surface is completed. The next step was to couple the mediator, FcA, onto the bridge aryl amine. In chapter 4 (**section 4.5.4**) however, data shows that the monocarboxylic acid group is essential for the appearance of the separated O_2 catalytic peak. By using the single carboxylic acid group to complete the coupling reaction with the aryl amine the coupling may affect the overall electron density [57] in the FcA, therefore, potentially altering the separated O_2 catalytic peak characteristic. For this reason both ferrocene carboxylic acid NHS ester (FcA-Ester) **figure 5.5.2.2.5.1** and 1, 1'-ferrocene carboxylic acid NHS ester (FcDA-Ester) **figure 5.5.2.2.5.2** were used for the surface coupling. The hypothesis was that while one of the carboxylic acid functional groups

may be involved in the aryl amine-mediator coupling reaction the second functional carboxylic acid group would be preserved for the separated O_2 catalytic peak reaction. FcA-Ester coupling was investigated first.
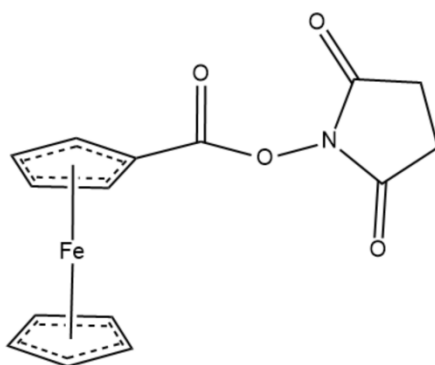
Chemical Formula: $C_{15}H_{13}FeNO_4$
Molecular Weight: 327.11
m/z: 327.02 (100.0%), 328.02 (19.1%), 325.02 (6.4%), 329.02 (1.6%), 329.03 (1.3%), 326.03 (1.1%)

Figure 5.5.2.2.5.1 Structure of FcA-Ester.
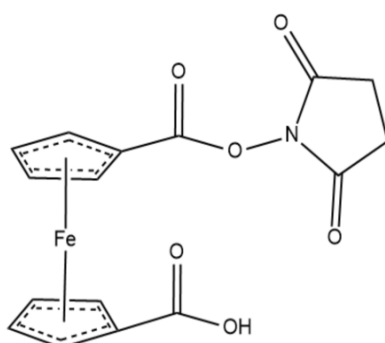
Chemical Formula: $C_{16}H_{13}FeNO_6$
Molecular Weight: 371.12
m/z: 371.01 (100.0%), 372.01 (20.2%), 369.01 (6.4%), 373.01 (2.0%), 373.02 (1.5%), 370.02 (1.1%)

Figure 5.5.2.2.5.2 Structure of FcDA-Ester.

Basic procedures were followed as in **section 5.5.2.2.1** and **figure 5.5.2.2.1.1** however diazonium grafting time, FcA-Ester coupling concentration and coupling incubation time were changed. Diazonium was grafted onto ITO surfaces for 25 seconds as shown to be optimal is **section 5.5.2.2.2**, FcA-Ester coupling concentration was tested at 1.2, 2, 3, and 5 mM in ethanol to test for the optimal concentration. Finally the incubation time was set for 24 hours to ensure incubation was sufficient for the coupling reaction to occur. All samples were sonicated for 5 minutes in ethanol prior to CVs being performed.

CVs were performed on each sample in PBS scanning from 0 V to 0.6 V back to 0 V at scan rate 100 mV sec^{-1} (**figure 5.5.2.2.5.3**). Data shows that the coupling efficiency was very low, and there was no significant difference between the different FcA-Ester coupling concentrations tested.

Figure 5.5.2.2.5.3 Typical CVs obtained from PBS solution scanned at 100 mV sec^{-1} with di

surface after incubated in 0 (Di), 1.2, 2, 3, and 5 mM FcA-Ester in ethanol for 24 hours.

(n=2)

In an attempt to improve the coupling efficiency alternative solvents were used for the

coupling reaction. The same procedure was employed to produce di-Fc surfaces, with the

exception of replacing ethanol with dichloromethane (DCM) and dimethylformamide (DMF).

CVs were performed on each sample in PBS scanning from 0 V to 0.6 V back to 0 V at scan

rate 100 mV sec^{-1} (**figure 5.5.2.2.5.4**). These alternative solvents however, did not show any

improvement of the FcA-Ester coupling efficiency. In addition, a colour change was observed

when the FcA-Ester was diluted in DCM and DMF. FcA-Ester diluted in ethanol stays

yellow-orange, while FcA-Ester diluted in DCM and DMF change to a dark brown colour

(**figure 5.5.2.2.5.5**).
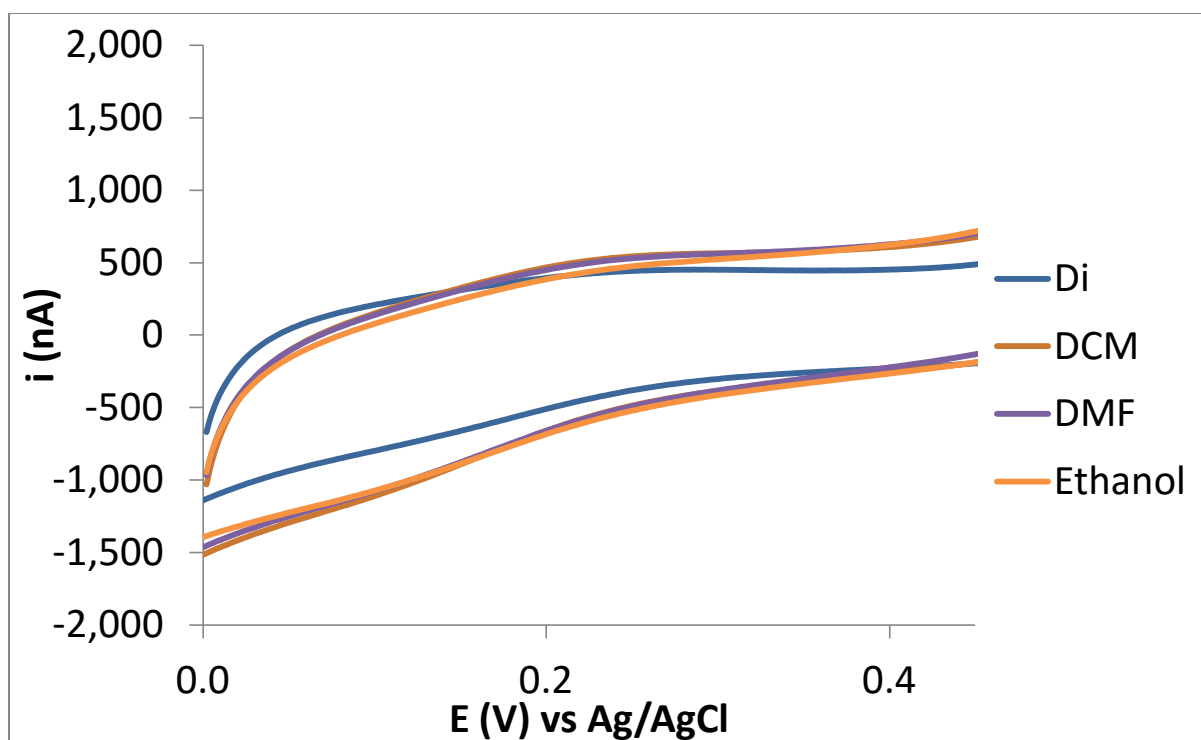
Figure 5.5.2.2.5.4 Typical CVs obtained from PBS solution scanned at 100 mV sec^{-1} with di surface after incubated in 5 mM FcA-Ester in ethanol, DCM and DMF for 24 hours. The blue line, Di, is the di surface alone negative control. n=2

Figure 5.5.2.2.5.5 Image of FcA-Ester dilated in Ethanol (left) and DMF (right) after 2 hours.

Triethylamine (TEA) is commonly used tertiary amine base in NHS ester - carboxylic acid reaction as it facilities the reaction [58]. The next batch of di-Fc samples were prepared by incubating di surface in 5 mM FcA-Ester and TEA in DCM for 24 hours. CVs were then performed using the samples as before (**figure 5.5.2.2.5.6**). The results show, there is no different between the coupling of the samples with and without TEA added.
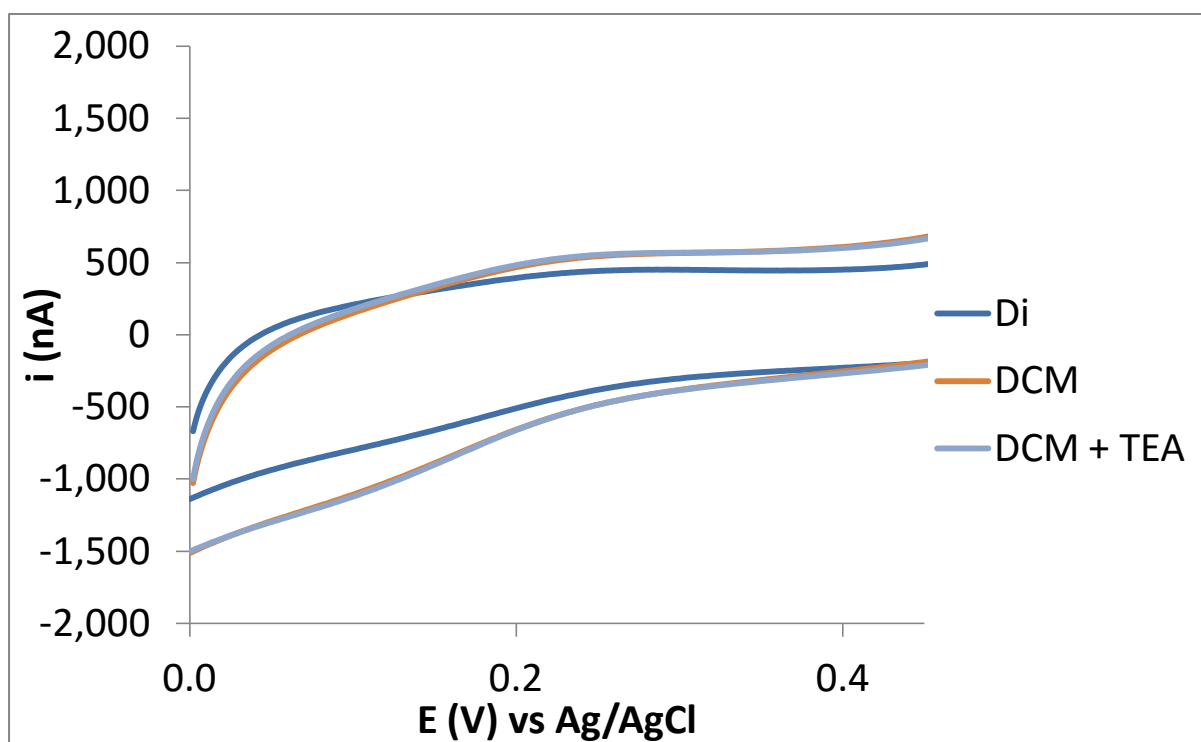
Figure 5.5.2.2.5.6 Typical CVs obtained from PBS solution scanned at 100 mV sec^{-1} with di surface after incubated in 5 mM FcA-Ester in DCM with or without TEA for 24 hours. The blue line, Di, is the di surface alone negative control. n=2

Having achieved only very low coupling efficiency at this point using FcA-Ester to synthesis the electrode surface, experiments were repeated with FcDa-Ester as an alternative mediator. The coupling reaction was repeated in ethanol, DMF and DCM with TEA solution. The same

result as FcA-Ester coupling was obtained, coupling efficiency remains very low (**figure 5.5.2.2.5.7**).

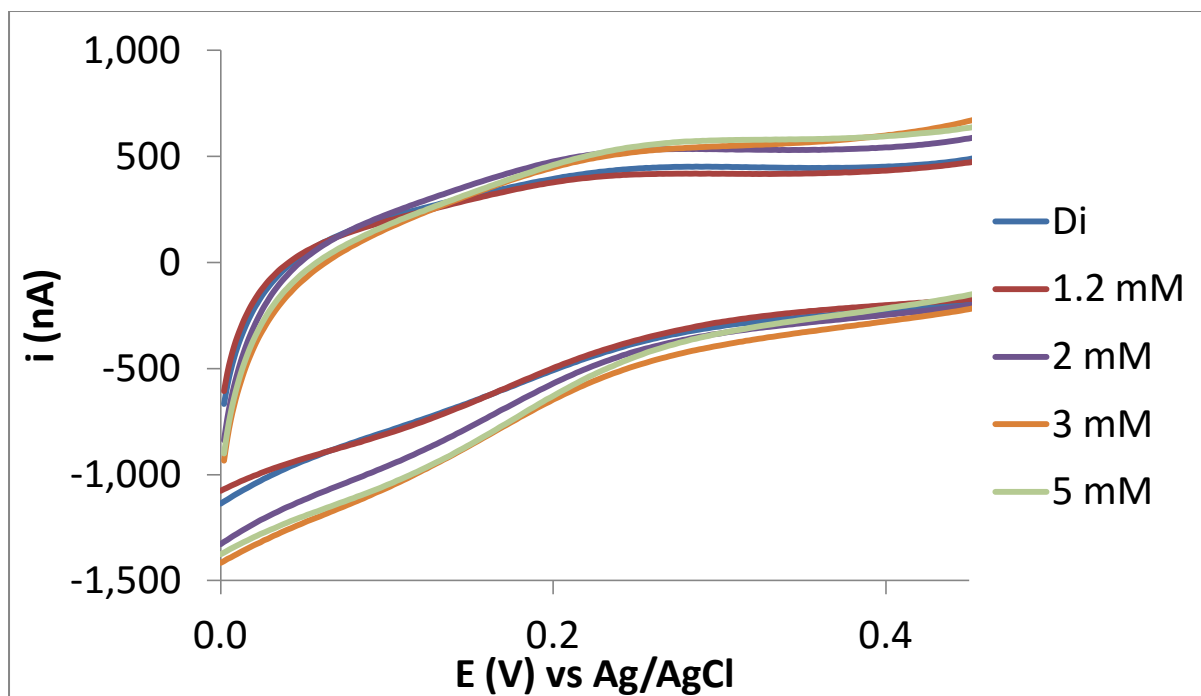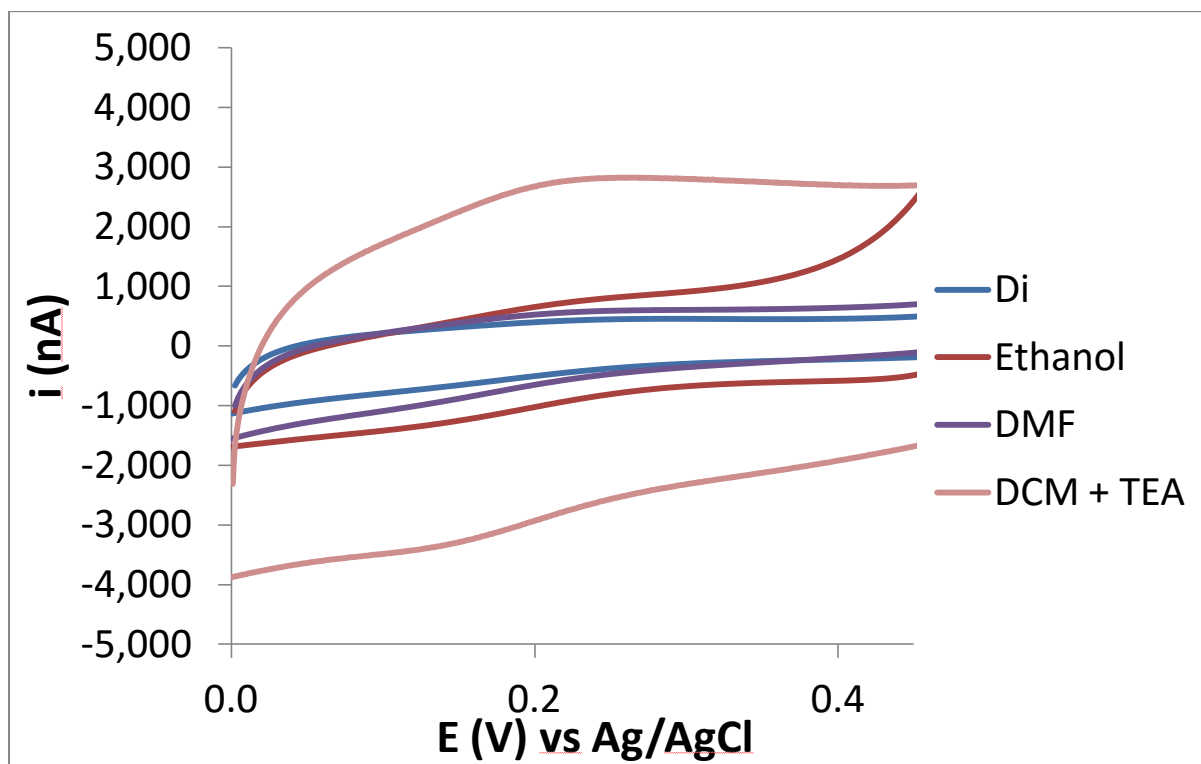**Figure 5.5.2.2.5.7** Typical CVs obtained from PBS solution scanned at 100 mV sec^{-1} with di surface after incubated in 5 mM FcDA-Ester in ethanol, DMF and DCM with TEA for 24 hours. The blue line, Di, is the di surface alone negative control. n=2

Four different coupling conditions were attempted, including having the reaction in ethanol, DMF, DCM with and without addition of TEA. However, none of the conditions has improved the coupling efficiency. As observed, after a few hours both FcA-Ester and FcDA-Ester were diluted in DMF, DCM with or without TEA, the solutions' colour turned from yellow-orange to dark brown with some visible precipitation. Investigation was needed to

ascertain what reaction is occurring between the different solvents and the FcA-Ester and FcDA-Ester molecules, for this a series of mass spectrometry experiments were conducted.

5.5.2.2.6 FcA-Ester and FcDA-Ester mass spectrometry in different solvents

Mass spectrometry (MS) was conducted to monitor the stability of FcA-Ester and FcDA-Ester in the different solvents used for the coupling reaction for surface immobilisation. An Alliance e2695 liquid chromatography (LC) system directly attached to a Xevo-G2-XS-ToF mass spectrometer were used to conduct the experiments. The LC system was used to directly inject the relevant samples and deliver the sample in methanol mobile phase at 100 µl/min, using electrospray ionisation (ESI) technique for MS analysis. The capillary voltage for ESI analysis was set to 3 kV in positive polarity, and the sampling cone voltage was set to 40 V. The source temperature was set to 130 °C, desolvation temperature set to 350 °C. Dry nitrogen gas was used as nebuliser gas (100 L/hr), desolvation gas (800 L/hr) and sample cone gas (60 L/hr).

Samples of FcA-Ester and FcDA-Ester were prepared at 0.5 mg/ml in each of the following solvents, ethanol, dichloromethane (DCM), tetrahydrofuran (THF) another commonly used solvent, and DMF both with and without 1 mM TEA.

The mass spectrum was analysed using two criteria. Criteria 1, as mentioned in the method (see **Chapter 2 section 2.4**), both FcA-Ester and FcDA-Ester could form adducts with the solvent used, and the adducts it can possibly form are $[M]^+$ the molecular ion, $[M+H]^+$

hydrogen adduct from the solvent, $[M+Salt]^+$ with salt being sodium (Na) or potassium (K) from the glassware, $[M+S]^+$ adduct with the solvent, or combinations of all of these. In addition, criteria 2, isotope distribution of the molecular weight is also used to confirm the presence of iron (Fe). Fe in nature exists in four isoforms with relative abundance ^{54}Fe (5.81%), ^{56}Fe (91.64%), ^{57}Fe (2.21%) and ^{58}Fe (0.34%) [59]. The iron isotope pattern was used to confirm that the molecular weight of the ions observed contain iron. These parameters were used in the interpretation of the MS data.

The samples in solvents without 1 mM TEA were injected (5 µl) at time points 0 and 48 hrs after dissolving in the relevant solvents. Mass Spectrometry analysis of FcA-Ester and FcDA-Ester prepared in dichloromethane (DCM) was also analysed (data not shown). The mass spectrometry data was inconclusive, no FcA-Ester or FcDA-Ester ions were observed in the mass spectrum. This may be because FcA-Ester and FcDA-Ester in DCM does not form positively or negatively charged ions by electrospray ionisation technique. Therefore, at this stage, using electrospray ionisation it is not clear if FcA-Ester and FcDA-Ester is stable in DCM. **Figure 5.5.2.2.6.1** and **figure 5.5.2.2.6.2** summarise the result of the stability of FcA-Ester and FcDA-Ester in ethanol (**i**), THF (**ii**) and DMF (**iii**) at 0 hrs and after 48 hrs in solution, respectively. The following molecular weight ions were observed for FcA-Ester in ethanol (**figure 5.5.2.2.6.1 i**) at time = 0 hrs; $[M]^+ = 327$ and $[M+Na]^+ = 350$, please see **figure 5.5.2.2.5.1** for the molecular structure, formula, weight and relative % of isotopes of FcA-Ester (obtained from Chemdraw). After 48 hrs, molecular weight ions $[M+Na]^+ = 350$ and $[M+Na+Ethanol]^+ = 396$ were observed. FcA-Ester in THF (**figure 5.5.2.2.6.1 ii**) only showed molecular weight ion $[M]^+ = 327$ in both time points 0 and 48 hrs. No molecular ions for FcA-Ester were observed in DMF (**figure 5.5.2.2.6.1 iii**) at time point 0 and 48 hrs. The

MS results suggest FcA-Ester is stable in both ethanol and THF for up to 48 hrs, but not in DMF.
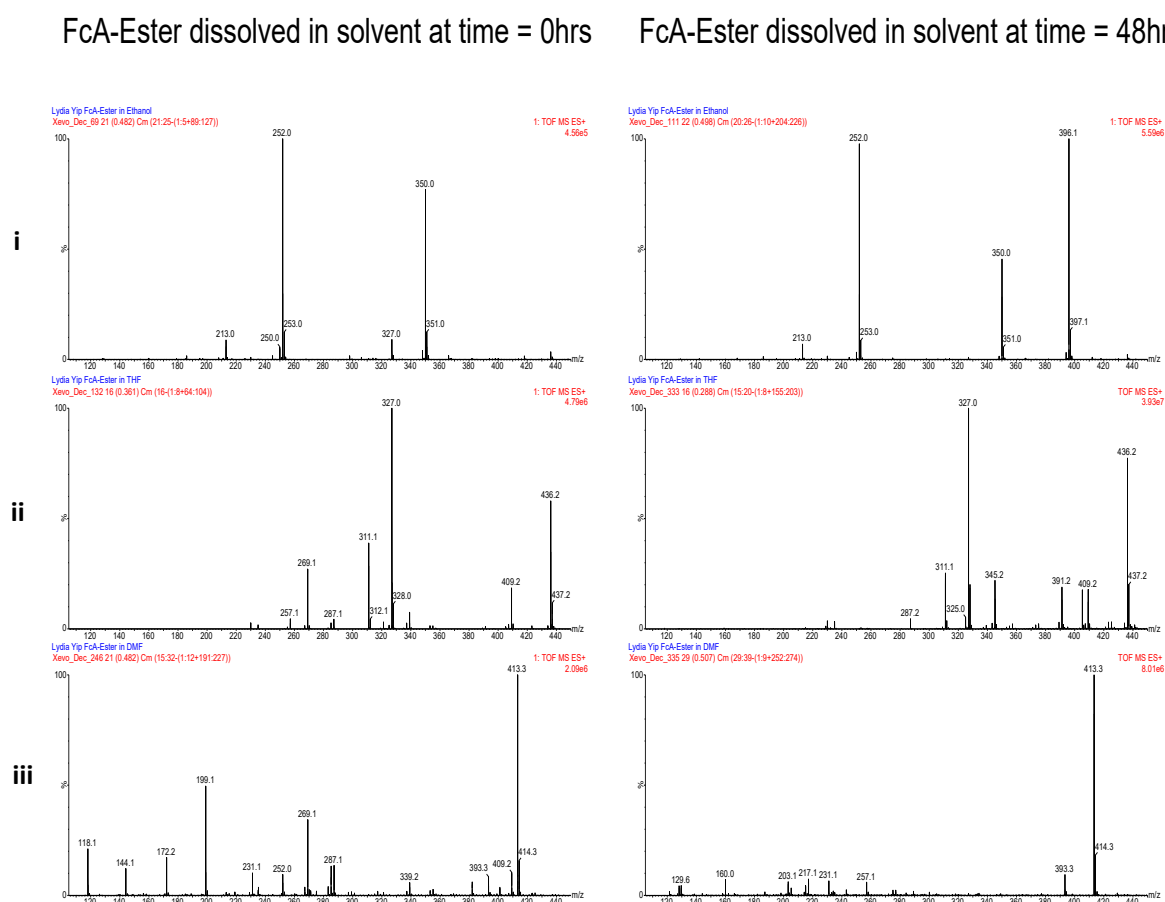
Figure 5.5.2.2.6.1 Mass spectrometry data obtained after FcA-Ester was diluted in (**i**) ethanol, (**ii**) THF and (**iii**) DMF after 0 and 48 hours.

FcDA-Ester (**figure 5.5.2.2.6.2)**, on the other hand, in ethanol shows molecular weight ions $[M+Na]^+ = 394$ at time point 0 hrs but at 48 hrs shows mainly $[M+Na+Ethanol]^+ = 440$, please see **figure 5.5.2.2.5.2** for the molecular structure, formula, weight and relative % of isotopes of of FcDA-Ester (obtained from Chemdraw). FcDA-Ester in THF and DMF show $[M+Na]^+ = 394$, but this disappears after 48 hrs. The MS data suggest FcDA-Ester is only stable in ethanol for up to 48 hrs, but not stable in THF or DMF.

FcDA-Ester dissolved in solvent at time = 0hrs   FcDA-Ester dissolved in solvent at time = 48hrs
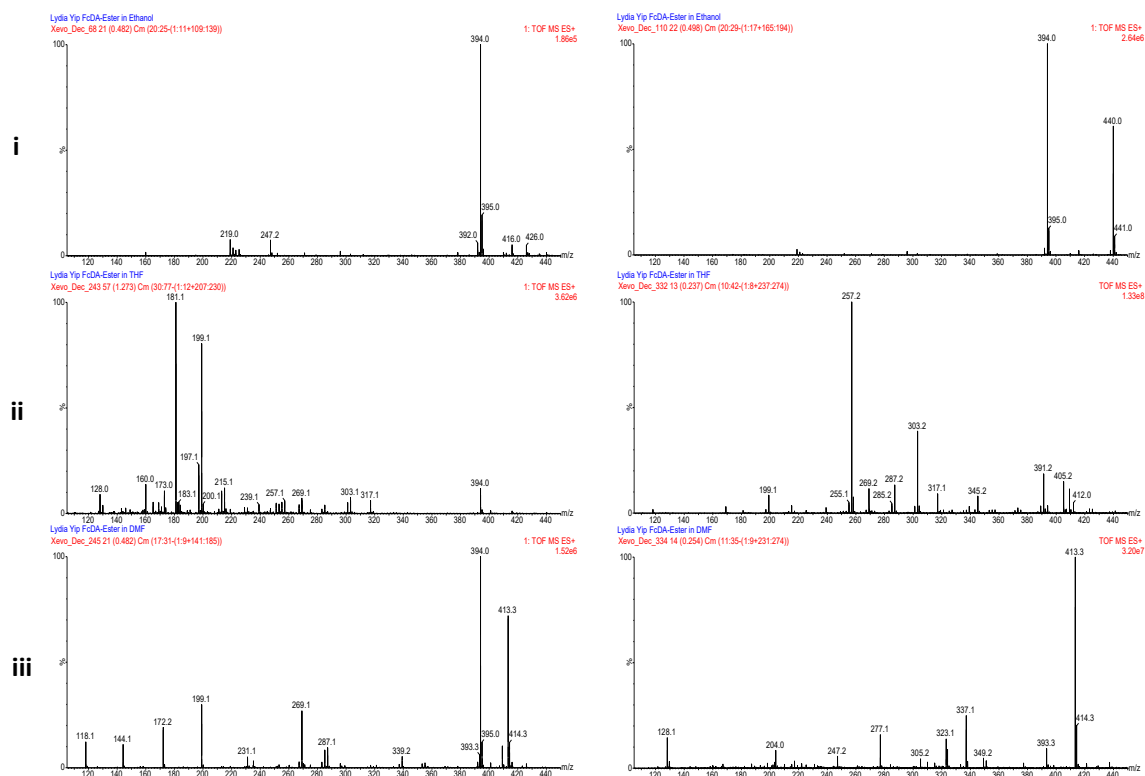
Figure **5.5.2.2.6.2** Mass spectrometry data obtained after FcDA-Ester was diluted in (**i**) ethanol, (**ii**) THF and (**iii**) DMF after 0 and 48 hours.

The MS data of FcA-Ester and FcDA-Ester suggested both compounds are stable in ethanol, therefore, only the MS data for FcA-Ester and FcDA-Ester in ethanol + 1 mM TEA is shown in **figure 5.5.2.2.6.3**. This was to confirm if TEA also reacted with the FcA-Ester and FcDA-Ester (**section 5.5.2.2.5**). The samples in ethanol and 1 mM TEA were injected (5 µl) at time points 0, 1, 2, 24, and 48 hrs to monitor the stability of FcA-Ester and FcDA-Ester in presence of 1 mM TEA. FcA-Ester in the presence of 1 mM TEA forms different molecular weight ions, when compared to samples without 1 mM TEA. At time point 0 hrs, the molecular weight ions $[M+Na+methanol]^+ = 382$ and $[M+Na+ethanol]^+ = 396$ are observed, the former being formed as a result of the mobile phase solvent used in the delivery of the

sample for ESI. In the first two hours we observe the switching of adduct formation from primarily [M+Na+methanol]$^+$ seen at 0 hr, to [M+Na+ethanol]$^+$ primarily seen at 2 hrs. At the 2 hr time point, a molecular weight of 196, which does not contain iron as confirmed by the lack of iron isotope pattern, starts to appear. This molecular weight ion increases as [M+Na+ethanol]$^+$ decreases at the 24 and 48 hr time points, and at 48 hr the major ion species seen is the 196 molecular weight and the [M+Na+ethanol]$^+$ ion has significantly decreased.
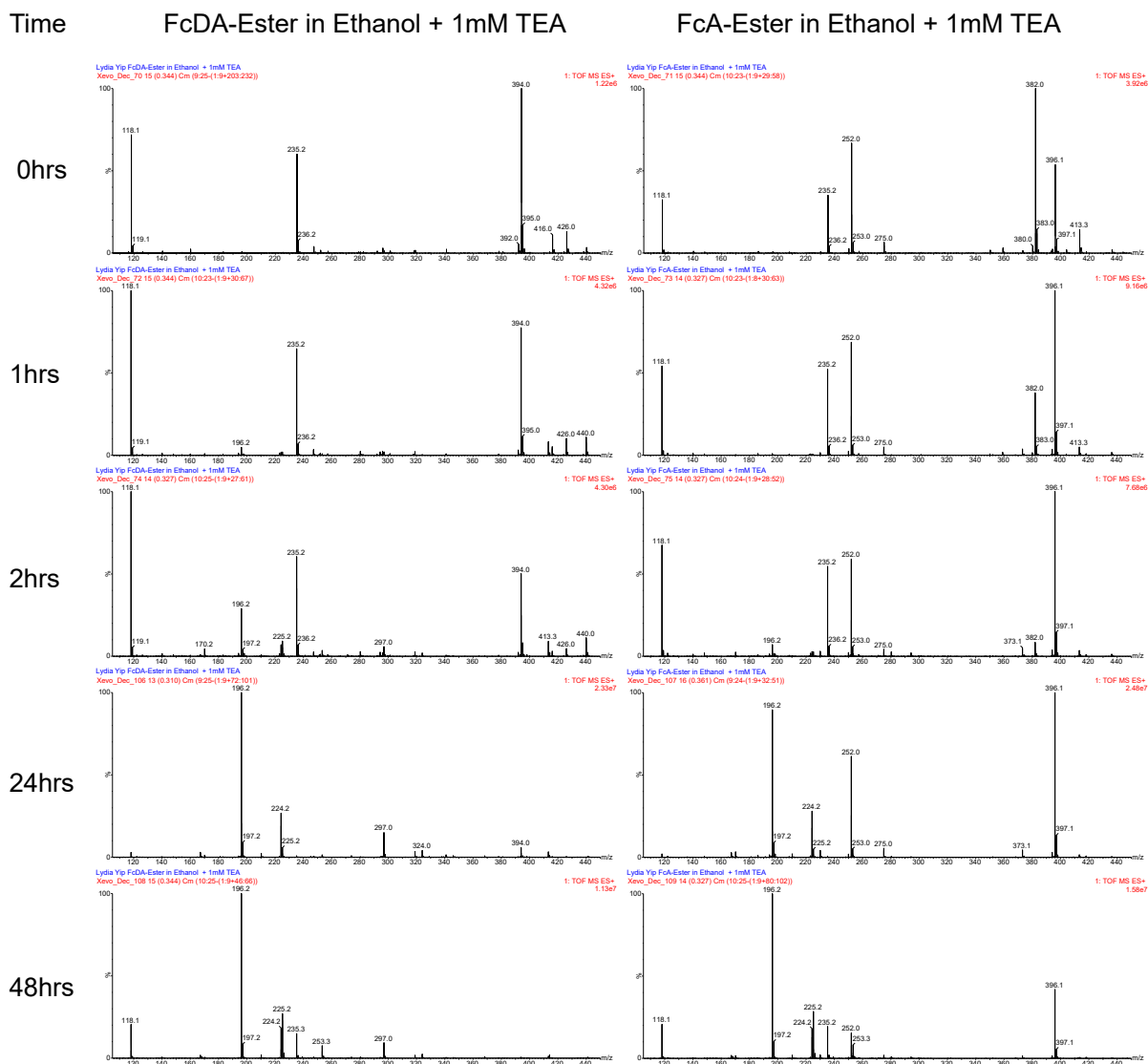
Figure **5.5.2.2.6.3** Mass spectrometry data obtained after FcDA-Ester and FcDA-Ester was diluted in ethanol, after 0 1, 2, 24 and 48 hours.

The FcDA-Ester only appears as the $[M+Na]^+ = 394$ molecular weight ion in the presence of 1 mM TEA and none of the other adducts are seen at any time point. Interestingly the 196 molecular weight ion, not containing the iron isotope pattern, shows up also in the FcDA-Ester experiment. Moreover, this 196 molecular weight ion appears at time point 1 hr, and progressively increases over time and the $[M+Na]^+ = 394$ molecular weight ion decreases over time. At 48 hr, the $[M+Na]^+ = 394$ molecular weight ion completely disappears.

In both cases of FcA-Ester and FcDA-Ester in ethanol with 1 mM TEA, experiments show a considerable MS spectrum difference from 2 hrs to 24 hrs. It's after the 2 hr time point that the 196 molecular weight ion significantly increases and the sample ion decreases. This suggests that both FcA-Ester and FcDA-Ester are relatively stable in the coupling mixture for up to 2 hrs.

The molecular weight ion 196 could possibly be due to further oxidation of the cyclopentadienides by TEA to dihydrofulvalene [60] from the reaction seen in **figure 5.5.2.2.6.4**
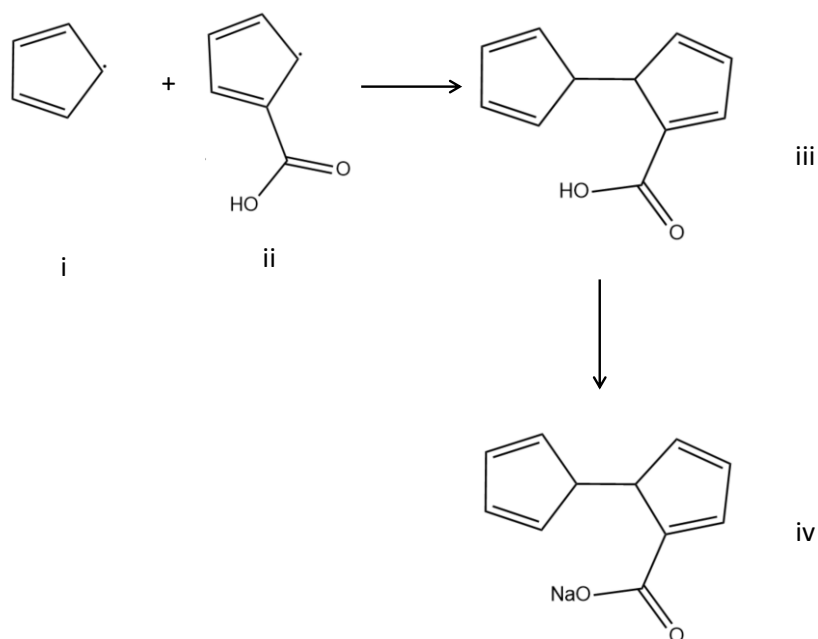
Figure 5.5.2.2.6.4 Shows the proposed reaction occurring for the increased presents of molecular weight ion 196. C_5H_5 (1,3-cyclopentadie-2-nide) (**i**) and $C_6H_5O_2$.(1,3-cyclopentadie-2-nide-1-carboxylic acid) (**ii**) was further oxidised by TEAleading to the iron falling off from FcA and FcDA to form (iii) [1,1'-bi(cyclopentane)]-2,2',4,4'-tetraene-2-

carboxylate. Substitution of the carboxylic acid hydrogen with sodium (Na) would produce (iv) sodium [1,1'-bi(cyclopentane)]-2,2',4,4'-tetraene-2-carboxylate (Mw = 196).

The molecular weight of [1,1'-bi(cyclopentane)]-2,2',4,4'-tetraene-2-carboxylic acid (**figure 5.5.2.2.6.4 iii)** is 174, molecular ion 196 comes from the replacement of the carboxylic acid hydrogen with a sodium (174-1+23 = 196) (**figure 5.5.2.2.6.4 iv)**. This would lead to the dissociation of the iron, thus explaining the loss of the iron isotope as observed in the MS data.

In the process of ferrocene synthesis, a base, KOH, was used to produces potassium cyclopentadienide salt from cyclopentadiene [61] which is dark brown in colour. Potassium cyclopentadienide would then mixed with iron chloride to form ferrocene [61]. MS data showed that, in the presence of TEA, the iron is being removed effectively reversing this last step in the synthesis process. Both FcA-Ester and FcDA-Ester are also not stable in DMF. From observation in **section 5.5.2.2.5**, FcA-Ester and FcDA-Ester also turns brown when diluted in DMF, DCM and DCM with TEA. It is concluded that the cyclopentadiene ring in both ferrocene molecules reacted with the solvent and the base (TEA) which caused the iron molecule to detach from the ring. This is supported by both the observed colour changed of the sample and the disappearance of the ferrocene ion from the MS data. TEA is a common additive that facilities ester – carboxylic acid reaction, however, in this case the TEA has been shown to disturb the structure of the raw material, in this case ferrocene. MS data shows that both FcA-Ester and FcDA-Ester are stable in ethanol however, the coupling efficiency was shown to be very low for unknown reasons. Further investigation would be required for a suitable solvent and coupling method for the FcA or FcDA chemical coupling onto surface to work.

5.6 Conclusion

In this chapter, some of the most commonly used methods of mediator immobilisation were investigated for production of electrodes with FcA mediator. Immobilisation was viewed as the next logical step for the reason mentioned previously some of which include, increased practicality, removal of mediator diffusion rate limiting step, and improvement to data accuracy. Initially the decision was made to attempt immobilisation without chemically altering the FcA mediator as it was shown in **chapter 4** the system was highly dependent on the preservation of the carboxylic acid functional group. To this end screen printing techniques were employed. Assuming a simple mix and print methodology, where a carbon ink was chosen as carbon had been previously used as an electrode material. Initial results were positive showing preservation of the separated O_2 catalytic peak shown in **chapter 4** however there were problems with the system. While the system showed the increased signal strength expected this was later found to also be due to the porous nature of the carbon ink. By increasing the surface area of the electrode to an unknown area and also the addition of another diffusion gradient as the sample solution has to diffuse through the ink the initial positive results showed the system needed more investigation. Along with experts from Gwent further investigation was carried out and while remaining functional the issue of the carbon ink being porous remained.

With no resolution found the next logical step was to use a commercially manufactured carbon electrode and immobilise the FcA into the surface of the electrode with an oxygen porous membrane. While this would introduce a diffusion layer it should prevent the issues found with the carbon ink being porous as found in the screen printing approach. Many membranes were considered with the criteria of being gas and aqueous permeable, however

few were found to be compatible. Many of the aqueous and gas permeable membranes are charge selective for example and therefore would be unsuitable for this purpose. AC membrane was finally chosen for further investigation as it fit the criteria well. FcA was drop coated onto the manufactured carbon electrodes followed by AC membrane. Results showed that while the system worked and the separated O_2 catalytic peak was preserved, when consecutive cycles were run the signal strength continues to reduce. Further investigation showed signs that the membrane during the process of conduction the CV analysis was being removed form the surface of the electrode. Optimisation was attempted by changing the concentration of membrane used in the preparation of the electrode and also the preparation methodology. All approaches that still preserved the functionality of the system gave rise to the same problem of removal of the membrane during CV analysis.

Having found screen printing and drop coating methods to be problematic, another approach was needed. While seemingly at risk of loss of the functional group of the FcA a surface chemistry approach was taken for mediator immobilisation. SAM and diazonium would be the chosen means for this chemical immobilisation approach. Having less chemical steps and therefore seemingly more simple SAM would be investigated first. Initially a SAM coupled with ferrocene was purchased, and when coupled onto a gold substrate electrode exhibited the separate O_2 catalytic peak. This confirmed that the chemical coupling of ferrocene with the SAM molecule, had left the carboxylic acid functional group activity undisrupted. A significant drop in ferrocene current was being observed over the 10 CV cycles which indicated there was a decrease of ferrocene concentration on the electrode surface. Investigation was carried out to verify the point at which the ferrocene was being removed, and via desorption it was verified to be a weakness of the thiol-Au bond under the

electrochemical conditions. Alternative SAM molecules were tried however it was not possible to produce a SAM system stable at the required electrochemical conditions.

Having found the thiol-Au bond to be the weak point in the SAM system of immobilisation but, that the chemical coupling of the ferrocene to still exhibits a ferrocene peak, diazonium surface grafting was attempted. Results showed that the grafting process was successful, and the di surface was electrochemically stable. Having established a strongly bonded bridge the project moved onto coupling of the ferrocene on to the diazonium bridge molecule. This was performed with different solvents and TEA to facilitate the reaction however each displayed little to no coupling efficiency. Having observed unexpected colour changes to the coupling solution and the low yield coupling the ferrocene mediator and coupling solutions were put to MS analysis. MS analysis showed that FcA-Ester was stable in ethanol and THF and FcDA-Ester was only stable in ethanol. It remains unclear as to why the coupling efficiency is so low. Further investigation is required in order to have ferrocene molecule couple onto di surface.

5.7 References

1.   Guadagno, T.M., et al., *A Link Between Cyclin A Expression and Adhesion-Dependent Cell Cycle Progression.* Science, 1993. 262(5139): p. 1572-1575.

2.   Reddig, P. and R. Juliano, *Clinging to life: cell to matrix adhesion and cell survival.* Cancer and Metastasis Reviews, 2005. 24(3): p. 425-439.

3.   Tyrrell, H.J., *The Origin and Present Status of Fick's Diffusion Law*. 1964.

4.   Clark, L.C., Jr. and C. Lyons, *Electrode systems for continuous monitoring in cardiovascular surgery.* Ann N Y Acad Sci, 1962. 102: p. 29-45.

5.   Putzbach, W. and N. Ronkainen, *Immobilization Techniques in the Fabrication of Nanomaterial-Based Electrochemical Biosensors: A Review.* Sensors, 2013. 13(4): p. 4811.

6.   Kochius, S., et al., *Immobilized redox mediators for electrochemical NAD(P)+ regeneration.* Appl Microbiol Biotechnol, 2012. 93(6): p. 2251-64.

7.   Ohfuji, K., et al., *Construction of a glucose sensor based on a screen-printed electrode and a novel mediator pyocyanin from Pseudomonas aeruginosa.* Biosensors and Bioelectronics, 2004. 19(10): p. 1237-1244.

8.   Nagata, R., et al., *A glucose sensor fabricated by the screen printing technique.* Biosensors and Bioelectronics, 1995. 10(3–4): p. 261-267.

9.   Xu, H., et al. *A glucose oxidase sensor based on screen-printed carbon electrodes modified by polypyrrole*. in *Engineering in Medicine and Biology Society, 2005. IEEE-EMBS 2005. 27th Annual International Conference of the*. 2006. IEEE.

10.   Ikeda, T., F. Matsushita, and M. Senda, *Amperometric fructose sensor based on direct bioelectrocatalysis.* Biosensors and Bioelectronics, 1991. 6(4): p. 299-304.

11.   Cinti, S., et al., *Cholesterol biosensor based on inkjet-printed Prussian blue nanoparticle-modified screen-printed electrodes.* Sensors and Actuators B: Chemical, 2015. 221: p. 187-190.

12. Gilmartin, M.A.T. and J.P. Hart, *Fabrication and characterization of a screen-printed, disposable, amperometric cholesterol biosensor.* Analyst, 1994. 119(11): p. 2331-2336.

13. Wu, L., et al., *Electrochemical immunoassay for CA125 based on cellulose acetate stabilized antigen/colloidal gold nanoparticles membrane.* Electrochimica Acta, 2006. 51(7): p. 1208-1214.

14. Moyo, M., J.O. Okonkwo, and N.M. Agyei, *Recent Advances in Polymeric Materials Used as Electron Mediators and Immobilizing Matrices in Developing Enzyme Electrodes.* Sensors, 2012. 12(1): p. 923.

15. Liu, G., et al., *The modification of glassy carbon and gold electrodes with aryl diazonium salt: The impact of the electrode materials on the rate of heterogeneous electron transfer.* Chemical Physics, 2005. 319(1–3): p. 136-146.

16. Taleat, Z., A. Khoshroo, and M. Mazloum-Ardakani, *Screen-printed electrodes for biosensing: a review (2008–2013).* Microchimica Acta, 2014. 181(9-10): p. 865-891.

17. Li, M., et al., *Recent developments and applications of screen-printed electrodes in environmental assays—A review.* Analytica Chimica Acta, 2012. 734: p. 31-44.

18. Dai, K.-S. and C. Lin, *Electrochemical test strip for multi-functional biosensor*. 2006, Google Patents.

19. Ambrózy, A., L. Hlavatá, and J. Labuda, *Protective membranes at electrochemical biosensors*, in *Acta Chimica Slovaca*. 2013. p. 35.

20. Karunakaran, C., K. Bhargava, and R. Benjamin, *Biosensors and Bioelectronics*. 2015: Elsevier Science.

21. Gilmartin, M.A.T. and J.P. Hart, *Novel, reagentless, amperometric biosensor for uric acid based on a chemically modified screen-printed carbon electrode coated with cellulose acetate and uricase.* Analyst, 1994. 119(5): p. 833-840.

22. Gilmartin, M.A.T. and J.P. Hart, *Rapid detection of paracetamol using a disposable, surface-modified screen-printed carbon electrode.* Analyst, 1994. 119(11): p. 2431-2437.

23.   Eckermann, A.L., et al., *Electrochemistry of redox-active self-assembled monolayers.* Coordination Chemistry Reviews, 2010. 254(15–16): p. 1769-1802.

24.   Prashar, D., *Self assembled monolayers-a review.* Int J ChemTech Res, 2012. 4(1): p. 258-265.

25.   Mandler, D. and S. Kraus-Ophir, *Self-assembled monolayers (SAMs) for electrochemical sensing.* Journal of Solid State Electrochemistry, 2011. 15(7-8): p. 1535-1558.

26.   Chaki, N.K. and K. Vijayamohanan, *Self-assembled monolayers as a tunable platform for biosensor applications.* Biosensors and Bioelectronics, 2002. 17(1–2): p. 1-12.

27.   Lehr, J., et al., *Reaction of gold substrates with diazonium salts in acidic solution at open-circuit potential.* Langmuir, 2009. 25(23): p. 13503-13509.

28.   Marshall, N. and J. Locklin, *Reductive Electrografting of Benzene (p-Bisdiazonium Hexafluorophosphate): A Simple and Effective Protocol for Creating Diazonium-Functionalized Thin Films.* Langmuir, 2011. 27(21): p. 13367-13373.

29.   Kariuki, J.K. and M.T. McDermott, *Formation of Multilayers on Glassy Carbon Electrodes via the Reduction of Diazonium Salts.* Langmuir, 2001. 17(19): p. 5947-5951.

30.   Maldonado, S., et al., *Surface Modification of Indium Tin Oxide via Electrochemical Reduction of Aryldiazonium Cations.* Langmuir, 2006. 22(6): p. 2884-2891.

31.   Rawson, F., et al., *Tailoring 3D single-walled carbon nanotubes anchored to indium tin oxide for natural cellular uptake and intracellular sensing.* Nano letters, 2012. 13(1): p. 1-8.

32.   Ketenoğlu, D. and B. Ünal, *Influence of surface roughness on the electrical conductivity of semiconducting thin films.* Physica A: Statistical Mechanics and its Applications, 2013. 392(14): p. 3008-3017.

33.   Sreedhar, N.Y., M. Sunil Kumar, and K. Krishnaveni, *Sensitive determination of chlorpyrifos using Ag/Cu alloy nanoparticles and graphene composite paste electrode.* Sensors and Actuators B: Chemical, 2015. 210: p. 475-482.

34. Klingler, R. and J. Kochi, *Electron-transfer kinetics from cyclic voltammetry. Quantitative description of electrochemical reversibility.* The Journal of Physical Chemistry, 1981. 85(12): p. 1731-1741.

35. Matsue, T., et al., *Electron-transfer reactions associated with host-guest complexation. Oxidation of ferrocenecarboxylic acid in the presence of .beta.-cyclodextrin.* Journal of the American Chemical Society, 1985. 107(12): p. 3411-3417.

36. Hoornstra, J., et al., *The importance of paste rheology in improving fine line, thick film screen printing of front side metallization*. 1997: Netherlands Energy Research Foundation ECN.

37. Chiu, K.-C. *Application of neural network on LTCC fine line screen printing process*. in *Neural Networks, 2003. Proceedings of the International Joint Conference on*. 2003.

38. Alias, R. and S.M. Shapee, *Rheological Behaviors and Their Correlation with Printing Performance of Silver Paste for LTCC Tape*. 2012: INTECH Open Access Publisher.

39. Hobby, A. *Screen Printing For The Industrial User*. March 1997 [cited 2015 16th December]; Available from: http://www.gwent.org/gem_screen_printing.html.

40. Foster, C., R. Kadara, and C. Banks, *Fundamentals of Screen-Printing Electrochemical Architectures*, in *Screen-Printing Electrochemical Architectures*. 2016, Springer International Publishing. p. 13-23.

41. Jańczuk, B., W. Wójcik, and A. Zdziennicka, *Wettability and surface free energy of glass in the presence of cetyltrimethylammonium bromide.* Materials Chemistry and Physics, 1999. 58(2): p. 166-171.

42. Sawada, S., et al., *Micropatterning of Copper on a Poly(ethylene terephthalate) Substrate Modified with a Self-Assembled Monolayer.* Langmuir, 2006. 22(1): p. 332-337.

43. Altankov, G., F. Grinnell, and T. Groth, *Studies on the biocompatibility of materials: Fibroblast reorganization of substratum-bound fibronectin on surfaces varying in wettability.* Journal of biomedical materials research, 1996. 30(3): p. 385-391.

44.   Erbil, H.Y., et al., *Determination of the Receding Contact Angle of Sessile Drops on Polymer Surfaces by Evaporation.* Langmuir, 1999. 15(21): p. 7378-7385.

45.   Švancara, I., et al., *A microscopic study on carbon paste electrodes.* Electroanalysis, 1996. 8(1): p. 61-65.

46.   Inaba, R., et al., *Electrochemical desorption of self-assembled monolayers for engineering cellular tissues.* Biomaterials, 2009. 30(21): p. 3573-3579.

47.   Gorman, C.B., H.A. Biebuyck, and G.M. Whitesides, *Control of the Shape of Liquid Lenses on a Modified Gold Surface Using an Applied Electrical Potential across a Self-Assembled Monolayer.* Langmuir, 1995. 11(6): p. 2242-2246.

48.   Liu, Y. and L. Xu, *Electrochemical Sensor for Tryptophan Determination Based on Copper-cobalt Hexacyanoferrate Film Modified Graphite Electrode.* Sensors, 2007. 7(10): p. 2446.

49.   Kim, T., K.C. Chan, and R.M. Crooks, *Polymeric self-assembled monolayers. 4. chemical, electrochemical, and thermal stability of ω-functionalized, self-assembled diacetylenic and polydiacetylenic monolayers.* Journal of the American Chemical Society, 1997. 119(1): p. 189-193.

50.   Xue, Y., et al., *Quantifying thiol–gold interactions towards the efficient strength control.* Nat Commun, 2014. 5.

51.   Oguchi, S., et al., *pH Condition in temperature shift cultivation enhances cell longevity and specific hMab productivity in CHO culture.* Cytotechnology, 2006. 52(3): p. 199-207.

52.   Simons, B.M., et al., *Formation of Thick Aminophenyl Films from Aminobenzenediazonium Ion in the Absence of a Reduction Source.* Langmuir, 2014. 30(17): p. 4989-4996.

53.   Mahouche-Chergui, S., et al., *Aryl diazonium salts: a new class of coupling agents for bonding polymers, biomacromolecules and nanoparticles to surfaces.* Chemical Society Reviews, 2011. 40(7): p. 4143-4166.

54. Anariba, F., S.H. DuVall, and R.L. McCreery, *Mono- and Multilayer Formation by Diazonium Reduction on Carbon Surfaces Monitored with Atomic Force Microscopy "Scratching"*. Analytical Chemistry, 2003. 75(15): p. 3837-3844.

55. Delamar, M., et al., *Covalent modification of carbon surfaces by grafting of functionalized aryl radicals produced from electrochemical reduction of diazonium salts.* Journal of the American Chemical Society, 1992. 114(14): p. 5883-5884.

56. Garrett, D.J., et al., *Robust Forests of Vertically Aligned Carbon Nanotubes Chemically Assembled on Carbon Substrates.* Langmuir, 2010. 26(3): p. 1848-1854.

57. Batterjee, S.M., et al., *The electrochemistry of some ferrocene derivatives: redox potential and substituent effects.* Applied Organometallic Chemistry, 2003. 17(5): p. 291-297.

58. Joullié, M.M. and K.M. Lassen, *Evolution of amide bond formation.* Arkivoc, 2010. 8: p. 189-250.

59. White, J. and A. Cameron, *The natural abundance of isotopes of stable elements.* Physical Review, 1948. 74(9): p. 991.

60. Moulton, R.D., R. Farid, and A.J. Bard, *Electrochemical reactions of cyclopentadienes in non-aqueous media.* Journal of Electroanalytical Chemistry and Interfacial Electrochemistry, 1988. 256(2): p. 309-326.

61. Cordes, H., *Production of ferrocene compounds*. 1965, Google Patents.

Chapter 6

Conclusion and future work

6.1 Conclusion

Proof of concept and development of a brand new BOD system has been completed in this project, and the patent application has been filed. The O_2 catalytic property of ferrocene derivatives was first reported by Cassidy's research group in 1999 [1]. However, the O_2 catalytic properties between different ferrocene derivatives which is governed by the different functional groups has never been investigated, let alone put into practical applications. This project undertook to investigate the practical use of both the O_2 catalytic property and to investigate the interaction of the different ferrocene derivatives with O_2. FcA, FcDA and FcMeOH were each found to exhibit different O_2 catalytic properties but it was the unique interaction of FcA due to the single carboxylic acid group that was most of interest. It exhibits the O_2 catalytic property but more importantly has a unique separated O_2 catalytic peak compared to the convoluted O_2 catalytic peak with normal oxidation peak in the case of FcDA and FcMeOH. This allows with just a single cycle of CV to measure the concentration of O_2 in a sample and with a small calculation of diffusion rate with a second cycle to measure the near real time consumption of O_2.

The FcA mediated BOD system offers potentially the fastest, and cheapest BOD developed to date, and a near real-time measurement of BOD that can be calculated down to single cell O_2 consumption measurement scale. The system requires no incubation time compare to the ferricyanide mediated BOD assay or standard BOD5. Any influence chemical or otherwise

introduced by the assay upon the targeted cell or cell line are minimised because there is no need for an incubation period due to the fast FcA O_2 catalytic kinetics rate. The assay offers result acquisition of dissolve oxygen measured in just 4 minutes, and BOD requiring 2 cycles of CV to be run in just 8 minutes. The cost of the machine could be as low as currently commercially available glucose meters, and potentially similar costing for the electrode chips. Also of great importance, the system would require little to no maintenance.

Pushing the concept to its full potential and a practical product range remains a challenge. In the current dissolved FcA mediated system, high accuracy, repeatability, and rapid measurement have been demonstrated. *E.coli* cell density was accurately measured, showing smaller standard error than using a viability assay compare to conventional agar plate colony count assay. Moreover and of great importance, it works with little or unnoticeable influence from complex media, e.g. LB broth. However improvements including sensitivity, portability, assay simplicity, and cost effectiveness are needed to truly optimise the system to a highly marketable product. This could potentially all be accomplished by successful immobilisation of FcA onto an electrode surface. The most commonly used immobilisation methods were tested in this project including screen printing, use of semi-permeable membrane and surface coupling chemistry. The unique requirements of this assay, namely the importance of preserving the mono-carboxylic acid group in the FcA and the multiple cycle CV have proven to greatly complicate this process. All attempts to date at immobilisation have shown promising signs for future development in various ways.

Screen printing with FcA mixed carbon paste ink initially seemed to be the ideal immobilisation method for the FcA mediated BOD system. It is cost effective, easy to

synthesise, and more importantly, it preserved the important single carboxylic acid group in the FcA. It has demonstrated an enlarged O_2 catalytic peak (**chapter 5 section 5.5.1.1**) compare to the FcA dissolved system (**chapter 4 section 4.5.4**). However, the porous property of the carbon paste ink has proved to be problematic for this particular system. In other single cycle systems such as glucose or cholesterol a porous ink would not cause a problem, however a system such as this that involving multiple cycles, it causes two main problems. Firstly the carbon paste ink being porous introduces an extra unpredictable diffusion layer for the O_2 molecule after the first CV cycle. This makes the system impossible to calibrate for the O_2 diffusion rate from the control samples for BOD assay purpose. In addition, as the sample is soaking through the electrode, the working area changed from a known 2D area to an unknown 3D area. The unknown 3D working area invalidates the current to concentration calculation.

The use of a semi-permeable membrane for trapping a mediator or enzymes onto an electrode surface is very common. This seemed the obvious next approach however it was proven that the selection of the correct membrane for this system would be a big challenge. This system in particular necessitates the use of a biocompatible membrane that will not filter out oxygen and negatively charged ions, for example HO_2^- and OH^-, like the Nifron membrane. This is because the oxygen detection relies upon the reduction of oxygen producing negatively charged ROS which react with the FcA mediator. CA seemed the logical choice fitting seemingly all the criteria however it was proved not to be the case as seemingly under assay conditions the membrane is removed from the surface of the electrode.

Chemical immobilisation using SAM as bridge seems to be the next logical method to test. SAM-modified surfaces are wildly used for biosensor development and very easy to prepare. However, the thiol-Au bond is only stable in a very narrow range of potential [2]. After we tested the SAM-modified surface under the FcA mediated BOD assay's working potential scanning range, surfaces have been shown to be unstable. This result was the same with different types of SAM molecules. Therefore, it was concluded, SAM is not suitable for this particular system.

On the other hand, diazonium has been successfully grafted onto the electrode surface and tested stable under the operating conditions of this system. The biggest advantage of using diazonium as a bridge for FcA surface immobilisation is, the strong and stable bond shown by the finding of this project with ITO. ITO is transparent, which allows the system to be easily integrated with microscopy techniques, even fluorescence microscopy techniques. This gives the potential of the system to be used for dual purposes, allowing BOD to be recorded while at the same time using fluorescence microscopy, for example Fluo-4AM for intercellular Ca^{2+} level [3]. By allowing this dual data acquisition running in parallel on the same sample of cells, it provides much greater control, as well as, improved comparison between samples. It would potentially reduce the amount of cellular work involved in such experiments, offering a most cost effective, and time efficient workflow.

The challenge with diazonium chemical immobilisation has arisen with the coupling stage of the reaction fixating FcA onto the diazonium post grafting on to the electrode surface. Following much investigation including coupling concentration, solvent coupling efficiency, and addition of base, coupling efficiency remains extremely low. MS was carried out and the

review of the data suggests, the cyclopentadiene ring structure in the ferrocene mediators tested are being deprotonated in the presents of base and certain solvents e.g. DMF. The peak with iron isotope pattern can be seen in the MS data to decrease over time and eventually disappear. This may have explained why the yield of diazonium-FcA-Ester or diazonium-FcDA-Ester coupling is so low in DMF and when TEA is added. However, the low yield in coupling that is done in ethanol remains unclear, as MS data has shown that both FcA-Ester and FcDA-Ester are stable in ethanol, however, coupling efficiency remains extremely low. More work is required to optimise the coupling efficiency.

6.2 Future work

The concept of the FcA-mediated BOD system is there and proven. The future work revolves around optimisation and refinement of the system, and for the main part this would be to develop a solution for surface immobilisation. Screen printing shows great promise in terms of developing the system into a portable, cost effective and fast system for environment studies, food industry and waste water processing in particular. The future work would involve either development of a non-porous carbon paste ink, thus resolving the issues found in this project. Alternatively finding another stable conducting material that does not interfere with the FcA property to act as an ink carrier for electrode synthesis could prove a solution.

On the other hand, diazonium bridged chemical immobilisation could potentially be ideal for the laboratory working environment. Dual measurement with integration of microscopy technologies via the utilisation of ITO as an electrode substrate by taking advantage of its transparency shows great potential. There is a risk that even with optimisation of coupling

completed that the system still may not sense oxygen. This would likely be due to the modification of the functional group leading to the loss of the separated O_2 catalytic peak properties. It is also yet to be seen if the diazonium layer will block the initial reduction of the O_2 molecule into HO_2^- and OH^- as was shown to be the mechanism of FcA catalysis in **chapter 4**. Having stated this, it is still worthwhile carrying out optimization of the coupling as even if detection of dissolved O_2 concentration is lost it can still be used as a ROS sensor. ROS is an important secondary messenger in cell signaling and closely related to cell metabolic rate. The system can still be developed into an important tool for molecular study. In addition, if carbon nano tube (CNT) can be coupled on top of the diazonium molecule before coupling FcA-Ester or FcDA-Ester on top, it could even give the potential for intracellular ROS detection.

6.3 References

1. Cassidy, J., et al., *Note on the voltammetry of ferrocene carboxylate in aqueous solution.* Electrochemistry communications, 1999. **1**(2): p. 69-71.

2. Kim, T., K.C. Chan, and R.M. Crooks, *Polymeric self-assembled monolayers. 4. chemical, electrochemical, and thermal stability of ω-functionalized, self-assembled diacetylenic and polydiacetylenic monolayers.* Journal of the American Chemical Society, 1997. **119**(1): p. 189-193.

3. Lai, P., N.C. Yip, and F. Michelangeli, *Regucalcin (RGN/SMP30) alters agonist-and thapsigargin-induced cytosolic [Ca 2+] transients in cells by increasing SERCA Ca 2+ ATPase levels.* FEBS letters, 2011. **585**(14): p. 2291-2294.